

McGraw-Hill Nanoscience and Technology Series

POLYMER NANOCOMPOSITES

PROCESSING, CHARACTERIZATION,
AND APPLICATIONS

JOSEPH H. KOO

Polymer Nanocomposites

McGraw-Hill Nanoscience and Technology Series

Series Editor: Omar Manasreh

MICHAEL H. PETERS • *Molecular Thermodynamics and Transport Phenomena*

KEN GILLES • *MEMS/MOEM Packaging: Concepts, Designs, Materials and Processes*

WILLIAM W. LIU AND YICHUAN FANG • *Microfluid Mechanics: Principles and Modeling*

NICOLAE O. LOBONTIU • *Mechanical Design of Microresonators: Modeling and Applications*

JENS TOMM AND JUAN JIMÉNEZ • *Quantum-Well Laser Array Packaging*

Z. M. ZHANG • *Nano/Microscale Heat Transfer*

Polymer Nanocomposites

Processing, Characterization, and Applications

Joseph H. Koo

McGraw-Hill

New York Chicago San Francisco Lisbon London Madrid
Mexico City Milan New Delhi San Juan Seoul
Singapore Sydney Toronto

Copyright © 2006 by The McGraw-Hill Companies, Inc. All rights reserved. Manufactured in the United States of America. Except as permitted under the United States Copyright Act of 1976, no part of this publication may be reproduced or distributed in any form or by any means, or stored in a database or retrieval system, without the prior written permission of the publisher.

0-07-149204-6

The material in this eBook also appears in the print version of this title: 0-07-145821-2.

All trademarks are trademarks of their respective owners. Rather than put a trademark symbol after every occurrence of a trademarked name, we use names in an editorial fashion only, and to the benefit of the trademark owner, with no intention of infringement of the trademark. Where such designations appear in this book, they have been printed with initial caps.

McGraw-Hill eBooks are available at special quantity discounts to use as premiums and sales promotions, or for use in corporate training programs. For more information, please contact George Hoare, Special Sales, at george_hoare@mcgraw-hill.com or (212) 904-4069.

TERMS OF USE

This is a copyrighted work and The McGraw-Hill Companies, Inc. (“McGraw-Hill”) and its licensors reserve all rights in and to the work. Use of this work is subject to these terms. Except as permitted under the Copyright Act of 1976 and the right to store and retrieve one copy of the work, you may not decompile, disassemble, reverse engineer, reproduce, modify, create derivative works based upon, transmit, distribute, disseminate, sell, publish or sublicense the work or any part of it without McGraw-Hill’s prior consent. You may use the work for your own noncommercial and personal use; any other use of the work is strictly prohibited. Your right to use the work may be terminated if you fail to comply with these terms.

THE WORK IS PROVIDED “AS IS.” McGRAW-HILL AND ITS LICENSORS MAKE NO GUARANTEES OR WARRANTIES AS TO THE ACCURACY, ADEQUACY OR COMPLETENESS OF OR RESULTS TO BE OBTAINED FROM USING THE WORK, INCLUDING ANY INFORMATION THAT CAN BE ACCESSED THROUGH THE WORK VIA HYPERLINK OR OTHERWISE, AND EXPRESSLY DISCLAIM ANY WARRANTY, EXPRESS OR IMPLIED, INCLUDING BUT NOT LIMITED TO IMPLIED WARRANTIES OF MERCHANTABILITY OR FITNESS FOR A PARTICULAR PURPOSE. McGraw-Hill and its licensors do not warrant or guarantee that the functions contained in the work will meet your requirements or that its operation will be uninterrupted or error free. Neither McGraw-Hill nor its licensors shall be liable to you or anyone else for any inaccuracy, error or omission, regardless of cause, in the work or for any damages resulting therefrom. McGraw-Hill has no responsibility for the content of any information accessed through the work. Under no circumstances shall McGraw-Hill and/or its licensors be liable for any indirect, incidental, special, punitive, consequential or similar damages that result from the use of or inability to use the work, even if any of them has been advised of the possibility of such damages. This limitation of liability shall apply to any claim or cause whatsoever whether such claim or cause arises in contract, tort or otherwise.

DOI: 10.1036/0071458212

*I would like to dedicate this book
to my wife Penelope and my
daughter Hilary, whose
understanding, support, and
encouragement made the
completion of this book possible.*

This page intentionally left blank

Contents

Preface	xi
Chapter 1. Introduction	1
1.1 What Is Nanotechnology?	1
1.2 Why Is This Length Scale So Important?	2
1.3 What Does <i>Nano</i> Really Mean?	2
1.4 Uniqueness of Nanostructured Materials	3
1.5 Polymer Nanomaterials	4
1.6 Scope of the Book	5
References	7
Chapter 2. An Overview of Nanoparticles	9
2.1 Current Polymer Nanocomposite Technology	9
2.2 Different Types of Nanoparticles	9
2.2.1 Montmorillonite nanoclays	10
2.2.2 Carbon nanofibers (CNFs)—vapor-grown carbon fibers (VGCFs)	19
2.2.3 Polyhedral oligomeric silsesquioxane (POSS)	26
2.2.4 Carbon nanotubes	29
2.2.5 Nanosilica	38
2.2.6 Nanoaluminum oxide	44
2.2.7 Nanotitanium oxide	46
2.2.8 Others	47
2.3 Summary	48
References	48
Chapter 3. Selecting Resin Matrix and Nanoparticles for Applications	51
3.1 Characteristics of Polymer Nanostructured Materials	51
3.2 Polymer Matrices	52
3.2.1 Thermoplastic-based nanocomposites	52
3.2.2 Thermoset-based nanocomposites	53
3.2.3 Elastomer-based nanocomposites	55
3.3 Summary	56
References	56

Chapter 4. Processing of Nanomaterials	61
4.1 Synthesis Methods	61
4.2 Solution Intercalation	64
4.2.1 Solution intercalation from polymers in solution	64
4.2.2 Solution intercalation from prepolymers in solution	65
4.3 Melt Intercalation	66
4.3.1 Thermoplastic nanocomposites	66
4.3.2 Elastomer nanocomposites	67
4.4 Roll Milling	67
4.5 Emulsion Polymerization	68
4.6 In-Situ Polymerization	69
4.6.1 Thermoplastic nanocomposites	70
4.6.2 Thermoset nanocomposites	71
4.6.3 Rubber modified epoxy nanocomposites	71
4.7 High-Shear Mixing	72
4.8 Summary	74
References	74
Chapter 5. Characterization of Polymer Nanomaterials	79
5.1 Characterization Methods	79
5.2 X-Ray Diffraction	80
5.3 Transmission Electron Microscopy and Spectroscopy	81
5.3.1 Transmission electron microscopy (TEM)	81
5.3.2 Energy-dispersive x-ray spectroscopy (EDS)	86
5.4 Small-Angle X-Ray Scattering (SAXS)	86
5.5 The Cone Calorimeter (CC)	88
5.6 The Mass Loss Calorimeter (MLC)	91
5.7 Summary, Future Needs, and Assessments	92
References	93
Chapter 6. Properties of Polymer Nanostructured Materials	95
6.1 Materials Properties	95
6.2 Thermoplastic Nanocomposites	95
6.2.1 Nylon 6 nanocomposites	95
6.3 Thermoset Nanocomposites	103
6.3.1 Epoxy nanocomposites	104
6.4 Elastomer Nanocomposites	118
6.4.1 TPO nanocomposites	118
6.5 Summary	122
References	122
Chapter 7. Polymer Nanostructured Materials for High-Temperature Applications	125
7.1 Thermoplastic Nanocomposites	125

7.1.1	Nonhalogenated, flame-retardant polymers for cabling jackets	126
7.1.2	Waterborne fire-retardant nanocomposite coating	132
7.1.3	Flame-retardant polymer nanocomposites for rapid manufacturing	138
7.2	Thermoset Nanocomposites	159
7.2.1	Nanocomposites for rocket ablative materials (NRAMs)	159
7.2.2	Flammability properties of polymer nanostructured materials	176
7.2.3	Nanomodified carbon/carbon composites (NCCCs)	182
7.2.4	Nanocomposites for carbon-fiber reinforced polymer matrix composites (NCPMCs)	198
7.3	Thermoplastic Elastomer Nanocomposites	214
7.3.1	Elastomer nanocomposites for propulsion systems	215
7.3.2	Thermoplastic elastomer nanocomposites for propulsion systems	217
7.3.3	Flame-retardant thermoplastic polyurethane nanocomposites	220
7.4	Summary	228
	References	228
 Chapter 8. Current Status, Trends, Future Directions, and Opportunities		 235
8.1	Nanotechnology Research Funding	235
8.1.1	Government R&D investments	235
8.2	Nanotechnology Research Output	237
8.2.1	Publication output	237
8.2.2	Patent output	238
8.2.3	Research areas of focus	238
8.2.4	Private sector activity	239
8.3	Nanotechnology Commercialization Prospects	239
8.4	Economics of Nanoparticles	242
8.5	Current Nanotechnology Commercial Applications	243
8.5.1	Hybrid compounds for cosmetics	245
8.5.2	Hybrid materials for protective and decorative coatings	246
8.5.3	Hybrid materials for dental applications	247
8.5.4	Hybrid materials (polymer-clay nanocomposites - PCNs) with structural properties	248
8.5.5	Hybrid materials (PCNs) with gas barrier properties	249
8.5.6	Hybrid materials (PCNs) with flame-retardant properties	251
8.5.7	Hybrid materials (PCNs) with other properties	252
8.6	Future Directions of the National Nanotechnology Initiative	253
8.6.1	Budget summary	255
8.7	Identified Areas of Opportunity	257
8.7.1	Near-term (1 to 5 years)	257
8.7.2	Mid-term (5 to 10 years)	257
8.7.3	Long-term (20+ years)	258
8.8	Nanotech's Safety Risks	258
8.9	Summary	260
	References	260
 Index		 263

This page intentionally left blank

Preface

Nanotechnology is the study and control of matter at dimensions of roughly 1 to 100 nanometers (nm), where unique phenomena enable novel applications. Nanotechnology is also the design, fabrication, and application of nanostructures or nanomaterials. The excitement surrounding nanoscale science and technology gives us unique opportunities to develop revolutionary materials. Nanoscale science and technology is a young field that encompasses nearly every discipline of science and engineering. Nanophase and nanostructured materials, a new branch of materials research, are attracting a great deal of attention because of their potential applications in areas such as electronics, optics, catalysis, ceramics, magnetic data storage, and polymer nanocomposites.

The research on nanotechnology is evolving and expanding very rapidly, which makes it impossible for a volume of this size to cover all aspects of the field. This book focuses primarily on polymer nanostructured materials. I have outlined a logical progression of what polymer nanomaterials are, how they are made, what their assets and deficiencies are, what they are used for, and to what extent they are commercially exploited. Each specialized chapter is part of a sequence of developing polymer nanostructured materials. One of the primary goals of this text is to aid the reader who wishes to engage in the research and development of polymer nanostructured materials. To this end, Chap. 2 consists of an overview of the commonly used nanoparticles and their origins, manufacture, properties, and potential applications. The remaining chapters cover the selection of resin matrix and nanoparticles, processing, characterizing, properties, performance, and applications. Finally, I offer a brief overview of nanotechnology—current status, trends, applications, future directions, and opportunities. Throughout the book, the theme is developed that polymer nanostructured materials are a whole family of materials whose properties are capable of being tailored to meet specific applications. This volume can serve as a general introduction to researchers just entering the field

and as a source for scholars from other subfields. This book is a solid textbook for upper-level undergraduate, graduate, and professional short courses.

During my preparation and writing, a great deal of help in terms of information and images was provided by a number of people and organizations. I would like to thank them, in no particular order: Dr. Richard A. Vaia of Air Force Research Laboratory/MLBP; Max L. Lake and Tom Hughes of Applied Sciences, Inc.; Thomas Pitstick of Carbon Nanotechnologies, Inc.; Alan Hedgepeth of Degussa AG; Dr. Stephan Sprenger of Hanse Chemie AG; Dr. Joseph D. Lichtenhan of Hybrid Plastics; and Dr. Doug Hunter of Southern Clay Products.

Many thanks are due to my friend Dr. Louis A. Pilato of Pilato Consulting/KAI, Inc., for his help in proofreading the manuscript and collaborating with me on numerous research and tutorial projects that have been used as examples throughout this book. I would also like to thank Dr. Charles Y-C Lee of Air Force Office of Scientific Research/NL; Dr. Shawn Phillips; Dr. Rusty Blanski; and Dr. Steven A. Svejda of Air Force Research Laboratory/Propulsion Directorate, Edwards AFB, California, for supporting our numerous research programs. I'm thankful to all my colleagues and students who have contributed to our research programs. Many thanks go to McGraw-Hill and to Jennifer Welsch and her staff at BookMasters Inc. for their tolerance and assistance.

JOSEPH H. KOO
Department of Mechanical Engineering
The University of Texas at Austin
Austin, Texas, USA
e-mail: jkoo@mail.utexas.edu
<http://www.me.utexas.edu/~koo/>

Polymer Nanocomposites

This page intentionally left blank

Introduction**1.1 What Is Nanotechnology?**

The National Nanotechnology Initiative Strategic Plan, developed by the Nanoscale Science, Engineering, and Technology Subcommittee, defines nanotechnology in the following way:

Nanotechnology is the understanding and control of matter at dimensions of roughly 1 to 100 nanometers, where unique phenomena enable novel applications. A nanometer is one-billionth of a meter; a sheet of paper is about 100,000 nanometers thick. Encompassing nanoscale science, engineering, and technology, nanotechnology involves imaging, measuring, modeling, and manipulating matter at this length scale.

At this level, the physical, chemical, and biological properties of materials differ in fundamental and valuable ways from the properties of individual atoms and molecules or bulk matter. Nanotechnology R&D is directed towards understanding and creating improved materials, devices, and systems that exploit these new properties.¹

Since its inception in fiscal year (FY) 2001, the National Nanotechnology Initiative (NNI, website: <http://www.nano.gov>) has sought to accelerate the responsible development and application of nanotechnology to create jobs and economic growth, to enhance national security, and to improve the quality of life for all citizens. Funding under the NNI has more than doubled since FY 2001, to a request in FY 2005 of nearly \$1 billion government-wide. R&D supported by the NNI is expected to result in cleaner and less wasteful methods of manufacture, stronger and lighter building materials, smaller yet faster computers, and more powerful ways to detect and treat disease.

1.2 Why Is This Length Scale So Important?

Wavelike (quantum mechanical) properties of electrons inside matter and atomic interactions are influenced by materials variations on the nanometer (nm) scale. By creating nanometer-scale structures, it is possible to control the fundamental properties of materials, such as their melting temperature, magnetic properties, charge capacity, and even their color, without changing the materials' chemical compositions. Making use of this potential will lead to new, high-performance products and technologies that were not possible before. Nanoscale structures such as nanoparticles and nanolayers have very high surface-to-volume and aspect ratios, making them ideal for use in polymeric materials.

1.3 What Does Nano Really Mean?

A nanometer is one billionth of a meter (10^{-9} m), about four times the diameter of an atom. Figure 1.1 depicts the diameters of a few interesting materials: a human red blood cell is 10,000 nm; a cell of the bacterium *E. coli* is 1000 nm; a viral cell is 100 nm; a polymer coil is 40 nm; a Q-rod is 30 nm with a 10:1 aspect ratio; and a quantum dot (QD) is 7 nm in diameter.

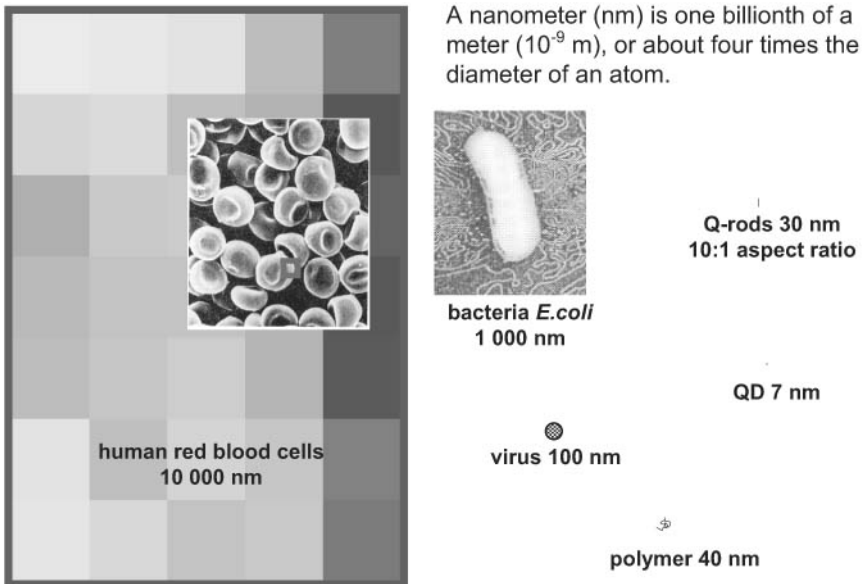
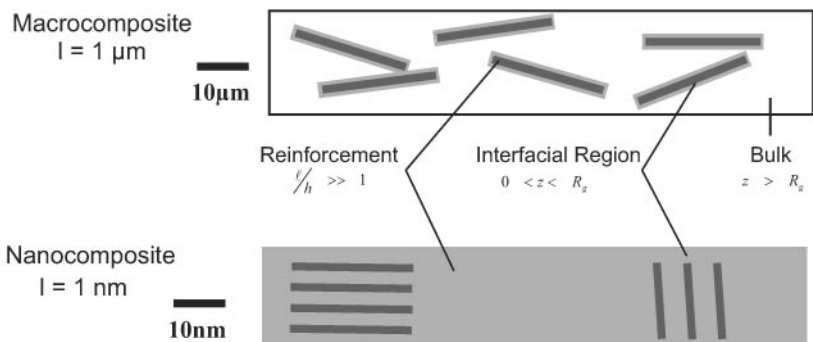


Figure 1.1 What nano really means. (Courtesy of R. Vaia.)

1.4 Uniqueness of Nanostructured Materials

For decades we have been dealing with macrocomposites such as filled polymers², where the length scale of the polymer fillers is in micrometers, as shown in Fig. 1.2. The reinforcement length scale is in micrometers, and the interface of fillers is close to the bulk polymer matrix. In the case of nanocomposites, where the length scale of the reinforcement (nanoparticles) is in nanometer scale (Fig. 1.2), they have ultralarge interfacial area per volume, and the distances between the polymer and filler components are extremely short. Polymer coils are 40 nm in diameter, and the nanoparticles are on the same order of magnitude as the polymer; as a result, molecular interaction between the polymer and the nanoparticles will give polymer nanocomposites unusual material properties that conventional polymers do not possess.

The excitement surrounding nanoscale science and technology gives us unique opportunities to develop revolutionary materials. Nanoscale science and technology is a young field that encompasses nearly every discipline of science and engineering. Nanophase and nanostructured materials, a new branch of materials research, is attracting a great deal of attention because of its potential applications in areas such as electronics, optics, catalysis, ceramics, magnetic data storage, and polymer nanocomposites. The unique properties and improved performance of nanomaterials are determined by their sizes, surface structures, and interparticle interactions. The role played by particle size is comparable to the role of the particle's chemical composition, adding



Characteristic

Ultralarge interfacial area per volume
 High fraction interfacial (interphase) material
 Short distances between components

Nanopolymer Nanoinorganic

Hierarchical
 Morphology
 Control
 Nano, Meso, Micro

Figure 1.2 Uniqueness of nanostructured materials. (Courtesy of R. Vaia.)

another parameter for designing and controlling particle behavior. To fully understand the impacts of nanomaterials in nanoscale science and technology, one needs to know why nanomaterials are so special!

1.5 Polymer Nanomaterials

Nanomaterials can be classified into *nanostructured materials* and *nanophase/nanoparticle materials*. The former usually refer to condensed bulk materials that are made of grains (agglomerates), with grain sizes in the nanometer size range, whereas the latter are usually the dispersive nanoparticles. The nanometer size covers a wide range, from 1 nm to as large as 100 to 200 nm. To distinguish nanomaterials from bulk, it is crucial to demonstrate the unique properties of nanomaterials and their prospective impacts in science and technology.

The introduction of inorganic nanoparticles as additives into polymer systems has resulted in polymer nanocomposites (PNs) exhibiting multifunctional, high-performance polymer characteristics beyond what traditional filled polymeric materials possess. The development of these new materials will enable the circumvention of classic material performance trade-offs by accessing new properties and exploiting unique synergies between materials that only occur when the length scale of morphology and the fundamental physics associated with a property coincide, i.e., on the nanoscale level. Multifunctional features attributable to polymer nanocomposites consist of improved thermal resistance and/or flame resistance, moisture resistance, decreased permeability, charge dissipation, and chemical resistance. Through control/alteration of the additives at the nanoscale level, one is able to maximize property enhancement of selected polymer systems to meet or exceed the requirements of current military, aerospace, and commercial applications. The technical approach involves the incorporation of nanoparticles into selected polymer matrix systems whereby nanoparticles may be surface-treated to provide hydrophobic characteristics and enhanced inclusion into the hydrophobic polymer matrix.

The reinforcement of polymers using fillers, whether inorganic or organic, is common in modern plastics. Polymer nanocomposites, or the more inclusive term, polymer nanostructured materials (PNMs), represent a radical alternative to these traditional filled polymers or polymer compositions. In contrast to traditional polymer systems where reinforcement is on the order of microns, polymer nanocomposites are exemplified by discrete constituents on the order of a few nanometers.

Uniform dispersion of these nano-sized fillers (nanoparticles) produces ultralarge interfacial area per volume between the nanoparticle and the host polymer. The immense internal interfacial area and the

nanoscopic dimensions between nanoparticles fundamentally differentiate polymer nanostructured composites from traditional filled plastics and composites. These materials' characteristics simply imply that the overall performance of PNMs cannot be understood by simple scaling rules that apply to traditional polymer composites. Thus, new combinations of properties derived from the nanoscale structure of PNMs provide opportunities to circumvent traditional performance associated with conventional reinforced plastics, epitomizing the promise of PNMs.

Many examples can be found in the literature demonstrating substantial improvements in physical and mechanical properties. When using the term "nanocomposite" to describe properties comparisons, it is intended to relate to traditional unfilled and filled polymers and not fiber-reinforced polymer matrix composites. Polymer nanocomposites may provide matrix resins with "multifunctionality", but they should not be considered in the near and intermediate term as a potential one-for-one replacement for current state-of-the-art carbon fiber-reinforced polymer matrix composites.

The value of PNM technology is not based solely on mechanical enhancements of the neat resin. Rather, its value comes from providing value-added properties not present in the neat resin, without sacrificing the inherent processibility and mechanical properties of the neat resin. Traditionally, the preparation of a blend or composite with multifunctionality requires a trade-off between desired performance, mechanical properties, cost, and processibility.

Development of materials with multifunctionality, whether micro-scale or nanoscale, must simultaneously balance four interdependent areas: constituent selection, processing, fabrication, and performance. Two main PNM processing methodologies have been developed: in-situ routes and exfoliation. Currently, exfoliation of layered silicates, carbon nanofiber/nanotubes, and polyhedral oligomeric silsesquioxanes (POSS[®]) in commodity and high-performance resins are the most investigated PNMs by government, academic, and industrial institutions all over the world.

1.6 Scope of the Book

Development of nanotechnology involves several key steps. First, synthesis of size- and even shape-controlled nanoparticles is the key for developing polymer nanostructured materials. Second is selection of the proper processing and fabrication techniques to achieve nanodispersions (uniform dispersibility) of the nanoparticles in a selective polymer matrix. Third, characterization of nanoparticles is indispensable to understanding the behavior and properties of nanoparticles, striving to

incorporate them into polymer systems in designing new nanomaterial systems with improved performance. Finally, the ultimate goal is to determine the performance of these polymer nanostructured materials using established test methods for specific applications.

This book aims to introduce the uniqueness of polymer nanostructured materials, addressing the importance of processing and characterization of the nanomaterials to achieve multifunctional polymeric materials. The book is divided into eight chapters: an introduction (Chap. 1); an overview of different types of nanoparticles (Chap. 2); selecting the proper resin matrix and nanoparticles for specific applications (Chap. 3); processing of the nanomaterials (Chap. 4); characterization of the structures of these polymer nanomaterials (Chap. 5); obtaining properties of the polymer nanocomposites/polymer nanostructured materials (Chap. 6); obtaining properties and evaluating the performance of these polymer nanostructured materials for high-temperature applications (Chap. 7); and presenting the current status, trends, applications, future directions, and opportunities (Chap. 8).

This book summarizes the author's research activities in the areas of: (a) developing *processes* to disperse nanoparticles uniformly in the different types of polymers; (b) using wide angle x-ray diffraction (WAXD), transmission electron microscopy (TEM), and scanning electron microscopy (SEM) techniques to characterize polymer nanocomposite *structures*; (c) studying the *structure-property* relationship of these types of new materials; and (d) evaluating the *performance* of these materials for different applications using established laboratory devices.

In these studies, four different processing methods were used to disperse nanoparticles in a variety of polymers. These methods were (a) high shear mixing for liquid resins, (b) three roll milling for liquid resins, (c) Brabender-type mixing for high viscosity resins, and (d) twin screw extrusion for solid polymers. The degree of nanodispersion was characterized by WAXD, TEM, and SEM analyses. These imaging techniques allowed the screening of formulations and distinguishing of compositions that exhibited either favorable or unfavorable nanodispersed nanoparticle/polymer blends. Furthermore, these analytical techniques facilitated and provided guidelines in the scale-up of favorable compositions.

Different types of polymers, including thermosets, thermoplastics, and elastomers, are presented as examples in this volume. Several types of nanoparticles including (a) montmorillonite (MMT) organoclays, (b) nanosilica, (c) carbon nanofibers (CNF), (d) polyhedral oligomeric silsesquioxanes (POSS), and (e) carbon nanotubes: small-diameter carbon nanotubes (SDNT), multiwall carbon nanotubes (MWNT), and

single-wall carbon nanotubes (SWNT) were used to disperse into the above families of polymers. Selected laboratory devices, such as a cone calorimeter, a mass loss calorimeter, a simulated solid rocket motor (SSRM), and a subscale solid rocket motor, were used to evaluate the materials' performance for fire and rocket propulsion applications. Physical, mechanical, and thermal properties of these polymer nanostructured materials were obtained using ASTM methods to evaluate performance of materials.

The field of nanotechnology is rapidly growing, with novel ideas appearing at a swift pace. Some of the technologies outlined in this text have already made their appearance in commercial products, with more to follow. Still in its infancy, nanometer-scale science and technology is an area that is only bounded by the interest, creativity, and imagination of a new generation of multidisciplinary scientists and engineers eager to take it to its limit.

References

1. *The National Nanotechnology Initiative Strategic Plan*, Nanoscale Science, Engineering and Technology Subcommittee, Committee on Technology, National Science and Technology Council, Arlington, VA, December 2004.
2. J.-F. Gerard (ed.), *Fillers and Filled Polymers*, Wiley-VCH Verlag GmbH, Weinheim, Germany, 2001.
3. G. Cao. *Nanostructures and Nanomaterials: Synthesis, Properties & Applications*, Imperial College Press, London, England, 2004.
4. H.-J. Fecht and M. Werner (eds.), *The Nano-Micro Interface: Bridging the Micro and Nano Worlds*, Wiley-VCH Verlag GmbH, Weinheim, Germany, 2004.
5. B. Karn, T. Mascinangioli, W. Zhang, V. Colvin, and P. Alivisatos (eds.), *Nanotechnology and the Environment—Applications and Implications*, ACS Symposium Series 890, American Chemical Society, Washington DC, 2005.
6. R. Krishnamoorti and R. A. Vaia (eds.), *Polymer Nanocomposites: Synthesis, Characterization, and Modeling*, ACS Symposium Series 804, ACS, Washington, DC, 2001.
7. R. N. Kostoff, J. A. Stump, D. Johnson, J. S. Murday, C. G. Y. Lau, and W. M. Tolles, "The structure and infrastructure of the global nanotechnology literature," *J Nanopart Res*, **8** (2006).
8. R. N. Kostoff, J. S. Murday, C. G. Y. Lau, W. M. Tolles, "The seminal literature of nanotechnology research," *J Nanopart Res*, **8** (2006).
9. A. W. Miziolek, S. P. Karna, J. M. Mauro, and R. A. Vaia (eds.), *Defense Applications of Nanomaterials*, ACS Symposium Series 891, American Chemical Society, Washington DC, 2005.
10. T. J. Pinnavaia and G. W. Beall (eds.), *Polymer-Clay Nanocomposites*, John Wiley & Sons, New York, 2000.
11. M. J. Schulz, A. D. Kelkar, and M. J. Sundaresan (eds.), *Nanoengineering of Structural, Functional, and Smart Materials*, CRC Press, Boca Raton, FL, 2006.
12. R. A. Vaia, "Polymer Nanocomposites Open a New Dimension for Plastics and Composites," *The AMPTIAC Newsletter*, **6**:17–24, 2002.
13. M. Di Ventra, S. Evoy, and J. R. Heflin, Jr., *Introduction to Nanoscale Science and Technology*, Kluwer Academic Publishers, Norwell, MA, 2004.
14. A. L. Wang (ed.), *Characterization of Nanophase Materials*, Wiley-VCH Verlag GmbH, Weinheim, Germany, 2000.

8 Chapter One

15. Z. L. Wang, Y. Liu, and Z. Zhang (eds.), *Handbook of Nanophase and Nanostructured Materials, Vol. 4: Materials Systems and Applications (II)*, Kluwer Academic/Plenum Publishers, New York, 2003.
16. N. Yao and Z. L. Wang (eds.), *Handbook of Microscopy for Nanotechnology*, Kluwer Academic Publishers, Boston, MA, 2005.

An Overview of Nanoparticles

2.1 Current Polymer Nanocomposite Technology

Polymer nanocomposites (PNs) consist of a polymeric material (e.g., thermoplastics, thermosets, or elastomers) and a reinforcing nanoscale material (nanoparticle). The nanoparticle has at least one dimension in nanometer scale. Polymer nanocomposites show major improvements in mechanical properties, gas barrier properties, thermal stability, fire retardancy, and other areas. There are many factors that affect the polymer nanocomposite properties:

- Synthesis methods such as melt compounding, solvent blending, in-situ polymerization, and emulsion polymerization
- Polymer nanocomposite morphology
- Types of nanoparticles and their surface treatments
- Polymer matrix such as crystallinity, molecular weight, polymer chemistry, and whether thermoplastic or thermosetting

Understanding property improvement related to PN properties is a very complex matter. Table 2.1 shows several benefits and disadvantages when nanoparticles are incorporated into the polymer matrix.

2.2 Different Types of Nanoparticles

There are different types of commercially available nanoparticles that can be incorporated into the polymer matrix to form polymer nanocomposites. Depending on the application, the researcher must determine the type of nanoparticle needed to provide the desired effect. A brief

TABLE 2.1 Characteristics of Nanoparticles to Polymers

Improved properties	Disadvantages
<ul style="list-style-type: none"> ■ Mechanical properties (tensile strength, stiffness, toughness) ■ Gas barrier ■ Synergistic flame retardant additive ■ Dimensional stability ■ Thermal expansion 	<ul style="list-style-type: none"> ■ Viscosity increase (limits processability) ■ Dispersion difficulties ■ Optical issues ■ Sedimentation ■ Black color when different carbon containing nanoparticles are used
<ul style="list-style-type: none"> ■ Thermal conductivity ■ Ablation resistance ■ Chemical resistance ■ Reinforcement 	

discussion will include the most commonly used nanoparticles in the literature:

- Montmorillonite organoclays (MMT)
- Carbon nanofibers (CNFs)
- Polyhedral oligomeric silsesquioxane (POSS®)
- Carbon nanotubes [multiwall (MWNTs), small-diameter (SDNTs), and single-wall (SWNTs)]
- Nanosilica (N-silica)
- Nanoaluminum oxide (Al_2O_3)
- Nanotitanium oxide (TiO_2)
- Others

2.2.1 Montmorillonite nanoclays

Origin. Nanoclay is the most widely investigated nanoparticle in a variety of different polymer matrices for a spectrum of applications.^{1,2} The origin of bentonite (natural clay) is most commonly formed by the in-situ alteration of volcanic ash, as shown in Fig. 2.1. Another, less common, origin is the hydrothermal alteration of volcanic rocks. Bentonite contains montmorillonite but also can contain glass, mixed-layer clays, illite, kaolinite, quartz, zeolite, and carbonates. Clay soil has particle size of less than 2 μm . The expanding clays are phyllosilicates, smectite, and montmorillonite, and the nonexpanding clays are talc, kaolin, and mica. The starting material of Southern Clay Products' (SCP, located in Gonzales, Texas) commercial clay products is from volcanic eruptions in the Pacific Ocean and the western United States during the Cretaceous period (85 to 125 million years ago).



Figure 2.1 Bentonite comes from the deposition and alteration of volcanic ash from inland sea beds from 85 million years ago.

Molten rock within the planet, magma, under extreme pressure, forced its way through the earth's crust and exploded into the atmosphere in a volcanic eruption. The rain of airborne ash carried by the prevailing winds from the eruption clouds subsequently fell to earth, forming deposits characterized by high-volume bedding of well- to moderately-sorted ash. The parent ash was deposited under marine conditions, and there was some minor accumulation in alkaline lakes, as illustrated in Fig. 2.2.³ The passing of geologic time resulted in the alteration of ash beds in the western United States' inland sea areas to form deposits into what is now the clay producing areas of Montana, Wyoming, and the Dakotas. Opinions differ concerning the process and time of alteration of the ash to clay. It is estimated that the resulting deposits in Wyoming alone contain over 1 billion tons of available clay.³

Structure. Silica is the dominant constituent of the montmorillonite clays, with alumina being essential. The chemical structure of montmorillonite clays is illustrated in Fig. 2.3, showing its sheet structure consisting of layers containing the tetrahedral silicate layer and the octahedral alumina layer. The tetrahedral silicate layer consists of SiO_4 groups linked together to form a hexagonal network of the repeating units of composition Si_4O_{10} . The alumina layer consists of two sheets of closely packed oxygens or hydroxyls, between which octahedrally

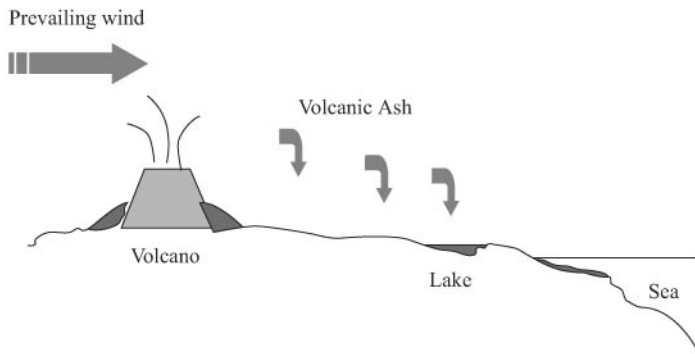


Figure 2.2 Formation of natural clays by the in-situ alteration of volcanic ash.

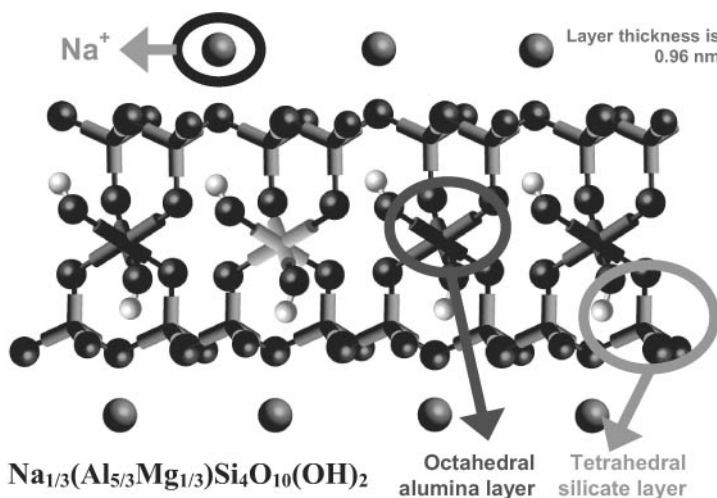


Figure 2.3 Chemical structure of montmorillonite nanoclays.

coordinated aluminum atoms are imbedded in such a position that they are equidistant from six oxygens or hydroxyls. The two tetrahedral layers sandwich the octahedral layer, sharing their apex oxygens with the latter. These three layers form one clay sheet that has a thickness of 0.96 nm. The chemical formula of the montmorillonite clay is $\text{Na}_{1/3}(\text{Al}_{5/3}\text{Mg}_{1/3})\text{Si}_4\text{O}_{10}(\text{OH})_2$. In its natural state Na^+ cation resides on the MMT clay surface.

Importance of organic treatment. Because layered silicates are hydrophilic materials, they must be made organophilic (hydrophobic) to become compatible with most host polymers that are hydrophobic polymers. Without organic treatment, layer silicates will only disperse and phase separate in the presence of very polar polymers. Organic

treatment is typically accomplished via ion exchange between inorganic alkali cations on the clay surface with the desired organic cation. The organic treatment, at the interface between inorganic silicate and organic polymer, is a vital part of the polymer nanocomposite, and therefore, it must be tailored to synthetic conditions. Synthetic methods for polymer nanocomposite preparation include solvent mixing, in-situ polymerization, and melt compounding. One of the most “industry-friendly” methods of making polymer nanocomposites is the use of melt compounding. The polymer and organically treated clay are heated to the melting point of the polymer, and the two are mixed together using compounding equipment such as an extruder or a mixing head. There are several types of clay surface treatments, which are listed below:

- Quaternary ammonium salts (current) based on textile antistatic agents
- Alkyl imidazoles which provides improved thermal stability
- Coupling and tethering agents, reactive diluents and can be functional amino compounds
- Others consist of cation types containing phosphorous ionic compounds

Dispersing nanoclay. Achieving exfoliation of organomontmorillonite in various polymer continuous phases is a function of the surface treatment of the MMT clays and the mixing efficiency of the dispersing apparatus or equipment. For hydrophilic nanoclay such as SCP’s Cloisite® Na⁺, it is recommended that it be dissolved in either water using high-shear mixing or to add Cloisite Na⁺ directly into a water soluble, aqueous polymer solution. Three types of mixing equipment are recommended to disperse hydrophobic nanoclays such as Southern Clay Products’ Cloisite 10A, 20A, 25A, 30B, and 93A into different resin systems. The recommended equipment is as follows: high-shear mixer or 3 roll mill for liquid resins, Brabender mixer for viscous resins, or twin-screw extruder for solid resins.

The preparation of polymer-clay nanocomposites is clearly illustrated in Fig. 2.4. Depending on the physical state of the polymer, one can incorporate the clay into the polymer by solution blending, melt blending, or in-situ polymerization processes to form polymer-clay nanocomposites. Polymer-clay nanocomposites can be classified morphologically into (a) unmixed, (b) intercalated, and (c) exfoliated (delaminated) states, as shown in Fig. 2.5. The most desirable morphological state for the polymer-clay nanocomposites is exfoliation, followed by intercalation. The processing challenge of nanoclay is to disperse the 8- μ m particles into > 1 million platelets using the proper processing technique and conditions, as shown in Fig. 2.6. The dispersion mechanism can

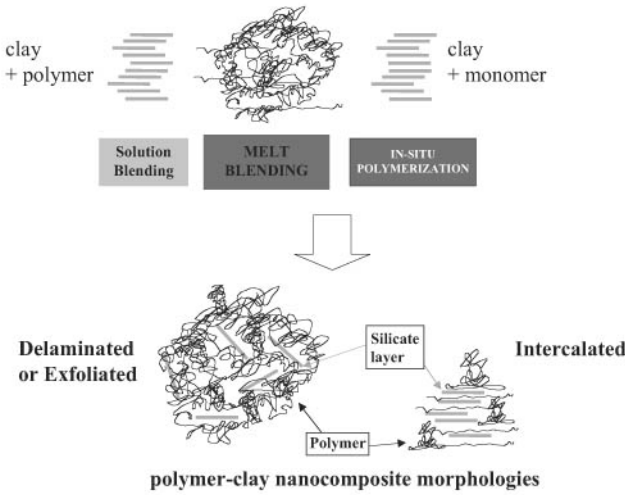


Figure 2.4 Schematic showing the preparation of polymer-clay nanocomposites. (Courtesy of J. Gilman.)

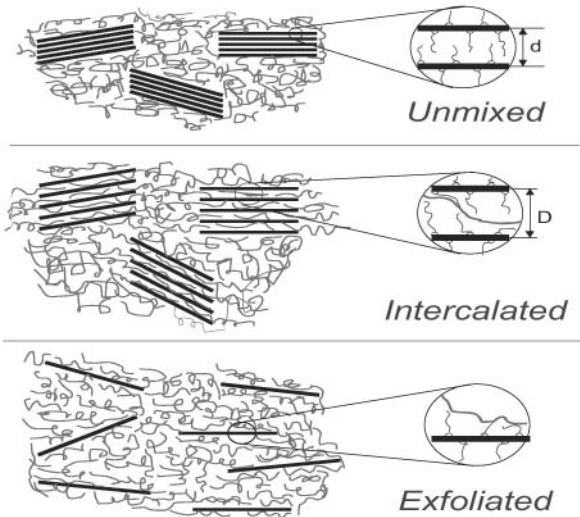


Figure 2.5 Schematic showing polymer-clay nanocomposite classifications.

be: (a) via a chemistry route, as with in-situ polymerization; (b) via a processing route, as in extrusion; or (c) by combining the chemistry and the processing routes (the optimal way), as is summarized in Fig. 2.7.

Figures 2.8 and 2.9 further illustrate the concept of particles shearing apart and platelets peeling apart in cartoon (Fig. 2.8) and in transmission electron micrographs (TEM) (Fig. 2.9). TEM is the most useful

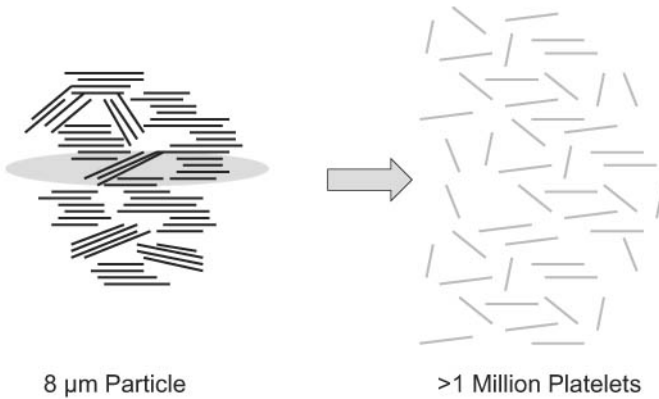


Figure 2.6 The processing challenge of nanoclay is turning 8- μm particles into > 1 million platelets. (Courtesy of SCP.)

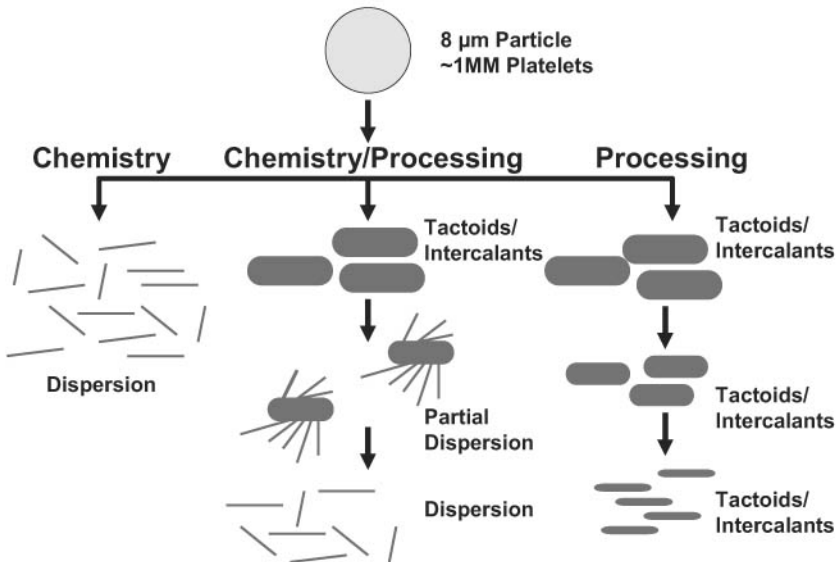


Figure 2.7 Different mechanisms for dispersing nanoclays. (Courtesy of SCP.)

tool to determine the degree of dispersion of the nanoparticles in the polymer matrix. This will be discussed in more detail in Chap. 5.

Organoclay suppliers. There are several worldwide suppliers for organoclays. In the United States, the two major suppliers are Southern Clay Products (SCP) and NanoCor. Southern Clay Products, located in Gonzales, Texas, produces Cloisite and Laponite, types of clay materials. Cloisite materials are based on natural occurring MMT while Laponites are chemically synthesized clays. Product information

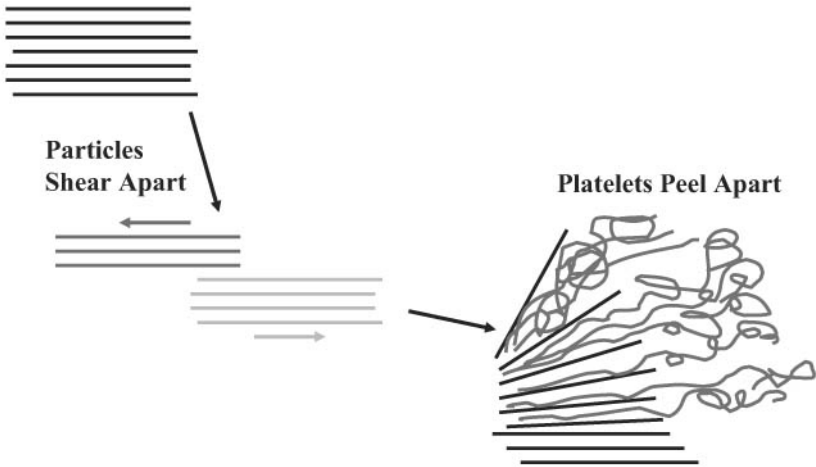
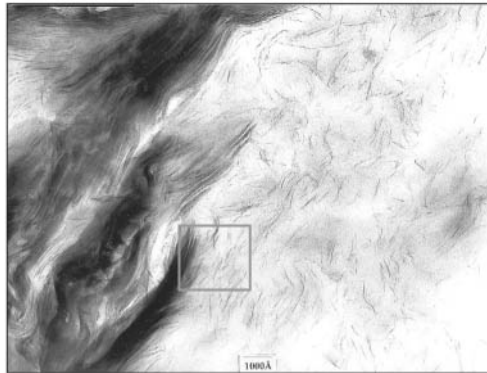


Figure 2.8 Cartoon showing particles shearing and platelets peeling apart. (Courtesy of SCP.)



Particles Shear Apart



Platelets Peel Apart

Figure 2.9 TEM micrographs showing particles shearing and platelets peeling apart. (Courtesy of SCP.)

can be obtained at the company's website: <http://www.nanoclay.com>. NanoCor, located in Chicago, Illinois, produces I.xxE (e.g. I.28E and I.30E) a type of clay product. Product information can be obtained at NanoCor's website: <http://www.nanocor.com>.

Other suppliers are Rheox, Source Clay Mineral, COOP (Japan), Kunimine (Japan), Sud Chemie (Germany), Laviosa Chimica Mineraria (Italy), and several Chinese companies.

Cloisite additives. Southern Clay Products (SCP) manufactures and markets Cloisite additives. These montmorillonite organoclays are

surface modified to allow complete dispersibility and miscibility with many different resin systems for which they were designed to improve. Cloisite MMT clays such as Cloisite Na⁺, 15A, 20A, 30B, 93A, 25A, and 10A are referenced in this section. Several of these MMT clays are mentioned also in Chap. 7.

Cloisite Na⁺ is a natural montmorillonite. This plastic additive improves various plastic physical properties, such as reinforcement, heat deflection temperature (HDT), coefficient of linear thermal expansion (CLTE), and barrier properties. Typical properties, chemical structure, dry particle size, and density data of Cloisite Na⁺, 15A, 20A, 30B, 93A, 25A, and 10A are shown in Tables 2.2, 2.3, 2.4, and 2.5, respectively.

Cloisite 15A and 20A are natural montmorillonite modified with a quaternary ammonium salt. Specific chemical pretreatment modifier (2M2HT: dimethyl, dehydrogenated tallow, quaternary ammonium salt) was used to generate Cloisite 20A and 15A.

Cloisite 30B is a natural montmorillonite modified with a quaternary ammonium salt. Specific chemical pretreatment modifier (MT2EtOH: methyl, tallow, bis-2-hydroxyethyl, quaternary ammonium) was used for the preparation of Cloisite 30B.

Cloisite 93A is a natural montmorillonite modified with a ternary ammonium salt. Specific chemical pretreatment modifier (M2HT: methyl, dehydrogenated tallow ammonium salt) was used to prepare Cloisite 93A.

Cloisite 25A is a natural montmorillonite modified with a quaternary ammonium salt. Specific chemical pretreatment modifier (2MHTL8: dimethyl, hydrogenated tallow, 2-ethylhexyl quaternary ammonium) led to Cloisite 25A.

TABLE 2.2 Properties of Several SCP Cloisite MMT Clays

MMT clay/ properties	Organic modifier [#]	Cation exchange capacity (meq/100g clay)	% Moisture	% Weight loss on ignition	X-ray results d ₀₀₁ (Å)
Cloisite Na ⁺	None	92.6	<2%	7%	11.7
Cloisite 15A	2M2HT (1)	125	<2%	43%	31.5
Cloisite 20A	2M2HT (1)	95	<2%	38%	24.2
Cloisite 30B	MT2EtOT (2)	90	<2%	30%	18.5
Cloisite 93A	M2HT (3)	90	<2%	40%	23.6
Cloisite 25A	2MHTL8 (4)	95	<2%	34%	18.6
Cloisite 10A	2MBHT (5)	125	<2%	39%	19.2

[#] See TABLE 2.3 for chemical data

TABLE 2.3 Cloisite MMT Clay Organic Modifier and Chemical Structures

MMT clay/organic modifier/chemical structure	Organic modifier	Chemical structure
Cloisite Na ⁺	None	None
Cloisite 15A	(1) 2M2HT: dimethyl, dehydrogenated tallow, quaternary ammonium	$\begin{array}{c} \text{CH}_3 \\ \\ \text{CH}_3 - \text{N}^+ - \text{HT} \\ \\ \text{HT} \end{array}$ <p>Where HT is Hydrogenated Tallow (~65% C18; ~30% C16; ~5% C14), Anion: Chloride</p>
Cloisite 20A	Same as Cloisite 15A	Same as Cloisite 15A
Cloisite 30B	(2) MT2EtOH: methyl, tallow, bis-2-hydroxyethyl, quaternary ammonium	$\begin{array}{c} \text{CH}_2\text{CH}_2\text{OH} \\ \\ \text{CH}_3 - \text{N}^+ - \text{T} \\ \\ \text{CH}_2\text{CH}_2\text{OH} \end{array}$ <p>Where T is Tallow (~65% C18; ~30% C16; ~5% C14), Anion: Chloride</p>
Cloisite 93A	(3) M2HT: methyl, dehydrogenated tallow ammonium	$\begin{array}{c} \text{H} \\ \\ \text{CH}_3 - \text{N}^+ - \text{HT} \\ \\ \text{H} \end{array}$ <p>Where HT is Hydrogenated Tallow (~65% C18; ~30% C16; ~5% C14), Anion: HSO₄</p>
Cloisite 25A	(4) 2MHTL8: dimethyl, hydrogenated tallow, 2-ethylhexyl quaternary ammonium	$\begin{array}{c} \text{CH}_3 \\ \\ \text{CH}_3 - \text{N}^+ - \text{CH}_2\text{CH}(\text{CH}_2\text{CH}_2\text{CH}_2\text{CH}_2\text{CH}_3) \\ \qquad \qquad \qquad \\ \text{HT} \qquad \qquad \qquad \text{CH}_3 \end{array}$ <p>Where HT is Hydrogenated Tallow (~65% C18; ~30% C16; ~5% C14), Anion: methyl sulfate</p>
Cloisite 10A	(5) 2MBHT: dimethyl, benzyl, hydrogenated tallow, quaternary ammonium	$\begin{array}{c} \text{CH}_3 \\ \\ \text{CH}_3 - \text{N}^+ - \text{CH}_2 - \text{C}_6\text{H}_5 \\ \\ \text{HT} \end{array}$ <p>Where HT is Hydrogenated Tallow (~65% C18; ~30% C16; ~5% C14), Anion: Chloride</p>

TABLE 2.4 Typical Dry Particle Sizes of Cloisite Clays (Microns, by Volume) and Color

MMT clay/ particle size	10% less than:	50% less than:	90% less than:	Color
Cloisite Na ⁺ , 15A, 20A, 30B, 93A, 25A, 10A	2 μ	6 μ	13 μ	Off-white

TABLE 2.5 Typical Dry Particle Sizes of Cloisite Clays (Microns, by Volume)

MMT clay/ properties	Loose bulk (lbs/ft ³)	Packed bulk (lbs/ft ³)	Specific gravity (g/cc)
Cloisite Na ⁺	12.45	20.95	2.86
Cloisite 15A	10.79	18.64	1.66
Cloisite 20A	7.35	13.55	1.77
Cloisite 30B	14.25	22.71	1.98
Cloisite 93A	10.56	18.03	1.88
Cloisite 25A	12.08	20.48	1.87
Cloisite 10A	10.21	16.52	1.90

Cloisite 10A is a natural montmorillonite modified with a quaternary ammonium salt. Specific chemical pretreatment modifier (2MBHT: dimethyl, benzyl, hydrogenated tallow, quaternary ammonium) was used to obtain Cloisite 10A.

2.2.2 Carbon nanofibers (CNFs)—vapor-grown carbon fibers (VGCFs)

Origin. Carbon nanofibers (CNFs) are a form of vapor-grown carbon fiber which is a discontinuous graphitic filament produced in the gas phase from the pyrolysis of hydrocarbons.⁴⁻⁸ With regard to properties of physical size, performance improvement, and product cost, CNFs complete a continuum bounded by carbon black, fullerenes, and single-wall to multiwall carbon nanotubes on one end and continuous carbon fiber on the other,⁶ as illustrated in Fig. 2.10. Carbon nanofibers are able to combine many of the advantages of these other forms of carbon for reinforcement in commodity and high performance engineering polymers. Carbon nanofibers have transport and mechanical properties that approach the theoretical values of single-crystal graphite, similar to the fullerenes, but they can be made in high volumes at low cost—ultimately lower than that of conventional carbon fibers. In equivalent production volumes, CNFs are projected to have a cost comparable to E-glass on a per-pound basis, yet they possess properties that far exceed those of glass and are equal to, or exceed, those of much more costly

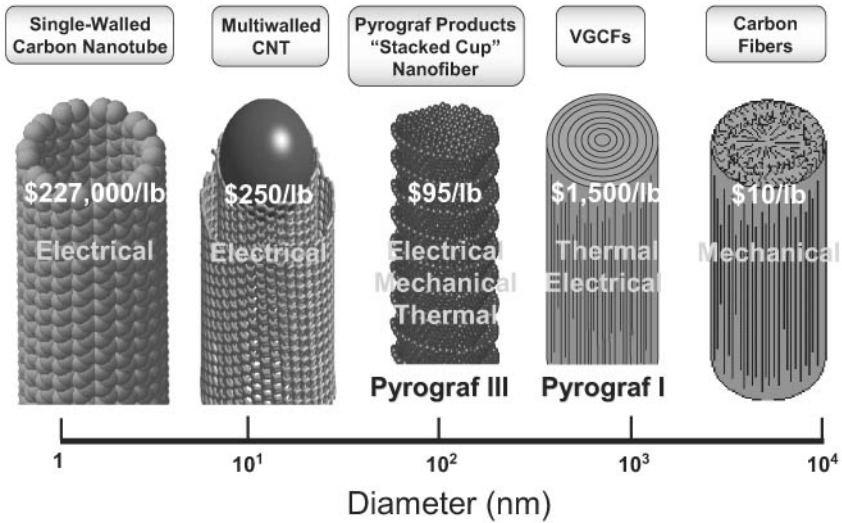


Figure 2.10 Sizes and costs from single-wall carbon nanotubes to conventional carbon fibers. (Courtesy of ASI.)

commercial carbon fiber. Maruyama and Alam published an excellent review of carbon nanotubes and nanofibers in composite materials.⁷

Manufacturing. Carbon nanofibers are manufactured by Applied Sciences, Inc./Pyrograf® Products (ASI) located in Cedarville, Ohio (website: <http://www.apsci.com>), by pyrolytic decomposition of methane in the presence of iron-based catalyst particles at temperatures above 900°C. Figure 2.11 shows how Pyrograf carbon nanofibers are produced at ASI. Typically, about 100 mg of powdered catalyst is placed in a ceramic boat, which is positioned in a quartz tube located in a horizontal tube furnace. The catalyst is reduced in a dilute hydrogen-helium stream at 600°C and quickly brought to the desired reaction temperature. Following this step, a mixture of hydrocarbon, hydrogen, and inert

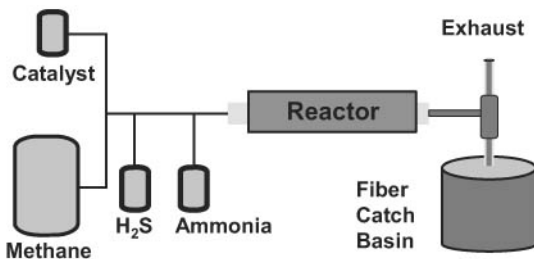


Figure 2.11 Schematic showing the production of raw Pyrograf carbon nanofibers. (Courtesy of ASI.)

gas is introduced into the system, and the reaction is allowed to proceed for about two hours. This method produces about 20 g of carbon fibers from the more active catalyst systems.

Properties. Pyrograf-I, an early product, possessed a diameter in micrometers and was the first generation of the Applied Sciences product, as shown in a SEM micrograph in Fig. 2.12. Pyrograf-III is a patented, very fine, highly graphitic CNF. Pyrograf-III is available in diameters ranging from 50 to 200 nm and lengths of 50 to 100 μm . Therefore, CNFs are much smaller than conventional continuous or milled carbon fibers (5 to 10 μm) but significantly larger than carbon nanotubes (1 to 10 nm). Compared to PAN and pitch-based carbon fiber, the morphology of CNFs is unique in that there are far fewer impurities in the filament, providing for graphitic and turbostratic graphite structures, and the graphene planes are more preferentially oriented around the axis of the fiber. Consequences of the circumferential orientation of high-purity graphene planes are a lack of cross-linking between the graphene layers and a relative lack of active sites on the fiber surface, making CNFs more resistant to oxidation and less reactive for bonding to matrix materials. Also, in contrast to carbon fiber derived from PAN or pitch precursors, CNFs are produced only in a discontinuous form, where the length of the fiber can be varied from about 100 μm to several centimeters, and the diameter is on the order of 100 nm. As a result, CNFs possess an aspect ratio of about 1,000.

Carbon nanofibers exhibit exceptional mechanical and transport properties, thus demonstrating their excellent potential as an attractive component for engineering materials. Table 2.6 lists the

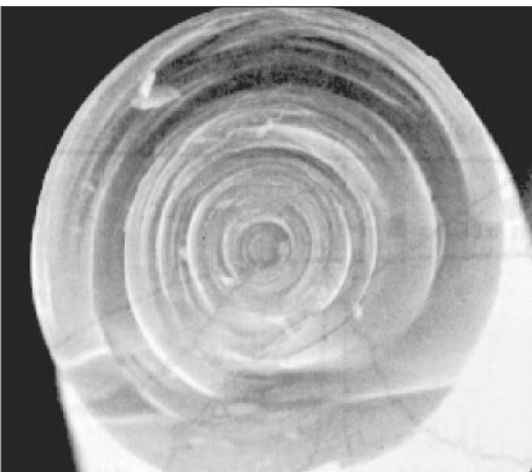


Figure 2.12 TEM micrographs of Pyrograf-I VGCF. (Courtesy of ASI.)

TABLE 2.6 Properties of CNFs

Property (units)	As grown	Heat treated
Tensile strength (GPa)	2.7	7.0
Tensile modulus (GPa)	400	600
Ultimate strain (%)	1.5	0.5
Density (g/cc)	1.8	2.1
Electrical resistivity ($\mu\Omega\text{-cm}$)	1000	55
Thermal conductivity (W/m-K)	20	1950

properties of vapor-grown carbon fibers, both as grown and after a graphitizing heat treatment to 3000°C. Note that, due to the difficulty of direct measurements of the nanofibers, the values in Table 2.6 are measured on vapor-grown fibers that have been thickened to several micrometers in diameter.⁶ Such fibers consist almost exclusively of chemical vapor deposition (CVD) carbon, which is less graphitic and more defective than the catalytically grown carbon core that constitutes the CNFs. Thus, the properties listed in the table represent an estimate for the properties of CNFs.

One of the goals for the broad utility of CNFs is to provide mechanical reinforcement comparable to that achieved with continuous tow carbon fiber at a price that approaches that of glass fiber reinforcement, and with low-cost composite fabrication methods such as injection molding. Theoretical models⁶ suggest that reinforcement by discontinuous fibers such as CNFs can closely approach that of continuous fibers, as long as the aspect ratio of the fibers is high and the alignment is good. Work is ongoing to improve the mechanical benefits of CNFs through fiber surface modification to provide physical or chemical bonding to the polymer matrix. Such modifications have resulted in strength and modulus improvements of four to six times the values of neat resin; however, these values are still a modest fraction of what may be anticipated from idealized fiber-matrix interphase and alignment of the fibers within the matrix. The more immediate opportunities for use in structural composites lie in the prospect of modifying the properties of the matrix material. For example, use of small volume loadings of CNFs in epoxy may allow for improvement of interlaminar shear strength of PAN or pitch-based composites. The CNF additives to fiberglass composites could provide benefits to a suite of properties, including thermal and electrical conductivity, coefficient of thermal expansion, and mechanical properties, as suggested by the data in Table 2.7.⁶ Figures 2.13 and 2.14 show the SEM micrograph of a CNF bundle and a close-up of Pyrograf-III CNF, respectively. Figure 2.15 shows the TEM micrograph of an individual CNF with the hollow core in two distinct regions, catalytic and deposited.⁶

TABLE 2.7 Thermoset Polyester/Pyrograf-III Composite Properties

Fiber content (wt%)	Tensile strength (MPa)	Tensile modulus (GPa)	Electrical resistivity (ohm-cm)
17% PR-19	51.5	4.55	3.2
17% PR-19, OX	47.4	4.55	7.1
5% PR-19 in 10% ¼" glass	44.1	11.52	5.0
5% PR-19, OX in 10% ¼" glass	33.8	8.92	7.0

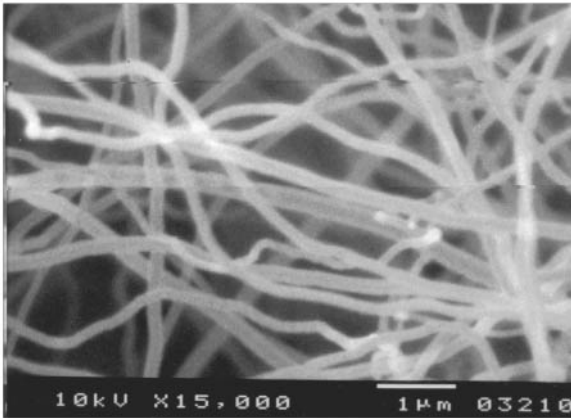


Figure 2.13 SEM micrograph showing Pyrograf-III carbon nanofibers in bundles. (Courtesy of ASL)

Pyrograf-III is available as PR-19 and PR-24 in three different grades. They are AG (as grown CNF), PS (pyrolytically stripped CNF), and HT (heat treated CNF) grades. PR-19 CNF has fiber diameters of 100 to 200 nm and fiber lengths of 30 to 100 micron. PR-24 CNF has fiber diameters of 60 to 150 nm and fiber lengths of 30 to 100 micron.

Carbon nanofiber nanocomposites can offer multifunctional performance for several potential aerospace and other commercial applications, as follows:

- EMI shielding, electrostatic painting, antistatic
- Thermal conductivity of spacecraft, batteries, and electronics
- Improved mechanical properties in polymers (composite structure, injection-molded parts, tires)
- Reduced coefficient of thermal expansion (CTE) for spacecraft resin systems

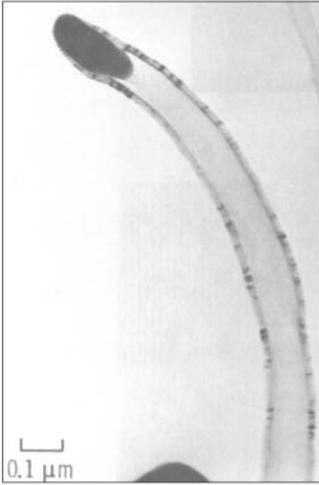


Figure 2.14 TEM micrograph showing single Pyrograf-III carbon nanofibers. (Courtesy of ASI.)



Figure 2.15 TEM micrograph showing carbon nanofibers have a hollow core and two distinct regions, catalytic and deposited. (Courtesy of ASI.)

Applied Sciences, Inc. has suggested that CNFs can be used for the following applications: (a) for improving strength and modulus, as shown in Table 2.8; (b) for lowering resistance, as shown in Table 2.9; (c) for CTE control, as shown in Table 2.10; and (d) as strain-compliant conductors, as shown in Table 2.11.

Recently Glasgow et al.⁸ demonstrated that the achievement of significant mechanical reinforcement in CNF composites requires high

TABLE 2.8 CNF for Structural Applications for Better Strength and Modulus

Generic area	Military	Civilian
Synthetic rubber	Tank tracks, aircraft tires, ship structures	Automotive tires, aircraft tires, ship structures, sporting goods
Thermoplastic structures	Aircraft, satellite structures, ship structures, optical components	Auto body structures, sporting goods, optical components
Thermoset structures	Aircraft, satellite structures, ship structures, optical components	Auto body structures, sporting goods, optical components
Carbon/epoxy structures	Airframes, especially Z-direction enhancement	Sporting goods, automobiles, aerospace structures

TABLE 2.9 CNF for Applications for Lower Resistance

Generic area	Military	Civilian
Static dissipation	Satellite charge control, fuel lines, hoses, tubing, ordnance	Fuel hoses and tubing for automobiles, electronics assembly
Electrostatic paint spray	Aircraft, ground vehicles, ships, other structures	Auto body components, aircraft, other vehicles
Electromagnetic interference mitigation	Plane crash reduction, avionics, RF, secure facilities	High speed computing, communications
Lightning strike mitigation	Aircraft (especially composite airframe), ships, radomes, ordnance bunkers	Aircraft, ground structures
Compliant contacts	Solar cells, electronics, scanning electron microscopy	Electronics

TABLE 2.10 CNF for Applications for CTE Control

Generic area	Military	Civilian
Optics	Low cost injection moldable mirrors, laser	Low cost injection moldable optics
Structures	Satellite structures (especially where stability in orbit is important), aircraft, ground vehicles, ships	Auto body components (match aluminum or steel) and for aerospace and ships
Electronics	MCT devices, electronic boards, high power electronics	Electronic boards, computers, cooling components

TABLE 2.11 CNF for Applications for Strain-Compliant Conductors

Generic area	Military	Civilian
Compliant contacts	Solar cell contacts for spacecraft, electronic boards	Electronic boards, solar cell contacts, high temperature lead free solder alternative
Thermal control devices		Temperature actuators, temperature measurement devices

fiber loadings and is somewhat dependent on generating an appropriate interphase between the CNF and the matrix. Novel surface treatments under development have yielded good improvements in the tensile modulus and strength of CNF-reinforced polypropylene. Adding surface functional groups, particularly oxygen groups, has also demonstrated benefits for interphase development. Carboxyl and phenolic groups contributing to a total surface oxygen concentration in the range of 5 to 20 atom percent have been added to CNF and have been used to fabricate epoxy polymer matrix composites to provide improved flexural strength and modulus. The effect of similarly functionalized CNF in bismaleimide (BMI) polymer matrix composites also shows promise. Data for propylene, epoxy, and BMI/CNF-reinforced composites indicate that higher fiber volume loadings will find a role in structural composite markets as price and availability improve.

2.2.3 Polyhedral oligomeric silsesquioxane (POSS)

Origin. A departure from the use of natural occurring clays and CNF is the concept involving the creation of inorganic-organic structured materials. One approach to developing better materials is to create inorganic-organic composite materials in which inorganic building blocks are incorporated into organic polymers. Polyhedral oligomeric silsesquioxane nanostructured materials, representing a merger between chemical and filler technologies, can be used as multifunctional polymer additives, acting simultaneously as molecular level reinforcements, processing aids, and flame retardants. These nanostructured materials are manufactured by Hybrid Plastics, Inc., located in Hattiesburg, Mississippi (website: <http://www.hybridplastics.com>).

Properties. Polyhedral oligomeric silsesquioxane possesses two unique structural features: (1) the chemical composition is a hybrid, intermediate ($\text{RSiO}_{1.5}$) between that of silica (SiO_2) and silicones (R_2SiO); and (2) POSS molecules are nanoscopic in size, ranging from approximately 1 to 3 nm. These materials are thermally and chemically more robust than silicones, and their nanostructured shape and size provide unique properties by controlling polymer chain motion at the molecular level. Polyhedral oligomeric silsesquioxane molecules are extremely tailorable, permitting a wealth of new nanostructured materials to be designed and synthesized from the bottom up. The POSS material has the multifunctional properties and inorganic framework of silicone oxide. It has been proven that this framework is ceramiclike in nature, especially in severe environments. The other

key factor for POSS property enhancement is the length scale effect. The anatomy of a POSS nanostructured chemical is illustrated in Fig. 2.16. It is a precise, three-dimensional silicone and oxygen cage structure for molecular-level reinforcing of polymer segments and coils. Hybrid Plastics currently offers over 250 nanostructured chemicals, as shown in Fig. 2.17, the POSS chemical tree. The key purpose of POSS technology (Fig. 2.18) is to create hybrid materials that are tough, lightweight, and as easy to process as polymers, yet with the characteristics of high use temperature and oxidation resistance, like ceramics. A list of property enhancements via POSS is listed in Fig. 2.19.

Features. Polyhedral oligomeric silsesquioxane materials are one type of hybrid inorganic-organic material of the form $(\text{RSiO}_{1/2})_n$ or R_nT_n , where organic substituents are attached to a silicon-oxygen cage.⁹ The most common POSS cage is the T_8 (e.g., Vinyl_8T_8 , shown in Fig. 2.20), although other cages with well-defined geometries include $n = 6, 10, 12, 14, 16$ and 18 .¹⁰ By incorporating these Si-O cages into organic polymers, properties superior to the organic material alone are realized, offering exciting possibilities for the development of new materials.¹¹⁻¹⁵ Vinyl and phenyl-based POSS materials have been used in composites that have shown excellent fire resistance performance.¹⁶

Another example of POSS-molecular silica blends is shown in Fig. 2.21, where each of four types of POSS has a different R group that was blended into 2 million MW polystyrene. The morphology of the polystyrene-POSS nanocomposites was changed significantly, as shown in the TEM images in Fig. 2.21a to d. Figure 2.21a illustrates R = cyclopentyl (C_5H_9) in the POSS material when blended with the polystyrene, where a snowflake domain was formed. Figure 2.21b

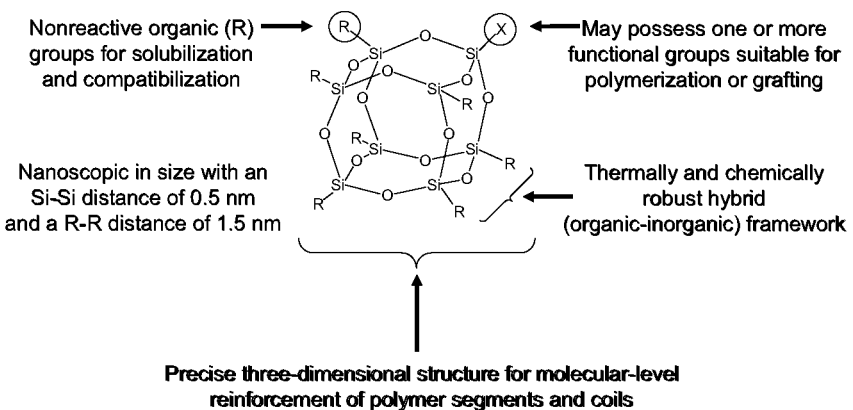


Figure 2.16 Anatomy of a POSS molecule. (Courtesy of Hybrid Plastics.)

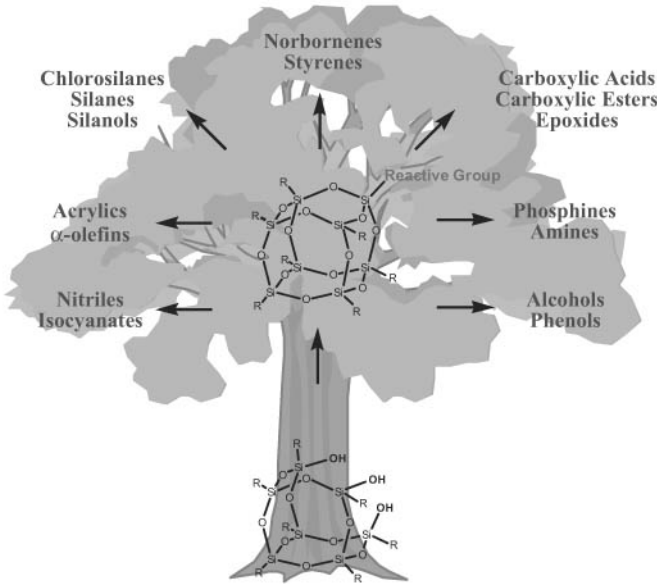


Figure 2.17 The POSS chemical tree. (Courtesy of Hybrid Plastics.)

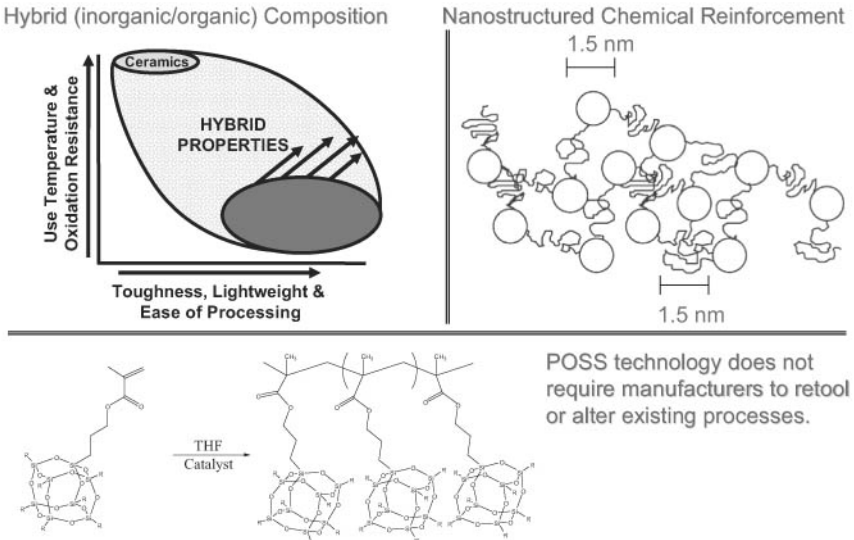


Figure 2.18 Key aspects of POSS technology. (Courtesy of Hybrid Plastics.)

shows R = cyclopentyl (CP₇T₈Styrenyl) in the POSS material when blended with the polystyrene, where partial compatibility was shown. Figure 2.21c demonstrates R = styrenyl (Styrenl₈T₈) of the POSS material when blended with polystyrene, where a phase inversion

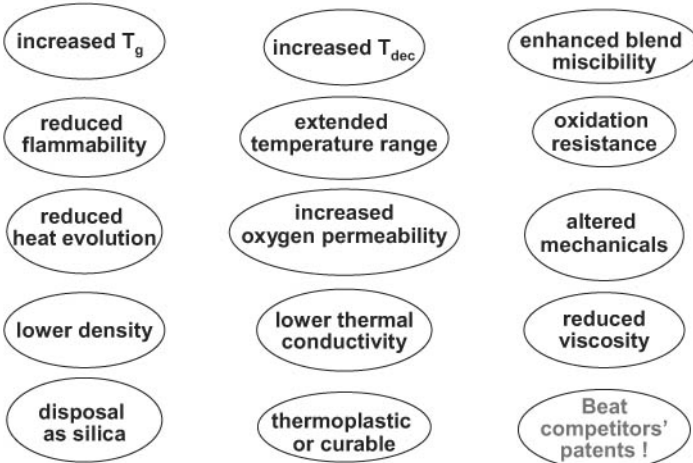


Figure 2.19 Property enhancements of polymers via POSS. (Courtesy of Hybrid Plastics.)

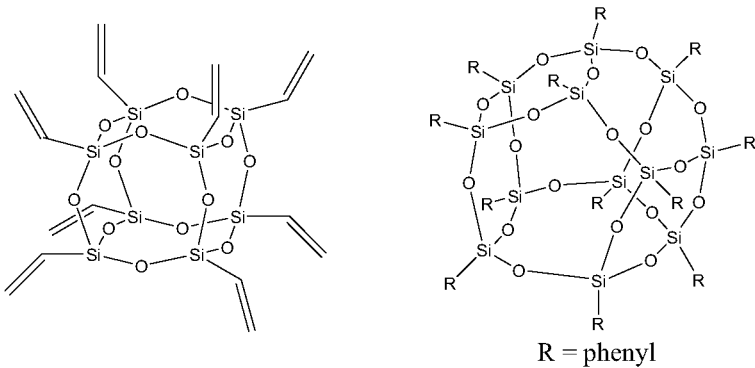


Figure 2.20 The chemical structures of Vinyl₈T₈ and Phenyl₁₂T₁₂.

occurred. Figure 2.21d illustrates R = Phenethyl (Phenethyl₈T₈) in the POSS material when blended with 50 wt% loading of POSS into the polystyrene, it is a transparent material! This example shows that the POSS material can be customized to control the morphology and the properties of the resulting nanocomposite blends.

2.2.4 Carbon nanotubes

Origin. There are excellent reviews and publications on the synthesis and the physical properties of carbon nanotubes.¹⁷⁻²⁰ In this section, only a brief summary of the classification of carbon nanotubes will be presented. Carbon nanotubes have attracted much attention in the past

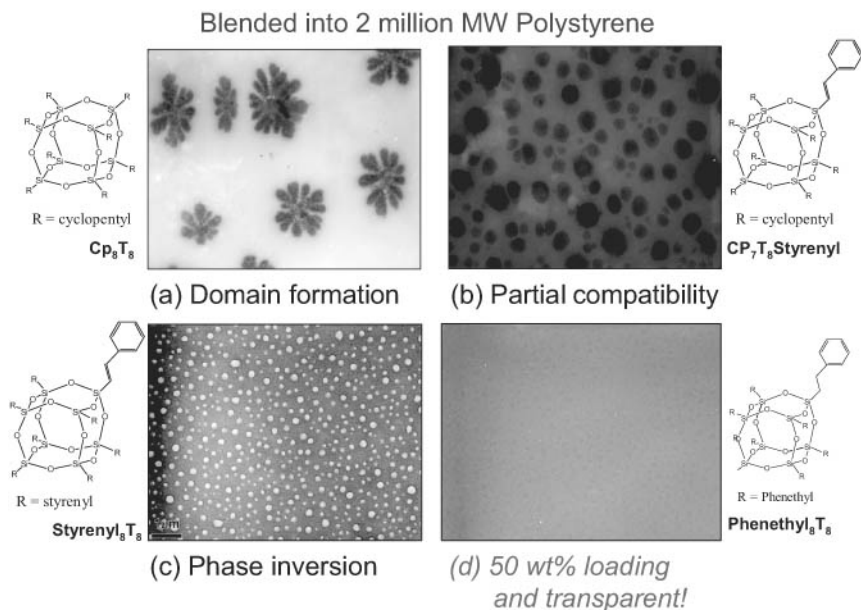


Figure 2.21 TEM micrographs showing the change of morphologies of polystyrene by changing the R group of the POSS materials. (Courtesy of A. Lee.)

several years because of their unique potential uses for structural, electrical, and mechanical properties.²¹ Nanotubes have high Young's modulus and tensile strength, and they can be metallic, semiconducting, or semimetallic, depending on the helicity and diameter.²¹

Manufacturing. Carbon nanotubes can be prepared by arc evaporation,²² laser ablation,²³ pyrolysis,²⁴ PECVD,²⁵ and electrochemical methods.^{26,27} Carbon nanotubes were first synthesized in 1991 by Iijima in the carbon cathode by arc discharge.²⁸ However, the experimental discovery of single-wall carbon nanotubes came in 1993.^{29,30} In 1996 a much more efficient synthesis route, involving laser vaporization of graphite to prepare arrays on the order of SWNTs.³¹ The process offered major new opportunities for quantitative experimental studies of carbon nanotubes.

Properties. Properties of carbon nanotubes have been studied extensively. Carbon nanotubes are excellent candidates for stiff and robust structures, because the carbon-carbon bond in the graphite is one of the strongest in nature. Transmission electron microscopy data revealed that carbon nanotubes are flexible and do not break upon bending.³² Thermal conductivity of carbon nanotubes can be extremely high, and the thermal conductivity of individual carbon nanotubes was found to

be much higher than that of graphite and bulk nanotubes.³³ Carbon nanotubes have a wide spectrum of potential applications. Examples include use in catalysis, storage of hydrogen and other gases, biological cell electrodes, quantum resistors, nanoscale electronic and mechanical devices, electron field emission tips, scanning probe tips, flow sensors, and nanocomposites.³⁴

Classifications. Carbon nanotubes can be grouped as single-wall (SWNT), multiwall (MWNT), and the newly established small-diameter (SDNT) material, based on the number of walls present in the carbon nanotubes, as illustrated in Fig. 2.22. By definition, SWNTs are single-walled carbon nanotubes about 1 nm in diameter with micrometer-scale lengths; MWNTs are multiwalled carbon nanotubes with an inner diameter of about 2 to 10 nm, an outer diameter of 20 to 70 nm, and a length of about 50 μm ; and SDNTs have diameters of less than 3.5 nm and have lengths from several hundred nanometers to several micrometers. These SDNTs generally have one to three walls.

Single-wall carbon nanotubes. Carbon Nanotechnologies, Inc. (CNI) is transitioning into the production of SWNTs via multiple pilot plants and a commercial demonstration unit operating in Houston, Texas (website: <http://www.cnanotech.com>), where the company produces buckytubes. Buckytubes are tubular fullerenes, polymers that are part of the fullerene family of carbon molecules discovered by Dr. Richard E. Smalley and colleagues in 1985. Buckytubes comprise single-wall carbon nanotubes (SWNTs) and nested (endohedral or endotopic) SWNTs (i.e., one, two, or more tubular fullerenes) inside another tubular fullerene, as depicted in Figs. 2.23 and 2.24.

Buckytubes are carbon nanotubes that are graphene (layers of graphite) rolled up into seamless tubes. Graphene consists of a hexagonal

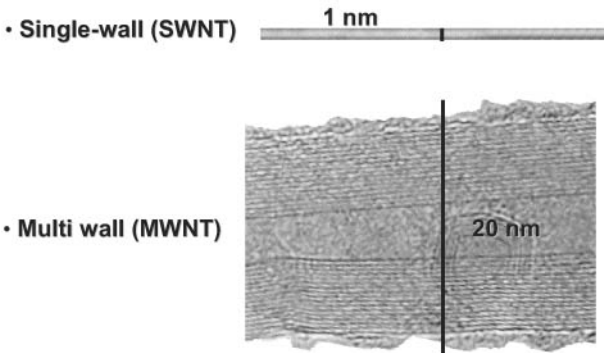
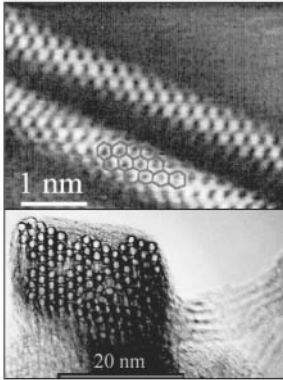


Figure 2.22 Definition of single- and multiwall carbon nanotubes. (Courtesy of CNI.)



- **SWNTs are Perfect: each atom in its place**

Ropes of SWNTs

- **Created by strong Van der Waals forces between SWNT surfaces**
- **Enable self-assembly**
- **Make dispersion challenging**

Figure 2.23 TEM micrographs showing SWNTs and ropes of SWNTs. (Courtesy of CNI.)

SWNTs are unique:

- Molecules
- Perfect structures
- Polymers of pure carbon

SWNTs have extraordinary properties:

- Strength (~100x steel)
- Electrical conductivity (~ copper)
- Thermal conductivity (3x diamond)
- Accessible surface

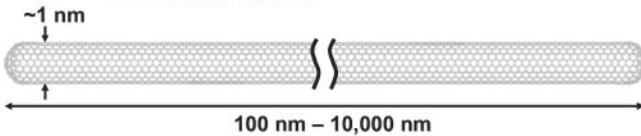


Figure 2.24 SWNTs are the perfect material with unique and extraordinary properties. (Courtesy of CNI.)

structure similar to chicken wire. Rolling up graphene into seamless tubes can be accomplished in various ways. For example, carbon-carbon bonds (like the wires in chicken wire) can be parallel or perpendicular to the tube axis, resulting in a tube where the hexagons circle the tube like a belt, but they are oriented differently. Alternatively, the carbon-carbon bond need not be either parallel or perpendicular, in which case the hexagons will spiral around the tube with a pitch, depending on how the tube is wrapped. Buckytubes have extraordinary electrical conductivity, thermal conductivity, and mechanical properties. They are the best electron field-emitter. As polymers of pure carbon, they can be reacted and manipulated using the chemistry of carbon. This carbon chemistry characteristic provides the opportunity to modify the structure and to optimize solubility and dispersion. Buckytubes

(Fig. 2.25) are molecularly perfect, which means that they are free of property-degrading flaws in the nanotube structure. Their material properties can therefore approach closely the very high levels intrinsic to them. Buckytubes have extraordinary properties: their strength is about 100 times that of steel, their electrical conductivity is close to that of copper, their thermal conductivity is about three times that of diamond, and they have tremendous accessible surface area. These extraordinary characteristics give buckytubes potential in numerous applications. In most applications, raw buckytubes need to be customized. The customization can be precisely controlled using organic chemistry on open ends, closed ends, and sidewalls, as illustrated in Fig. 2.25.

Single-walled nanotubes offer incredible opportunities in electrical properties, mechanical properties, thermal properties, and field emission, as shown below:

- *Electrical properties.* Electrically conductive composites for electrostatic dissipation, shield, and conductive sealants; energy storage for super capacitors and fuel cells; electronic materials and devices for conductive inks and adhesives; electronic packaging; device and microcircuit components
- *Mechanical properties.* High-performance composites; coatings for wear-resistance and low friction; high performance fibers; reinforced ceramic composites
- *Thermal properties.* Thermally conductive polymer composites; thermally conductive paints and coatings
- *Field emission.* Flat-panel displays; electron device cathodes and lighting

In most applications, raw SWNTs will need to be customized

This customization can be precisely controlled using everyday organic chemistry

- Open ends
- Closed ends
- Sidewalls

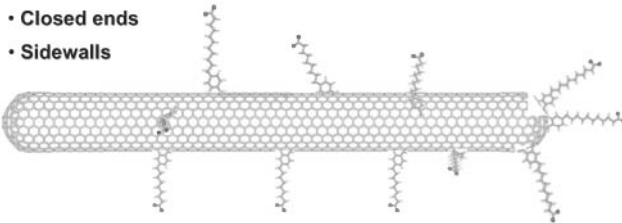


Figure 2.25 SWNTs can be customized and controlled using organic chemistry. (Courtesy of CNI.)

Figure 2.26 shows the timeline of how CNI is transforming SWNTs from the laboratory to industry. A pilot plant is shown in Fig. 2.27.

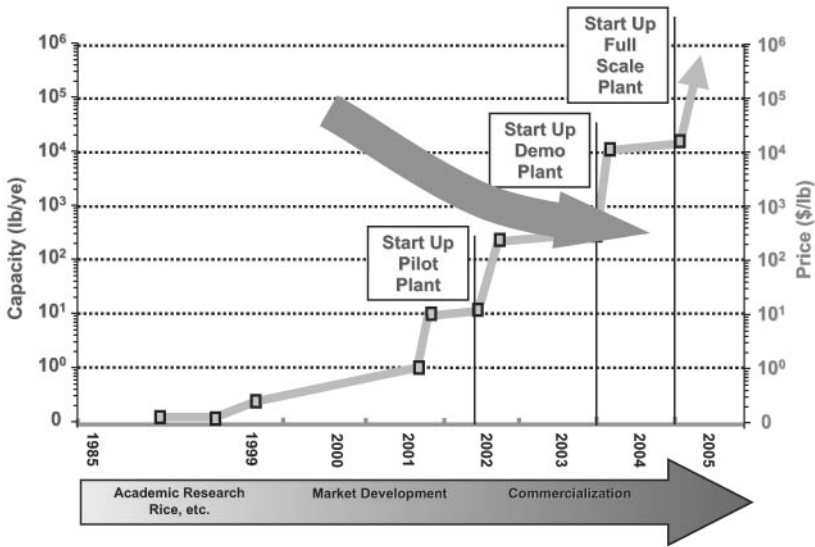


Figure 2.26 Taking SWNT from the laboratory to industry. (Courtesy of CNI.)



Figure 2.27 CNI pilot plant producing SWNTs. (Courtesy of CNI.)

Small-diameter carbon nanotubes (SDNTs). Carbon Nanotechnologies, Inc. (CNI) is the leading producer of small-diameter carbon nanotubes (SDNTs) and single-wall carbon nanotubes (SWNTs). Small-diameter carbon nanotubes are linear polymers of pure carbon with diameters less than 3.5 nm and lengths from several hundred nanometers to several micrometers.³⁵ Small-diameter carbon nanotubes are more cost-effective and affordable than SWNTs. These SDNTs generally have one to three walls. Like buckytubes, SDNTs are molecules, not particles or structures like their larger multiwall or vapor-grown carbon fiber relatives, so accordingly, they have a high degree of molecular perfection. It is this high degree of molecular perfection that provides SDNTs with their amazing properties. Small-diameter carbon nanotubes are the strongest, stiffest, toughest molecules available. They have the electrical conductivity of copper and various band-gap semiconductors depending upon their diameter and chirality, which allows them to compete with metals as well as with silicon and other semiconductors. They are the most conductive of the inherently conducting polymers. Small-diameter carbon nanotubes are also the best known conductor of thermal energy along their length, and their thermal stability in air of up to 550 or 1400°C in anaerobic conditions makes them the most thermally stable polymer known. Finally, SDNTs can be customized using standard organic chemistry to modify the way they interact with each other, as well as with various materials and solvents; they can be functionalized on their ends or their sidewalls, either covalently or noncovalently. Figures 2.28a and b show two TEM micrographs of some typical SDNTs.³⁵

Multiwall carbon nanotubes. Multiwall carbon nanotubes have an interior diameter of 2 to 10 nm, an exterior diameter of 20 to 75 nm, and a

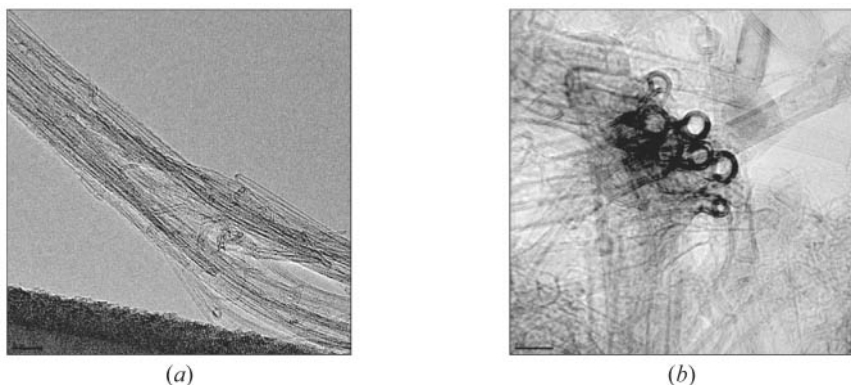


Figure 2.28 High-resolution TEM micrographs of typical SDNTs in ropes are shown in a progressive manner, where the scale bar is 20 nm for the left image and 5 nm for the right image. (Courtesy of CNI)

length of 50 μm , as shown in Fig. 2.29. Multiwall carbon nanotubes are produced by CVD synthesis of xylene-ferrocene composition at a relatively low temperature of 725°C, and with high purity > 95 percent xylene (Fig. 2.30). Multiwall carbon nanotubes are nanoscale carbon fibers with a high degree of graphitization. Multiwall carbon nanotubes are technically neither fullerenes nor molecular. They are attractive materials intermediate between SWNT and CNF with properties vastly superior to graphite and carbon black (Figs. 2.31 and 2.32). Hyperion

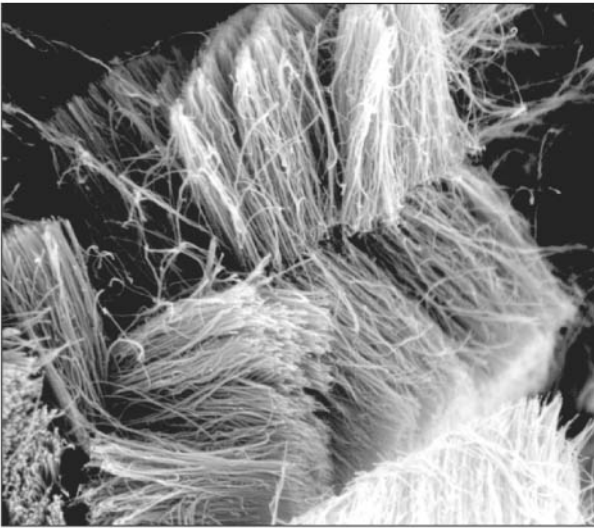
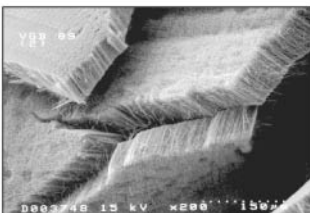
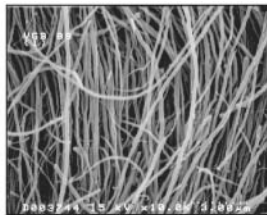


Figure 2.29 MWNTs have dimensions of 2 to 10 nm ID, 20 to 75 nm OD, and are 50 μm long.

- CVD synthesis
 - xylene / ferrocene
 - low temperature, 725°C
 - high purity, > 95%



- aligned normal to substrate
- easily dispersed

Figure 2.30 MWNTs are produced using CVD synthesis.

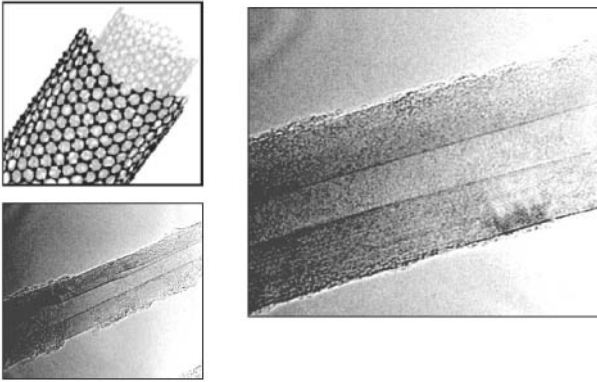


Figure 2.31 Microstructures of MWNTs in cartoon and TEM micrographs.

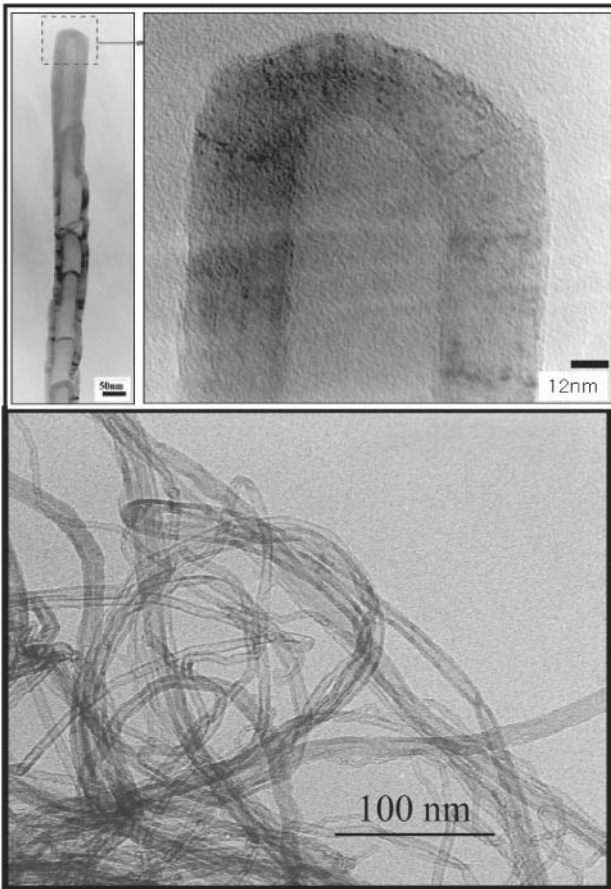


Figure 2.32 TEM micrographs showing MWNTs in bundles, as individual nanotube, and in high magnification. (Courtesy of CNI.)

is a manufacturer of MWNTs and they compound their MWNTs with different types of polymers and market them as MWNT polymer masterbatches.

2.2.5 Nanosilica

Origin. In 1941 Degussa patented a high temperature hydrolysis process of metallic oxides to produce extremely fine particle oxides. It was converted into large scale production in the 1950s and has become the process for the preparation of nanoparticles based on silicon dioxide, aluminum oxide and titanium dioxide. Under TEM analyses, the primary particles of the three oxides show cubic forms with rounded off corners. All materials exhibit no internal surface. Silicon dioxide under the trademark of AEROSIL made it debut at this time.

Properties. AEROSIL is highly dispersed, amorphous, very pure silica that is produced by high-temperature hydrolysis of silicon tetrachloride in an oxyhydrogen gas flame.³⁶⁻³⁸ It is a white, fluffy powder consisting of spherically shaped primary particles. AEROSIL OX 50 has the largest average primary particle size of 40 nm; AEROSIL 300 and 380 have the smallest size of 7 nm. The primary particles are spherical and free of pores. The primary particles in the flame interact to develop aggregates, which join together reversibly to form agglomerates. Figure 2.33 shows a TEM micrograph of AEROSIL 300 in which the primary particles, aggregates, and agglomerates can be clearly seen.³⁸ The average diameters of the primary particles are in the range of 7 to 40 nm, according to the AEROSIL grade. The specific surface areas range between 50 and 380 m²/g. In contrast to precipitated silicas,

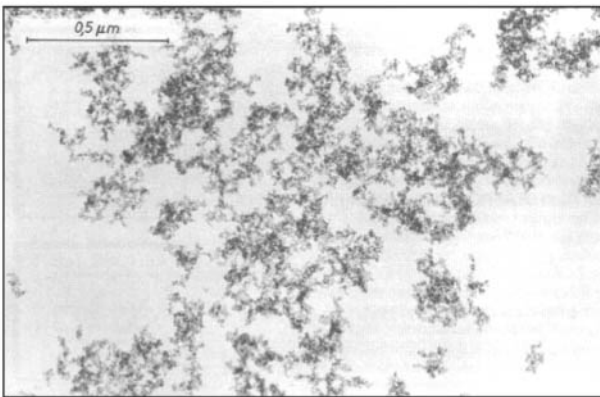


Figure 2.33 TEM micrograph of AEROSIL 300 showing particles in aggregates. (Courtesy of Degussa.)

AEROSIL does not have a clearly defined agglomerate size. Particle size distribution becomes wider as the average primary particle size increases, and the tendency to form agglomerates is reduced (Fig. 2.34). The extremely small particles naturally result in a large specific surface area, ranging from approximately $50 \text{ m}^2/\text{g}$ (AEROSIL OX 50 has an average primary particle size of 40 nm) to $380 \text{ m}^2/\text{g}$ (AEROSIL 380 has an average primary particle size of 7 nm). The size of the surface area is easily illustrated if one considers that approximately 20 g of AEROSIL 200 (average primary particle size is 12 nm) has the same surface area as an American football field. AEROSIL consists entirely of amorphous silicon dioxide. It starts to sinter and turn into glass above 1200°C . Crystallization only occurs after heat treatment. AEROSIL is nearly insoluble in water. It is also insoluble in acids. It does, however, dissolve in strong alkaline media to form silicates.

Applications. Siloxane and silanol groups are situated on the surface of the AEROSIL particles. The latter is responsible for the hydrophilic behavior of the untreated AEROSIL. These silanol groups also determine the interaction of the AEROSIL with solids, liquids, and gases. One gram of AEROSIL 200 with a specific surface area of $200 \text{ m}^2/\text{g}$ contains approximately 1 mmol of silanol groups. The surface of AEROSIL particles can be easily chemically modified by reacting the silanol groups with various silanes and silazanes, resulting in hydrophobic AEROSIL particles. For example, AEROSIL R972 and R812 are made hydrophobic with dimethylsilyl or trimethylsilyl groups, which are stable against hydrolysis. Hydrophilic and hydrophobic grades of

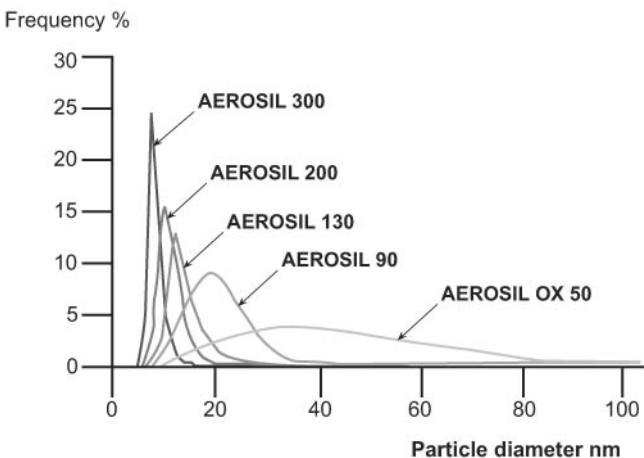


Figure 2.34 Particle size distributions of various grades of AEROSIL nanosilicas. (Courtesy of Degussa.)

AEROSIL are successfully used in numerous applications such as a reinforcing filler, a thickening and thixotropic agent, an antisetling agent, and a free-flow aid.

AEROSIL is a submicrometer amorphous silica that has been used successfully for decades as a thickening agent and thixotrope in liquid systems. It is also used to adjust the rheological properties of epoxy resins. It also serves as a rheological aid to provide effective, stable thickening and thixotropy of epoxy systems.³⁶⁻³⁸ AEROSIL fumed silica for rheology control is widely used in silicone rubber, coatings, plastics, printing inks, adhesives, lubricants, creams, ointments, and toothpaste. Nelson and coworkers used this nanoparticle with polystyrene in their recent study demonstrating significant improvement in reduced flammability of polystyrene.³⁹ Properties of AEROSIL R805 and R202 are listed in Table 2.12.

The introduction of most nanoparticles into low-viscosity, reactive resin systems such as epoxies, vinyl esters, cyanate esters, BMI, and phenolics results in a rapid increase in viscosity as the nanoparticle content is increased to 5 to 7 percent and leads to limited use of the nanomodified reactive resin system in many “low- to medium-viscosity” demanding processing applications like vacuum assisted resin transfer molding (VARTM), impregnation of fabric, filament winding, and other processing methods. Although there are instances that indicate 5 to 7 percent nanoparticle content is optimum, reduction in viscosity through the use of solvent and/or increased temperature allows reasonable dispersion of the nanoparticles into the resin matrix system. Questionable uniformity of nanoparticle dispersion using high-shear mixing conditions followed by removal of solvent is an additional issue, as is “scale-up.”

As it was mentioned above, there are processing problems (viscosity increase) associated with the introduction of 5 to 7 percent nanoparticles into low viscosity reactive resin systems (epoxies, VE, etc.) A novel technique of preparing “macrosurfaced silica” appears to

TABLE 2.12 Material Properties of AEROSIL R805 and R202

Properties	AEROSIL R805	AEROSIL R202
Specific surface area (BET) (m ² /g)	150 ± 25	100 ± 20
Carbon content (%)	4.5–6.5	3.5–5.0
Average primary particle size (nm)	12	14
Tapped density standard material (g/l)	50	50
Moisture 2 hours at 105°C	0.5	0.5
Ignition loss 2 hours at 1,000°C based on material dried for 2 hours at 105°C	5.0–7.0	4.0–6.0
pH value in 4% dispersion	3.5–5.5	4.0–6.0
SiO ₂ -content based on ignited material (%)	> 99.8	> 99.8

avoid the “increased viscosity” problem when 5-7% nanoparticles are introduced.

Macrosurfaced nanosilica. The use of the recently reported Hanse Chemie Technology⁴⁰⁻⁴² of “macrosurface” treated spherical nanosilica allows the introduction of ≥ 10 percent Hanse nanosilica with minimal increase in viscosity in the nanomodified reactive resin system and still provide “multifunctionality” to the resulting cured resin system. Hanse’s proprietary synthesis of silica nanocomposites is shown in Fig. 2.35. A silicate solution is transformed into a silica sol using the sol-gel method. The silicas were surface-modified to be compatible with selective polymer matrices to form transparent polymer nanocomposites with low viscosity and no sedimentation. Hanse is able to create homogeneous dispersions of amorphous silicon dioxide in standard, chemically unchanged organic monomers, prepolymers, and oligomers using this technique. The silica phase consists of discrete nanospheres (20 nm) with an extremely narrow size distribution, as shown in Fig. 2.36. Owing to agglomerate-free colloidal dispersion of the nanosilica particles, the nanocomposites are highly transparent, with low viscosity, and they do not show sedimentation even with SiO_2 loading up to 60 percent, as shown in a TEM micrograph in Fig. 2.37. This nanosilica serves as both performance additive and filler!

Properties. Hanse claims that nanosilica particles can easily penetrate “closed meshed fabrics” and are therefore well suited for reinforcement of composites, especially VARTM. This characteristic would similarly apply to uniform impregnation of fabric in prepreg preparation.

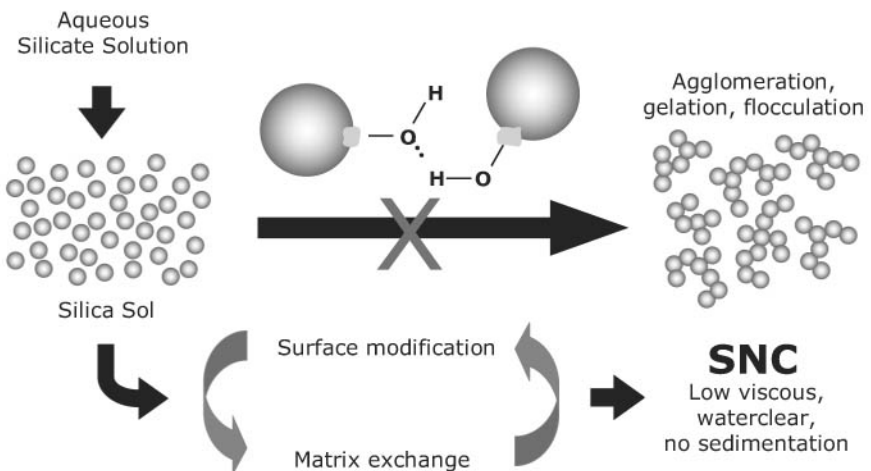


Figure 2.35 Hanse Chemie’s route to produce nanosilicas. (Courtesy of Hanse Chemie.)

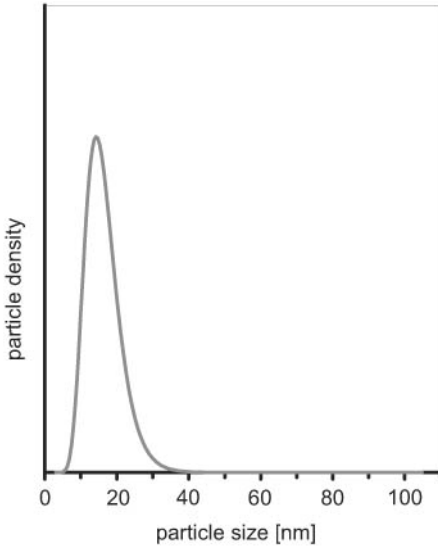


Figure 2.36 Narrow particle size distribution is a characteristic of Hanse Chemie's nanosilicas. (Courtesy of Hanse Chemie.)

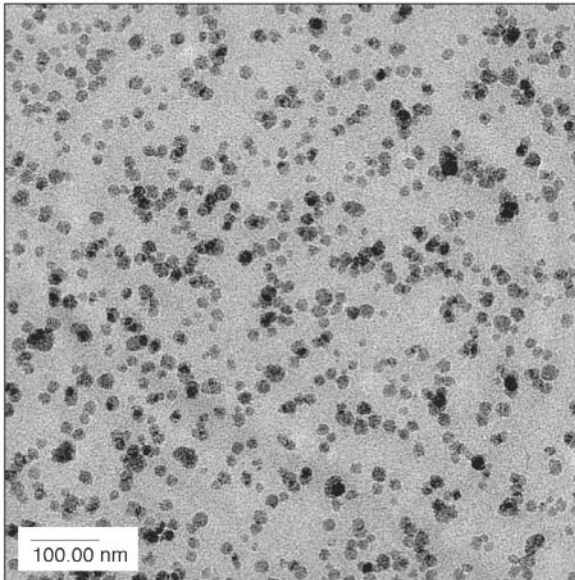


Figure 2.37 TEM micrographs showing Hanse Chemie's homogenous dispersion of nanosilica in polymer. (Courtesy of Hanse Chemie.)

Furthermore, it is possible that with a further increase in nanosilica content to 15 to 20 percent, with a modest increase in viscosity and

reasonable economics for the nanosilica, that flame-resistant epoxy polymer matrix composites (PMCs) may emerge without jeopardizing the expected benefits of nanomodification—improved heat strength, higher T_g , improved toughness, and others.

NANOCRYL[®] is a product of Hanse Chemie, produced when nanosilica are dispersed in unsaturated acrylates. It can be used for applications such as radiation curing coatings, adhesives, raw materials for coating resins, and medical compounds. Figure 2.38 illustrates that there is no viscosity buildup of nanosilica in acrylate ester up to 50 wt%. Other products such as NANOPOL for polyurethane foams, etc, NANOCONE for silicone polymers have been developed.

Applications. A variety of applications can be considered with the diversity of Hanse Chemie nanosilica products ranging from epoxies, acrylates, polyurethanes, silicone elastomers for FRP, structural adhesives, coatings, castings. The Hanse Chemie nanosilica products have the following features:

Process:

- commercially available, stable dispersions for reactive systems such as epoxies, acrylates, urethanes, silicones
- ease of processing, low viscosity providing excellent wet-out of woven fabric with reduced heat of reaction, reduced cure shrinkage
- cure rate unaffected
- combine with typical fillers

Nanomaterials Products:

- Enhanced scratch, abrasion resistance, and transparent products

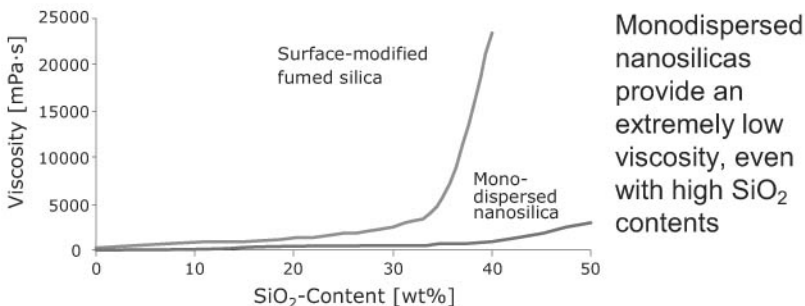


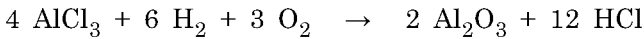
Figure 2.38 Viscosities of fumed silica and monodispersed nanosilica in acrylate ester. (Courtesy of Hanse Chemie.)

- Unique toughness and stiffness
- Reduced thermal yellowing, thermal expansion
- Depending on Hanse material, improved electrical insulation or enhanced thermal conductivity

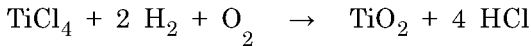
2.2.6 Nanoaluminum oxide

Origin. In 1941 Degussa developed and patented a process where silicon tetrachloride was vaporized and hydrolyzed in an oxyhydrogen flame. AEROSIL nanosilicas were produced using this process. The basis of the AEROSIL process is the hydrolysis of the gaseous metallic chlorides under the influence of water that develops during the oxyhydrogen reaction, and at the temperature characteristics for such a reaction. The formation of the highly dispersed oxides takes place schematically, according to the following equations:³⁷

Aluminum Oxide C



Titanium Dioxide P 25



Under TEM analyses, the primary particles of the three oxides show cubic forms, with the corners rounded off. Similar to AEROSIL particles, they have no internal surface.

Properties. Aluminum Oxide C has an average primary particle size of about 13 nm and a specific surface of about 100 m²/g. The aluminum oxides produced through precipitation of aluminum hydroxide from aluminate solution followed by calcinations consist of particles in the order of magnitude of micrometers. High surface aluminum oxide gels, in contrast to Aluminum Oxide C, have a high proportion of internal surface. Figure 2.39 shows a TEM micrograph of Aluminum Oxide C. The specific surface is also a function of the specific weight, and for “heavy” oxides, these must be evaluated correspondingly higher. In Fig. 2.40, the BET surfaces are represented in comparison with the specific weights of four nanoparticles.

The compacted apparent density of Aluminum Oxide C is about 80 g/L. For use in powdered coatings or as a free-flow aid in powders, which tend to form lumps, a less compact material with a compacted apparent density of about 50 g/L is offered as Aluminum Oxide CS.

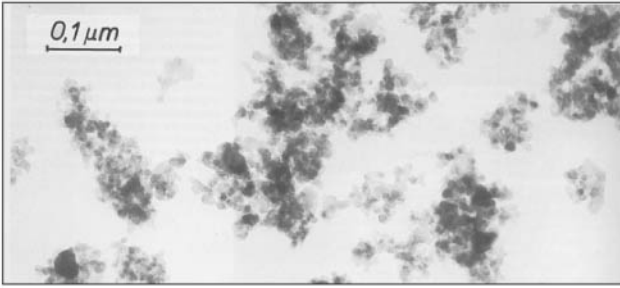


Figure 2.39 TEM micrograph of Aluminum Oxide C. (Courtesy of Degussa.)

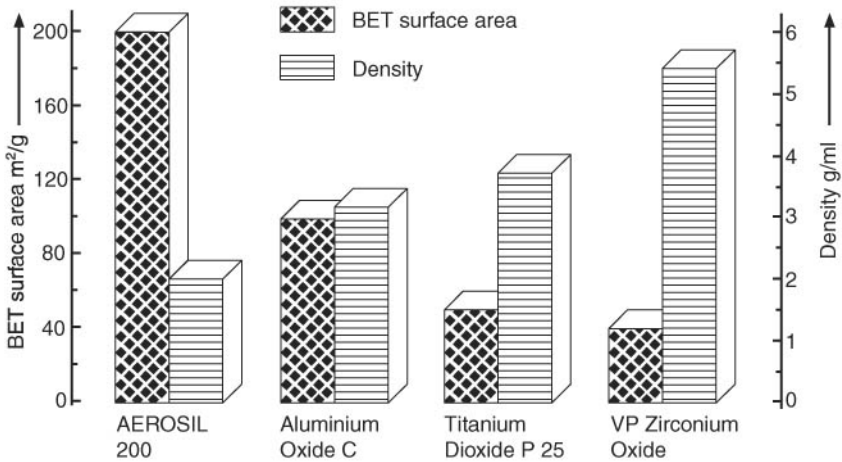


Figure 2.40 Comparison of BET surface areas and densities of AEROSIL 200, Al₂O₃C, TiO₂ P 25, and ZrO. (Courtesy of Degussa.)

Through dispersion of Aluminum Oxide C in water, followed by drying and grinding, a compacted apparent density of about 500 g/L can be attained. Figure 2.41 shows 10 g each of commercial Aluminum Oxide C (compacted apparent density about 80 g/L) and a variant compacted via an aqueous dispersion (compacted apparent density about 500 g/L). In combination with AEROSIL, Aluminum Oxide C has proven to be effective in the thickening and the formation of thixotropes of polar liquids. For the thickening and the formation of thixotropes of water, AEROSIL COK 84, a mixture of 84 percent AEROSIL 200 and 16 percent Aluminum Oxide C has been established as optimum for this application.

A partial listing of potential Aluminum Oxide C applications includes: production of aluminum nitride, ink-jet papers, thermo-transfer printing, cable insulation, high voltage insulators, transparent coatings, acrylate suspensions containing pigments, solder-resistant



Figure 2.41 Comparison of 10 g of commercial Aluminum Oxide C (compacted apparent density about 80 g/L) (left) and 10 g of Aluminum Oxide C compacted by the wet process (compacted apparent density about 550 g/L) (right). (Courtesy of Degussa.)

masks, photoresists for the production of ICs, coating of steel, heat insulation mixtures, powdered coating, and hair shampoo. Aluminum oxide nanoparticles have been used to form a nanocomposite for improved stereolithographs.⁴³

2.2.7 Nanotitanium oxide

Origin. Titanium Dioxide P 25 has an average primary particle size of about 21 nm and a specific surface of about 50 m²/g.³⁷ It is therefore considerably more finely divided in structure than the titanium dioxides that are produced on a major industrial scale by the sulphate or chloride process for pigment applications with a particle diameter of about 0.3 μm. Their specific surfaces are about 10 m²/g. Figure 2.42 shows a TEM micrograph of Titanium Dioxide P 25, and Fig. 2.43 shows the compacted apparent density of a commercial titanium dioxide pigment and of Titanium Dioxide P 25.

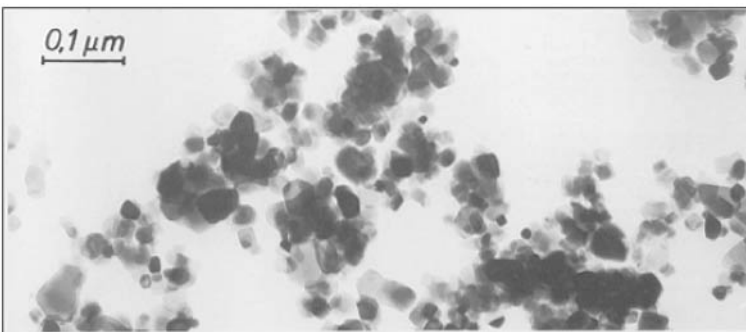


Figure 2.42 TEM micrograph of Titanium Dioxide P 25. (Courtesy of Degussa.)

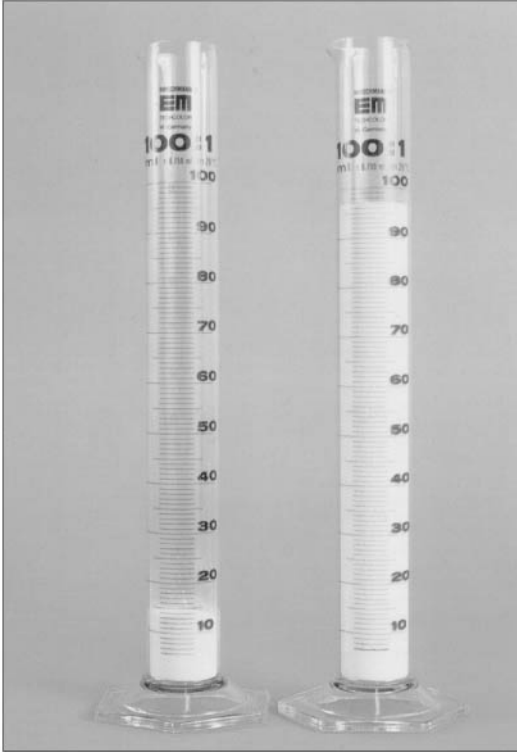


Figure 2.43 Comparison of the compacted apparent densities of a commercial TiO_2 pigment (left) and of TiO_2 P 25 (right). (Courtesy of Degussa.)

Properties. Titanium Dioxide (TiO_2) P 25 has been shown to be an excellent additive to improve the heat stability of room temperature vulcanized (RTV) silicone adhesive/sealant. Titanium Dioxide P 25 can offer long-term heat stability at high temperatures. It also has the added benefit of flame retardancy to RTV silicone using only a small amount of P 25. It also can offer semi-reinforcing qualities, which larger-particle-size heat stabilizers cannot. For optimum properties, a minimum loading level of three parts is recommended.

Potential Titanium Dioxide P 25 applications consist of high-voltage insulation material, IC substrate boards, toners, fluorescent tubes, toners, battery separators, UV sun screen lotion, and polystyrene.

2.2.8 Others

There are other nanoparticles such as exfoliated graphite⁴⁴⁻⁴⁷ and silicon carbide (SiC)⁴⁸ that have been used to form polymer nanocomposites with enhanced material properties.

2.3 Summary

In this chapter several popular and commercially available nanoparticles that are required to form polymer nanocomposites were discussed. The origin, properties, and applications of these nanomaterials are presented to provide interested persons with the fundamentals and properties of these nanomaterials and the knowledge to select the proper nanoparticles for specific applications.

References

1. R. Krishnamoorti and R. A. Vaia (eds.), *Polymer Nanocomposites: Synthesis, Characterization, and Modeling*, ACS Symposium Series 804, ACS, Washington, DC, 2001.
2. T. J. Pinnavaia and G. W. Beall (eds.), *Polymer-Clay Nanocomposites*, John Wiley & Sons, New York, 2000.
3. B. Briell, "Nanoclay—Counting on Consistency," presented at *Nanocomposite 2000*, Southern Clay Products, Gonzales, TX, 2000.
4. G. G. Tibbetts, "Why Are Carbon Filaments Tubular?" *J. Crystal Growth*, **66**:632–638 (1984).
5. M. L. Lake and J.-M. Ting, "Vapor Grown Carbon Fiber Composites," in *Carbon Materials for Advanced Technologies*, T.D. Burchell (ed.), Pergamon, Oxford: England, 1999.
6. G. G. Tibbetts, J. C. Finegan, J. J. McHugh, J.-M. Ting, D. G. Glasgow, and M. L. Lake, "Applications Research on Vapor-Grown Carbon Fibers," in *Science and Application of Nanotubes*, E. Tomanek and R. J. Enbody (eds.), Kluwer Academic/Plenum Publishers, New York, 2000.
7. B. Maruyama and K. Alam, "Carbon Nanotubes and Nanofibers in Composite Materials," *SAMPE J*, **38**(3):59–70 (2002).
8. D. G. Glasgow, G. G. Tibbetts, M. J. Matuszewski, K. R. Walters, and M. L. Lake, "Surface Treatment of Carbon Nanofibers for Improved Composite Mechanical Properties," *Proc. SAMPE 2004 Int'l Symposium*, SAMPE, Covina, CA, 2004.
9. M. G. Voronkov, V. I. Vavrent'yev, *Top Curr Chem*, **102**:199–236 (1982).
10. P. A. Agaskar, W. G. Klempner, *Inorg Chim Acta*, **229**:355–364 (1995).
11. R. H. Baney, M. Itoh, A. Sakakibara, and T. Suzuki, *Chem Rev*, **92**:1409–1430 (1995).
12. J. D. Lichtenhan, *Comments Inorg Chem* **17**:115–130 (1995).
13. J. D. Lichtenhan, in *Polymeric Materials Encyclopedia*, J. C. Salamore, (ed.), CRC Press, Boca Raton, FL, 1996, pp. 7769–7778.
14. G. Z. Li, L. C. Wang, H. L. Ni, and C. U. Pittman, *Inorg Organomet Polym.* **11**:123–154 (2001).
15. S. H. Phillips, T. S. Haddad, and S. J. Tomczak, *Curr Opin Sol State Mater Sci*, **8**:21–29 (2004).
16. U. Sorathia and I. Perez, "Improving Fire Performance Characteristics of Composite Materials for Naval Applications," *Polymeric Materials: Science & Engineering*, **91**:292–296 (2004).
17. M. Terrones, *Ann Rev Mater Res* **33**:419 (2003).
18. P. J. F. Harris, *Carbon Nanotubes and Related Structures, New Materials for the Twenty-First Century*, Cambridge University Press, Cambridge, 1999.
19. K. Tanaka, T. Yamabe, and K. Fukui, *The Science and Technology of Carbon Nanotubes*, Elsevier, Amsterdam, 1999.
20. R. Saito, G. Dresselhaus, and M. S. Dresselhaus, *Physical Properties of Carbon Nanotubes*, Imperial College Press, London, 1998.
21. M. S. Dresselhaus, G. Dresselhaus, and P. C. Eklund, *Science of Fullerenes and Carbon Nanotubes*, Academic Press, San Diego, CA, 1996.
22. T. W. Ebbesen, *Ann Rev Mater Sci*, **24**:235 (1994).

23. T. Guo, P. Nikolaev, A. Thess, D. T. Colbert, and R. E. Smalley, *J Phys Chem*, **55**:10694 (1995).
24. M. Endo, K. Takeuchi, S. Igarashi, K. Kobori, M. Shiraiishi, and H. W. Kroto, *J Phys Chem Solids*, **54**:1841 (1993).
25. O. Groning, O. M. Kuttel, C. Emmenegger, P. Groning, and L. Schlapbach, *J Vac Sci Technol*, **B18**:665 (2000).
26. W. K. Hsu, J. P. Hare, M. Terrones, H. W. Kroto, D. R. M. Walton, and P. J. F. Harris, *Nature*, **377**:687 (1995).
27. W. K. Hsu, M. Terrones, J. P. Hare, H. Terrones, H. W. Kroto, and D. R. W. Walton, *Chem Phys Lett*, **262**:161 (1996).
28. S. Iijima, *Nature*, **354**:56 (1991).
29. S. Iijima and T. Ichihashi, *Nature*, **363**:603 (1993).
30. D. S. Bethune, C. H. Kiang, M. S. de Vries, G. Gorman, R. Savoy, J. Vazquez, and R. Beyers, *Nature*, **363**:605 (1993).
31. A. Thess, R. Lee, P. Nikolaev, H. Dai, P. Petit, J. Robert, C. Xu, Y. H. Lee, S. G. Kim, A. G. Rinzler, D. T. Colbert, G. E. Scuseria, D. Tomanek, J. E. Fischer, and R. E. Smalley, *Science*, **273**:483 (1996).
32. P. M. Ajayan, O. Stephan, C. Colliex, and D. Trauth, *Science*, **265**:1212 (1994).
33. P. Kim, L. Shi, A. Majumdar, and P. L. McEuen, *Phys Rev Lett*, **87**:215502 (2001).
34. Cao, G., *Nanostructures & Nanomaterials Synthesis, Properties & Applications*, Imperial College Press, London, England, 2004.
35. T. Pitstick, Carbon Nanotechnologies, Inc., Houston, TX, personal communication, June 2005.
36. Technical Bulletin AEROSIL® No. 27, Degussa AG, D-63403 Hanau-Wolfgang, Germany, 10/2001.
37. Technical Bulletin AEROSIL® No. 56, Degussa AG, D-63403 Hanau-Wolfgang, Germany, 10/1990.
38. Technical Bulletin AEROSIL® Fumed Silica, Degussa AG, D-63403 Hanau-Wolfgang, Germany, 9/2002.
39. F. Yang, R. Yngard, G. L. Nelson, *J Fire Sciences*, **23**:209–226 (May 2005).
40. S. Sprenger and M. Pyrlík, "Nanoparticles in Composites and Adhesives: Synergy with Elastomers," *Proc. 11th International Conference on Composites/Nano Engineering*, Hilton Head Island, SC, Aug. 2004.
41. U.S. Patent Application, 20040147029, dated July 29, 2004.
42. J. Cinquin, S. Bechtel, K. Schmidtke, and T. Meer, "Polymer Nano-Composites of Aeronautic Applications: From Dream to Reality?" *Proc. 11th International Conference on Composites/Nano Engineering*, Hilton Head Island, SC, Aug. 2004.
43. A. D. Pool and H. T. Hahn, "A Nanocomposite for Improved Stereolithography," *Proc. 2003 SAMPE ISSE*, SAMPE, Covina, CA, 2003.
44. Y.-X. Pan, Z.-A. Yu, Y.-C. Ou, and G.-H. Hu, "A New Process of Fabricating Electrically Conducting Nylon 6/Graphite Nanocomposites via Intercalation Polymerization," *J Polym Sci B Phys*, **88**:1626 (2000).
45. G.-H. Chen, D.-J. Wu, W.-G. Weng, and W.-L. Yan, "Preparation of Polymer/Graphite Conducting Nanocomposites by Intercalation Polymerization," *J Appl Polym Sci*, **82**:2506 (2001).
46. L. T. Drzal and H. Fukushima, "Exfoliated Graphite as a Nano-Reinforcement for Polymers," *Proc. 2003 SAMPE ISSE*, SAMPE, Covina, CA, 2003.
47. O. Choi, H. T. Hahn, S. Gilje, and R. B. Kaner, "Graphite Nanoplatelet Reinforced Epoxy Composites: The Effect of Exfoliated and Surface Treatment," *Proc. 2005 SAMPE ISTC*, SAMPE, Covina, CA, 2005.
48. V. Yong and H. T. Hahn, "Kevlar/Vinyl Ester Composites with SiC Nanoparticles," *Proc. 2004 SAMPE ISSE*, SAMPE, Covina, CA, 2004.

This page intentionally left blank

Selecting Resin Matrix and Nanoparticles for Applications

3.1 Characteristics of Polymer Nanostructured Materials

There are two main challenges to developing polymer nanostructured materials after the desired nanoparticle has been selected for the polymer of interest. First, the choice of nanoparticles requires an interfacial interaction and/or compatibility with the polymer matrix. Second, the proper processing technique should be selected to uniformly disperse and distribute the nanoparticles or nanoparticle aggregates within the polymer matrix. In this chapter the selection process of several resin matrices and nanoparticles based on the author's research and the efforts of other researchers will be described. In Chap. 2, the different types of nanoparticles were briefly described. In this chapter, different types of polymers and polymer nanocomposites will be discussed.

In most cases, polymer nanostructured materials exhibit multifunctionality. Several of the functions of these materials are listed below:

- *Thermal*: increased thermal resistance, higher glass transition temperature (T_g) or heat deflection temperature (HDT), reduced coefficient of thermal expansion (CTE)
- *Mechanical*: increased modulus, strength, toughness, elongation (in some cases)
- *Chemical*: improved solvent resistance, improved moisture resistance
- *Electrical*: improved thermal conductivity, lower resistivity (depends on the nanoparticles)

- *Barrier*: reduced oxygen, moisture transmission
- *Optical*: clear, transparency provided in selective systems
- *Others*: abrasion resistance, reduced shrinkage

3.2 Polymer Matrices

In general, polymers can be classified into the three basic families of resins namely *thermoplastics*, *thermosets*, and *elastomers*. Table 3.1 lists several characteristics of the thermosetting and thermoplastic resin systems.

3.2.1 Thermoplastic-based nanocomposites

Materials are often classified as metals, ceramics, or polymers. Polymers differ from the other materials in a variety of ways, but generally they exhibit lower densities, and moduli. The lower densities of polymeric materials offer an advantage in applications where lighter weight is desired. The addition of thermally and/or electrically conducting fillers allows the polymer formulator the opportunity to develop materials from insulating to conducting type characteristics.

Thermoplastic materials are used in a vast array of products. In the automotive area, they are used for interior parts and in under-the-hood applications. The packaging applications area is a large area for thermoplastics, from carbonated beverage bottles to plastic wrap.

TABLE 3.1 Comparisons of Thermoplastic and Thermosetting Resin Characteristics

Thermoplastic resin	Thermosetting resin
<ul style="list-style-type: none"> ▪ High MW solid ▪ Stable material ▪ Reprocessable, recyclable ▪ Amorphous or crystalline ▪ Linear or branched polymer ▪ Liquid solvent resistance 	<ul style="list-style-type: none"> ▪ Low MW liquid or solid ▪ Low to medium viscosity, requires cure ▪ Cross-linked, nonprocessable ▪ Liquid or solid ▪ Low MW oligomers ▪ Excellent environmental and solvent resistance
<ul style="list-style-type: none"> ▪ Short process cycle ▪ Neat up to 30% filler ▪ Injection/compression/extrusion 	<ul style="list-style-type: none"> ▪ Long process cycle ▪ Long or short fiber reinforced ▪ Resin transfer molding (RTM)/filament winding (FW)/sheet molding compound (SMC)/prepreg/pultrusion
<ul style="list-style-type: none"> ▪ Limited structural components ▪ Neat resin + nanoparticles ▪ Commodity: high-performance areas for automotive, appliance housings, toys 	<ul style="list-style-type: none"> ▪ Many structural components ▪ Neat or fiber reinforced + nanoparticles ▪ Commodity: advanced materials for construction, marine, aircraft, aerospace

Application requirements vary widely; fortuitously, plastic materials can be formulated to meet these different business opportunities. It remains for designers to select from the array of thermoplastic materials that are available to meet the particular needs of their applications.

Many thermoplastics have been nanomodified into polymer nanocomposites by incorporating nanoparticles into the polymers as shown in Table 3.2. Several of these nanomaterials will be described in detail in Chaps. 4 through 7.

3.2.2 Thermoset-based nanocomposites

Thermosetting type resins consist of solid, semi-solid, or liquid organic reactive intermediate material that cures or crosslinks into a high

TABLE 3.2 Thermoplastic-Based Nanocomposite Examples

Thermoplastic polymer	Reference
Acetal (POM)	1
Biodegradable polymers	2
Cellulose	3
Fluoropolymers	4
Polyamide	5, 6
Polyacrylonitrile	7
Polyamide-imide (PAI)	8
Polyarylate	9
Polybenzimidazole (PBI)	10
Polybutylene (PB)	11
Polycarbonate (PC)	12, 13
Polyester thermoplastic	14
Polyetherimide (PEI)	15
Polyethylene (PE)	16
Polyethylene copolymer	17
Polyimide (PI)	18
Polyketone	19
Poly(methylmethacrylate) (PMMA)	20
Polymethylpentene (PMP)	21
Polyphenylene oxide (PPO)	22
Polyphenylene sulphide (PPS)	23
Polypropylene (PP)	24
Polyurethane (PUR)	25
Acrylonitrile butadiene styrene (ABS) terpolymer	26, 27
Polystyrene (PS)	28
Styrene-acrylonitrile copolymer (SAN)	29, 30
Sulfone-based resin [polyether sulfone (PES)]	31
Sulfone-based resin [polysulfone (PSU)]	32
Vinyl-based resin [polyvinyl chloride (PVC)]	33
Vinyl-based resin (chlorinated PVC)	34
Other polymer blend	35

molecular weight product with no observable melting point. The basic characteristic of these intermediate reactive thermosetting resins is that they will, upon exposure to elevated temperature from ambient to above 450°F, undergo an irreversible chemical reaction often referred to as *polymerization*, or *cure*. Each family member has its own set of individual chemical characteristics based on its molecular structure and its ability to either homopolymerize, copolymerize, or both. This transformation process separates the thermosets from the thermoplastic polymers. The important beneficial factor lies in the inherent enhancement of the physical, electrical, thermal, and chemical properties of thermoset resins because of that chemical cross-linking polymerization reaction, which contributes to their ability to maintain and retain these enhanced properties when exposed to severe environmental conditions.

An intermediate reactive thermosetting species is defined as a liquid, semi-solid, or solid composition capable of curing at some defined temperature that can be from ambient to several hundred degrees and cannot be reshaped by subsequent reheating. In general, these intermediate reactive thermosetting compositions contain two or more components: a reactive resinous material with a curing agent that causes the intermediate material to polymerize (cure) at room temperature, or a low molecular weight resinous material and curing agent that, when subjected to elevated temperatures, will commence polymerization and cure.

Several thermosetting resins have been nanomodified into polymer nanocomposites by introducing the nanoparticle into the thermosetting resin as shown in Table 3.3. These intermediate thermosetting nanocomposites can be impregnated into fiber reinforcements such as glass, silica, quartz, carbon/graphite, aramid, poly(p-phenylene-2-6-benzobisoxazole) (PBO), polyethylene, boron, or ceramic and upon

TABLE 3.3 Thermoset-Based Nanocomposite Examples

Thermoset resin	Reference
Aminos: urea and melamine	36, 37
Bismaleimide (BMI)	38
Epoxy	39, 40
Phenolic	41, 42
Polyesters (thermosetting)	43
Vinyl ester	44
Polyimide (thermosetting)	45
Polyurethane	46, 47
Silicone	48
Cyanate ester and phenolic triazine	49, 50
Others	51, 52

curing lead to laminates or nanomodified polymer matrix composites (PMCs). Several of these nanomaterials will be described in detail in Chaps. 4 through 7.

3.2.3 Elastomer-based nanocomposites

Another important group of polymers is the group that is elastic or rubberlike, known as elastomers. These elastomeric materials can be block copolymers or multi-phase systems containing soft (low T_g) segments and hard segments (high T_g , possibly crystalline). They are processable under thermoplastic conditions. A few elastomers have been nanomodified into elastomer nanocomposites as shown in Table 3.4. Several of these nanomaterials will be described in detail in Chaps. 4 through 7. For completeness, some rubber materials (synthetic, isoprene, natural, etc.) that are nanomodified are also listed in Table 3.4.

TABLE 3.4 Elastomer-Based Nanocomposite Examples

Elastomer type	Polymer	Reference
Thermoplastic elastomers (TPEs)	Styrenics	53
Thermoplastic elastomers (TPEs)	Olefenics	54
Thermoplastic polyolefin elastomers (TPOs)		55
Polyurethane thermoplastic elastomers (TPUs)	Copolyesters	56–58
Polyurethane thermoplastic elastomers (TPUs)	Polyamides	59
Thermoplastic vulcanicate (TPV)		60
Synthetic rubbers (SRs)	Acrylonitrile butadiene copolymer	61
Synthetic rubbers (SRs)	Butadiene rubber (BR)	62
Synthetic rubbers (SRs)	Butyl rubber	63
Chlorosulfonated polyethylene (CSM)		64
Epichlorohydrin (ECH, ECO)		65, 66
Ethylene propylene copolymer (EPDM)		58, 67, 68
Fluoroelastomer (FKM)		69
Polyacrylate acrylic rubber (ACM)		70
Polychloroprene (neoprene) (CR)		71
Polyisoprene (IR)		72
Polysulfide rubber (PSR)		73
Silicone rubber (SiR)		74
Styrene butadiene rubber (SRB)		75
Natural rubber (NR)		76

3.3 Summary

Scientists and engineers can develop formulations for a range of polymer nanocomposites to fit their requirements and applications. The challenge is to select the baseline polymers with the proper nanoparticles to solve specific problems. Processing and morphological characterization are the keys to understanding the fundamentals of this new class of nanomaterials. These topics will be further explored in later chapters.

References

1. C. Sanchez, B. Julian, P. Belleville, and M. Popall, "Applications of Hybrid Organic-Inorganic Nanocomposites," *J. Mater. Chem.* **15**:3559–3592 (2005).
2. S. Kalambur, S. H. S. Rizvi, "Biodegradable and Functionally Superior Starch-Polyester Nanocomposites from Reactive Extrusion," *J. Appl. Polym. Sci.* **96**:1072–1082 (2005).
3. X. Liu, Q. Wu, and L. A. Berglund, "Cellulose Nanocomposites," presented at: Seventh International Conference on Woodfiber-Plastic Composites, Madison, WI, 2003, pp. 213–216.
4. H. Shah, R. Szerw, D. Carroll, L. S. Goldner, J. Hwang, J. Ballato, and D. W. Smith Jr., "Fluoropolymer Nanotube Composites for Coatings and Nanoscopic Probes," *Polym. Mater. Sci. Eng.* **82**:300 (2000).
5. K. Masenelli-Varlot, E. Reynaud, G. Vigier, and J. Varlet, "Mechanical Properties of Clay-Reinforced Polyamide," *J. Polym. Sci. Part B: Polym. Phys.* **40**:272–283 (2001).
6. J. H. Koo, L. A. Pilato, G. Wissler, J. Cheng, D. Ho, K. Nguyen, H. Stretz, and Z. P. Luo, "Flammability and Mechanical Properties of Nylon 11 Nanocomposites," *Proc. SAMPE 2005 ISSE*, SAMPE, Covina, CA, 2005.
7. T. Yu, J. Lin, J. Xu, T. Chen, and S. Lin, "Novel Polyacrylonitrile Nanocomposites Containing Na-Montmorillonite and Nano SiO₂ Particle," *Polymer* **46**:5695–5697 (2005).
8. A. Ranade, N. A. D'Souza, and B. Gnade, "Exfoliated and Intercalated Polyamide-Imide Nanocomposites with Montmorillonite," *Polymer* **43**:3759–3766 (2002).
9. A. P. Krasnov, E. E. Said-Galiev, L. N. Nikitin, O. V. Afonicheya, I. O. Volkov, V. K. Popoy, V. N. Bagratashvili, and A. D. Aliev, "Friction and Wear of the Polyarylate Impregnated by Copper Hexafluoroacetylacetonate in Supercritical CO₂-Solution," *Trenie I Iznos* **19**:90–96 (1998).
10. A. Gultek, M. G. Icduygu, and T. Seekin, "Preparation and Characterization of Polybenzimidazole-Clay Hybrid Materials," *Mater. Sci. Eng. Part B: Solid-State Mater. Adv. Tech.* **B107**:166–171 (2004).
11. Y.-W. Chang, S. Kim, and Y. Kyung, "Poly(Butylene Terephthalate)-Clay Nanocomposites Prepared by Melt Intercalation: Morphology and Thermomechanical Properties," *Polym. Int.* **54**:348–353 (2005).
12. P. J. Yoon, D. L. Hunter, and D. R. Paul, "Polycarbonate Nanocomposites: Part 1. Effect of Organoclay Structure on Morphology and Properties," *Polymer* **44**:5323–5339 (2003).
13. P. J. Yoon, D. L. Hunter, and D. R. Paul, "Polycarbonate Nanocomposites: Part 2. Degradation and Color Formation," *Polymer* **44**:5341–5354 (2003).
14. J.-H. Chang, B.-S. Seo, and D.-H. Hwang, "An Exfoliation of Organoclay in Thermotropic Liquid Crystalline Polyester Nanocomposites," *Polymer* **43**:2969–2974 (2002).
15. J. Lee, T. Takekoshi, and E. P. Giannelis, "Fire Retardant Polyetherimide Nanocomposites," *Mater. Res. Soc. Symp. Proc.* **457**:513–518 (1997).

16. S. Su, D. D. Jiang, and C. A. Wilkie, "Poly(Methyl Methacrylate), Polypropylene and Polyethylene Nanocomposite Formation by Melt Blending Using Novel Polymerically-Modified Clays," *Polym. Degrad. Stab.* **83**:321–331 (2004).
17. B. Liao, M. Song, H. Liang, and Y. Pang, "Polymer-Layered Silicate Nanocomposites. 1. A Study of Poly(Ethylene Oxide)/Na⁺-Montmorillonite Nanocomposites as Polyelectrolytes and Polyethylene-block-poly(ethylene glycol) Copolymer/Na⁺-Montmorillonite Nanocomposites as Fillers for Reinforcement of Polyethylene," *Polymer* **42**:10007–10011 (2001).
18. T. Agag, T. Koga, and T. Takeichi, "Studies on Thermal and Mechanical Properties of Polyimide-Clay Nanocomposites," *Polymer* **42**:3399–3408 (2001).
19. N. Bulakh, S. M. Kulkarni, J. P. Jog, and R. V. Chaudhari, "Preparation and Characterization of Polyketone/Clay Nanocomposites," *J. Macromol. Sci. Part B: Phys.* **B42**:963–973 (2003).
20. Q. Zhao and E. T. Samulski, "In-Situ Polymerization of Poly(Methyl Methacrylate)/Clay Nanocomposites in Supercritical Carbon Dioxide," *Macromolecules* **38**:7967–7971 (2005).
21. S. D. Wanjale and J. P. Jog, "Poly(4-Methyl-1-Pentene)/Clay Nanocomposites: Effect of Organically Modified Layered Silicates," *Polym. Int.* **53**:101–105 (2004).
22. Y. Li and H. Shimizu, "Novel Morphologies of Poly(Phenylene Oxide) (PPO)/Polyamide 6 (PA6) Blend Nanocomposites," *Polymer* **45**:7381–7388 (2004).
23. M. H. Cho and S. Bahadur, "Study of the Tribological Synergistic Effects in Nano CuO-Filled and Fiber-Reinforced Polyphenylene Sulfide Composites," *Wear* **258**:835–845 (2005).
24. J.-M. Hwu and G.-J. Jiang, "Preparation and Characterization of Polypropylene-Montmorillonite Nanocomposites Generated by In-Situ Metallocene Catalyst Polymerization," *J. Appl. Polym. Sci.* **95**:1228–1236 (2005).
25. A. Pattanayak and S. C. Jana, "Synthesis of Thermoplastic Polyurethane Nanocomposites of Reactive Nanoclay by Bulk Polymerization Methods," *Polymer* **46**:3275–3288 (2005).
26. L. W. Jang, C. M. Kang, and D. C. Lee, "A New Hybrid Nanocomposite Prepared by Emulsion Copolymerization of ABS in the Presence of Clay," *J. Polym. Sci. Part B: Polym. Phys.* **39**:719–727 (2001).
27. H. A. Stretz, D. R. Paul, and P. E. Cassidy, "Poly(styrene-co-acrylonitrile)/Montmorillonite Organoclay Mixtures: A Model System for ABS Nanocomposites," *Polymer* **46**:3818–3830 (2005).
28. A. B. Morgan, L.-L. Chu, and J. D. Harris, "A Flammability Performance Comparison between Synthetic and Natural Clays in Polystyrene Nanocomposites," *Fire and Mater.* **29**:213–229 (2005).
29. M. H. Noh, L. W. Jang, and D. C. Lee, "Intercalation of Styrene-Acrylonitrile Copolymer in Layered Silicate by Emulsion Polymerization," *J. Appl. Polym. Sci.* **74**:179–188 (1999).
30. H. A. Stretz, D. R. Paul, R. Li, H. Keskkula, and P. E. Cassidy, "Intercalation and Exfoliation Relationships in Melt-Processed Poly(styrene-co-acrylonitrile)/Montmorillonite Nanocomposites," *Polymer* **46**:2621–2637 (2005).
31. J. Lu, M. Qin, Y. Ke, Z. Qi, and X. Yi, "Study on Polymer Layered Silica Nanocomposites of a Few Typical High Performance Plastic Resins," *Gaofenzi Xuebao* **1**:73–77 (2002).
32. G. S. Sur, H. L. Sun, S. G. Lyu, and J. E. Mark, "Synthesis, Structure, Mechanical Properties, and Thermal Stability of Some Polysulfone/Organo-Clay Nanocomposites," *Polymer* **42**:9783–9789 (2001).
33. M. Lee, B.-K. Lee, and K.-D. Choi, "Foam Compositions of Polyvinyl Chloride Nanocomposites," *PCT Int. Appl. WO Patent* 2004074357, 2004.
34. Y. Kim and J. L. White, "Melt-Intercalation Nanocomposites with Chlorinated Polymers," *J. Appl. Polym. Sci.* **90**:1581–1588 (2003).
35. A. H. Tsou and A. J. Dias, "Low Permeability Nanocomposites," *PCT Int. Appl. WO Patent* 2002100923, 2002.

36. S. Ananthakumar, K. Prabhakaran, U. S. Hareesh, P. Manohar, and K. G. K. Warriar, "Gel Casting Process for Al_2O_3 -SiC Nanocomposites and Its Creep Characteristics," *Mater. Chem. Phys.* **85**:151–157 (2004).
37. C. Zilg, R. Mulhaupt, and J. Finter, "Synthesis of Melamine-Modified Organophilic Layered Phyllosilicates in Fabrication of Nanocomposites and Molded Polymer Parts," *PCT Int. Appl.* WO Patent 2000044669, 2000.
38. J. Meng and X. Hu, "Synthesis and Exfoliation of Bismaleimide-Organoclay Nanocomposites," *Polymer* **45**:9011–9018 (2004).
39. F. Bondioli, V. Cannillo, E. Fabbri, and M. Messori, "Epoxy-Silica Nanocomposites: Preparation, Experimental Characterization, and Modeling," *J. Appl. Polym. Sci.* **97**:2382–2386 (2005).
40. J. H. Koo, L. A. Pilato, G. Wissler, A. Lee, A. Abusafieh, and J. Weispfenning, "Epoxy Nanocomposites for Carbon Fiber Reinforced Polymer Matrix Composites," *Proc. SAMPE 2005 ISSE*, SAMPE, Covina, CA, 2005.
41. J. Pappas, K. Patel, and E. B. Nauman, "Structure and Properties of Phenolic Resin/Nanoclay Composites Synthesized by In-Situ Polymerization," *J. Appl. Polym. Sci.* **95**:1169–1174 (2005).
42. J. H. Koo, H. Stretz, J. Weispfenning, Z. P. Luo, and W. Wootan, "Nanocomposite Rocket Ablative Materials: Subscale Ablation Test," *Proc. SAMPE 2004 ISSE*, SAMPE, Covina, CA, 2004.
43. Y. Zhang, S. Fu, C. Huang, L. Li, G. Li, and Q. Yan, "Advances in Thermosetting Polymer-Based Nanocomposites," *Jinshu Xuebao* **40**:833–840 (2004).
44. G. Chigwada, P. Jash, D. D. Jiang, and C. A. Wilkie, "Fire Retardancy of Vinyl Ester Nanocomposites: Synergy with Phosphorus-Based Fire Retardants," *Polym. Degrad. Stab.* **89**:85–100 (2005).
45. Y. Zhang, S. Fu, C. Huang, L. Li, G. Li, and Q. Yan, "Advances in Thermosetting Polymer-Based Nanocomposites," *Jinshu Xuebao* **40**:833–840 (2004).
46. D. Martin, P. Halley, R. Truss, M. Murphy, S. Meusburger, and O. Jackson, "The Development of Nanocomposites to Enhance Functionality of Materials for Rotational Molding," Annual Tech. Conf.—Soc. Plastics Eng., 60th, 1:1292–1295 (2002).
47. Z. Wang, P. C. LeBaron, and T. J. Pinnavaia, "Nanolayer Reinforcement of Thermoset Polymers," Eighth Int. Additives Conference, 1999, Paper 10/1–10/9.
48. S. Wang, C. Long, X. Wang, Q. Li, and Z. Qi, "Synthesis and Properties of Silicone Rubber/Organomontmorillonite Hybrid Nanocomposites," *J. Appl. Polym. Sci.* **69**:1557–1561 (1998).
49. S. Ganguli, D. Dean, K. Jordan, G. Price, and R. Vaia, "Chemorheology of Cyanate Ester-Organically Layered Silicate Nanocomposites," *Polymer* **44**:6901–6911 (2003).
50. J. H. Koo, L. A. Pilato, P. Winzek, S. Shivakumar, C. U. Pittman, Jr., and Z. P. Luo, "Thermo-Oxidative Studies of Nanomodified Carbon/Carbon Composites," *Proc. SAMPE 2004 ISSE*, SAMPE, Covina, CA, 2004.
51. C. Y. Wang and T. Zhao, "Polynaphthoxazine–Montmorillonite Nanocomposites: Synthesis and Characterization," *Chinese Chem. Letters* **12**:935–936 (2001).
52. C. Wang, T. Zhao, B. Han, and Y. Ke, "Polynaphthoxazine–Montmorillonite Nanocomposites: Synthesis and Characterization," *Gaofenzi Xuebao* **2**:217–220 (2002).
53. H. Xu, Y. Li, and D. Yu, "Studies on the Poly(styrene-*b*-butadiene-*b*-styrene)/Clay Nanocomposites Prepared by Melt Intercalation," *J. Appl. Polym. Sci.* **98**:146–152 (2005).
54. B. Herrero, M. Arroyo, and M. A. Lopez-Manchado, "Preparation and Characterization of Thermoplastic Vulcanizates-Organoclay Nanocomposites," *Mater. Sci. Forum* **480–481**:333–338 (2005).
55. P. D. Fasulo, W. R. Rodgers, R. A. Ottaviani, and D. L. Hunter, "Extrusion Processing of TPO Nanocomposites," *Polym. Eng. Sci.* **44**:1036–1045 (2004).
56. B. Finnigan, K. Jack, K. Campbell, P. Halley, R. Truss, P. Casey, D. Cookson, S. King, and D. Martin, "Segmented Polyurethane Nanocomposites: Impact of Controlled Particle Size Nanofillers on the Morphological Response to Uniaxial Deformation," *Macromolecules* **38**:7386–7396 (2005).

57. J. H. Koo, D. Marchant, G. Wissler, P. Ruth, S. Barker, R. Blanski, and S. Phillips, "Polymer Nanostructured Materials for Solid Rocket Motor Insulation: Processing, Microstructure, and Mechanical Properties," *Proc. 52nd JANNAF Propulsion Meeting*, CPIA, Columbia, MD, 2004.
58. R. Blanski, J. H. Koo, P. Ruth, N. Nguyen, C. Pittman, and S. Phillips, "Polymer Nanostructured Materials for Solid Rocket Motor Insulation: Ablation Performance," *Proc. 52nd JANNAF Propulsion Meeting*, CPIA, Columbia, MD, 2004.
59. J. Kelnar, J. Kotek, L. Kapralkova, and B. S. Munteanu, "Polyamide Nanocomposites with Improved Toughness," *J. Appl. Polym. Sci.* **96**:288–293 (2005).
60. J. K. Mishra, G.-H. Kim, I. Kim, I.-J. Chung, and C.-S. Ha, "A New Thermoplastic Vulcanizate (TPV)/Organoclay Nanocomposite: Preparation, Characterization, and Properties," *J. Polym. Sci. Part B: Polym. Phys.* **42**:2900–2908 (2004).
61. S. Kaang, J. Wonseop, M. Abdul Kader, and C. Nah, "Effects of Blend Composition and Mixing Method on Mechanical and Morphological Properties of Zinc Dimethacrylate-Reinforced Acrylonitrile-Butadiene Copolymer Nanocomposites," *Polym.-Plastics Tech. Eng.* **43**:1517–1538 (2004).
62. L. Zheng, A. F. Xie, and J. T. Lean, "Polystyrene Nanoparticles with Anionically Polymerized Polybutadiene Brushes," *Macromolecules* **37**:9954–9962 (2004).
63. J. Jin, V. Nguyen, W. Gu, X. Lu, B. J. Elliott, and D. L. Gin, "Cross-Linked Lyotropic Liquid Crystal-Butyl Rubber Composites: Promising 'Breathable' Barrier Materials for Chemical Protection Applications," *Chem. Mater.* **17**:224–226 (2005).
64. G. Markovic, B. Radovanovic, J. B. Simendic, and M. Marinovic-Cincovic, "Thermostability and Surface Morphology of Nano- and Micro-Filled NBR/CSM and CR/CSM Rubber Blends," *J. Serbian Chem. Soc.* **69**:167–173 (2004).
65. C. H. Lee, H. B. Kim, S. T. Lim, H. J. Choi, and M. S. Jhon, "Biodegradable Aliphatic Polyester-Poly(Epichlorohydrin) Blend/Organoclay Nanocomposites: Synthesis and Rheological Characterization," *J. Mater. Sci.* **40**:3981–3985 (2005).
66. S. T. Lim, C. H. Lee, H. B. Kim, H. J. Choi, and M. S. Jhon, "Polymer/Organoclay Nanocomposites with Biodegradable Aliphatic Polyester and Its Blends: Preparation and Characterization," *Mater. Res. Innov.* **8**:130–131 (2004).
67. H. Acharya, M. Pramanik, S. K. Srivastava, and A. K. Bhowmick, "Synthesis and Evaluation of High-Performance Ethylene-Propylene-Diene-Terpolymer/Organoclay Nanoscale Composites," *J. Appl. Polym. Sci.* **93**:2429–2436 (2004).
68. P. Ruth, R. Blanski, and J. H. Koo, "Preparation of Polymer Nanostructured Materials for Solid Rocket Motor Insulation," *Proc. 52nd JANNAF Propulsion Meeting*, CPIAC, Columbia, MD, 2004.
69. M. A. Kader and C. Nah, "Influence of Clay on the Vulcanization Kinetics of Fluoroelastomer Nanocomposites," *Polymer* **45**:2237–2247 (2004).
70. A. Bandyopadhyay, M. De Sarkar, and A. K. Bhowmick, "Synthesis and Characterization of Acrylic Rubber/Silica Nanocomposites by Sol-Gel Technique," Technical Papers: ACS, Rubber Division (Fall Technical Program), 124–144, 2003.
71. Y. Kim and J. L. White, "Melt-Intercalation Nanocomposites with Chlorinated Polymers," *J. Appl. Polym. Sci.* **90**:1581–1588 (2003).
72. M. Knite, V. Teteris, B. Polyakov, and D. Ertis, "Electric and Elastic Properties of Conductive Polymeric Nanocomposites on Macro- and Nanoscales," *Mater. Sci. Eng. C: Biomimetic Supramol. Sys.* **C19**:15–19 (2002).
73. J. Xue and F. Xue, "New Anticorrosive and Scale-Inhibiting Water-Injection Tube of Nano Ti/Polymer Composite," Faming Zhuanli Shenging Gongkai Shuomingshu, Patent CN 1482190, 2004.
74. A. H. El-Hag, L. C. Simon, S. H. Jayaram, and E. A. Cherney, "Physicochemical Properties of Silica Filled Silicone Rubber Nanocomposites," Annual Report: Conference on Electrical Insulation and Dielectric Phenomena, 688–691, 2004.
75. L. Zhang, Y.-Z. Wang, Y.-G. Wang, S. Yuan, and D. Yu, "Morphology and Mechanical Properties of Clay/Styrene-Butadiene Rubber Nanocomposites," *J. Appl. Polym. Sci.* **78**:1873–1878 (2000).
76. M. A. Lopez-Manchado, B. Herrero, and M. Arroyo, "Organoclay- Natural Rubber Nanocomposites Synthesized by Mechanical and Solution Mixing Methods," *Polym. Int.* **53**:1766–1772 (2004).

This page intentionally left blank

Processing of Nanomaterials

4.1 Synthesis Methods

After the selection of a particular polymer matrix and the appropriate nanoparticles for a specific application, the next challenge is to determine the proper synthesis method to create the desired polymer nanocomposite. Figure 4.1 shows the processing challenge of transforming $8\mu\text{m}$ particles into > 1 million platelets. In general, for solid

Challenge

Age-old Blend Questions:

- Process from Agglomerate to Dispersion: Activation Energy?
- Final Dispersion: Thermodynamic vs. Kinetic Stability?

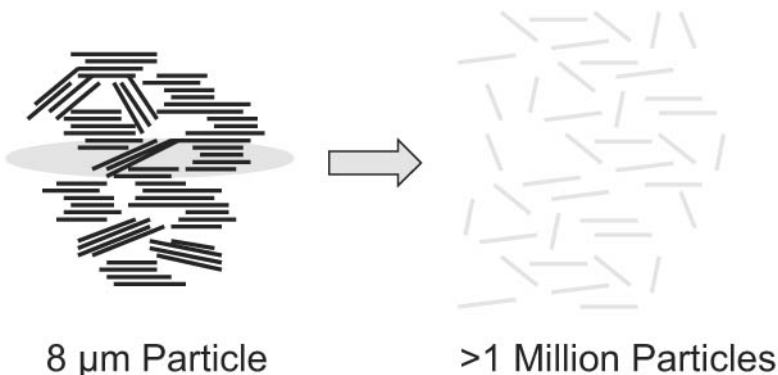


Figure 4.1 Processing challenge of layered silicate. (Courtesy of SCP.)

thermosetting reactive prepolymers or thermoplastic polymers with solid nanoparticles, the following processing methods are recommended:

- Solution intercalation
- Melt intercalation
- Roll milling

For liquid thermosetting reactive prepolymers or thermoplastic polymers with solid nanoparticles, the following processing methods are recommended:

- In-situ polymerization
- Emulsion polymerization
- High-shear mixing

Examination of Figs. 4.2 and 4.3 identifies the “real” challenge that confronts the investigator as conditions are considered to suitably disperse the chosen polymer into the aggregated or layered nanoparticle(s). Solution intercalation, mesophase mediated (emulsion or suspension), in-situ polymerization, and melt processing are considered convenient methods to disperse layered silicates into nanocomposites in

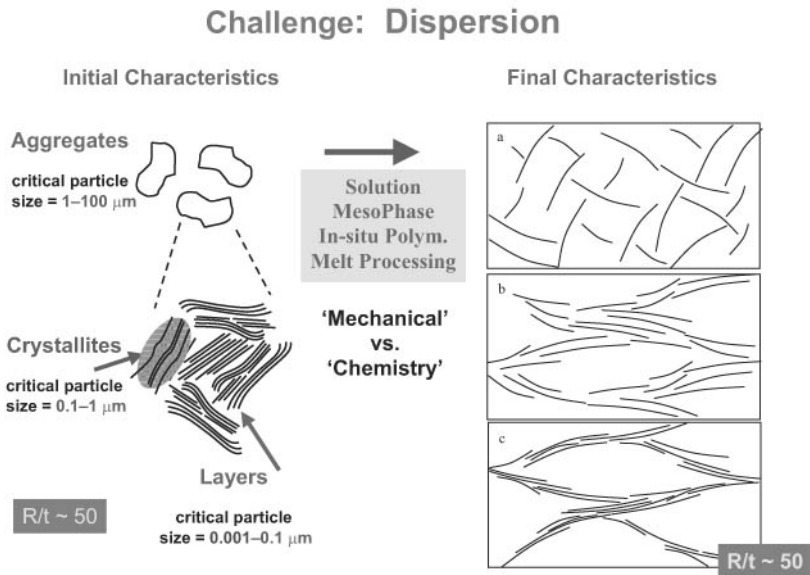


Figure 4.2 Dispersion of layered silicates using different processing methods. (Courtesy of R. Vaia.)

an intercalated or exfoliated state (Fig. 4.3). As it will be mentioned later, optimum mechanical properties of the resulting nanocomposite are obtained when the layered silicate is fully exfoliated with polymer inserted into the silicate galleries. Intercalation of layered silicate with polymer is somewhat beneficial in polymer properties enhancement but not as optimum as exfoliated systems.¹⁻⁹ An excellent review by Alexandre and Dubois lists recent developments in synthesis, properties, and future applications of polymer-layered silicate nanocomposites.⁸ Different approaches and a wide range of polymer matrices (i.e., thermoplastics, thermosets, and elastomers) were considered. Parallel to process selection is the use of WAXD and TEM (Chap. 5) to characterize the uniformity or lack thereof of the dispersion. TEM is vital for an appreciation of “viewing” an intercalated or exfoliated nanocomposite system.

Two types of structures are obtained, namely intercalated nanocomposites, where the polymer chains are sandwiched between silicate layers, and exfoliated nanocomposites, where the separated, individual silicate layers are more or less uniformly dispersed in the polymer matrix. This new family of materials exhibits enhanced properties such as increased Young’s modulus and storage modulus, increased thermal stability and gas barrier properties, and good flame retardancy at a low filler level, usually about 5 wt%.

Sanchez et al. surveyed the applications of hybrid organic-inorganic nanocomposites in their recent review.⁹ This new generation of hybrid

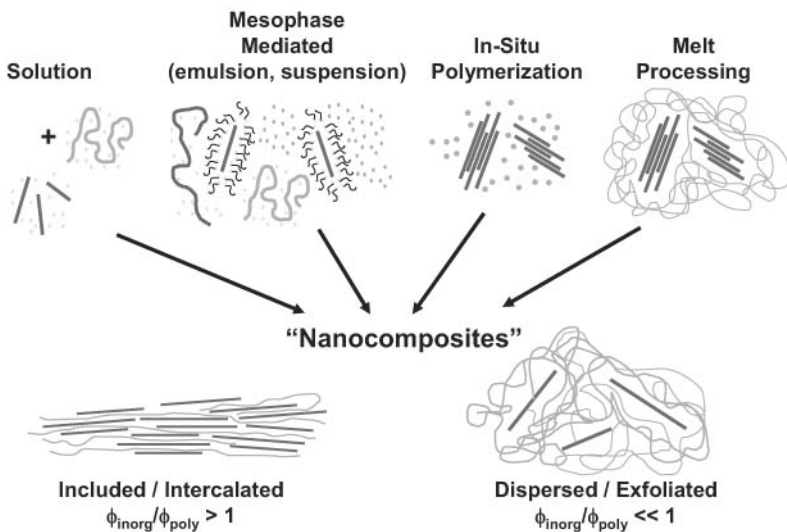


Figure 4.3 Various synthesis methods to disperse layered silicate into nanocomposites. (Courtesy of R. Vaia.)

materials is opening many promising applications in several diverse areas: optics, electronics, ionics, mechanics, energy, environment, biology, medicine, functional smart coatings, fuel and solar cells, catalysts, sensors, and more. These hybrid materials will be described in Chap. 8.

In the following sections, we will show how to use these six synthesis approaches and different types of nanoparticles to form polymer nanocomposites.

4.2 Solution Intercalation

The layered silicate is exfoliated into single layers using a solvent in which the polymer (or a thermosetting reactive prepolymer, in the case of insoluble polymers such as polyimide) is soluble. It is well known that such layered silicates, due to the weak forces that stack the layers together, can be easily dispersed in an adequate solvent. The polymer then absorbs onto the delaminated sheets, and when evaporated (or the mixture precipitated), the sheet reassembles, sandwiching the polymer to form an ordered, multilayered structure.

4.2.1 Solution intercalation from polymers in solution

This technique has been widely used with water-soluble polymers to produce intercalated nanocomposites^{10,11} based on polyvinyl alcohol (PVOH),^{12,13} polyethylene oxide (PEO),¹³⁻¹⁷ polyvinyl pyrrolidone (PVPyr),¹⁸ or polyacrylic acid (PAA).¹⁷ When polymeric aqueous solutions are added to dispersions of fully delaminated sodium layered silicate, the strong interaction existing between the water soluble macromolecules and the silicate layers often triggers the reaggregation of the layers as it occurs for PVPyr¹⁸ or PEO.¹³ In the presence of PVOH, the silicate layers are colloiddally dispersed resulting in a colloidal distribution of nanoparticles in PVOH.¹³

Polymer intercalation using this technique can also be performed in organic solvents. Polyethylene oxide has been successfully intercalated in sodium MMT and sodium hectorite by dispersion in acetonitrile,¹⁹ allowing stoichiometric incorporation of one or two polymer chains between the silicate layers and increasing the intersheet spacing from 0.98 to 1.36 and 1.71 nm, respectively. Study of the chain conformation using two-dimensional, double-quantum nuclear magnetic resonance (NMR) on ¹³C-enriched PEO intercalated in sodium hectorite²⁰ reveals that the conformation of the -OC-CO- bonds of PEO is $90 \pm 5\%$ gauche, inducing constraints on the chain conformation in the interlayer.

4.2.2 Solution intercalation from prepolymers in solution

The Toyota Research group was the first to use solution intercalation technique to produce polyimide (PI) nanocomposites.²¹ The polyimide-montmorillonite (MMT) nanocomposite has been synthesized by mixing in dimethylacetamide, a modified montmorillonite with the polyimide precursor, i.e., a polyamic acid obtained from the step polymerization of 4,4'-diaminodiphenyl ether with pyromellitic dianhydride. The organic-modified montmorillonite was prepared by previous intercalation with dodecylammonium hydrochloride. After elimination of the solvent, an organoclay-filled polyamic acid film was recovered, which was thermally treated up to 300°C to trigger the imidization reaction and to produce the polyimide nanocomposite. The WAXD patterns (Chap. 5) of these filled PI films do not show any diffraction-peak-typical structure of an intercalated morphology. This led the authors to conclude that an exfoliated structure was formed and explained the excellent gas barrier properties of the resultant films. Enhanced properties and excellent gas barrier performance are attributable to the exfoliated nanocomposite structure. This experiment has been extended to other layered silicates (hectorite, saponite, and synthetic mica) with different aspect ratios, as shown in Table 4.1.²²

X-ray diffraction (see Chap. 5 where absence of a peak for layered silicates is strong evidence for exfoliation) data of the resulting polyimide-based nanocomposites show no noticeable peak, indicating a possible exfoliated structure for the montmorillonite and the synthetic mica. For both hectorite and saponite, a broad peak, centered on a value of 15 Å, is observed, indicating that for these layered silicates, polymer intercalation occurs, probably mixed with some exfoliation. For saponite, the measured interlayer spacing is even smaller than the value measured for the starting organically modified clay (18 Å), suggesting that the organic cation may have been expelled from the clay interlayer during the imidization reaction.

TABLE 4.1 Nature, CEC, and Length of the Layered Silicates Used in the Synthesis of Polyimide²²

Layered silicate	CEC (meq/100 g)	Length of dispersed particles (angstroms)*
Hectorite Na ⁺	55	460
Saponite Na ⁺	100	1650
Montmorillonite Na ⁺	119	2180
Synthetic mica Na ⁺	119	12,300

*Longer particle dimension as determined by TEM observation.

4.3 Melt Intercalation

The layered silicate is mixed with the solid polymer matrix in the molten state. Under these conditions and if the layer surfaces are sufficiently compatible with the selected polymer, the polymer can be inserted into the interlayer space and form either an intercalated or an exfoliated nanocomposite. No solvent is required.

4.3.1 Thermoplastic nanocomposites

Vaia and Giannelis²³ have studied polystyrene (PS) as the matrix for dispersing different types of clays. Li-fluorohectorite [cation exchange (CEC) = 150 meq/100 g], saponite (100 meq/100 g), and sodium montmorillonite (80 meq/100 g) were modified accordingly, using various ammonium cations: dioctadecyldimethylammonium, octadecyltrimethylammonium, and a series of primary alkylammonium cations with carbon chains of 6, 9–16, and 18 carbon atoms. The nanocomposites were synthesized by statically annealing (without any mixing or shearing) a pelletized intimate mix of the modified silicate in PS ($M_w = 30,000$, $M_w/M_n = 1.06$) under vacuum at 170°C, a temperature well above the PS glass transition, as shown in Table 4.2.²⁴

Comparison of the first three entries indicates that, for a given alkyl surfactant, increasing the cation exchange from 80 to 120 meq/100 g allows PS intercalation to occur. At a low CEC and for single alkyl chain build up cations (entries 1 and 2), no intercalation is observed. Under these conditions, the aliphatic alkyl chain of the organic cation adopts a pseudo-monolayer arrangement characterized by low gallery height. Intercalation can take place at lower CECs when the clay surface

TABLE 4.2 Characteristics of Polystyrene Melt Intercalation Within Octadecylammonium Modified Clays.

Entry	Clay (CEC in meq/100 g)*	Ammonium cation	Initial gallery height (nm)	Final gallery height (nm)	Net change (nm)
1	M (80)	PODA [†]	0.75	0.75	0
2	S (100)	PODA [†]	0.83	0.83	0
3	F (120)	PODA [†]	1.33	2.16	0.83
4	F (120)	QODA [‡]	1.57	2.69	1.12
5	M (80)	DODMDA [§]	1.43	2.25	0.82
6	S (100)	DODMDA [§]	1.50	2.35	0.85
7	F (120)	DODMDA [§]	2.85	2.85	0

*M = montmorillonite, S = saponite, F = fluorohectorite.

[†]PODA: primary octadecylammonium.

[‡]QODA: quaternized octadecylammonium.

[§]DODMDA: dioctadecyldimethylammonium.

possesses an ammonium cation bearing two long alkyl chains (entries 5 and 6). However, excessive packing of the chains all along the layer surface (high CEC and two long alkyl chains per cationic head, entry 7) leads to the formation of a nonintercalated structure, as predicted by the theory introduced by Vaia and Giannelis.²⁴ The authors also found that polymer intercalation depends on the length of the exchange ammonium cation as well as on the annealing temperature.

4.3.2 Elastomer nanocomposites

Burnside and Giannelis²⁵ have described the two-step preparation of silicon-rubber-based nanocomposites. First, silanol-terminated polydimethylsiloxane (PDMS, $M_w = 18,000$) was melt blended at room temperature with dimethyldiallowammonium-exchanged montmorillonite. Then the silanol end groups were cross-linked with tetrathylorthosilicate (TEOS) in the presence of tin bis(2-ethylhexanoate) as a catalyst at room temperature. To obtain exfoliated nanocomposites (as determined by absence of peak WAXD patterns, Chap. 5), several conditions were required, such as mixing the modified clay and PDMS under sonication (for better mixing) and with the addition of a small quantity of water extending/crosslinking TEOS end groups. The nature of both the silicone matrix and the clay modifier plays an important role. Neither exfoliation nor intercalation can occur if MMT is modified with a different surfacing agent, such as benzyl dimethyloctadecylammonium cation, or if too much water is added. On the other hand, only intercalation was observed when a PDMS-polydiphenylsiloxane random copolymer containing 14 to 18 mol% diphenylsiloxane units was used. The results stress the key importance of selecting the right match between the matrix and the organoclay to optimize the layered silicate exfoliation.

Elastomer nanocomposites and thermoplastic elastomer nanocomposites that possess enhanced ablation and fire retardancy characteristics were developed by the Air Force Research Laboratory/Polymer Working Group at Edwards AFB, CA.²⁶⁻³¹

4.4 Roll Milling

Three-roll milling is considered as low-shear mixing for incorporating solid nanoparticles into a liquid polymer, as compared to high-shear mixing, which will be discussed in Section 4.7.

Polymer nanocomposites were developed by incorporating different POSS nanostructured chemicals in Derakane™ Momentum™ 441-400 epoxy vinyl ester (EVE) resin.³² The various POSS polymers and monomers used in this study were polyphenylsilsesquioxane

uncured (phenyl resin), polyvinyl silsesquioxane uncured (vinyl resin), polyvinyl silsesquioxane fully cured (Firequench[®]), and vinyl-POSS-cage mixture (vinyl POSS). These formulations were prepared by blending POSS (15 wt%) into the EVE resin using three-roll milling, low-shear mixing, and solvent-assisted blending synthesis methods. Three-roll milling was the preferred method for this study. It is very fast, cost-effective, and results in the optimum POSS dispersion in the EVE resin. The E-glass-reinforced EVE-POSS nanocomposites exhibit better flammability properties than pure E-glass-reinforced Derakane Momentum 441-400 resin, with reduced smoke, a reduced heat release rate, and an increased ignition time using cone calorimetry. The EVE-POSS nanocomposites were reported to have equivalent or better mechanical, thermal, cure, and processing characteristics. The properties were also found to be comparable to or better than the halogenated EVE resin (Derakane Momentum 510A-40). The nanoreinforced polymers acquired fire retardancy via two major mechanisms: (a) reduced volatilization of fuel (organic monomer/polymer), and (b) the formation of thermo-oxidative stable, and nonpermeable surface chars.

A diglycidyl ether of bisphenol A (DGEBA) epoxy resin cured with methyl tetrahydrophthalic anhydride hardener was blended with Nanocor I.28E using three-roll milling.³³ Good dispersion was reported by the authors using this mixing technique.

4.5 Emulsion Polymerization

In a manner analogous to the solution intercalation technique, the layered silicate is dispersed in the aqueous phase, and the polymer nanocomposites are formed.

The emulsion polymerization technique has been used to study the intercalation of water insoluble polymers within Na⁺-MMT, which is well known to readily delaminate in water.³⁴⁻³⁶ Polymethyl methacrylate (PMMA) was first examined using this technique.³⁴ Emulsion polymerization was carried out in water in the presence of various amounts of MMT clay. Distilled methyl methacrylate monomer (MMA) was dispersed in the aqueous phase with the aid of sodium lauryl sulfate as a surfactant. Polymerization was conducted at 70°C for 12 hours, using potassium persulfate as the free-radical initiator. The resulting latex was coagulated, filtered, and dried under reduced pressure. The resulting composites were extracted with hot toluene for 5 days (Soxhlet extraction). The amounts of intercalated polymer were determined for both extracted and nonextracted materials and are shown in Table 4.3, with the molecular weights and polydispersities of the extracted polymers.

These results demonstrate that a portion of the PMMA chain remains immobilized onto and/or within the layered silicates and is not extracted. This finding is further confirmed by Fourier transform infrared spectroscopy (FTIR) of the extracted composite, which shows the absorption bands typical of PMMA chains. It can be observed that the relative content of clay does not substantially modify the PMMA molecular weights (M_w), the value of which is quite comparable to M_w of PMMA polymerized in the absence of clay (entry 1, Table 4.3). The presence of layered silicates does not seem to perturb the free-radical polymerization. Intercalation is evidenced by x-ray diffraction (WAXD), (Chap. 5) where an increase of about 5.5 Å is observed for PMMA 10, 20, and 30. This increase correlates reasonably well with the thickness of the polymer chain in its extended form. Differential scanning calorimetry (DSC) data obtained for the extracted nanocomposites did not show any glassy transition, in accordance with what is usually observed for intercalated polymers. Ion-dipole interactions are believed to be the driving force for the immobilization of the organic polymer chains that lay flat on the layered silicate surface.

4.6 In-Situ Polymerization

The layered silicate is swollen within the liquid monomer (or a monomer solution) so that the polymer formation can occur between the intercalated sheets. Polymerization can be initiated by different polymerization methods such as heat or radiation, diffusion of a suitable initiator, or an organic initiator or catalyst fixed through cationic exchange inside the inter layer before the swelling step of the monomer.

TABLE 4.3 Montmorillonite Feed Ratios, PMMA Contents in Nonextracted and Extracted Composites, Average Molecular Weights, and Polydispersities of Extracted PMMAs³⁴

Sample	Feed ratio of PMMA/clay (g/g)	PMMA content (wt%)* non-extracted	PMMA content (wt%)* extracted [†]	$M_n \times 10^{-3}$ (g/mol)	$M_w \times 10^{-3}$ (g/mol)	M_w/M_n
PMMA	100/0	—	—	23	160	6.6
PMMA10	100/10	87.4	58.7	44	250	5.8
PMMA20	100/20	79.3	49.6	60	200	3.4
PMMA30	100/30	60.4	33.4	63	150	2.4
PMMA40	100/40	58.6	22.8	82	390	4.8
PMMA50	100/50	46.1	18.4	38	290	7.6

*As determined by TGA.

[†]Composite recovered after Soxhlet extraction in toluene for 5 days.

4.6.1 Thermoplastic nanocomposites

Many “interlamellar” polymerization reactions were studied by various research groups in the 1960s and 1970s using layered silicate,^{11,37,38} but it is the work initiated by the Toyota research team^{39,40} about 15 years ago that the study of polymer-layered silicate nanocomposites became recognized. The Toyota team studied the Na-montmorillonite organically modified by protonated α,ω -amino acid ($^+\text{H}_3\text{N}-(\text{CH}_2)_{n-1}-\text{COOH}$, with $n = 2, 3, 4, 5, 6, 8, 11, 12, 18$) and swollen by the ϵ -caprolactam monomer at 100°C. Subsequently the nanomodified ϵ -caprolactam was transformed by ring opening polymerization to nylon-6-based nanocomposites.⁴⁰⁻⁴² A clear difference occurs in the swelling behavior between the montmorillonite with relatively short ($n < 11$) and longer alkyl chains, as shown in Table 4.4, indicating that a larger amount of monomer can be intercalated when longer alkyl chains are used.

Montmorillonite modified by 12-aminolauric acid ($n = 12$) was selected during the intercalative ring opening polymerization of ϵ -caprolactam.⁴⁰ The modified montmorillonite (12-Mont) was mixed with the monomer containing a small amount of 6-aminocaproic acid as a polymerization accelerator. The mixture was heated first at 100°C for 30 minutes, then at 250°C for 6 hours. The cooled and solidified product was crushed, washed with water at 80°C, and then dried. Depending on the amount of 12-Mont introduced, either exfoliated (for less than 15 wt%) or delaminated structure (from 15 to 70 wt%) was obtained, as evidenced by x-ray diffraction (WAXD) and transmission electron microscopy (TEM) measurements (Chap. 5). Comparison of the titrated amounts of COOH and NH_2 end groups present in the synthesized nanocomposites with given values, such as the cation exchange (CEC) of the montmorillonite used (119 meq/100 g), led to the conclusion that the COOH end groups present along the 12-Mont surface are

TABLE 4.4 Basal Spacing on Organomodified Montmorillonite in the Presence of ϵ -Caprolactam (ϵ -CLa) at 100°C

$^+\text{H}_3\text{N}-(\text{CH}_2)_{n-1}-\text{COOH}$ (n)	Interlayer spacing of the modified clay (Å)	Interlayer spacing when swollen by (ϵ -CLa) at 100°C (Å)
2	12.7	14.1
3	13.1	19.7
4	13.2	19.9
5	13.2	20.4
6	13.2	23.4
8	13.4	26.4
11	17.4	35.7
12	17.2	38.7
18	28.2	71.2

responsible for the initiation of polymerization. Nearly all of the $^+\text{NH}_3$ end groups present in the matrix should be interacting with the montmorillonite anions. Finally, the ratio of bonded to nonbonded polymer chains increased with the amount of incorporated MMT (from 32.3% of bonded chains for 1.5 wt% MMT to 92.3% of bonded chains for 59.6 wt% clay).

4.6.2 Thermoset nanocomposites

In-situ polymerization has also been explored to create thermoset-based nanocomposites. This method has been extensively used for the production of both intercalated and exfoliated epoxy-based nanocomposites. Messersmith and Giannelis⁴³ have analyzed the effects of different curing agents and conditions in the formation of epoxy nanocomposites based on the diglycidyl ether of bisphenol A (DGEBA) and a montmorillonite modified by bis(2-hydroxyethyl)methyl hydrogenated tallow alkyl ammonium cation. The observed increase in viscosity at relatively low shear rates and the transition of opaque to semi-transparent suspension indicated that the modified MMT clay dispersed quite readily in DGEBA when sonicated for a short period of time. The increase in viscosity was attributed to the formation of a "house-of-cards" structure, in which edge-to-edge and edge-to-face interactions between dispersed layers form percolation structures. WAXD patterns of uncured clay/DGEBA also indicate that intercalation occurred during mixing and that this intercalation improves as the temperature is increased from room temperature to 90°C.

4.6.3 Rubber modified epoxy nanocomposites

Lan and Pinnavaia⁴⁴ examined the formation of nanocomposites with a rubber-epoxy matrix obtained from DGEBA derivative (Epon 828) and cured with a polyether diamine (Jeffamine D2000) to obtain low glass transition temperature materials. Two montmorillonites modified by the protonated *n*-octylamine and the protonated *n*-octadecylamine, respectively, were used in this study. It was shown that depending on the alkyl chain length of the modified clays, an intercalated and partially exfoliated (*n*-octyl) or a totally exfoliated (*n*-octadecyl) nanocomposite can be obtained.

These authors have also studied other parameters such as the nature of alkylammonium cations present in the gallery and the effect of the cation-exchange capacity of the clay⁴⁵ when Epon 828 was cured with *m*-phenylene diamine. It was demonstrated that when mixed with the epoxide and variable length of the protonated primary alkylamine

(with 8, 10, 12, 16, or 18 carbons), the modified clays adopt a structure where the carbon chains are fully extended and oriented perpendicularly to the silicate plane incorporating a maximum of one monolayer of epoxide molecules.

4.7 High-Shear Mixing

The solid or liquid nanoparticles are mixed with the liquid polymer matrix using high-shear equipment (e.g., an IKA[®] mixer, IKA, Wilmington, NC). Under these conditions and if the surface treated nanoparticles are compatible with the selected polymer, the high-shear mixing will disrupt the nanoparticle aggregates and disperse the polymer matrix into the nanoparticle layers. An intercalated or an exfoliated nanocomposite will result. This technique may or may not, (especially in the case of water-based polymer) require solvent.

Mulhaupt et al.⁴⁶ used a mixture of two epoxy resins, tetraglycidyl 4,4'-diaminodiphenyl methane (TGDDM) and bisphenol-A-diglycidylether (BADGE), cured with 4,4'-diaminodiphenyl sulfone (DDS), as the matrix material for high-performance hybrid nanocomposites containing organophilic layered silicate (OLS, synthetic fluorohectorite) and functional liquid six-arm star poly(propylene oxide-block-ethylene oxide) (PPO) as a toughening agent. The hybrid nanocomposites were composed of OLS as well as separated liquid PPO spheres in the epoxy matrix. Synthetic fluorohectorite (Somasis ME-100) was supplied by Unicoo Japan Ltd. (Tokyo, Japan) and Octadecylamine (ODA) was supplied by Fluka (Buchs, Switzerland). The liquid PPO was supplied by Bayer AG (Leverkusen, Germany).

To prepare the epoxy hybrid nanocomposites, mixtures of equal amounts of BADGE (Araldite GY 250) and TGDDM (Araldite MY 720) were used as epoxy components. BADGE (130.5 g) and TGDDM (130.5 g) were mixed together with 20 g of the modified PPO with stearate end groups for tailored polarity as well as phenol end groups for covalent bonding to epoxy resin at 80°C and 8 hPa pressure over a period of 30 minutes with a Molteni Labmax high-shear mixer (Rheinfelder, Switzerland). Somasis/ODA (10 g) was then added to the liquid prepolymers and dispersed therein using an IKA Ultra-Turrax T25 basic high-performance disperser from IKA-Werke, Staufen, Germany, for 6 minutes. The organophilic layered silicate was swollen in the resin for 3 hours at 90°C under reduced pressure with the Labmax mixer. Then 109 g DDS (Hardener HT 976) was dissolved in the reaction mixture at 135°C over a period of 25 minutes of mixing at 8 hPa.

The epoxy resin was then poured into a mold and cured at 140°C for 3 hours and at 220°C for 7 hours in a vented oven to produce epoxy hybrid nanocomposites containing 5 wt% of PPO liquid polymer

and 2.5 wt% of Somasif/ODA OLS. Various other hybrid nanocomposites with different amounts of liquid PPO and OLS were produced by this method. Controls containing either liquid PPO toughening agent or surface treated clay (OLS) were also prepared for comparison.

Various analytical procedures such as gel permeation chromatography (GPC), differential scanning calorimetry (DSC), TEM, dynamic mechanical analyzer (DMA), linear coefficient of thermal expansion (CTE), tensile properties, and fracture toughness were determined. To evaluate the effect of morphology on the fracture mechanical response, the surface of broken compact-tension specimens was examined using scanning electron microscopy (SEM).

The hybrid nanocomposites possessed high glass transition temperature of 220°C. The T_g values were elevated compared to those of the neat resin (212°C) by the addition of the modified liquid PPO. The CTE of the composite material was increased by the addition of liquid polymer toughening agent. The stiffness was only slightly increased, and the strength of the hybrid composites was improved by 20%, mainly because of the addition of the layered silicates. The high toughness of the neat resin could not be preserved for the hybrid materials. The K_{Ic} was decreased by 15% to values of 1.15 MPa m^{-1/2}, compared to 1.35 MPa m^{-1/2} for the neat resin. Hence, the extensive matrix yielding of the neat resin with the generation of shear ribs was the most effective failure mode. The predominant failure mode of the hybrid nanocomposites initiated by the silicate particles, crack bifurcation and branching, was not effective. Crack pinning by the liquid PPO spheres could be resolved only when the modified polymer was used as a single additive and afforded the lowest K_{Ic} values.

Koo and coworkers have successfully used high-shear mixing techniques to incorporate layered silicates, nanosilicas, carbon nanofibers, and POSS to form polymer nanostructured materials in several of their research programs.⁴⁷⁻⁵³ Layered silicates and carbon nanofiber, and POSS were incorporated separately into resole phenolic (Borden SC-1008) using high-shear, nonsparking paint mixing equipment to form different types of polymer nanocomposites.⁴⁷⁻⁵⁰ Neat resin castings (without fiber reinforcement) were made for WAXD and TEM analyses (Chap. 5). The polymer nanocomposites were then impregnated onto carbon fabric to form polymer matrix composites. These nanocomposite rocket ablative materials (NRAMs) were tested under a simulated solid rocket motor environment. Ablation and heat transfer characteristics of these NRAMs will be discussed in more detail in Chap. 7.

Koo's research team^{51,52} also incorporated layered silicates, carbon nanofibers, and POSS into resole phenolic (Hitco 134A) and cyanate ester (Lonza PT-15 and PT-30) using high-shear mixing equipment to

form polymer nanocomposites. These polymer nanocomposites were used to create a new type of nanomodified carbon/carbon composite (NCCC). Wide-angle x-ray diffraction (WAXD) and TEM analyses (Chap. 5) were used to determine the degree of dispersion. Six resin/nanoparticle materials were selected to produce prepregs. These prepregs were fabricated into composites for carbonization and densification to produce C/C composites. Heat aging was conducted for 24 hours for the six candidates and the baseline Hitco CC139 materials. Mechanical properties such as the tensile, compressive, and flexural strengths and moduli were determined and compared with the baseline CCC.^{51,52} Thermo-oxidative studies of these NCCCs will be discussed in more detail in Chap. 7.

The incorporation of layered silicates, nanosilicas, and carbon nanofibers into a high-temperature, damage-tolerant epoxy resin system (CYCOM[®] 977-3, from Cytec Engineering Materials) was reported by the Koo group.⁵³ Wide-angle x-ray diffraction and TEM were used to determine the degree of dispersion. Dynamic mechanical thermal analysis (DMTA) was used to determine the T_g and complex modulus of the polymer nanocomposites. The TEM analyses indicated the layered silicates, nanosilicas, and CNFs dispersed very well in the epoxy resin system (Chap. 5). High T_g and complex modulus values from DMTA for the nanomodified materials are presented as evidence for nanophase presence in the epoxy system as compared to lower T_g and complex moduli for the epoxy resin control. The DMTA data of the neat epoxy nanosilica nanocomposite (2 wt% AEROSIL R202) show the high T_g (258°C) and the highest complex modulus (964 MPa). The epoxy nanocomposites for carbon-fiber-reinforced polymer matrix composites will be discussed in more detail in Chap. 7.

4.8 Summary

In this chapter we identified six synthesis approaches for incorporating different types of nanoparticles into polymer matrices. Selected literature examples were used to demonstrate these synthesis methods. Selective examples will be described in more detail in Chaps. 6 and 7, and will emphasize the properties and performance of these polymer nanostructured materials.

References

1. E. Tomanek and R. J. Enbody (eds.), *Science and Application of Nanotubes*, Kluwer Academic/Plenum Publishers, New York, 2000.
2. T. J. Pinnavaia and G. W. Beall (eds.), *Polymer-Clay Nanocomposites*, John Wiley & Sons, New York, 2000.

3. R. Krishnamoorti and R. A. Vaia (eds.), *Polymer Nanocomposites: Synthesis, Characterization, and Modeling*, ACS Symposium Series 804, ACS, Washington, DC, 2001.
4. Z. L. Wang, Y. Liu, and Z. Zhang (eds.), *Handbook of Nanophase and Nanostructured Materials*, vol. 4: *Materials Systems and Applications (II)*, Kluwer Academic/Plenum Publishers, New York, 2003.
5. G. Cao, *Nanostructures & Nanomaterials Synthesis, Properties & Applications*, Imperial College Press, London, 2004.
6. M. Di Ventra, S. Evoy, and J. R. Heflin, Jr. (eds.), *Introduction to Nanoscale Science and Technology*, Kluwer Academic Publishers, New York, 2004.
7. M. J. Schulz, A. D. Kelkar, and M. J. Sundareshan (eds.), *Nanoengineering of Structural, Functional, and Smart Materials*, CRC, Boca Raton, FL, 2006.
8. M. Alexandre and P. Dubois, "Polymer-Layered Silicate Nanocomposites: Preparation, Properties, and Uses of a New Class of Materials," *Mater. Sci. Eng.* **R28**:1–63 (2000).
9. C. Sanchez, B. Julian, P. Belleville, and M. Popall, "Applications of Hybrid Organic-Inorganic Nanocomposites," *J. Mater. Chem.* **15**:3559–3592 (2005).
10. M. Lerner and C. Oriakhi, in *Handbook of Nanophase Materials*, A. Goldstein (ed.), Mekker Decker, New York, 1997, pp. 199–219.
11. B. Lagaly, "Introduction from Clay Mineral-Powder Interactions to Clay Mineral-Polymer Nanocomposites," *Appl. Clay Sci.* **15**:1–9 (1999).
12. D. J. Greenland, "Adsorption of Polyvinyl Alcohols by Montmorillonite," *J. Colloid Sci.* **18**:647–664 (1963).
13. N. Ogata, S. Kawakage, and T. Orgihara, "Poly (Vinyl Alcohol)-Clay and Poly (Ethylene Oxide)-Clay Blend Prepared Using Water as Solvent," *J. Appl. Polym. Sci.* **66**:573–581 (1997).
14. R. L. Parfitt and D. L. Greenland, "Absorption of Poly (Ethylene Glycols) on Montmorillonites," *Clay Mineral* **8**:305–323 (1970).
15. X. Zhao, K. Urano, and S. Ogasawara, "Adsorption of Polyethylene Glycol from Aqueous Solutions on Montmorillonite Clays," *Colloid Polym. Sci.* **267**:899–906 (1989).
16. E. Ruiz-Hitzky, P. Aranda, B. Casal, and J. C. Galvan, "Nanocomposite Materials with Controlled Ion Mobility," *Adv. Mater.* **7**:180–184 (1995).
17. J. Billingham, C. Breen, and J. Yarwood, "Adsorption of Polyamide, Polyacrylic Acid and Polyethylene Glycol on Montmorillonite: An In-Situ Study using ATR-FTIR," *Vibr. Spectrosc.* **14**:19–34 (1997).
18. R. Levy and C. W. Francis, "Interlayer Adsorption of Polyvinyl Pyrrolidone on Montmorillonite," *J. Colloid Interface Sci.* **50**:442–450 (1975).
19. J. Wu and M. M. Lerner, "Structural, Thermal, and Electrical Characterization of Layered Nanocomposites Derived from Sodium-Montmorillonite and Polyethers," *Chem. Mater.* **5**:835–838 (1993).
20. D. J. Harris, T. J. Bonagamba, and K. Schmidt-Rohr, "Conformation of Poly (Ethylene Oxide) Intercalated in Clay and MoS₂ Studied by Two-Dimensional Double-Quantum NMR," *Macromolecules* **32**:6718–6724 (1999).
21. K. Yano, A. Usuki, A. Okada, T. Kurauchi, and O. Kamigaito, "Synthesis and Properties of Polyimide-Clay Hybrid," *J. Polym. Sci. Part A: Polym. Chem.* **31**:2493–2498 (1993).
22. K. Yano, A. Usuki, and A. Okada, "Synthesis and Properties of Polyimide-Clay Hybrid Films," *J. Polym. Sci. Part A: Polym. Chem.* **35**:2289–2294 (1997).
23. R. A. Vaia and E. P. Giannelis, "Polymer Melt Intercalation in Organically-Modified Layered Silicates: Model Predictions and Experiment," *Macromolecules* **30**:8000–8009 (1997).
24. R. A. Vaia, H. Ishii, and E. P. Giannelis, "Synthesis and Properties of Two-Dimensional Nanostructures by Direct Intercalation of Polymer Melts in Layered Silicates," *Chem. Mater.* **5**:1694–1696 (1993).
25. S. D. Burnside and E. P. Giannelis, "Synthesis and Properties of New Poly (Dimethylsiloxane) Nanocomposites," *Chem. Mater.* **7**:1597–1600 (1995).

26. R. Blanski, J. H. Koo, P. Ruth, N. Nguyen, C. Pittman, and S. Phillips, "Polymer Nanostructured Materials for Solid Rocket Motor Insulation: Ablation Performance," *Proc. 52nd JANNAF Propulsion Meeting*, CPIA, Columbia, MD, 2004.
27. J. H. Koo, D. Marchant, G. Wissler, P. Ruth, S. Barker, R. Blanski, and S. Phillips, "Polymer Nanostructured Materials for Solid Rocket Motor Insulation: Processing, Microstructure, and Mechanical Properties," *Proc. 52nd JANNAF Propulsion Meeting*, CPIA, Columbia, MD, 2004.
28. P. Ruth, R. Blanski, and J. H. Koo, "Preparation of Polymer Nanocomposites for Solid Rocket Motor Insulation," *Proc. 52nd JANNAF Propulsion Meeting*, CPIA, Columbia, MD, 2004.
29. R. Blanski, J. H. Koo, P. Ruth, N. Nguyen, C. Pittman, and S. Phillips, "Ablation Characteristics of Nanostructured Materials for Solid Rocket Motor Insulation," *Proc. National Space & Missile Materials Symposium*, Seattle, WA, June 21–25, 2004.
30. J. H. Koo, D. Marchant, G. Wissler, P. Ruth, S. Barker, R. Blanski, and S. Phillips, "Processing and Characterization of Nanostructured Materials for Solid Rocket Motors," *Proc. National Space & Missile Materials Symposium*, Seattle, WA, June 21–25, 2004.
31. D. Marchant, J. H. Koo, R. Blanski, E. H. Weber, P. Ruth, A. Lee, and C. E. Schlaefer, "Flammability and Thermophysical Characterization of Thermoplastic Elastomer Nanocomposites," *ACS National Meeting, Fire & Polymers Symposium*, Philadelphia, PA, Aug. 22–26, 2004.
32. S. K. Gupta, J. J. Schwab, A. Lee, B. X. Gu, and B. S. Hsiao, "POSS® Reinforced Fire Retarding EVE Resins," *Proc. SAMPE 2002 ISSE*, SAMPE, Covina, CA, 2002, pp. 1517–1526.
33. A. Yasmin, J. L. Abot, and I. M. Daniel, "Processing of Clay/Epoxy Nanocomposites with a Three-Roll Mill Machine," *Mater. Res. Soc. Symp. Proc. vol. 740:75–80* (2003).
34. D. C. Lee and L. W. Jang, "Preparation and Characterization of PMMA-Clay Hybrid Composite by Emulsion Polymerization," *J. Appl. Polym. Sci.* **62**:1117–1122 (1996).
35. D. C. Lee and L. W. Jang, "Characterization of Epoxy-Clay Hybrid Composite Prepared by Emulsion Polymerization," *J. Appl. Polym. Sci.* **68**:1997–2005 (1998).
36. M. W. Noh and D. C. Lee, "Synthesis and Characterization of PS-Clay Nanocomposite by Emulsion Polymerization," *Polym. Bull.* **42**:619–626 (1999).
37. G. Lagaly and K. Beneke, "Intercalation and Exchange Reactions of Clay Minerals and Non-Clay Layer Compounds," *Colloid Polym. Sci.* **269**:1198–1211 (1991).
38. M. P. Eastman, E. Bain, T. L. Porter, K. Manygoats, R. Whitehorse, R. A. Parnell, and M. E. Hagerman, "The Formation of Poly(Methyl-Methacrylate) on Transition Metal-Exchanged Hectorite," *Appl. Clay Sci.* **15**:173–185 (1999).
39. Y. Fukushima, A. Okada, M. Kawasumi, T. Kurauchi, and O. Kamigaito, "Swelling Behavior of Montmorillonite by Poly-6-Amide," *Clay Mineral* **23**:27–34 (1988).
40. A. Usuki, Y. Kojima, M. Kawasumi, A. Okada, Y. Fukushima, T. Kurauchi, and O. Kamigaito, "Synthesis of Nylon-6-Clay Hybrid," *J. Mater. Res.* **8**:1179–1183 (1993).
41. A. Usuki, M. Kawasumi, Y. Kojima, A. Okada, T. Kurauchi, and O. Kamigaito, "Swelling Behavior of Montmorillonite Cation Exchanged for ω -Amino Acids by ϵ -Caprolactam," *J. Mater. Res.* **8**:1174–1178 (1993).
42. Y. Kojima, A. Usuki, M. Kawasumi, A. Okada, T. Kurauchi, and O. Kamigaito, "Synthesis of Nylon-6-Clay Hybrid by Montmorillonite Intercalated with ϵ -Caprolactam," *J. Polym. Sci. Part A: Polym. Chem.* **31**:983–986 (1993).
43. P. B. Messersmith and E. P. Giannelis, "Synthesis and Characterization of Layered Silicate-Epoxy Nanocomposites," *Chem. Mater.* **6**:1719–1725 (1994).
44. T. Lan and T. J. Pinnavaia, "Clay-Reinforced Epoxy Nanocomposites," *Chem. Mater.* **6**:2216–2219 (1994).
45. T. Lan, P. D. Kaviratna, and T. J. Pinnavaia, "Mechanism of Clay Tactoid Exfoliation in Epoxy-Clay Nanocomposites," *Chem. Mater.* **7**:2144–2150 (1995).
46. J. Frohlich, R. Thomann, O. Gryshchuk, J. Karger-Kocsis, and R. Mulhaupt, "High-Performance Epoxy Hybrid Nanocomposites Containing Organophilic Layered Silicates and Compatibilized Liquid Rubber," *J. of Appl. Polym. Sci.* **92**:3088–3096 (2004).

47. J. H. Koo, H. Stretz, A. Bray, W. Wootan, S. Mulich, B. Powell, J. Weispfenning, and T. Grupa, "Phenolic-Clay Nanocomposites for Rocket Propulsion System," *Proc. SAMPE 2002 ISSE*, SAMPE, Covina, CA, 2002.
48. J. H. Koo, H. Stretz, A. Bray, J. Weispfenning, Z. P. Luo, and W. Wootan, "Nanocomposites Rocket Ablative Materials: Processing, Characterization, and Performance," *Proc. SAMPE 2003 ISSE*, SAMPE, Covina, CA, 2003, pp. 1156–1170.
49. J. H. Koo, W. K. Chow, H. Stretz, A. C-K. Cheng, A. Bray, and J. Weispfenning, "Flammability Properties of Polymer Nanostructured Materials," *Proc. SAMPE 2003 ISSE*, SAMPE, Covina, CA, 2003, pp. 954–964.
50. J. H. Koo, H. Stretz, J. Weispfenning, Z. P. Luo, and W. Wootan, "Nanocomposite Rocket Ablative Materials: Subscale Ablation Test," *Proc. SAMPE 2004 ISSE*, SAMPE, Covina, CA, 2004.
51. J. H. Koo, C. U. Pittman, Jr., K. Liang, H. Cho, L. A. Pilato, Z. P. Luo, G. Pruetz, and P. Winzek, "Nanomodified Carbon/Carbon Composites for Intermediate Temperature: Processing and Characterization," *Proc. SAMPE 2003 ISTC*, SAMPE, Covina, CA, 2003.
52. J. H. Koo, L. A. Pilato, P. Winzek, S. Shivakumar, C. U. Pittman, Jr., and Z. P. Luo, "Thermo-Oxidative Studies of Nanomodified Carbon/Carbon Composites," *Proc. SAMPE 2004 ISSE*, SAMPE, Covina, CA, 2004.
53. J. H. Koo, L. A. Pilato, G. Wissler, A. Lee, A. Abusafieh, and J. Weispfenning, "Epoxy Nanocomposites for Carbon Fiber Reinforced Polymer Matrix Composites," *Proc. SAMPE 2005 ISSE*, SAMPE, Covina, CA, 2005.

This page intentionally left blank

Characterization of Polymer Nanomaterials

5.1 Characterization Methods

There are three key steps in the development of nanomodified materials and these are: (a) materials preparation, (b) property characterization, and (c) material performance or device fabrication. The materials preparation involves the processing of nanoparticles with polymer matrix into a polymer nanocomposite. This was discussed in Chap. 4. The next challenge is to determine the degree and level of dispersion of the nanoparticles in the polymer matrix. Characterization involves two main processes: structure analysis and property measurements. Structure analysis is carried out using a variety of microscopic and spectroscopic techniques, while property characterization is rather diverse and depends on the individual application.

Due to the high selectivity of the size and structure of the polymer nanostructured materials (PNMs), the physical properties of these PNMs can be quite diverse. It is known that the physical properties of nanostructures depend strongly on their size and shape. The properties measured from a large quantity of nanomaterials could be an average of the overall properties, so that the unique characteristics of an individual nanostructure could be embedded. An essential task as one develops capability in the preparation of nanomaterials is property characterization of an individual nanostructure with a well-defined atomic structure.

Characterizing the properties of individual nanoparticles presents a challenge to many existing testing and measuring techniques because of the following constraints. First, the size (diameter and length) is rather small, prohibiting the application of well-established techniques. Second, the small size of nanostructures makes their manipulation

rather difficult, and specialized techniques are needed for identifying and analyzing individual nanostructures. Finally, new methods and analytical tools must be developed to quantify the properties of individual nanostructures. In this chapter, several commonly used structural characterization techniques are briefly discussed, along with examples demonstrating the techniques. More detailed characterization of nanophase materials can be found elsewhere.¹⁻⁴ Property characterization for the individual PNMs will be deferred to Chaps. 6 and 7. The commonly used characterization techniques are:

- Wide-angle x-ray diffraction (WAXD)
- Transmission electron microscopy (TEM) and spectroscopy
- Scanning electron microscopy (SEM)
- Small angle x-ray scattering (SAXS)
- Thermal gravimetric analyses (TGA)
- Differential scanning calorimetry (DSC)
- Dynamic mechanical thermal analyses (DMTA)
- Mechanical properties (tensile, flexural, and compressive strength and modulus, and Izod impact)
- Flammability (cone calorimeter and UL 94)

Other techniques:

- Nuclear magnetic resonance (NMR)
- Scanning probe microscopy (SPM)—atomic force microscopy (AFM) and scanning tunneling microscopy (STM)
- Neutron scattering
- Optical microscopy

5.2 X-Ray Diffraction

Wide-angle x-ray diffraction (WAXD) is the most commonly used technique to characterize the degree of nanodispersions of MMT organoclay in a specific polymer. Wide-angle x-ray diffraction measures the spacing between the ordered crystalline layers of the organoclay. By using Bragg's law: $\sin\theta = n\lambda/2d$ where d is the spacing between atomic planes in the crystalline phase and λ is the x-ray wavelength. The intensity of the diffracted x-ray is measured as a function of the diffraction angle 2θ and the specimen's orientation. This diffraction pattern is used to identify the specimen's crystalline phases and to measure its structural properties. WAXD is nondestructive and does not require elaborate

sample preparation which partly explains the wide usage of this technique in materials characterization. Spacing change (increase or decrease) information can be used to determine the type of polymer nanocomposite formed, such as:

- Immiscible (no d-spacing change)
- Decomposed/deintercalated (d-spacing decrease)
- Intercalated (d-spacing increase)
- Exfoliated (d-spacing outside of wide-angle x-ray diffraction, or so expansive and disordered as to give a signal)

However, WAXD can be affected by many parameters:

- Sampling (powder vs. solids, alignment of clay platelets)
- Experimental parameters (slit width, count time, angle step rate)
- Layered silicate order (disordered/amorphous materials exhibit no pattern by WAXD)
- WAXD measures d-spacing, not overall (global) clay dispersion in the sample

To reveal the capabilities of a modern x-ray characterization of nanoparticles and the fundamentals of WAXD, the reader should refer to other sources.³ Figure 5.1 displays the WAXD data showing the intensity of various wt% (5, 10, and 15 wt%) of SCP's Cloisite 30B MMT organoclay dispersed in a resole phenolic (Borden's SC-1008).⁵ The fact that no peaks were shown at diffraction angle around 2.5 for all three wt% indicates that all three formulations were possibly in an exfoliated state.

5.3 Transmission Electron Microscopy and Spectroscopy

5.3.1 Transmission electron microscopy (TEM)

One of the characteristics of polymer nanostructured materials is their extremely small particle size of the added nanoparticles. Although some structural features can be revealed by x-ray and neutron diffraction, direct imaging of individual nanoparticles is only possible using transmission electron microscopy (TEM) and scanning probe microscopy. Transmission electron microscopy is unique because it can provide a real space image on the atom distribution in the nanocrystal and on its surface.^{1,6} Today's TEM is a versatile tool that provides not only atomic

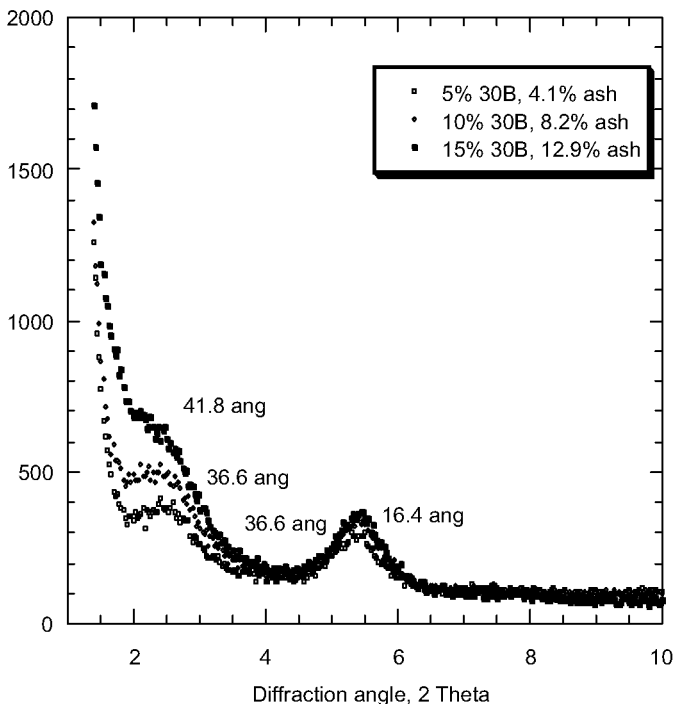


Figure 5.1 WAXD data showing the intensity of 5, 10, and 15% of Cloisite 30B MMT nanoclay in resole phenolic.⁵

resolution lattice images, but also chemical information at a spatial resolution of 1 nm or better, allowing direct identification of the chemistry of a single nanocrystal. With a finely focused electron probe, the structural characteristics of a single nanoparticle can be fully characterized. To reveal the capabilities of a modern TEM and the fundamentals of TEM and its applications in characterization of nanophase materials, the reader should refer to other sources.^{1,2,4,6,7}

A modern TEM, which is composed of an illumination system, a specimen stage, an objective lens system, a magnification system, a data recording system, and a chemical analysis system, is shown schematically in Fig. 5.2.¹ The electron gun, which typically uses a LaB_6 thermionic emission source or a field emission source, is the heart of the illumination system. The LaB_6 gun fires a high-illumination current, but the current density and the beam coherence are not as high as those of a field emission source. When a field emission source is used it is primarily for performing high-coherence lattice imaging, electron holography, and high spatial resolution microanalysis. The TEM illumination system also includes condenser lenses, which are vitally critical for forming a fine electron probe. The specimen stage is vital for

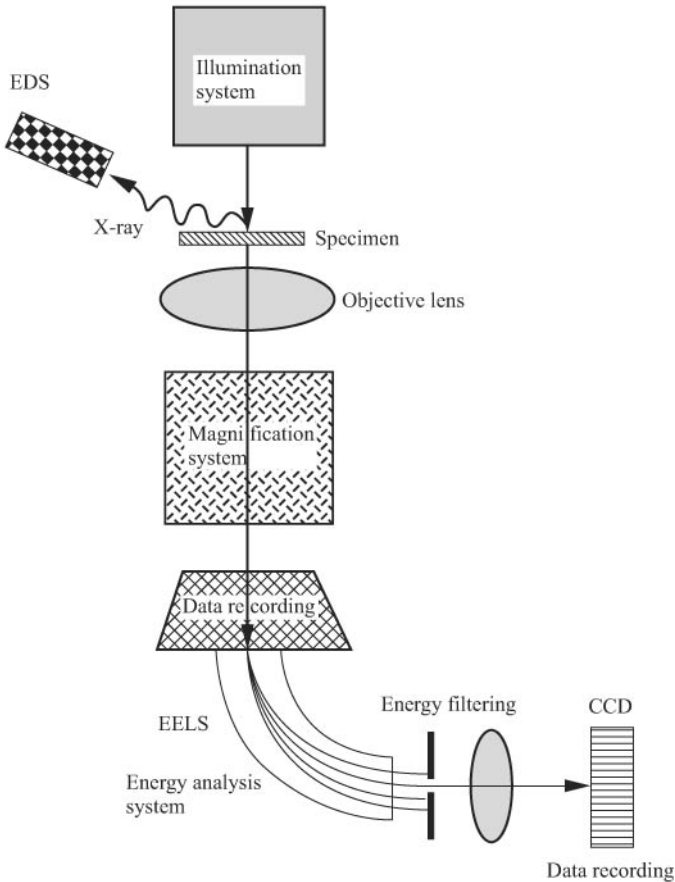


Figure 5.2 Schematic structure of transmission electron microscopy.

structure analysis, because it can be used to perform in-situ observations of phenomena induced by annealing, electric fields, or mechanical stress, making it possible to characterize the physical properties of individual nanostructures. The objective lens, which determines the limit of image resolution, is extremely critical for TEM. The TEM magnification system consists of intermediate lenses and projection lenses, and it provides a magnification of up to 1.5 million times. The data recording system is digital because of its use of a charge coupled device (CCD), to allow quantitative data processing and quantification. Finally, the chemical analysis system is the energy-dispersive x-ray spectroscopy (EDS) and electron energy-loss spectroscopy (EELS); these can be used in a complimentary manner to quantify the chemical composition of the specimen. Electron energy-loss spectroscopy can also provide information related to the electronic structure of the specimen.

TEM sample preparation is of utmost importance in obtaining a TEM with good resolution. Figure 5.3 illustrates the sequence of TEM sample preparation that the author has followed in his studies. The basic requirements are that the specimen has to be thin enough to be transparent to the electron beam, must be clean, without much damage or contamination. There are several common methods for TEM specimen preparation:

- *Ion-milling*: for nearly all kinds of materials
- *Electropolishing*: for conductive bulk materials
- *Crushing powders*: the simplest way to prepare TEM specimens, but microstructural details may be lost

The bulk sample is first cut into thin slices about 0.6 mm thick. The thin sample slices are then either core-drilled or punched to obtain a 3-mm-diameter disk with a thickness of $\sim 60 \mu\text{m}$. The disk is then dimpled until the thickness in the center reaches about 10–20 μm , and the specimen is then ion-milled until it is penetrated.

Figure 5.4 shows TEM micrographs of three types of nanoparticles in IPA solvent as a 99.5% solution in IPA.⁵ The unit bar is 500 nm on all three micrographs. Cloisite 30B in Fig. 5.4(a) shows intercalated nanoclay. Figure 5.4(b) shows PR-24-PS CNFs entangled in bundles. Figure 5.4(c) shows Trisilanolphenyl-POSS-SO1458 ($\text{C}_{48}\text{H}_{38}\text{O}_{12}\text{Si}_7$)

- *Basic requirements*:
 - Thin enough to be transparent to the electron beam
 - Clean, without much damage or contamination
- *Several common methods*:
 - *Ion-milling*: for almost all kinds of materials
 - *Electropolishing*: for conductive bulk materials
 - *Crushing powders*: the simplest way to prepare the TEM samples, but microstructural details may be lost

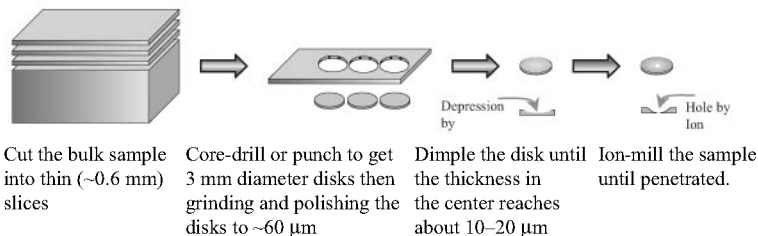


Figure 5.3 TEM sample preparation process by ion-milling.

and Fig. 5.4(d) shows polyvinyl silsesquioxane uncured-PM1285 ($C_2H_3O_{1.5}Si$)_n in micron sizes.

Transmission electron microscopy allows the observation of the overall organoclay dispersion in the polymer nanocomposite sample. Clay dispersion and structure observed under the microscope can determine the nature of a clay nanocomposite as follows:

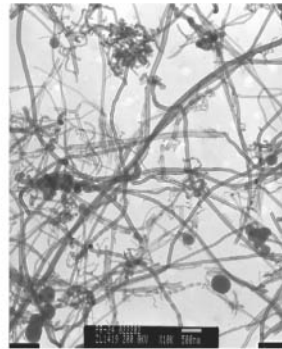
- *Immiscible*: usually large clay tactoids, undispersed clay particles
- *Intercalated*: clay layers in ordered stacks can be observed
- *Exfoliated*: single clay layers can be observed

Global microscale dispersion, as well as nanoscale dispersion and structure, can be determined.

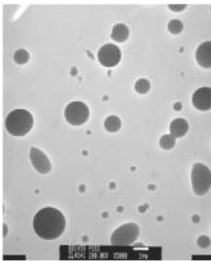
Transmission electron microscopy has several limitations and drawbacks, as follows:



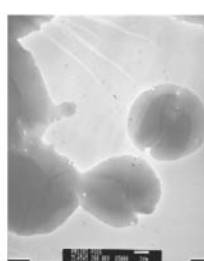
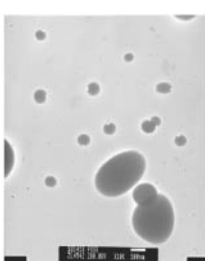
(a)



(b)



(c)



(d)

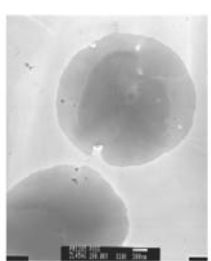


Figure 5.4 TEM micrographs of nanoparticles in IPA solvent (a) Cloisite, 30B, (b) PR-24-PS CNFs, (c) Trisilanolphenyl-POSS-SO1458, and (d) polyvinyl silsesquioxane uncured-PM1285.⁵

- In sampling, heterogeneous samples will give false results
- Labor-intensive analysis, involving expensive analytical instruments
- Cannot measure d-spacing of clay; therefore, cannot easily determine difference between intercalated clay nanocomposite and well-dispersed, immiscible nanocomposite

Transmission electron microscopy measures overall “characteristics” of clay dispersion such as uniformity, tactoids or non-uniformity of the clay within the material. It is recommended that TEM measurements should be combined with WAXD data for a thorough analyses of the nanomaterial.

5.3.2 Energy-dispersive x-ray spectroscopy (EDS)

X-rays emitted from atoms are characteristic of the elements, and the intensity distribution of the x-rays represents the thickness-projected atom densities in the specimen. This is known as energy-dispersive x-ray spectroscopy (EDS) which has played and is important for micro-analysis, particularly for heavier elements. EDS is a key tool for identifying the chemical composition of a specimen. A modern TEM is capable of producing a fine electron probe smaller than 2 nm, allowing direct identification of the local composition of an individual element. Examples will be provided in Chap. 7. When POSS materials were incorporated into the cyanate ester resin, EDS was used to demonstrate that a molecular dispersion was achieved by the PT-15 cyanate ester-Trisilanolphenyl-POSS nanocomposite. Figure 5.5 shows the TEM micrographs of PT-15/SO1458 POSS in progressive magnification. EDS shows Si is dispersed very well in the PT-15 resin system. Si counts were observed in the particle and matrix areas.⁸ Thus molecular dispersion of POSS particle in PT-15 CE resin is evident.

5.4 Small-Angle X-Ray Scattering (SAXS)

Small-angle x-ray scattering (SAXS) is an analytical x-ray application technique for the structural characterization of solid and fluid materials in the nanometer range. In SAXS experiments, the sample is irradiated by a well-defined, monochromatic x-ray beam, as shown in Fig. 5.6. When a nonhomogeneous medium, for example proteins in water, is irradiated, structural information about the scattering particles can be derived from the intensity distribution of the scattered beam at very low scattering angles.

With SAXS it is possible to study both monodisperse and polydisperse systems. In the case of monodisperse systems, one can determine

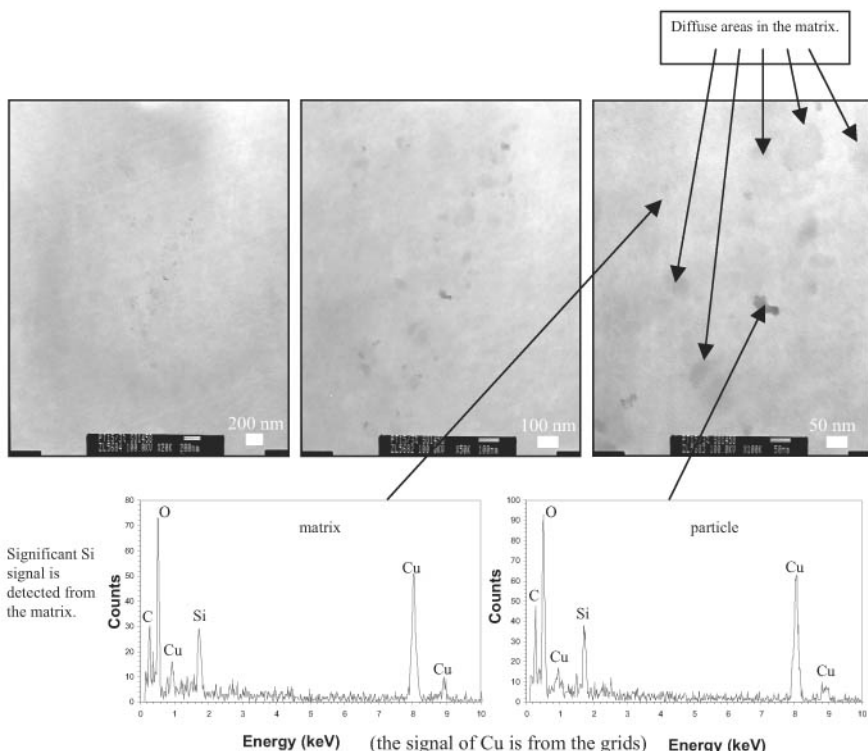


Figure 5.5 TEM micrograph of PT-15/SO1458 POSS in progressive magnification. Energy-dispersive x-ray spectroscopy (EDS) shows Si is dispersed very well in the PT-15 resin system.⁸

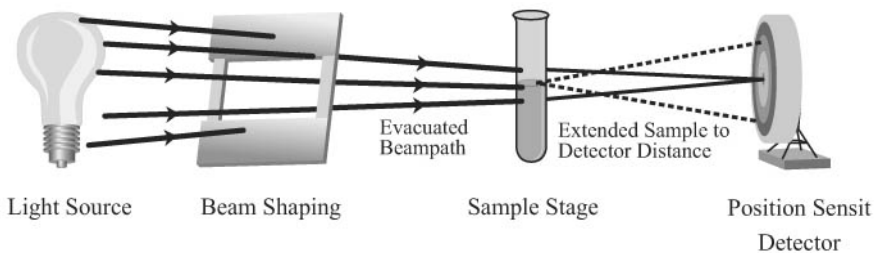


Figure 5.6 Schematic of small-angle x-ray scattering (SAXS).

size, shape, and internal structure of the particles. For polydisperse systems, a size distribution can be calculated assuming that all particles have the same shape. Small-angle x-ray scattering is used to investigate structural details in the 0.5 to 50 nm size range in materials such as:

- Suspended nanopowders
- Materials in life science and biotechnology (proteins, viruses, DNA complexes)
- Polymer films and fibers
- Catalyst surface per volume
- Microemulsions
- Liquid crystals

Small-angle x-ray scattering can provide the following information:

- Lamella repeat distance
- Radius of gyration
- Particle size and shape
- Large-scale structure and long-range order

Readers should refer to existing texts describing the SAXS technique.^{4,9,10}

5.5 The Cone Calorimeter (CC)

The potential fire hazard of any material depends on many factors, including ignitability, rate of surface flame spread, heat release rate (peak, average, and total), mass loss rate, smoke evolution, and evolution of toxic gases [e.g. carbon monoxide (CO)]. The Cone Calorimeter (CC) has been regarded as the most significant bench-scale instrument for evaluating reaction-to-fire properties of materials. Cone Calorimeter data address most of these factors, either directly [e.g. heat release rate (HRR)] or indirectly (e.g. time to ignition and HRR as functions of external heat flux as indicators of flame spread potential). The data obtained from the CC test are available in engineering units that are conducive to extrapolation to other fire sizes and scenarios. This section briefly discusses how the CC operates. Readers should refer to Babrauskas' excellent description in reference 11, the ASTM E 1354¹² or the ISO 5660¹³ for more details of the Cone Calorimeter.

A conceptual view of the CC is shown in Fig. 5.7. Figure 5.8 shows a commercial CC instrument. Figure 5.9 shows a test specimen ignited under the CC during testing. The CC is a fire-test instrument based on the principle of oxygen consumption calorimetry. This empirical principle is based on the observation that, generally, the net heat of combustion of any organic material is directly related to the amount of oxygen required for combustion. Approximately 13.1 MJ of heat are released per kilogram of oxygen consumed. At the core of the

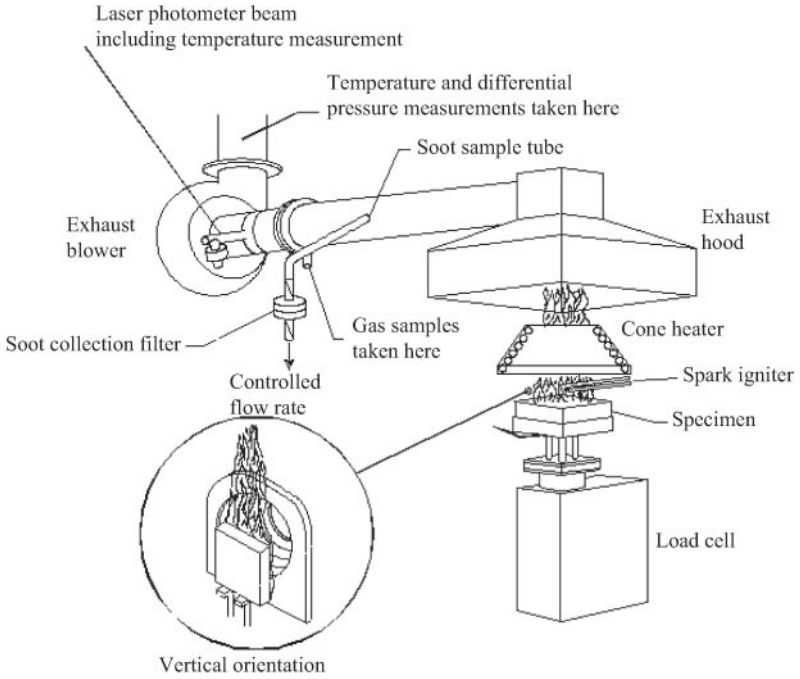


Figure 5.7 Schematic of a Cone Calorimeter.

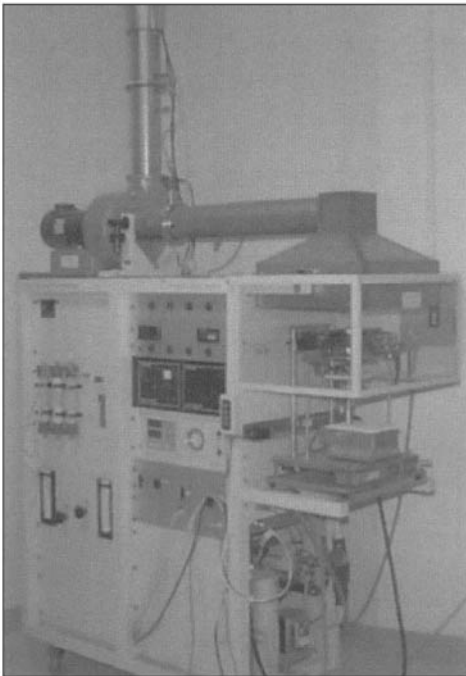


Figure 5.8 A commercial Cone Calorimeter



Figure 5.9 Close-up showing test specimen igniting during Cone Calorimeter testing.

instrument is a radiant electrical heater in the shape of a truncated cone (hence the name). This heating element irradiates a flat horizontal sample (100 mm \times 100 mm and up to 50 mm thick) placed beneath it at a preset heat flux of up to 100 kW/m². The sample is placed on a load cell for continuous monitoring of its mass as it burns. Ignition is provided by an intermittent spark igniter located 13 mm above the sample.

The gas stream containing the combined combustion products is captured through an exhaust duct system, consisting of a high-temperature centrifugal fan, a hood, and an orifice-plate flow meter. The typical air flow rate is 0.024 m³/s. Oxygen concentration in the exhaust stream is measured with an oxygen analyzer capable of an accuracy of 50 ppm, and the heat release rate is determined by comparing oxygen concentration with the value obtained when no sample is burning.

Smoke obscuration measurements are made in the exhaust duct using a helium-neon laser, with silicon photodiodes as the main beam and reference detectors, and appropriate electronics to derive the extinction coefficient and set the zero reading. Locations in the exhaust duct also provide additional sampling probes to determine concentrations of other combustion products such as carbon dioxide and

carbon monoxide. All data are collected with a PC, which continuously records data at fixed intervals of a few seconds during the test.

The CC is used to determine the following principal flammability properties:

- Heat release rate per unit area (kW/m^2)
- Cumulative heat released (kW)
- Effective heat of combustion (MJ/kg)
- Time to ignition (s)
- Mass loss rate (kg/s)
- Total mass loss (kg)
- Smoke density (m^2/kg)

Ignitability is defined as the propensity to ignition, as measured by the time in seconds to sustain flaming (the existence of flame on or over most of the specimen surface for periods of at least 4 seconds) at a specified heat flux. Ignitability is thus a measure of how quickly the material will ignite in a fire situation.

Heat release is defined as the heat generated in a fire due to various chemical reactions occurring within a given weight or volume of material. The major contributors are those reactions where carbon monoxide and carbon dioxide are generated, and oxygen is consumed. Heat release data provide a relative fire-hazard assessment for materials. Materials with low heat release per unit weight or volume will do less damage to the surroundings than materials with high heat release rate. The heat release rate, especially the peak amount, is the primary characteristic determining the size, growth, and suppression requirements of a fire environment. The rate of heat release is determined by measurement of the oxygen consumption as determined by the oxygen concentration and the flow rate in the exhaust product stream.

Effective heat of combustion, mass remaining, smoke ratio, carbon dioxide, and carbon monoxide are the additional CC data that are obtained during the experiment.

5.6 The Mass Loss Calorimeter (MLC)

The Mass Loss Calorimeter or Cone (MLC) per ASTM E2102¹⁴ or ISO 13927 is used to determine mass loss rate and ignitability at any heat flux condition defined within the Cone Calorimeter fire model of ISO 5660 or ASTM E1354. This instrument as shown in Fig. 5.10 is manufactured by Fire Testing Technology Ltd. (FTT), West Sussex, UK.

The complete assembly is also suitable to replace the cone heater/load cell assembly inside a Cone Calorimeter. As a stand-alone instrument, the MLC serves as a quality control tool. The instrument is supplied as two-part component system: the cone heater assembly (with conical heater, shutter mechanism, spark ignition, load cell) and the control as shown in Fig. 5.10. It can also be provided as an enclosed system in order to measure combustion products and toxicity yields or to use with low oxygen conditions. A heat release rate instrument can be used to determine the effect of combustion as a ratio of heat release rate and mass loss rate. Thus, if the effective heat of combustion is known, mass loss rate data can be used to calculate approximate values of heat release rate. The MLC is an inexpensive way of assessing fire properties of materials. Heat release is calculated using thermopile in the MLC.

5.7 Summary, Future Needs, and Assessments

No “single” technique provides sufficient analytical information related to the structural characteristics of a polymer nanocomposite. More than one technique is recommended to understand the structures and properties of the polymer nanocomposite. It is time consuming and costly to perform all the necessary experiments and to accumulate all of the data to verify the development of each polymer nanocomposite formulation. One needs to be selective in the choice of analytical tools to be used their in studies. There are other techniques that show promise for polymer nanocomposite analysis but more study is required before their value is recognized. These include:

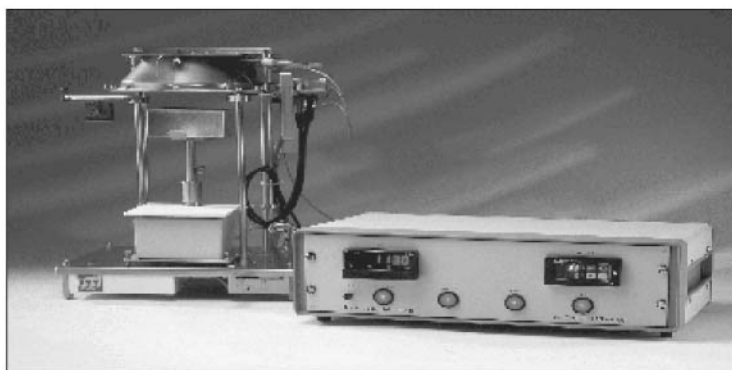


Figure 5.10 FTT Mass Loss Calorimeter setup with cone heat assembly (left) and control unit (right).

- *Neutron scattering*: the technique possesses similar limitations as WAXD. There is additionally limited access to its use because there are few nuclear labs providing this service.
- *Atomic force microscopy*: “tip” resolution and uncertainty around images of clay platelets (single clay platelet in stacks of 2–3 that are very tightly packed together).
- *Nuclear magnetic resonance*: NMR is successful only with the presence of iron as a component in the clay. Additional work is ongoing.
- *Rheology/differential scanning calorimetry*: It has been suggested in the literature that clay dispersions can be monitored by DSC with rheological changes but these findings may be specific to nanocomposites containing clay.

Polymer nanostructured materials present a complex analytical problem. Properties of PNMs are dependent on many factors. No one analytical technique can analyze all of these factors. Thermal gravimetric analyses, wide-angle x-ray diffraction, and transmission electron microscopy are currently the major tools to characterize these materials. Combining these techniques provides us with a better description and analysis of these PNMs. Each technique has its own advantages and shortcomings. To shorten the time to complete analysis on polymer nanostructured materials, new analytical techniques are necessary to facilitate analyses more rapidly to reduce the time lag for complete analysis of PNMs. Furthermore techniques that probe polymer-nanoparticle/polymer-organic treatment interactions are warranted.

References

1. Z. L. Wang (ed.), *Characterization of Nanophase Materials*, Wiley Vch, Weinheim, Germany, 2000, pp. 37–80.
2. N. Yan and Z. L. Wang (eds.), *Handbook of Microscopy for Nanotechnology*, Kluwer Academic Publishers, Boston, 2005.
3. Z. L. Wang (ed.), *Characterization of Nanophase Materials*, Wiley Vch, Weinheim, Germany, 2000, pp. 13–36.
4. G. Cao, *Nanostructures and Nanomaterials: Synthesis, Properties & Applications*, Imperial College Press, London, England, 2004, pp. 329–390.
5. J. H. Koo, H. Stretz, A. Bray, J. Weispfenning, Z. P. Luo, and W. Wootan, “Nanocomposite Rocket Ablative Materials: Processing, Microstructure, and Performance,” AIAA-2004-1996 paper, *44th AIAA/ASME/ASCE/AHS Structures, Structural Dynamics, and Materials Conference*, Palm Springs, CA, Apr. 19–22, 2004.
6. P. Buseck, J. M. Cowley, and L. Eyring (eds.), *High Resolution Transmission Electron Microscopy and Associated Techniques*, Oxford University Press, New York, 1988.
7. S. Y. Hobbs and V. H. Watkins, “Morphonology Characterization by Microscopy Techniques,” in *Polymer Blends* vol. 1: *Formulation*, D. R. Paul and C. B. Bucknall (eds.), John Wiley & Sons, New York, 2000, pp. 239–289.

8. J. H. Koo, C. U. Pittman, Jr., K. Liang, H. Cho, L. A. Pilato, Z. P. Luo, G. Pruetz, and P. Winzek, "Nanomodified Carbon/Carbon Composites for Intermediate Temperature: Processing and Characterization," *Int'l SAMPE Technical Conference* **35**:521–534 (2003).
9. A. Guinier and G. Fournet, *Small-Angle Scattering of X-Rays*, Wiley, New York, 1955.
10. O. Glatter and O. Kratky, *Small-Angle X-Ray Scattering*, Academic Press, London, 1982.
11. V. Babrauskas, "The Cone Calorimeter," in *Heat Release in Fires*, V. Babrauskas and S. J. Grayson (eds.), E & FN Spon, London, England, 1996, pp. 61–91.
12. Standard Test Method for Heat and Visible Smoke Release Rates for Materials and Products Using an Oxygen Consumption Calorimeter (E1354). American Society for Testing and Materials, Philadelphia, PA.
13. Fire Tests – Reaction to Fire – Part 1: Rate of Heat Release from Building Products. ISO DOS 5660. International Organization for Standardization, Geneva, Switzerland.
14. Standard Test Method for Screening Test for Mass Loss and Ignitability of Materials (ASTM E2102). American Society for Testing and Materials, Philadelphia, PA.

Properties of Polymer Nanostructured Materials

6.1 Materials Properties

In previous chapters, the different types of nanoparticles, selection of resin matrix and nanoparticles, processing of nanomaterials, and morphological characterization of polymer nanostructured materials were discussed. In this chapter, the properties and performance of this novel type of nanomodified polymeric material are described. Selective polymer nanocomposites for different applications will be presented to demonstrate the diversity of resulting PNMs and their utility. A list of thermoplastic nanocomposites, thermoset nanocomposites, and elastomer nanocomposites was surveyed in Chap. 3. Selective nylon 6 nanocomposites, epoxy nanocomposites, and thermoplastic polyolefin elastomer (TPO) nanocomposites are discussed in this chapter. Physical, mechanical, and thermal properties, as well as the performance of these polymer nanostructured materials, are reported.

6.2 Thermoplastic Nanocomposites

6.2.1 Nylon 6 nanocomposites

Mica-type silicates such as montmorillonite, hectorite, and saponite are attractive nanoclays¹⁻³ functioning as reinforcing fillers for polymers because of their high aspect ratio and unique intercalation and exfoliation characteristics. The incorporation of organoclays into polymer matrices has been known for many decades. In 1950, Carter et al.⁴ developed organoclays that were surface treated with organic bases to reinforce latex-based elastomers. In 1963, Nahin et al.⁵ incorporated organoclay into a thermoplastic polyolefin matrix. Organoclay modified

composites were obtained with improved solvent resistance and high tensile strength by irradiation-induced crosslinking procedure. In 1976, Fujiwara and Sakamoto⁶ of the Unitika patented the first organoclay hybrid nanocomposite. Ten years later, a Toyota research team disclosed improved methods to produce nylon 6–clay nanocomposites using in-situ polymerization, similar to the Unitika process.^{7–10} They reported that the resulting nylon 6–clay nanocomposites exhibited increased solvent resistance, decreased CTE, reduced permeability, and increased flame retardant characteristics. A very comprehensive review of polymer/layered silicate nanocomposites was published by Ray and Okamoto of Toyota Technical Institute in 2003.¹¹ These materials were commercialized in Japan by Ube and Unitika. Gianellis and Vaia et al.^{12–15} reported that nanocomposites can be obtained by direct polymer intercalation, where polymer chains diffuse into the space between the clay galleries. They also suggested that this approach can be combined with conventional polymer extrusion to decrease the time to form these hybrids, by shearing clay platelets leading to sample uniformity.

Dennis and Paul et al.¹⁶ demonstrated that the degree of exfoliation and dispersion of layered silicate nanocomposites formed from polyamide 6 by melt compounding is affected by both the chemistry of the clay surface and the type of extruder and its screw design. Increasing the mean residence time in the extruder generally improves the exfoliation and dispersion. It appears that an optimum extent of back mixing is necessary as judged by the broadness of the residence time distribution and optimal shear intensity. However, excessive shear intensity or back mixing also causes poor exfoliation and dispersion. Shear intensity is required to initiate the dispersion process by shearing particles apart into tactoids or intercalants. Residence time in a low-shearing or mildly shearing environment is required to allow polymer to enter the clay galleries and peel the platelets apart (Chap. 2). The nonintermeshing, twin-screw extruder used in the study yielded the best exfoliation and uniformity of dispersion. Excellent exfoliation and uniformity of dispersion can be achieved with both corotating and counter-rotating, intermeshing types of extruders when a fully optimized screw configuration is used. Figure 6.1 shows TEM micrographs of selective nylon 6–clay nanocomposites using different extruder and screw configurations. It is recognized that extruder processing conditions are important variables that must be optimized to affect a high degree of exfoliation and dispersion.

Cho and Paul¹⁷ prepared nylon 6–organoclay nanocomposites by melt compounding using a typical corotating twin-screw extruder and compared the resulting material with nylon 6 composites containing glass fibers and untreated clay. Transmission electron microscopy and WAXD indicate that the organoclay was well dispersed into the

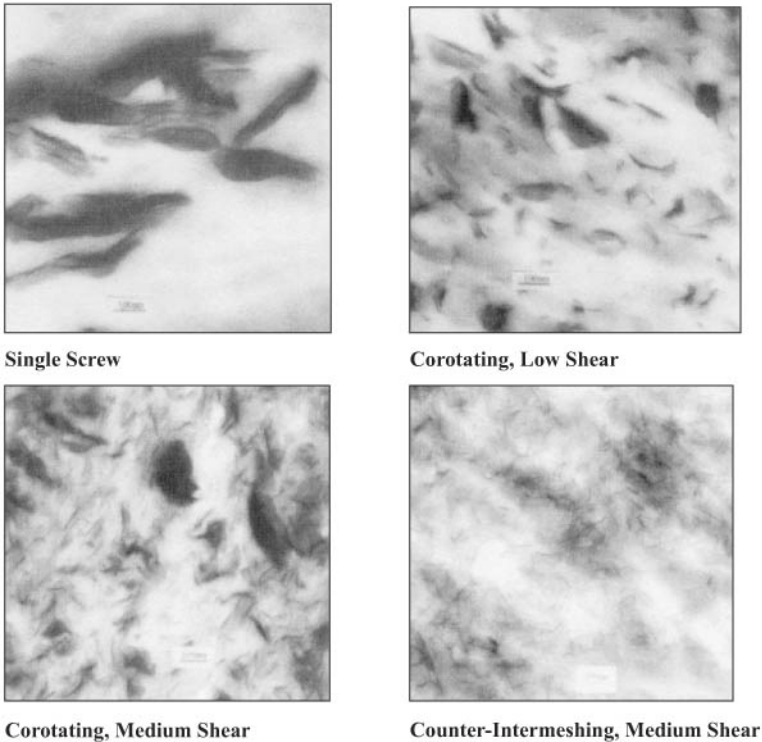


Figure 6.1 Transmission electron micrographs for elective nylon 6–Cloisite 15A nanocomposites using different extruders and screw configurations.¹⁶

nylon 6 matrix and that the mechanical properties of these materials compare well with nylon 6–clay nanocomposites formed by in-situ polymerization and by melt processing. Melt processing of these nylon 6–clay nanocomposites in a single-screw extruder failed to give similar levels of dispersion or exfoliation.

A high degree of exfoliation by melt processing requires an adequate residence time in the extruder, as well as sufficient shear. Although highly exfoliated nylon 6–clay nanocomposites show continuous improvement in strength and modulus relative to the neat nylon 6 matrix as more organoclay is added, there is a loss of ductility beyond a certain organoclay loading. The type of organotreatment and the speed of testing seem to have significant effect on ductility. Adding additional organoclay to nylon 6 significantly increases the ductile-to-brittle transition temperature. The mechanical properties of the organoclay nanocomposites showed greater values than glass fiber composites (Table 6.1).

Fornes and Paul et al.¹⁸ examined the effect of varying molecular weight of nylon 6 and nanoclay. Nylon 6 (low, or LMW; medium, or

TABLE 6.1 Mechanical Properties of Nylon 6 Composites¹⁷

Nylon 6 composites	Mineral content (%)	Izod impact strength (J/m)	Modulus (GPa)	Yield strength (MPa)	Elongation at break (%) [*]
Nylon 6	0	38 ± 4	2.66 ± 0.2	64.2 ± 0.8	200 ± 30
N6/glass fiber	5	53 ± 8	3.26 ± 0.1	72.6 ± 0.8	18 ± 1.3
N6/montmorillonite	5	40 ± 2	3.01 ± 0.1	75.4 ± 0.3	22 ± 6.0
N6/organoclay	3.16	38 ± 3	3.66 ± 0.1	83.4 ± 0.7	126 ± 25
N6/organoclay/glass fiber	8	44 ± 3	4.82 ± 0.1	95.0 ± 0.9	8 ± 0.5

^{*}Crosshead speed 0.51 cm/min

MMW; and high, or HMW) was prepared by a corotating twin-screw extruder. Wide-angle x-ray diffraction and TEM results collectively reveal a mixed structure for LMW-based nanocomposites having regions of intercalated and exfoliated clay platelets, whereas the MMW and HMW composites revealed highly exfoliated structures. Qualitative TEM observations were supported by quantitative analyses of high magnification TEM images. The average number of platelets per stack was shown to decrease with increasing nylon 6 molecular weights. The TEM particle density increased with increasing molecular weight, revealing clay platelets exfoliated for the nanocomposites in the order of HMW > MMW > LMW composites (Fig. 6.2). Tensile

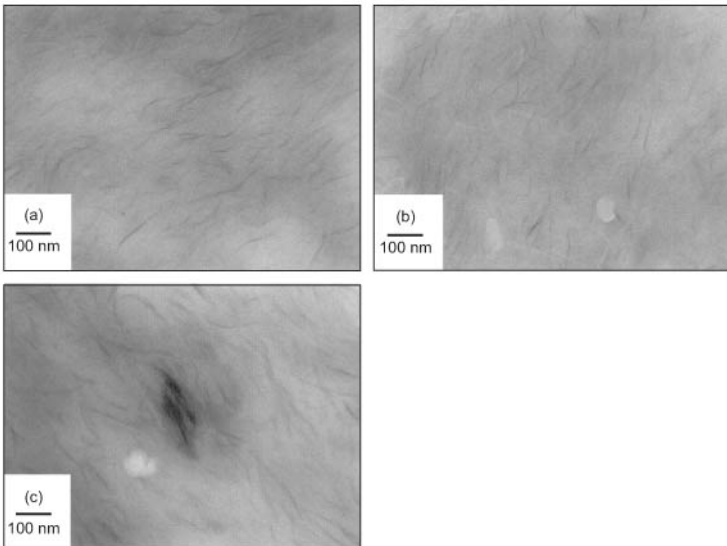


Figure 6.2 Transmission electron micrographs of melt-compounded nanocomposites containing ~3.0 wt% montmorillonite based on (a) HMW, (b) MMW, and (c) LMW nylon 6.¹⁸

properties revealed superior performance for the higher molecular weight nylon 6 composites, with highest tensile properties for HMW. Additionally the HMW-based nanocomposites had the highest moduli (Fig. 6.3), yield strengths (Fig. 6.4), and elongation at break (Fig. 6.5).

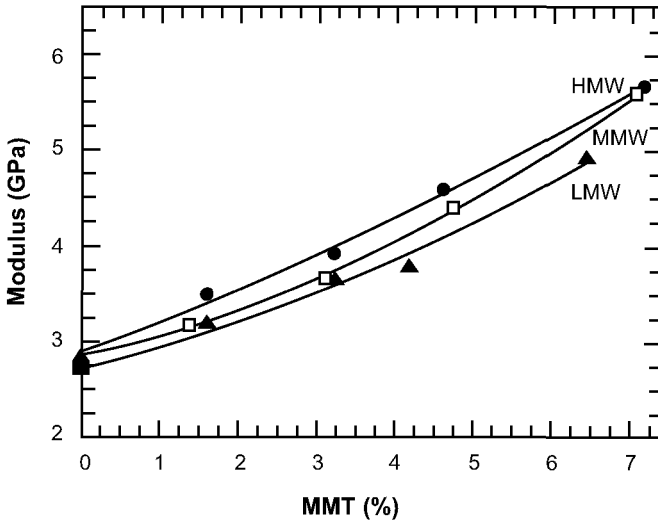


Figure 6.3 Effect of montmorillonite content on tensile modulus for LMW-, MMW-, and HMW-based composites.¹⁸

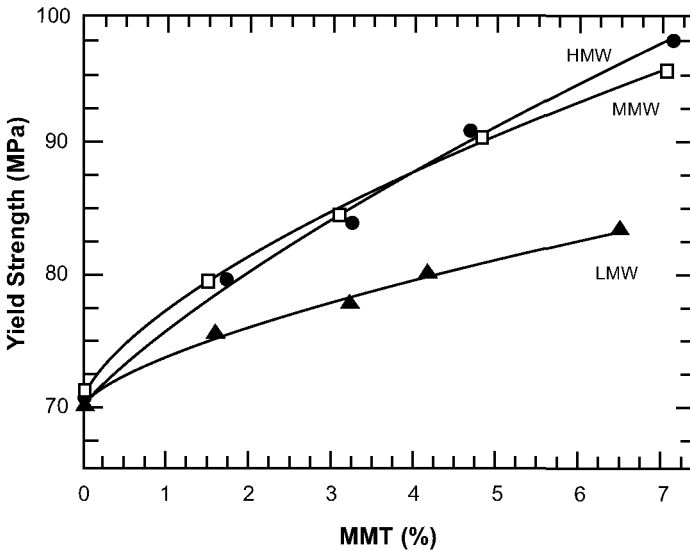


Figure 6.4 Effect of montmorillonite content on yield strength for LMW-, MMW-, and HMW-based composites.¹⁸

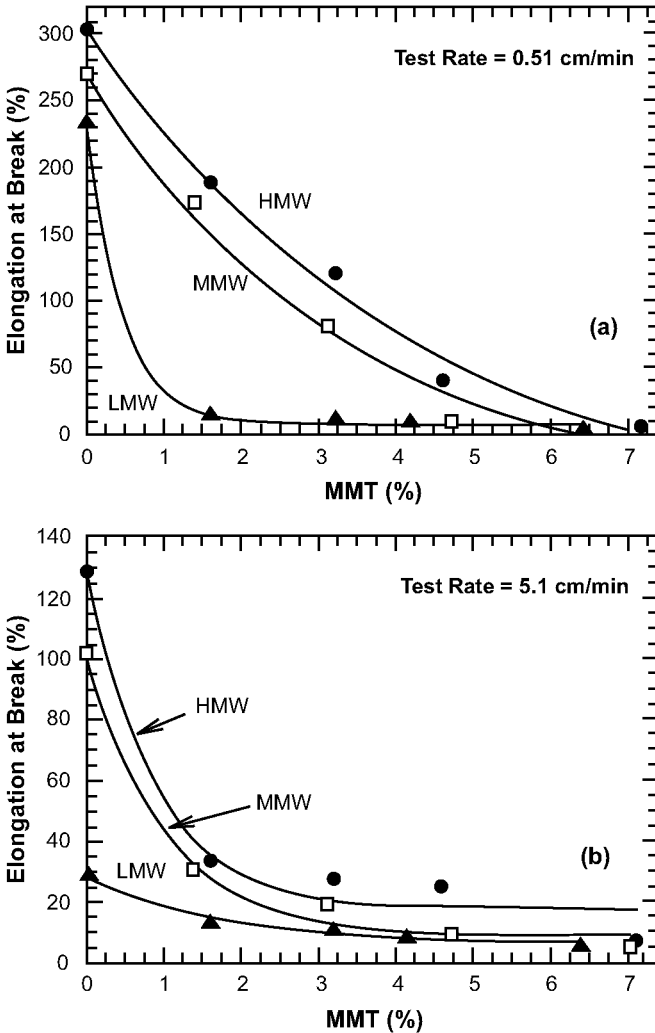


Figure 6.5 Effect of montmorillonite content on elongation at break for LMW-, MMW-, and HMW-based composites at a crosshead speed of (a) 0.51 cm/min and (b) 5.1 cm/min.¹⁸

The notched Izod impact strength, shown in Fig. 6.6, was relatively independent of clay concentration for the HMW and MMW composites, but gradually decreased for the LMW composites. The melt viscosity, and consequently the shear stress, increased with increasing nylon 6 molecular weight. The higher shear stress is believed to have been the major contributor to exceptional exfoliation of clay platelets in the higher molecular weight nylon 6-matrix.

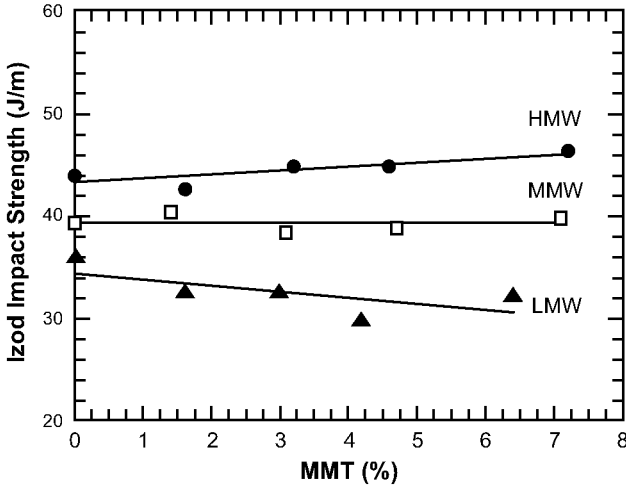


Figure 6.6 Effect of montmorillonite content on Izod impact strength for LMW-, MMW-, and HMW-based composites.¹⁸

Figure 6.7 schematically illustrates the various roles of shear stress during the melt compounding of nanocomposites. Initially, the stress should assist in rupturing large organoclay particles into dispersed stacks of silicate tactoids [Fig. 6.7(a)]. As the extrudate travels in extruder, transfer of the stress from the molten polymer to the silicate tactoids is proposed as shearing tactoids into smaller stacks of silicate platelets [Fig. 6.7(b)]. Ultimately, individual platelets peel apart through a combination of shear and diffusion of polymer chains in the organoclay gallery [Fig. 6.7(c)].

The Paul group¹⁹ also studied the structure-property relationships for nanocomposites formed by melt processing of a series of organically modified montmorillonite clays with high and low molecular weight nylon. The structure of the alkyl ammonium substituent on the clay was systematically varied to determine how specific groups affect nylon 6 nanocomposite morphology and the resulting physical properties. As demonstrated by WAXD, galleries of the organoclays expand in a systematic manner to accommodate the molecular size and the amount of amine surfactant exchanged for the inorganic cation of the natural occurring montmorillonite. The density of the organic material in the galleries is in the anticipated range for organic liquids and solids. Both the modulus and the yield strength of the nanocomposites appear to decrease as the original organoclay *d*-spacing increases, in contrast to some earlier suggestions in the literature.

Three distinct surfactant structural effects have been identified that lead to a high amount of exfoliation, high stiffness, and increased yield strengths for nanocomposites based on high molecular weight

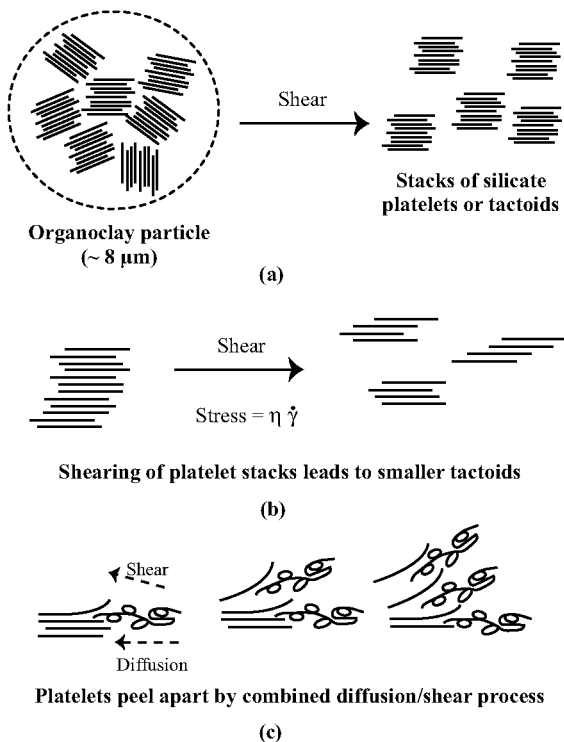


Figure 6.7 Stepwise mechanism of clay platelet exfoliation in the melt compounding of nanocomposites: (a) organoclay particle breakup, (b) clay tactoid breakup, and (c) platelet exfoliation.¹⁸

polyamide. They are (a) one long alkyl substituent group on the ammonium ion rather than two, (b) methyl groups rather than 2-hydroxy-ethyl groups on the amine, and (c) an equivalent amount of amine surfactant on the clay (to avoid an excess amount). Similar trends, but lower extents of exfoliation, were seen for a lower molecular weight grade of nylon 6. The authors proposed that these effects are due to the amount of exposed silicate surface. Alkyl ammonium ions, which cover a larger portion of the silicate surface, shield desirable polar polyamide-polar clay interactions and ultimately lead to reduced platelet exfoliation. However, this finding does not imply that unmodified clay, i.e., sodium montmorillonite, would be optimum. Organic surface modification of the clay is still required to overcome the cohesive forces between neighboring platelets so that polymer intercalation and exfoliation can occur during melt processing. It is possible that these observations may “only apply” to nylon 6 polymer. Thus, the nature of polymer-organoclay thermodynamic interactions

may be different for other polymers and may have different structure-property effects. Continued studies in this area are encouraged.

The molecular weight of the polyamide has a significant effect on nanocomposite morphology and mechanical properties. The higher molecular weight polyamide consistently leads to better exfoliation and greater reinforcement than lower molecular weight polyamides. In summary, with proper selection of the nylon 6, organoclay modifier, and processing conditions, one can produce high-performance nylon 6 nanocomposites by melt processing. These features contributed to the development of commercial nylon type products by Toyota, Ube, Unitika, Honeywell, and others.

6.3 Thermoset Nanocomposites

Epoxy resins are widely used in commercial and military applications because of their high mechanical/adhesion characteristics, solvent and chemical resistance combined with the versatility of cure over a range of temperatures without by-products. The properties of epoxy-based organic-inorganic composites can be fine-tuned by an appropriate choice of the structures of both epoxy prepolymer and hardener and of the type and amount of inorganic filler or fiber.

The use of inorganic nanoparticles can be particularly interesting for conventional epoxy-based polymer matrix composites (PMCs). Micrometer-sized inorganic particles are currently widely used for the reinforcement of epoxy matrices to lower shrinkage on curing, thermal expansion coefficients, improve thermal conductivity, and meet mechanical requirements. The final properties of the PMCs are affected by several factors, such as intrinsic characteristics of each component, the contact, the shape and dimension of fillers, and the nature of the interface. A strong interface between matrix and filler is needed to achieve high performance. It requires that the load applied to the PMCs is mainly transferred to the fillers via the interface. To enhance these properties, the use of submicron particles can lead to a significant improvement of the mechanical properties of the PMCs. In the past decade, a tremendous amount of research has been conducted in the preparation of submicron inorganic particles, leading to the possibility of preparing PMCs reinforced with nanofillers.²⁰ The enhanced modulus, decreased coefficient of thermal expansion, and potential rigid-phase toughening afford thermoset nanocomposites opportunities in PMCs. Epoxy resin reinforced with nanoparticles represents one of the most actively studied resin matrix. Details of epoxy nanocomposites studies are included in this section.

6.3.1 Epoxy nanocomposites

Brown, Curliss, and Vaia²¹ studied the role of various quaternary ammonium surfactants in the epoxy/diamine nanocomposite formation and processing conditions that are necessary in ultimately fabricating PMCs with a nanocomposite matrix resin. The use of a hydroxyl-substituted quaternary ammonium modifier provides flexibility to combine both catalytic functionality (increases the intragallery reaction rate), and enhanced miscibility toward both components (resin and clay). Balancing these two factors is necessary to maintain rheological properties that are compatible with PMCs.

Initially, the effect of various processing steps on nanocomposite formation was examined by the authors. Figure 6.8 outlines the generalized processing procedure to fabricate the Epon 828 layered silicate nanocomposites. In all three organically modified layered silicates (OLS) of this study, intercalation and not exfoliation of Epon 828 was observed. This study shows autoclave processing (evacuated bag with 100 psi hydrostatic pressure) was useful in producing bubble-free, uniform plaques, especially for systems containing greater than 10 wt% OLS. Figure 6.9 shows optical micrographs of the optically transparent plaques of autoclaved nanocomposites containing up to 20 wt% S30A in Epon 828/D400 resin, and turbid plaques containing up to 20 wt% B34 in Epon 828/D400 resin.

Detailed TEM verified the intercalated structure of B34-containing resin [Figs. 6.10(a) and 6.10(b)]. Individual layers, oriented perpendicular to the sample surface, appear as dark lines, with lateral size around 500 nm. Primary particles consisting of groups of parallel layers are larger, with dimensions from 0.5 to 1.5 μm . Although the S30A

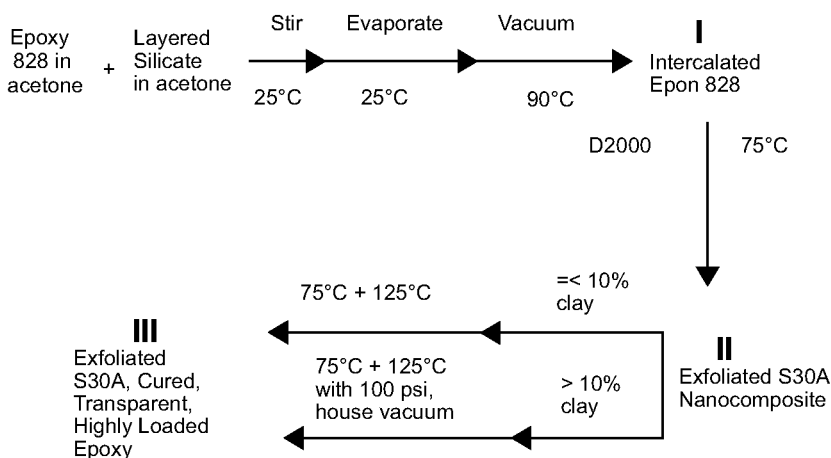


Figure 6.8 Generalized processing scheme.²¹

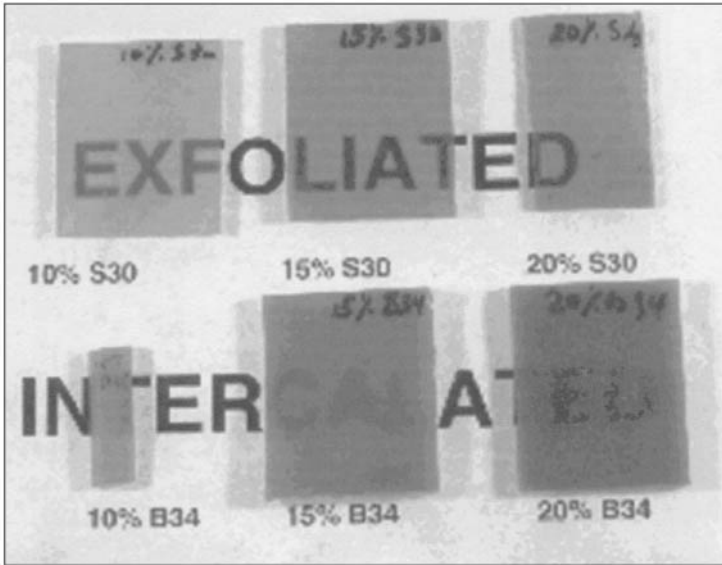


Figure 6.9 Optical image of 5-mm-thick plaques of Epon 828/D400 containing 10, 15, and 20% S30A and 10, 15, and 30% B34.²¹

nanocomposites were suggested as exfoliated by x-ray diffraction and the plaques were optically clear, a mixture of partially intercalated as well as exfoliated layers exists [Figs. 6.11(a) and 6.11(b)].

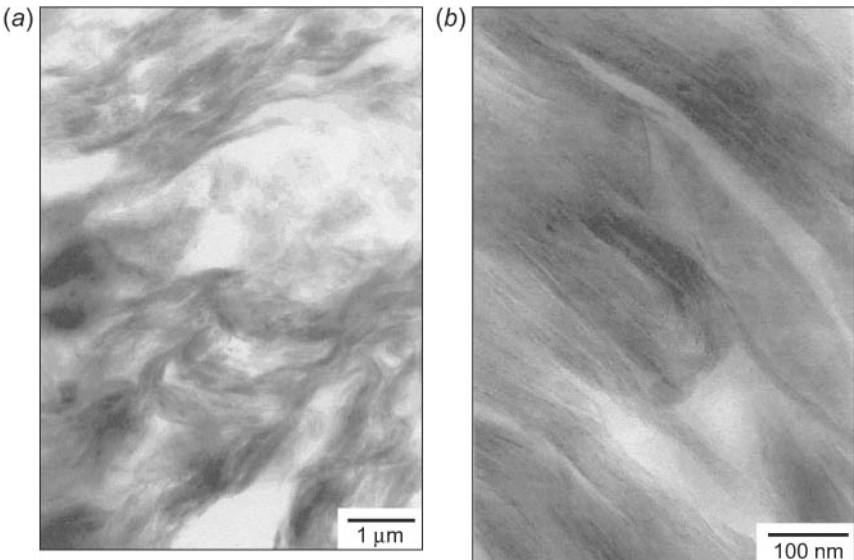


Figure 6.10 Bright-field TEM micrographs of 10% B34 in Epon 828 cured with D2000: (a) low magnification of large aggregate, and (b) high magnification within aggregate.²¹

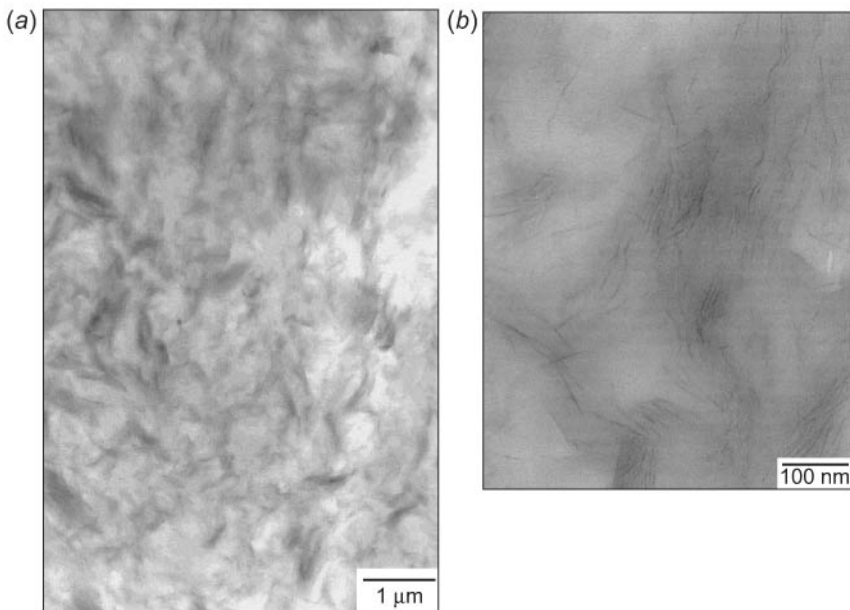


Figure 6.11 Bright-field TEM micrographs of 10% S30A in Epon 828 cured with D2000: (a) low and (b) high magnification.²¹

Figures 6.12(a) and 6.12(b) compare the temperature dependence of the dynamic shear moduli (1 Hz) from torsional bar measurements for unmodified Ep828/D2000 with nanocomposites containing 10 wt% OLS. Figure 6.13 compares the temperature dependency of the dynamic shear moduli at various concentrations of intercalated B34 and partially exfoliated S30A in Epon 828/D2000. Table 6.2 summarizes the glass transition temperature and dynamic shear moduli at various temperatures.

Incorporation of the layered silicate into the epoxy resulted in flammability²² and ablation resistance.²³ When exposed to an open flame, unmodified Epon 828/D2000 burns, leaving oily, tacky residue. Resin containing intercalated B34 burns but produces a rigid, graphitic char. Increased exfoliation of the layers, as in the S30A-containing resin, resulted in a self-extinguishing behavior upon removal of the flame. The resulting char exhibited a highly uniform microcellular microstructure consisting of 10- to 20- μm diameter cells separated by 1- to 2- μm struts of silica-alumina-oxycarbide (Fig. 6.14), as determined by the microprobe system.

This study suggests that surface modifiers should include a catalyst to enhance reactivity within the OLS crystallites. A critical balance must be maintained for use with PMCs. If miscibility between the OLS and the thermoset mixture is great, unacceptably large viscosity

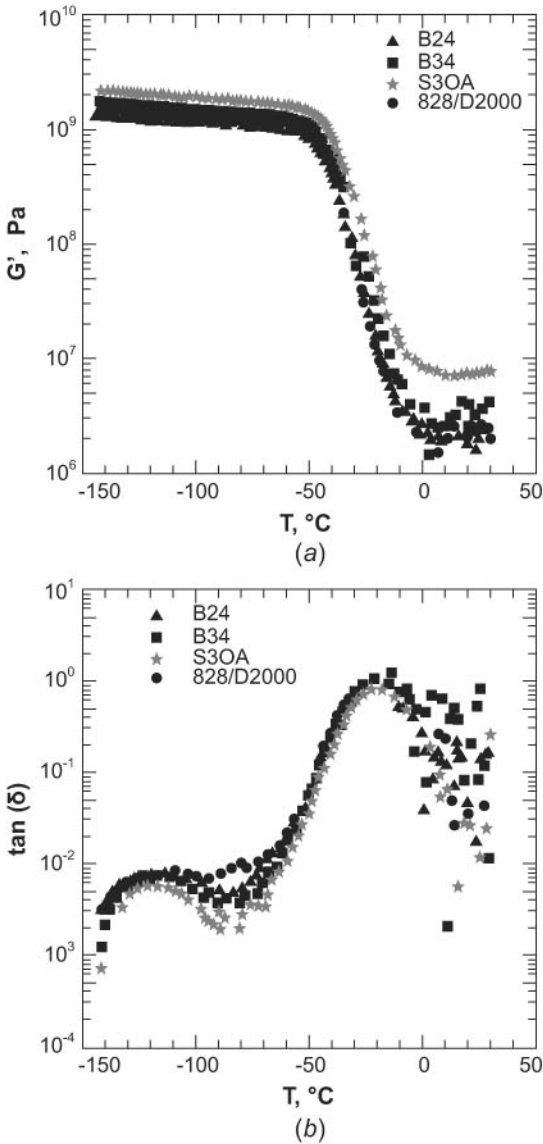


Figure 6.12 Temperature dependence of the (a) dynamic shear moduli and (b) $\tan(\delta)$ from torsional bar measurements (0.1% strain 1 Hz) for unmodified Epon 828/D2000 and nanocomposites containing 10 wt% OLS.²¹

increases and potential gelation of the system will occur through impingement of exfoliated sheets. If miscibility toward both components is insufficient, a nonstoichiometric mixture of reagents will

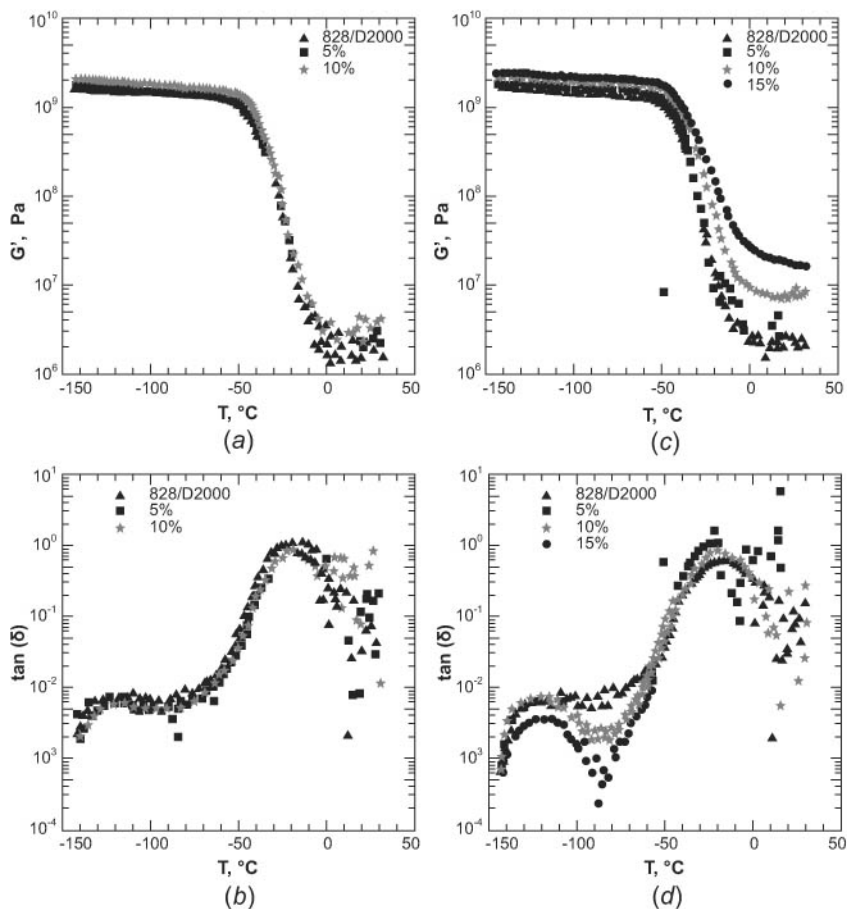


Figure 6.13 Temperature dependence of the dynamic shear moduli and δ from torsional bar measurements (0.1% strain, 1 Hz) for various concentrations of (a) and (b) intercalated B34 and (c) and (d) partially exfoliated S30A in Epon 828/D2000.²¹

be presented in the interlayer, and enhanced interlayer reactivity will not produce the desired network formation. Thus, optimal methodology for multicomponent thermosets would entail a choice of an OLS modification that (a) partially compatibilizes the mixture, leading to a disordered intercalate containing both components and separation of the OLS aggregates into individual crystallites (slight viscosity increase), and (b) catalyzes interlayer reactivity to enable rapid layer separation before matrix gelation. Overall, this study further refines the criteria for organic modifiers necessary to fabricate blends of nanoscopic inorganic phases in high performance resins.

TABLE 6.2 Dynamic Mechanical Summary for OLS/Epon 828/D2000²¹

	wt% OLS	T_g^a	$G (\pm 25\%)$			
			-140°C^b	-60°C^b	-25°C^c	0°C^c
828/D2000		-24	1.6	1.1	31	2.4 ^d
B34	2.5	-18	1.7	1.3	35	1.2 ^d
	5.0	-18	1.8	1.3	52	2.5 ^d
	10	-18	1.9	1.4	80	3.1
S30A	2.5	-18	1.7	1.3	90	2.5 ^d
	5.0	-22	1.8	1.3	50	1.0 ^d
	10	-15	2.3	1.7	120	8.0
	15	-12	2.4	1.9	270	23
B24	10	-22	1.4	1.1	28	2.9 ^d

^aPlus or minus 3°C. ^bIn GPa. ^cIn MPa. ^dLowest resolution for transducer ~1–2 MPa.

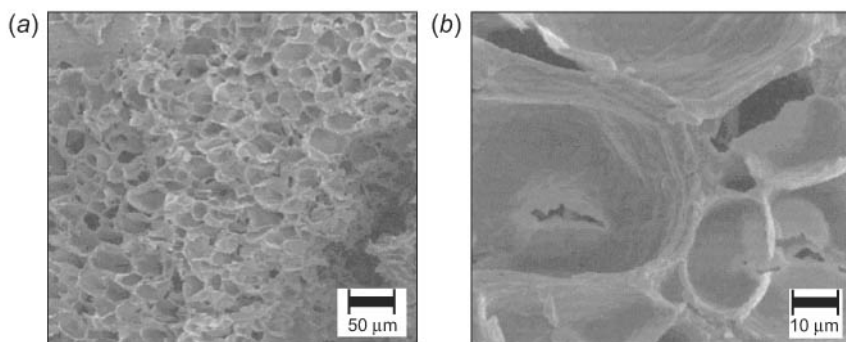


Figure 6.14 Scanning electron microscopy micrograph of char produced by burning 10% S30A/Epon 828/D2000 in air.²¹

Most of the recent focus on epoxy systems has been on difunctional resins, predominantly using the diglycidyl ether of bisphenol-A (DGEBA). The more highly crosslinked systems are difficult to toughen, and a smaller increase than those achieved for flexible and low glass transition epoxy systems may still prove to be beneficial, in comparison to using higher concentrations of more commonly used fillers. Although DGEBA is widely used, most aerospace materials and other high-performance applications require epoxies of higher functionality because of the required higher modulus and glass transition temperature.

Becker, Varley, and Simon²⁴ investigated the possibility of improving the mechanical properties of multi-functionality epoxy resins through dispersion of octadecyl ammonium ion-modified layered silicates within the polymer matrix. They used three different resins: (a) difunctional diglycidyl ether of bisphenol-A (DGEBA), (b) trifunctional triglycidyl *p*-amino phenol (TGAP) and (c) tetrafunctional tetraglycidyl diamino diphenylmethane (TGDDM) in their studies.^{24,25} All resins were cured

with diethyltoluene diamine (DETDA). The morphology of the final, cured materials was probed by wide-angle x-ray scattering (WAXS), optical, and atomic force microscopy. The α - and β -relaxation temperatures of the cured systems were determined using dynamic mechanical thermal analysis. It was found that the presence of organoclay steadily decreased both transition temperatures with increasing filler concentration. The effect of different concentration of the alkyl ammonium-modified layered silicate on the toughness and stiffness of the different epoxy resins was analyzed. All resin systems have shown improvement in both toughness and stiffness of the materials through the incorporation of layered silicates, despite the fact that it is often found that these two properties cannot be simultaneously achieved.

The clay used in the studies by Becker et al.^{24,25} is a commercially available octadecyl ammonium ion-modified montmorillonite layered silicate (Nanomer I.30E) from Nanacor, Inc. The three epoxy resins were DGEBA, TGAP, and TGDDM. The hardener is a mixture of two DETDA. Structures of these materials are shown in Table 6.3.

A wide range of epoxy nanocomposites with varying amounts of organoclay were prepared. Wide-angle x-ray scattering traces of the clay concentrations show that the organoclay, with an initial d -spacing

TABLE 6.3 Epoxy Resins and Hardener as Used for Nanocomposite Synthesis²⁴

Substance	Formula
DGEBA	
TGAP	
TGDDM	
DETDA	

of 23 Å, is exfoliated in the DGEBA-based system (Fig. 6.15). Only the 10 percent concentration shows a distinct peak correlating to a *d*-spacing of 48 Å. In contrast to the DGEBA-based system, resins of high functionality show distinctive peaks even at a lower organoclay concentration, indicating that these systems have a lower degree of exfoliated layered silicate. Wide-angle x-ray scattering traces are shown in Fig. 6.16 for TGAP and Fig. 6.17 for TGDDM.

Before investigating the microstructure of the nanocomposites, optical microscopy was applied to image the bulk surface. Optical micrographs, as shown in Fig. 6.18 for the DGEBA system containing

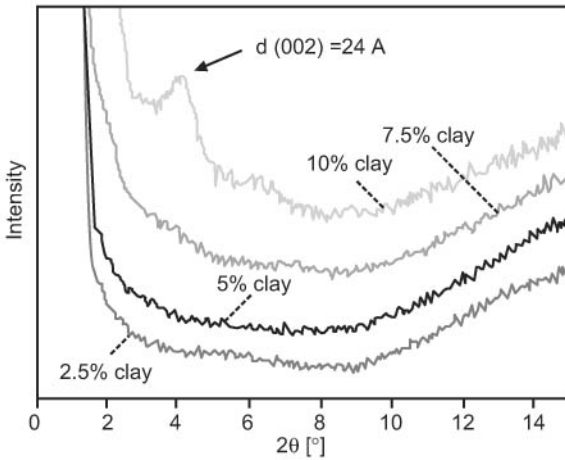


Figure 6.15 Wide-angle x-ray scattering of DETDA-cured DGEBA nanocomposites containing 0 to 10% organoclay.²⁴

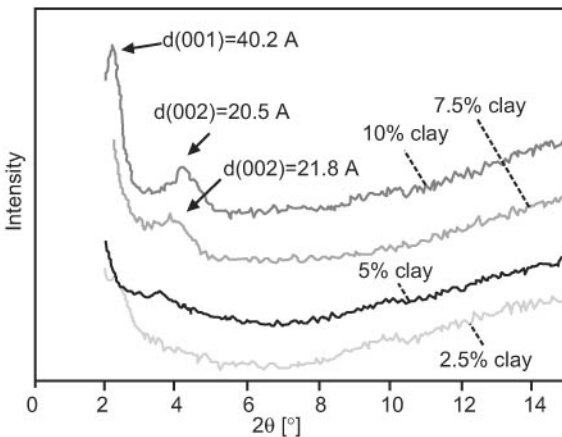


Figure 6.16 Wide-angle x-ray scattering of DETDA-cured TGAP nanocomposites containing 0 to 10% organoclay.²⁴

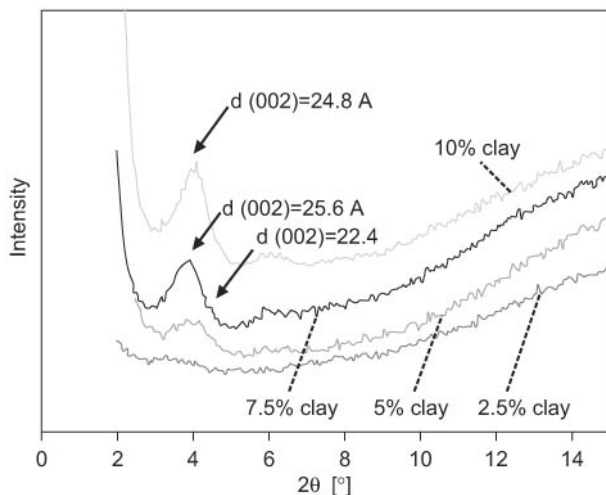


Figure 6.17 Wide-angle x-ray scattering of DETDA-cured TGDDM nanocomposites containing 0 to 10% organoclay.²⁴

5 percent of organoclay, show large particulate phases. This finding indicates that even for the DGEBA-based system, not all clay particles are fully dispersed in the polymer phase. Both optical microscopy and AFM images show that at least part of the silicate content remained in tactoids or stackings of layers, rather than forming a homogenous morphology through the whole material.

Dynamic mechanical thermal analysis was applied in two steps, from -100 to 50°C and from 50 to 300°C , to investigate the influence of the organoclay on the α - and β -transitions. Plots of the glass

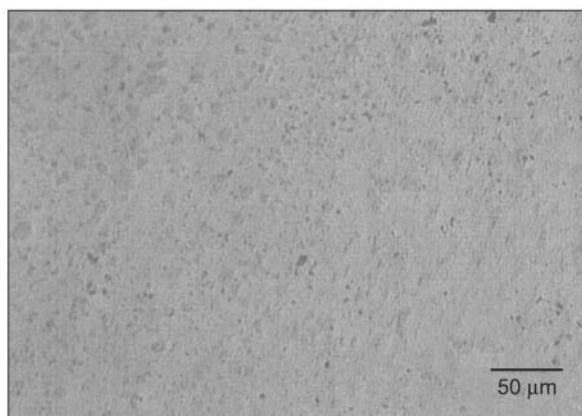


Figure 6.18 Optical micrograph showing large particles in the DETDA-cured DGEBA system containing 5% organoclay.²⁴

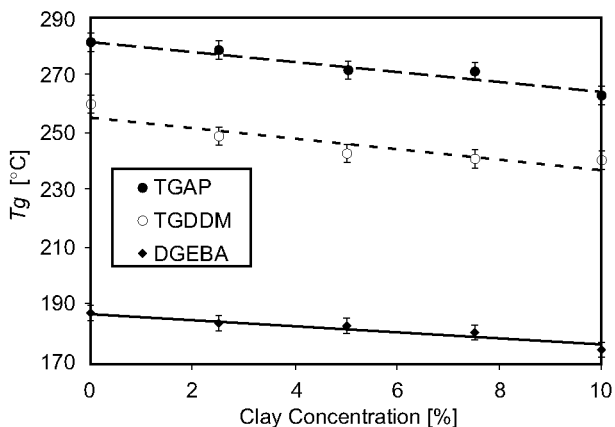


Figure 6.19 Glass transition temperatures as determined from the δ peak of DMTA measurements.²⁴

transition temperature (T_g) as a function of organoclay concentration are shown in Fig. 6.19. The value of T_g decreased steadily with increasing organoclay concentrations. The reduction in T_g was found to be about 15°C for TGAP- and DGEBA-based systems, and 20°C for the TGDDM-based system with an organoclay content of 10 percent. In summary, it appears that in all systems, incorporation of clay leads to a decrease in both glass transition and secondary relaxation temperatures, possibly because of a decrease in effective crosslink density.

Differential scanning calorimetry data of peak temperatures and percentage residual cure are summarized in Table 6.4. Differential scanning calorimetry traces for the DGEBA-based systems confirmed full cure while the TGAP and TGDDM-based nanocomposites show small peaks around 250°C, indicating further reaction. Although the amount of reaction is very small, the filled resin was more fully cured than the neat systems.

Density results of the various nanocomposites after curing, as determined by gas-displacement pycnometry, are shown in Fig. 6.20. Theoretical densities according to the rule-of-mixture were calculated

TABLE 6.4 DSC Results of Postcured Epoxy-Clay Nanocomposite Systems²⁴

Clay conc. (%)	TGAP		TGDDM	
	Peak (°C)	% Residual cure	Peak (°C)	% Residual cure
0	266.4	5.1	253.7	4.3
2.5	270.2	2.9	237.4	0.7
5	251.0	3.0	248.5	3.7
7.5	253.7	2.8	233.0	1.1
10	255.7	1.6	229.5	0.6

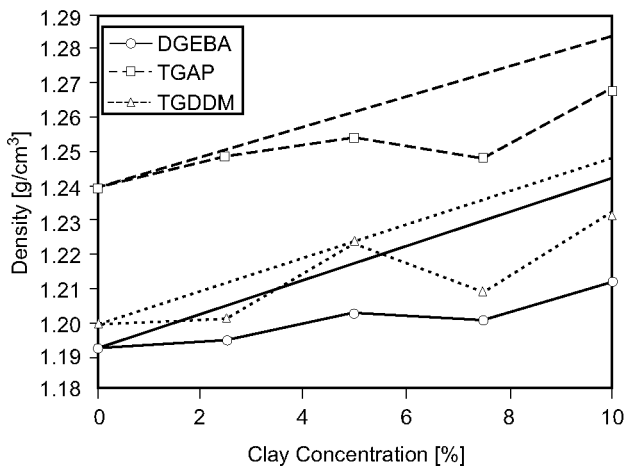


Figure 6.20 Density of cured-epoxy nanocomposites as determined from gas-displaced pycnometry. The dotted lines represent theoretical densities according to the rule-of-mixtures.²⁴

based on an organoclay density of 1.68 g/cm^3 . The rule-of-mixture data are represented as straight lines in Fig. 6.20. All densities are within a very small range of 1.19 to 1.23 g/cm^3 . The densities are generally slightly below predicted values according to the rule-of-mixture. The lower density is possibly related to poorer packing of the polymer molecules near the silicate layers.

Modulus was determined using the three-point bend test. All resin systems show a monotonic increase in modulus with increasing organoclay concentrations. A normalized modulus was calculated by dividing the actual nanocomposite modulus value through the modulus of the unfilled system. Figure 6.21 shows that the increase in modulus for all resin systems is about 20 percent for an organoclay concentration of 10 percent. The improved stiffness can be directly ascribed to the reinforcement of exfoliated, high-aspect-ratio platelets. In the work by Lan and Pinnavia,²⁶ it was found that a Jeffamine D2000-cured DGEBA nanocomposite increased the modulus by approximately 500 percent at an organoclay concentration of 10 wt%. The DGEBA system in this study shows only slightly greater relative improvement in modulus than the TGAP or TGDDM resin, respectively.

The fracture toughness, as quantified by stress intensity factor K_{IC} , was determined using the compact tension test. The normalized stress intensity factor data is shown in Fig. 6.22. Most toughening techniques show a loss in stiffness; however, in this study both toughness and stiffness were improved through the organoclay incorporation. The stress intensity factor indicates that DGEBA and TGDDM show an

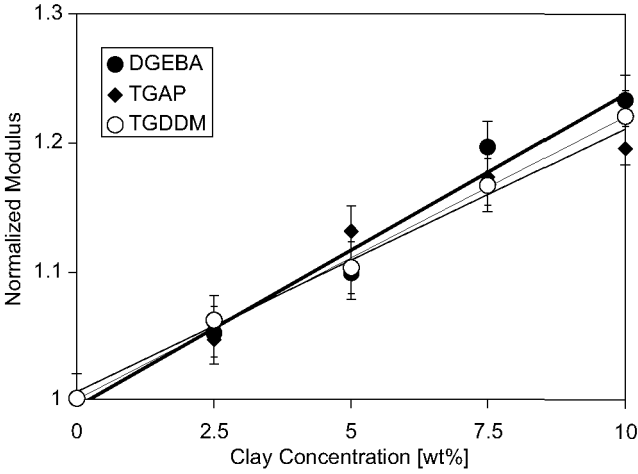


Figure 6.21 Normalized modulus of different DETDA-cured resins containing 0 to 10% organoclay.²⁴

increase in toughness in a similar range, whereas improvement in the TGAP system is significantly lower.

Improvement in stiffness of the high-functionality epoxy resins is comparable with those achieved for the difunctional (DGEBA) resin system. Although it is often found that improvement in modulus compromises toughness of the material, both toughness and stiffness were improved through the incorporation of organoclay. The improved modulus and toughness make nanocomposite strategy an attractive

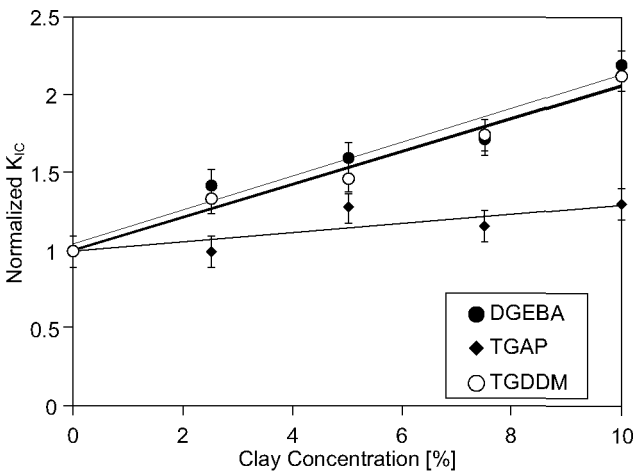


Figure 6.22 Normalized stress intensity factor of different DETDA-cured resins containing 0 to 10% organoclay.²⁴

alternative to the commonly used micrometer-sized impact modifying fillers.

Becker et al.²⁵ extended the above research to study the relationship between cure temperature, morphological, and mechanical properties of the di-, tri-, and tetrafunctional, high-performance, epoxy layered-silicate nanocomposites. Wide angle x-ray scattering was used to monitor the different stages of organoclay exfoliation kinetics. It was found that some degree of conversion was required to obtain significant intercalation. The polymer nanocomposite morphology was probed using TEM, WAXD, and positron annihilation lifetime spectroscopy. Comparison of the nanocomposite formation based on three different epoxy resins with different structures and functionalities has shown that the structure and chemistry of the epoxy resin, its mobility, and its reactivity are key factors controlling exfoliation, and therefore the morphology, of the cured nanocomposite. Two different effects have to be considered: improved dispersion and better exfoliation of the silicate platelets in the polymer matrix, and changes in the nature of the reaction and thus the network formation. The difunctional DGEBA resin gave better exfoliation than the high-functionality resins. It was observed for all resins that higher cure temperatures led to improved intercalation and exfoliation. Tactoids were observed in all three resin systems. This is attributed to better catalysis of the intragallery reaction by organo-ions, which reside within the galleries. The structural mobility (diffusion), as indicated by the viscosity of the resin, seemed less relevant.

High cure temperatures were found to improve clay exfoliation and simultaneously increase toughness and modulus in the case of DGEBA- and TGAP-based materials. The mechanical properties remained relatively unaffected by the cure temperature. It is assumed that the effect of cure temperature on the reaction chemistry and the effect on cross-link density also have a major impact on mechanical properties in addition to the changes in organoclay dispersion. More dramatic changes in the nanocomposite morphology may be required to significantly change the mechanical properties. Because the processing temperature window is limited by side reactions and thermal degradation, variation of cure temperature alone may not be sufficient to form a fully dispersed, "true" nanocomposite. Free volume properties did not vary significantly between resins or with curing temperature and generally followed the rule-of-mixtures, although there was a suggestion that the presence of clay leads to increased free volume. This finding was consistent with decreased T_g upon the addition of layered silicate and decreased cross-link density in interfacial regions of clay and epoxy matrix.

Wang et al.²⁷ developed a "slurry-compounding" process for the preparation of epoxy-clay nanocomposites. The microstructures of the

nanocomposites were characterized by optical and transmission electron microscopy. It was found that clay was highly exfoliated and uniformly dispersed in the resulting nanocomposite. Characterization of mechanical and fracture behaviors revealed that Young’s modulus increases monotonically with increasing clay concentration while the fracture toughness shows a maximum at 2.5 wt% of clay. The micro-deformation and fracture mechanisms were studied throughout TEM and SEM analyses of the microstructures of the arrested crack tips and damage zone. The initiation and development of the micro-cracks are the dominant micro-deformation and fracture mechanisms in these nanocomposites. The formation of a large number of micro-cracks and the increase in the fracture surface area due to crack deflection are the major toughening mechanisms.

Silica nanoparticles of different sizes were characterized by Bondioli et al.²⁸ using the sol-gel process. Epoxy-silica nanocomposites were prepared with nanosilicas (reaction of TEOS with methanol or ethanol) ranging from 1 to 5 wt%. Scanning electron microscopy analysis and tensile tests were carried out on these epoxy-silica nanocomposites, and the results indicated the absence of particle aggregation and enhanced elastic modulus. Mechanical properties were also modeled using a finite element code (OOF²⁹) that was able to construct a numerical model based on microstructural analyses of the material. Table 6.5 summarizes the mechanical properties (elastic moduli experimentally determined and modeled) for the nanocomposites. A more reliable three-phase model was developed by considering the presence of an interphase layer surrounding the particles with the intermediate elastic properties between the epoxy and the inclusion, and a characteristic size proportional to the particle radius. The composite elastic moduli were calculated from the stress-strain curves. The results were recorded (Table 6.5), as a function of particle concentration. The elastic modulus increased with a higher amount of

TABLE 6.5 Experimental and Model Elastic Modulus of Epoxy-Silica Nanocomposites²⁸

Composite	SiO ₂ content (wt %)	E (GPa) experimental	Standard deviation (experimental) (GPa)	E (GPa) two-phase model
Unfilled epoxy	—	2.000	0.100	2.000
Epoxy/SiO ₂ from ethanol	1	2.135	0.149	2.018
	3	2.272	0.181	2.062
	5	2.370	0.123	2.099
Epoxy/SiO ₂ from methanol	1	2.428	0.065	2.019
	3	2.506	0.147	2.061
	5	2.537	0.202	2.104

reinforcement, but the values predicted by the computational model are considerably lower. It is worth noting that analytical equations such as the Halpin-Tsai rule³⁰ or the Lewis-Nielsen equation,³¹ give estimates that are in good agreement with the numerical results and thus differ from the experimental data. This finding suggests that analytical and numerical approaches commonly used for particulate composites are not suitable when a nanophase is involved.

A more refined model was used by the authors by considering the interphase between the matrix and the particle as a third constituent phase. It was assumed that such an interphase had properties intermediate between the polymeric matrix and the inorganic filler. It was hypothesized that the dimension of the interphase's extension was proportional to the particle size. It was set equal to half of the average diameter. Nanocomposites with nanosilicas were modeled, and the respective elastic moduli were evaluated with the same procedure previously described. The results are plotted in Fig. 6.23.

The numerical results are in good agreement with the experimental data, especially if the error bars are taken into consideration. These results demonstrate that such a model is a reliable tool for the prediction of elastic properties of epoxy-silica nanocomposites. Future development of this work should aim at the experimental characterization of the nanocomposite interphase to support the hypotheses of this research. The characteristic size and stiffness should be determined. This determination could be achieved by means of AFM techniques³² or nanoindentation equipment.³³

6.4 Elastomer Nanocomposites

6.4.1 TPO nanocomposites

Most of the early work on the formation of nanocomposites focused on their preparation via in-situ polymerization of caprolactam (Toyota group and others) in the presence of expanded silicate material. Recently, researchers have investigated melt processing as the preferred method for the preparation of thermoplastic nanocomposites such as nylon,¹⁵⁻¹⁸ polystyrene,^{11,34} and polypropylene.^{35,36} These researchers have been primarily interested in the effect of processing conditions on physical and mechanical property enhancement of the resulting PNMs.

Fasulo et al.³⁷ conducted extrusion trials designed to determine the role of processing conditions with regard to the dispersion of the clay-based filler systems in thermoplastic polyolefin resin systems. The thermoplastic polyolefin (TPO) resins were supplied by Basell Polyolefins, Inc. These resins were based on a blend of polypropylene homopolymer, impact modified polypropylene, and ethylene-propylene-

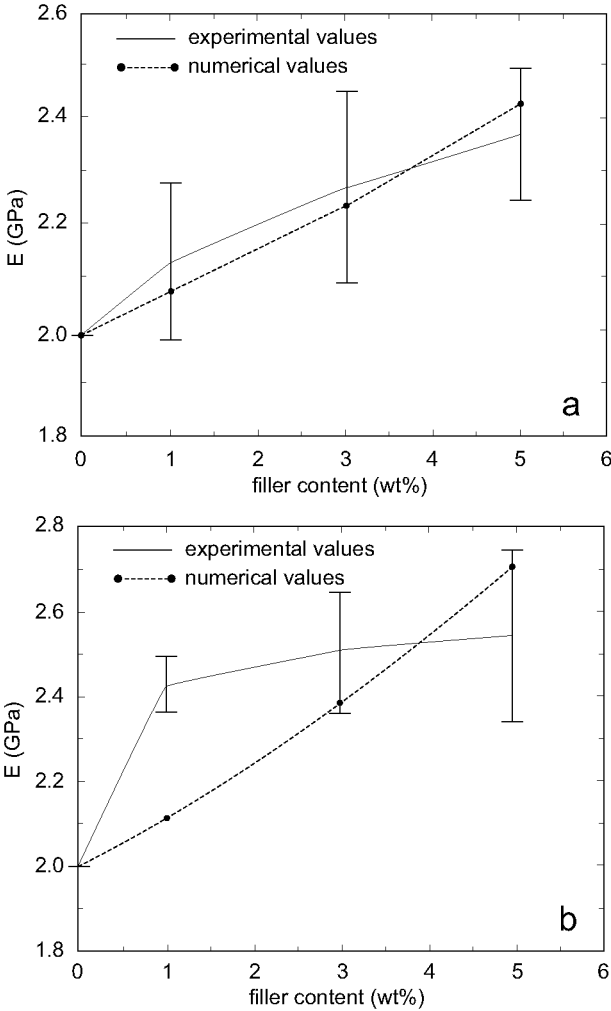


Figure 6.23 Elastic modulus as a function of filler content (three-phase model): (a) nanosilica from methanol and (b) nanosilica from ethanol.²⁸

based elastomers. The organically modified MMT fillers were provided by Southern Clay Products, Inc. These fillers were refined from Wyoming bentonite clay and were modified using an ammonium-based surfactant.

The authors examined more than 300 varying nanocomposite formulations and evaluated their surface appearance. The surface evaluation consisted of visual ranking, controls, and microscopy. Surface imperfections of the injection-molded samples were examined visually as well as by scanning electron microscopy (SEM). Energy-

dispersive x-ray spectroscopy (EDS) analysis was utilized to examine on the surfaces and cross-sections of these samples. Figure 6.24 shows a representative surface with a numerical ranking.

Property evaluation included physical and mechanical properties. The physical properties appeared to be relatively independent of the processing conditions. The only property that appeared to correlate with the amount of agglomerated material is the number of brittle failures from multiaxial instrumented impact, and even this result was minimal. Figure 6.25 shows two micrographs, the control formulation and a nanocomposite prepared using the same processing conditions. Both materials exhibited few imperfections. The imperfections visible on the control formulation can be attributed to either the coating process or poor elastomer dispersion.

Figure 6.26 shows micrographs of the painted surfaces from two of the worst-ranked processing conditions. These imperfections are more numerous and larger than those observed on the control panel and can be attributed only to the surface imperfections observed on the substrate. For the low-high-low processing conditions, the imperfections are small but are visible in bright light. For the high-high-low processing conditions, the imperfections are large and visible in any light. These

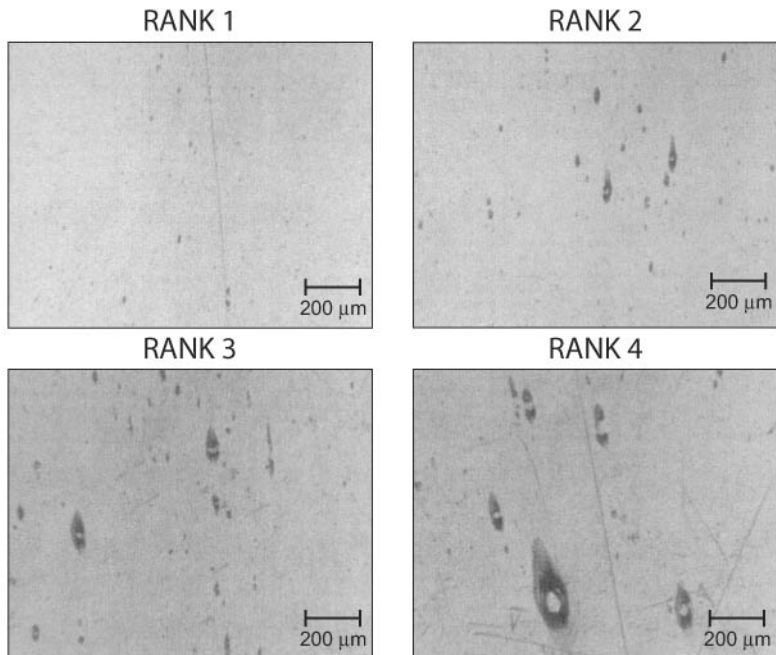


Figure 6.24 Micrographs showing representative surfaces with various ranks.³⁷

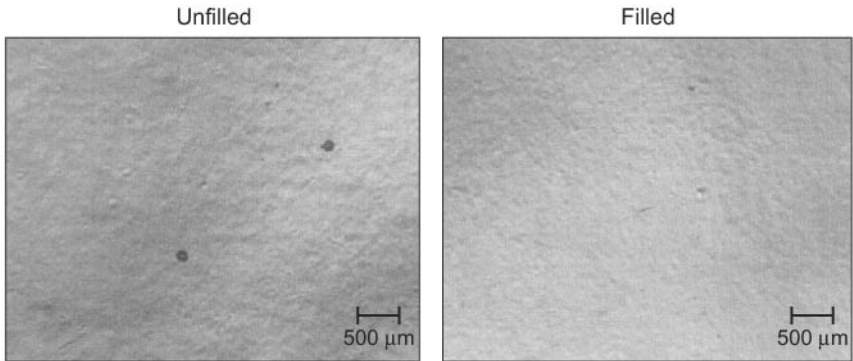


Figure 6.25 Micrographs of a coated, unfilled formulation and a coated nanocomposite formulation.³⁷

results provide a reasonable estimate of the size of surface imperfections required for the imperfection to be visible after the painting operation.

This work has shown that certain processing conditions maximize the clay agglomeration, whereas others will minimize it. A balance of processing parameters is required. The clay can agglomerate when the processing temperature is higher because there is opportunity to degrade the intercalant or surfactant that exists between the clay sheets prior to the wetting of the filler by the molten resin. Without the surfactant, the surface tension of the unmodified clay sheets leads to agglomeration. When the feed rate is high, there is a greater possibility of forming a mass of clay that can then experience increased pressure as it is processed in the extruder and creates agglomeration. A low screw rotation speed delivers less energy to the clay sheets, leading to slower reduction in the breakdown in the height of the clay stacks, and ultimately reduces the exfoliation of the filler material.

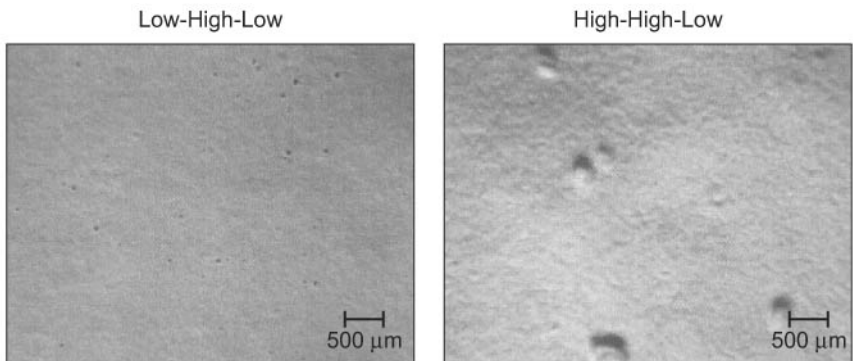


Figure 6.26 Micrographs of coated nanocomposite formulations processed under the worst conditions.³⁷

6.5 Summary

Several examples of thermoplastic-, thermoset-, and elastomer-based nanocomposites are presented in this chapter. These examples demonstrate that physical, mechanical, other material properties are enhanced with the proper selection of a nanoparticle that is compatible with the polymer. Suitable processing and curing conditions are essential to create polymer nanocomposites for a specific application. Characterization tools are useful to understand polymer nanocomposites' behavior, properties, and performance. Custom designed polymer nanocomposites can be prepared to meet specific needs and requirements.

References

1. T. J. Pinnavaia, "Intercalated Clay Catalysts," *Science* **220**:365–371 (1983).
2. V. Mehrotra and E. P. Giannelis, "Conducting Molecular Multilayers: Intercalation of Conjugated Polymers in Layered Media," *Mater. Res. Soc. Symp. Proc.* **171**:39–44 (1990).
3. E. P. Giannelis, "A New Strategy for Synthesizing Polymer-Ceramic Nanocomposites," *J. Minerals* **44**:28–30 (1992).
4. L. W. Carter, J. G. Hendricks, and D. S. Bolley, United States Patent No. 2531396 (1950) (assigned to National Lead Co.).
5. P. G. Nahin and P. S. Backlund, United States Patent No. 3084117 (1963) (assigned to Union Oil Co.).
6. S. Fujiwara and T. Sakamoto, Japanese Kokai Patent Application No. 109998 (1976) (assigned to Unitika K.K., Japan).
7. Y. Fukushima and S. Inagaki, "Synthesis of an Intercalated Compound of Montmorillonite and 6-Polyamide," *J. Inclusion Phenomena* **5**:473–482 (1987).
8. A. Okada, Y. Fukushima, M. Kawasumi, S. Inagaki, A. Usuki, S. Sugiyama, T. Kuraunch, and O. Kamigaito, United States Patent No. 4739007 (1988) (assigned to Toyota Motor Co., Japan).
9. M. Kawasumi, M. Kohzaki, Y. Kojima, A. Okada, and O. Kamigaito, United States Patent No. 4810734 (1989) (assigned to Toyota Motor Co., Japan).
10. A. Usuki, Y. Kojima, M. Kawasumi, A. Okada, Y. Fukusima, T. Kurauch, and O. Kamigaito, "Synthesis of Nylon 6–Clay Hybrid," *J. Mater. Res.* **8**:1179–1184 (1993).
11. S. S. Ray and M. Okamoto, "Polymer/Layered Silicate Nanocomposites: A Review From Preparation to Processing," *Prog. Polym. Sci.* **28**:1539–1641 (2003).
12. R. A. Vaia, H. Ishii, and E. P. Giannelis, "Synthesis and Properties of Two-Dimensional Nanostructures by Direct Intercalation of Polymer Melts in Layered Silicates," *Chem. Mater.* **5**:1694–1696 (1993).
13. R. A. Vaia, K. D. Jandt, E. J. Kramer, and E. P. Giannelis, "Kinetics of Polymer Melt Intercalation," *Macromolecules* **28**:8080–8085 (1995).
14. R. A. Vaia and E. P. Giannelis, "Lattice Model of Polymer Melt Intercalation in Organically-Modified Layered Silicates," *Macromolecules* **30**:7990–7999 (1997).
15. R. A. Vaia and E. P. Giannelis, "Polymer Melt Intercalation in Organically Modified Layered Silicates: Model Predictions and Experiment," *Macromolecules* **30**:8000–8009 (1997).
16. H. R. Dennis, D. L. Hunter, D. Chang, S. Kim, J. L. White, J. W. Cho, and D. R. Paul, "Effect of Melting Processing Conditions on the Extent of Exfoliation in Organoclay-Based Nanocomposites," *Polymer* **42**:9513–9522 (2001).
17. J. W. Cho and D. R. Paul, "Nylon 6 Nanocomposites by Melt Compounding," *Polymer* **42**:1083–1094 (2001).
18. T. D. Fornes, P. J. Yoon, H. Keskkula, and D. R. Paul, "Nylon 6 Nanocomposites: The Effect of Matrix Molecular Weight," *Polymer* **42**:9929–9940 (2001).

19. T. D. Fornes, P. J. Yoon, D. L. Hunter, H. Keskkula, and D. R. Paul, "Effect of Organoclay Structure on Nylon 6 Nanocomposite Morphology and Properties," *Polymer* **43**:5915–5933 (2002).
20. M. I. Baraton, *Synthesis, Functionalization and Surface Treatment of Nanoparticles*, American Science Publishers, Los Angeles, CA, 2002.
21. J. M. Brown, D. Curliss, and R. A. Vaia, "Thermoset-Layered Silicate Nanocomposites: Quaternary Ammonium Montmorillonite with Primary Diamine Cured Epoxies," *Chem. Mater.* **12**:3376–3384 (2000).
22. J. W. Gilman, "Flammability and Thermal Stability Studies of Polymer Layered-Silicate (Clay) Nanocomposites," *Appl. Clay Sci.* **15**:31–59 (1999).
23. R. A. Vaia, G. Price, P. N. Ruth, H. T. Nguyen, and J. Lichtenhan, "Polymer/Layered Silicate Nanocomposites as High Performance Ablative Materials," *Appl. Clay Sci.* **15**:67–92 (1999).
24. O. Becker, R. Varley, and G. Simon, "Morphology, Thermal Relaxations and Mechanical Properties of Layered Silicate Nanocomposites Based upon High-Functionality Epoxy Resins," *Polymer* **43**:4365–4373 (2002).
25. O. Becker, Y.-B. Cheng, R. J. Varley, and G. P. Simon, "Layered Silicate Nanocomposites Based on Various High-Functionality Epoxy Resins: The Influence of Cure Temperature on Morphology, Mechanical Properties, and Free Volume," *Macromolecules* **36**:1616–1625 (2003).
26. T. Lan and J. T. Pinnavaia, "Clay-Reinforced Epoxy Nanocomposites," *Chem. Mater.* **6**:2216–2219 (1994).
27. K. Wang, L. Chen, J. Wu, M. L. Toh, C. He, and A. F. Yee, "Epoxy Nanocomposites with Highly Exfoliated Clay: Mechanical Properties and Fracture Mechanisms," *Macromolecules*, **38**:788–800 (2005).
28. F. Bondioli, V. Cannillo, E. Fabbri, and M. Messori, "Epoxy-Silica Nanocomposites: Preparation, Experimental Characterization, and Modeling," *J. Appl. Polym. Sci.* **97**:2382–2386 (2005).
29. W. C. Carter, S. A. Langer, and E. R. Fuller, "OOF Manual: Version 1.0," [http: www.ctcms.nist.gov/oof](http://www.ctcms.nist.gov/oof) 1998.
30. E. J. Barbero, *Introduction to Composite Materials Design (Solution Manual)*, Taylor and Francis, New York, 1998.
31. T. B. Lewis and L. E. Nielsen, "Dynamic Mechanical Properties of Particulate-Filled Composites," *J. Appl. Polym. Sci.* **14**:1449–1471 (1970).
32. S.-L. Gao and E. Mader, "Characterisation of Interphase Nanoscale Property Variations in Glass Fibre Reinforced Polypropylene and Epoxy Resin Composites," *Composites Part A: Applied Science and Manufacturing* **33**:559–576 (2002).
33. H. Wang, Y. Bai, S. Liu, J. Wu, and C. P. Wong, "Combined Effects of Silica Filler and Its Interface in Epoxy Resin," *Acta Materialia* **50**:4369–4377 (2002).
34. B. Hoffmann, C. Dietrich, R. Thomann, C. Friedrich, and R. Mulhaupt, *Macromol. Rapid Commun.* **21**:57 (2000).
35. M. Kawasumi, N. Hasegawa, M. Kato, A. Usuki, and A. Okada, "Preparation and Mechanical Properties of Polypropylene-Clay Hybrids," *Macromolecules* **30**:6333–6338 (1997).
36. P. Reichert, H. Nitz, S. Klinke, R. Brahdtsch, R. Thomann, and R. Mulhaupt, "Poly (propylene)/Organoclay Nanocomposite Formation: Influence of Compatibilizer Functionality and Organoclay Modification," *Macromol. Mater. Eng.* **275**:8–17 (2000).
37. P. D. Fasulo, W. R. Rodgers, R. A. Ottaviani, and D. L. Hunter, "Extrusion Processing of TPO Nanocomposites," *Polym. Eng. Sci.* **44**:1036–1045 (2004).

This page intentionally left blank

Polymer Nanostructured Materials for High-Temperature Applications

In previous chapters, different types of nanoparticles, selecting resin matrix and nanoparticles, processing of nanomaterials, morphological characterization of polymer nanostructured materials, and properties of several widely studied thermoplastic nanocomposites, thermoset nanocomposites, and elastomer nanocomposites were described. In this chapter, the *properties and performance* of this novel type of *polymeric material for high-temperature applications* are discussed. Selective polymer nanocomposites or polymer nanostructured materials for different high-temperature applications are illustrated to demonstrate the technical approach. Thermoplastic nanocomposites, thermoset nanocomposites, and elastomer nanocomposites are included in this chapter. Physical, mechanical, and thermal properties, accompanied with the performance of these polymer nanostructured materials, are reported.

7.1 Thermoplastic Nanocomposites

Three applications are selected as examples for this section: (a) nonhalogenated, flame-retardant polymers for cabling jackets, (b) waterborne flame-retardant coatings for wood substrate, and (c) flame-retardant polymer nanocomposites for selective laser sintering allowing rapid manufacturing. These examples are used to illustrate the processing techniques used to form the resulting polymer nanocomposites. The flammability, mechanical properties, and performance characteristics of these PNMs for specific applications are included.

7.1.1 Nonhalogenated, flame-retardant polymers for cabling jackets¹

Current shipboard fiber optic cabling jackets contain halogen flame retardants to fulfill both the MIL-C-85045² and the UL-910³ standards for flammability. Funding was provided by the U.S. Navy to develop nonhalogenated flame retardant (FR) polymers using innovative flame-retardant concepts: MMT organoclay and phosphorus flame-retardant additives.¹

Selection of materials. Equistar Petrothene XL 07414, a nonhalogenated, nontarnishing, FR-crosslinkable polyolefin copolymer (based on polypropylene (PP)) containing approximately 40 percent alumina trihydrate (ATH) was selected as the baseline polymer. Two Southern Clay Products MMT clays, Cloisite 15A and 20A, were selected (Chap. 2). Clariant Exolit AP 750, a nonhalogenated, intumescent FR additive based on ammonium polyphosphate, APP ($(\text{NH}_4)_3\text{PO}_4$) was also selected for this study.

Material processing. All materials were dried overnight under vacuum at 80°C before processing. Polymer and nanoclays were extruded by a Haake CTW 100 conical intermeshing, counterrotating, twin-screw extruder. This model is considered a low-shear extruder because it has an L/D of 10/1 (inlet) and 15/1 (outlet). Materials were extruded at 60 rpm with a temperature profile of 113, 109, and 120°C. All test plaques were compression-molded into a size of 10 by 10 by 0.32 cm on a heated press and cured in an oven at 204°C for 15 minutes.

Flammability testing. Heat release rate (HRR) is important for characterizing the real-fire response properties of polymeric materials.⁴ Relatively small specimens (10 by 10 by 0.32 cm), using the laboratory-scale mass loss calorimeter according to ASTM E2102⁵ under the heat flux of real-scale fires, were used in this study (Chap. 5). Figure 7.1 shows the mass loss calorimeter. This test method was developed for material evaluation, mathematical modeling, design purposes, and research and development. It acquires the time to sustained ignition, peak heat release rate, average heat release rate (for 600 s), total heat release, and percentage mass loss during the experiment. The samples were exposed at heat fluxes of 35 and 65 kW/m² for 10 to 15 minutes by the mass loss calorimeter. An average of three samples was tested, and the flammability properties were averaged. Additional information of the mass loss calorimeter can be found in Chap. 5.



Figure 7.1 Mass loss calorimeter for flammability testing.

Discussion of results. Several studies were conducted, such as the (a) effect of MMT clays loading, (b) effect of heat fluxes for MMT clay, (c) effect of phosphorus loading, (d) synergistic effect of MMT clay and phosphorus, and (e) effect of FR additives on mechanical properties.

Effect of MMT clay loading. Three levels of organoclay loadings were used in this study: PP with 4, 6, and 8 wt% of Cloisite 20A; and PP with 4, 6, and 8 wt% Cloisite 15A. Figures 7.2 and 7.3 show the HRR and mass loss of Cloisite 15A clay at 35 kW/m^2 , respectively. Figures 7.4 and 7.5 show the HRR and mass loss of Cloisite 20A at 35 kW/m^2 , respectively. Peak heat release rate (PHRR) decreased and residual mass increased with the increase in weight percent of Cloisite 15A MMT clay. Peak heat release rate increased slightly and residual mass decreased slightly with the increase in weight percent of 20A MMT clay. The 8 wt% Cloisite 15A clay exhibited the optimal performance.

Figure 7.6 shows the transmission electron micrographs of the pretest PP-8% Cloisite 15A clay nanocomposite specimen at $5600\times$ and

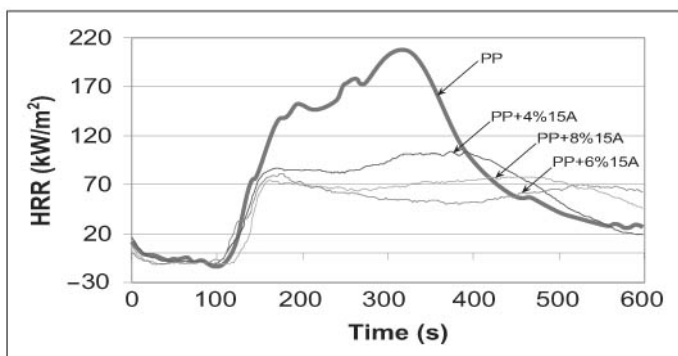


Figure 7.2 Heat release rate of Cloisite 15A MMT clay at 35 kW/m^2 .

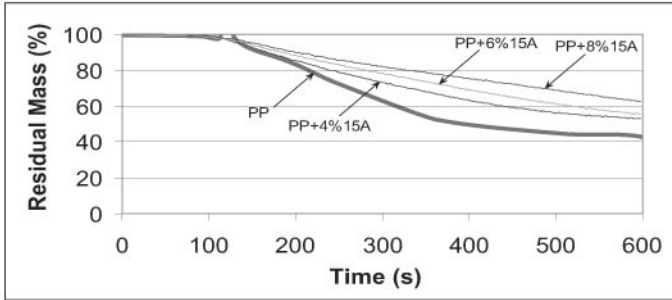


Figure 7.3 Residual mass of Cloisite 15A MMT clay at 35 kW/m^2 .

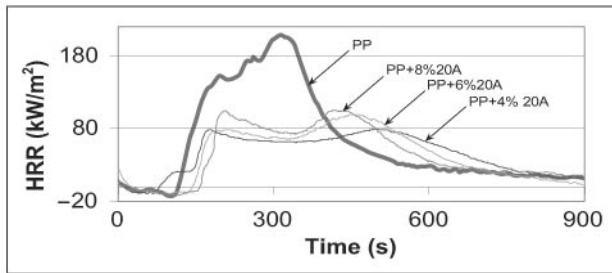


Figure 7.4 Heat release rate of Cloisite 20A MMT clay at 35 kW/m^2 .

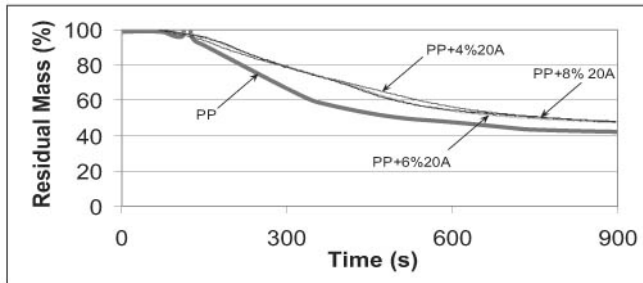


Figure 7.5 Residual mass of Cloisite 20A MMT clay at 35 kW/m^2 .

44,000 \times magnifications. The large particles are the micrometer-size ATH particles mixed well with the Cloisite 15A nanoclays. Figure 7.7 shows the transmission electron micrographs of the posttest PP-8% Cloisite 15A clay nanocomposite specimen at 5600 \times and 44,000 \times magnification. It is clearly shown in Fig. 7.7 that the ATH particles were not totally consumed and still partially remained in the ash residue. The membranelike Cloisite 15A nanoclays are clearly seen in the 44,000 \times magnification TEM micrograph in Fig. 7.7.

Effect of heat fluxes on PP-8% Cloisite 15A nanocomposite. Comparisons of PP and PP-8% Cloisite 15A were carried out at heat fluxes 35 and

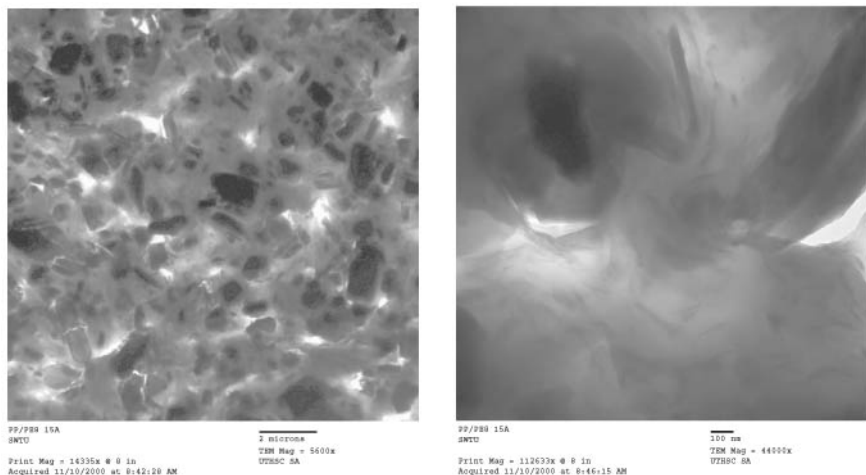


Figure 7.6 Transmission electron micrographs of the pretest PP-8% Cloisite 15A nanocomposite specimen at 5600 \times (left) and 44,000 \times (right) magnifications.

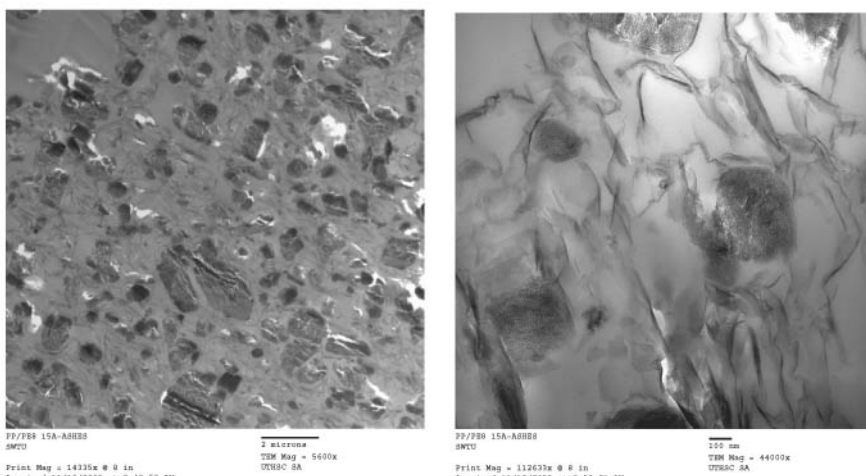


Figure 7.7 Transmission electron micrographs of the posttest PP-8% Cloisite 15A nanocomposite specimen at 5600 \times (left) and 44,000 \times (right) magnifications.

65 kW/m², as shown in Fig. 7.8. For 35 kW/m², the PHRR was lowered significantly from 211 to 86 kW/m² with the addition of 8 wt% of Cloisite 15A. For 65 kW/m², the PHRR was also lowered significantly from 328 to 143 kW/m² with the addition of 8 wt% of Cloisite 15A. Residual mass (Fig. 7.9) shows that MMT clay gives its best performance from 100 to 600 s for the lower heat flux; for the higher heat flux, this enhancement is from 100 to 500 s.

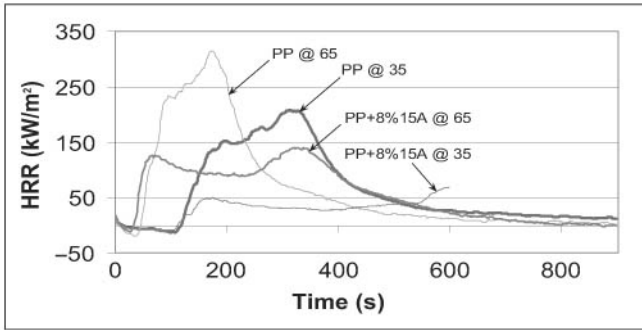


Figure 7.8 Heat release rate of 8% Cloisite 15A MMT clay at 35 and 65 kW/m².

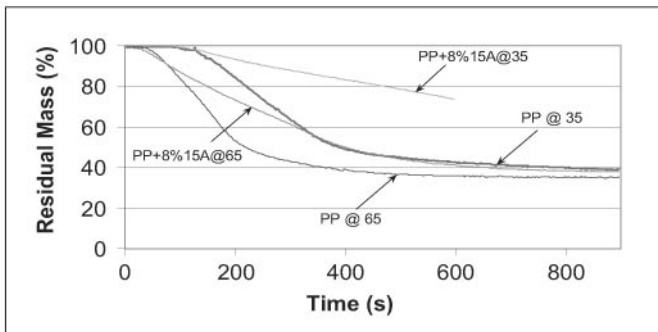


Figure 7.9 Residual mass of 8% Cloisite 15A MMT clay at 35 and 65 kW/m².

Effect of phosphorus loading. The addition of AP 750 (phosphorus FR additive) delayed the time of ignition substantially to over 200 s and also lowered the PHRR, as shown in Fig. 7.10. The 25 wt% AP 750 has the lowest PHRR, followed by the 35 wt% of AP 750, and then the 45 wt% AP 750 specimens. All three specimens had higher residual

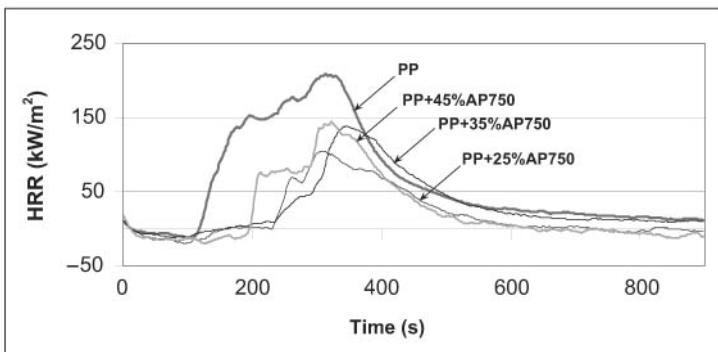


Figure 7.10 Heat release rate of AP 750 at 25, 35, and 45 wt% at 35 kW/m².

mass than the PP specimen, as shown in Fig. 7.11. It was demonstrated that Cloisite 15A nanoclay and Exolit AP 750 reduced flammability of Petrothene XL 07414 PP polymer dramatically.

Synergistic effect of MMT clay and phosphorus. The addition of 8 percent Cloisite 15A MMT clay to the PP polymer lowered the PHRR substantially, and the addition of 35 percent AP 750 delayed the time of ignition to 250 s. The combination of 8 percent Cloisite 15A and 35 percent AP 750 was blended with the PP system to study the synergistic effect of the two flame retardants. The HRR of the combined Cloisite 15A and AP 750 is shown in Fig. 7.12. The results, though not ideal, are encouraging. After reviewing the individual HRR plots of the three mass loss calorimeter runs of the PP/8% Cloisite/35% AP 750 polymer blend, a large variation in HRR data was noted. Most likely this variation is related to the addition sequence of components to PP. The sequence of processing is important, and it needs to be explored further to achieve more desirable results.

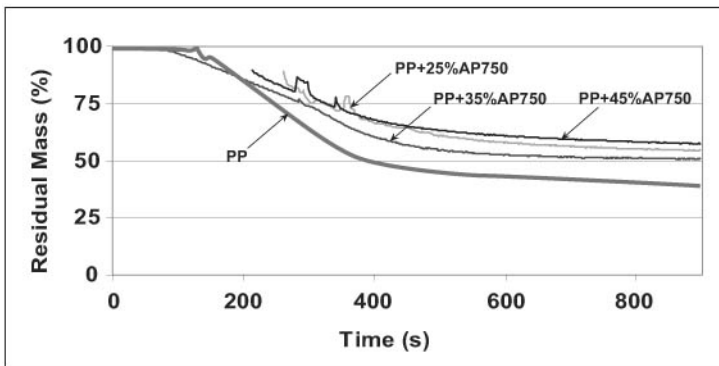


Figure 7.11 Residual mass of AP 750 at 25, 35, and 45 wt% at 35 kW/m².

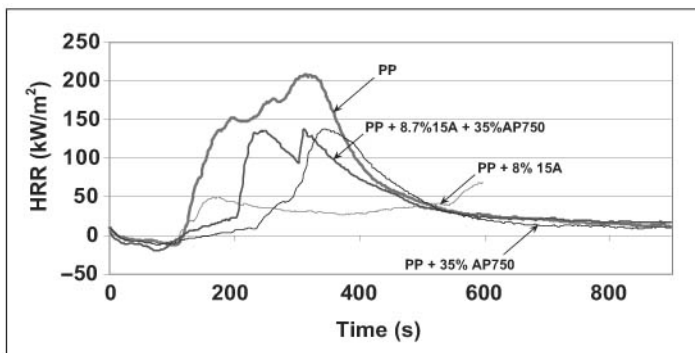


Figure 7.12 Heat release rate of the combined Cloisite 15A and AP 750.

Effect of flame retardants on mechanical properties. The modulus increased dramatically (up to 130%) with the addition of 8 percent MMT clay. Both Cloisite 15A and 20A MMT clays had about the same effect on modulus. The modulus only increased by 55 percent with the addition of 25 percent phosphate FR additive. A trade-off between modulus and strain at break and peak stress was noted; this effect is more sensitive in the PP-clay samples but not as sensitive in the PP-phosphate samples. Samples with both clay and phosphate resembled the phosphate-only sample, but the best mechanical properties were achieved when clay and phosphate were added to the feed simultaneously rather than sequentially.

Summary and conclusions. The feasibility of using nonhalogenated FR additives for shipboard optical fiber cables was demonstrated. Montmorillonite clay and phosphorus FR additives with PP polymer systems were formulated and tested. The most promising FR formulation is PP/8% Cloisite 15A MMT clay. Phosphorus FR additives can delay time of ignition. The synergetic effect of MMT clay with conventional phosphorus FR additives to the PP polymer system offers promise and should be further investigated. Modulus increased dramatically with the addition of 8 percent MMT clay.

7.1.2 Waterborne fire-retardant nanocomposite coating^{6,7}

Fire-retardant (FR) coatings are used to protect material surfaces against intensive heat from fire. These coatings sharply limit the flame spread and smoke development on building materials. American Society for Testing and Materials (ASTM) E 84⁸ is a standard used to evaluate flammability properties of building materials. It is more cost-effective to use a controlled laboratory device (cone calorimeter, see Chap. 5)⁴ for FR coating product development than to conduct a complete ASTM E 84 test. The author and coworkers have developed a cost-effective approach for screening experimental FR coatings.⁹

Materials and processing. The objective of this study is to formulate and evaluate clear, water-based FR polymer-clay nanocomposite coatings for building materials.^{6,7} Cloisite Na⁺ nanoclay (see Chap. 2) was dispersed in deionized water using a Dispermat (coating-type mixer) at high speed for about an hour. Then the slurry was allowed to stay at room temperature overnight. Next, the slurry was mixed with polyvinyl acrylic copolymer (PVA 5174, supplied by StanChem, East Berlin, CT) and/or intumescent components (APP, dipentaerythritol, and melamine) for about two hours for coating. Douglas fir plywood in plates

measuring 10 by 10 by 1.8 cm were used as the substrate for all test specimens. The coating thickness was monitored with a digital caliper until the required thickness, usually a dry thickness of 0.28 to 0.30 mm (0.011 to 0.012 inch), had been reached. The edges were then fully coated and the coating was allowed to dry at room temperature for about 24 hours before testing.

Discussion of results

Flammability properties. Samples were exposed to a mass loss calorimeter under a heat flux of 50 kW/m² for 15 minutes. Table 7.1 summarizes some of the main flammability properties of PVA 5174 (control) and the PVA-Clay FR coating systems prepared in this study with clay loading up to 60 percent (wt%). Figure 7.13 shows the heat release rate (HRR) of the PVA 5174 (control) at a heat flux of 50 kW/m². The first peak of the heat release rate appeared quite early, at 50 s after ignition. The average PHRR of three experiments was 220 kW/m². Figure 7.14 shows the heat release rates of PVA-Clay FR coating systems with different clay loadings at a heat flux of 50 kW/m². It is very clear that nanoclay

TABLE 7.1 Calorimeter Data for PVA-Clay FR Coating

MMT clay loading (%)	0	10	20	30	50	60
Sustained ignition time (s)	18	22	268	224	900	900
First peak heat release rate (PHRR) (kW/m ²)	220	123	53	49	26	23
Time to first PHRR (s)	39	37	267	257	No ignition	No ignition
Total heat release (THR) at 900 s (kJ)	629	419	280	249	115	111
Residual mass at 900 s (%)	32	44	54	56	69	70

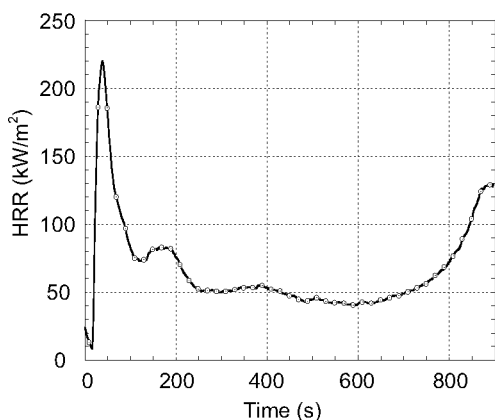


Figure 7.13 Heat release rate of PVA 5174 at 50 kW/m².

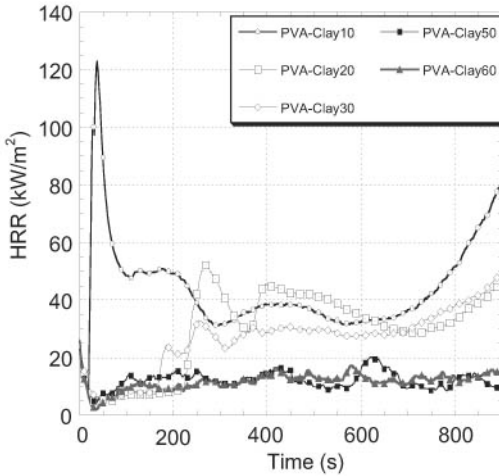


Figure 7.14 Heat release rate of PVA-clay FR coatings at 50 kW/m^2 .

plays a key role in reducing the flammability of these coating systems. With only 10 percent clay, the PHRR was dramatically reduced by almost 50 percent. With more clay applied, the PHRR continued to drop. Actually, with 50 and 60 percent clay loading, the testing specimen could not be ignited throughout the 15-minute test. Figure 7.15 shows the mass loss of the PVA-clay FR coating systems. It is noted that with the addition of clay the residual mass has been raised from 32% to 70%. Figure 7.16 shows the effect of nanoclay loading in the PVA-clay FR coatings on PHHR. It is determined that 30 wt% of nanoclay would be a good loading to study the synergistic effect between the clay and conventional intumescent FR additives. Photos (Fig. 7.17a to f) of combus-

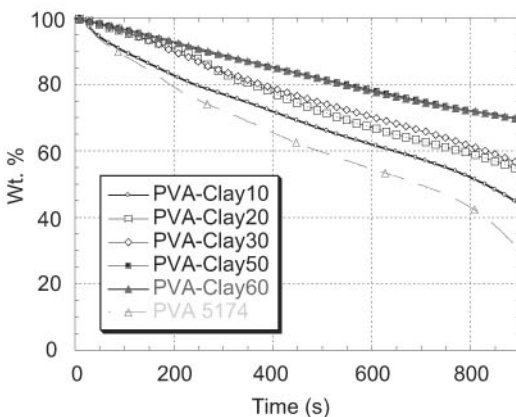


Figure 7.15 Residual mass of PVA-clay FR coatings at 50 kW/m^2 .

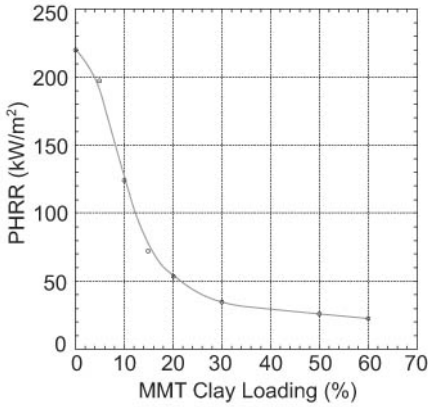


Figure 7.16 Effect of MMT clay loading on peak heat release rate of PVA-clay FR coatings.

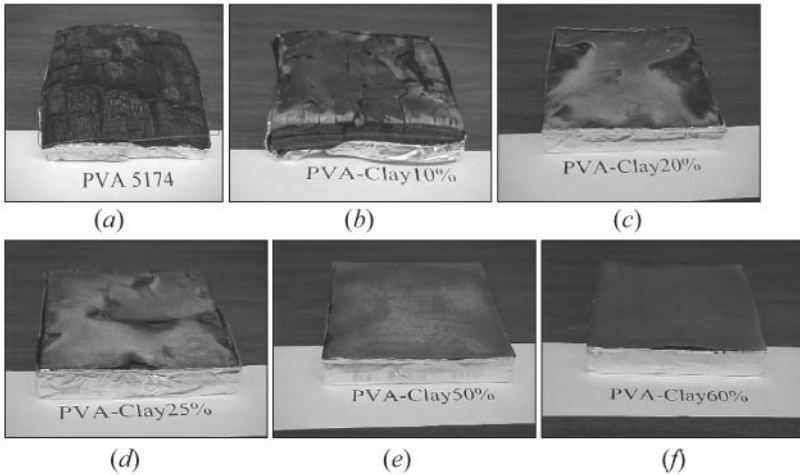


Figure 7.17 Digital photos of combustion residues of wood blocks coated with (a) PVA 5174, (b) PVA-10% MMT clay, (c) PVA-20% MMT clay, (d) PVA-25% MMT clay, (e) PVA-50% MMT clay, and (f) PVA-60% MMT clay.

tion residue indicate that a uniform ceramic layer forms on the top surface of the wood block. Furthermore, SEM micrographs (Figs. 7.18 and 7.19) of a posttest specimen with 30 percent clay indicate that the MMT clay formed protective layers underneath the charred top surface of the coating. In Fig. 7.18 scanning electron micrographs of posttest PVA-30% clay specimen shows ash and unburned PVA matrix (top left), layers of ash/MMT clay (top right), and different views of ash layers (bottom left and bottom right).

Synergistic effect. A synergistic effect between the clay and conventional intumescent FR additives (melamine, dipentaerythritol, and

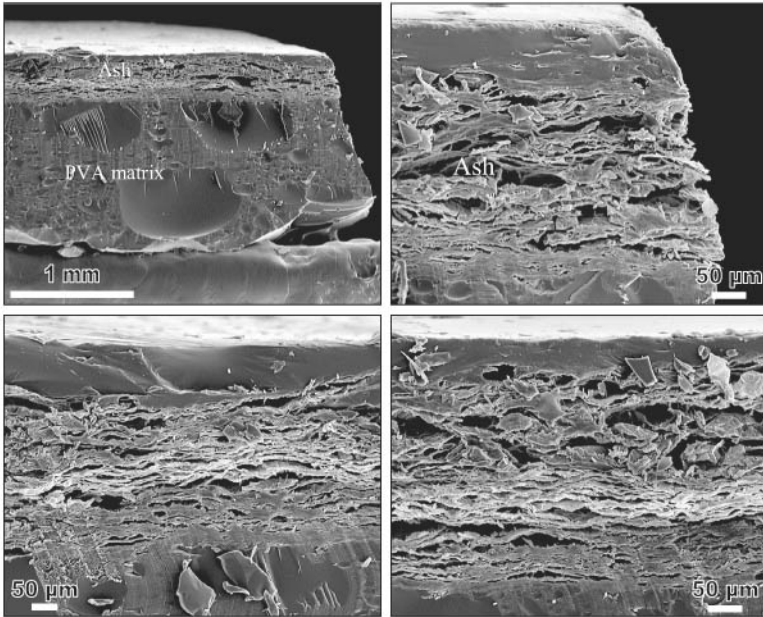


Figure 7.18 Scanning electron micrographs of posttest PVA-30% clay specimen showing ash and unburned PVA matrix (top left), layers of ash/MMT clay (top right), and different views of ash layers (bottom left and bottom right).

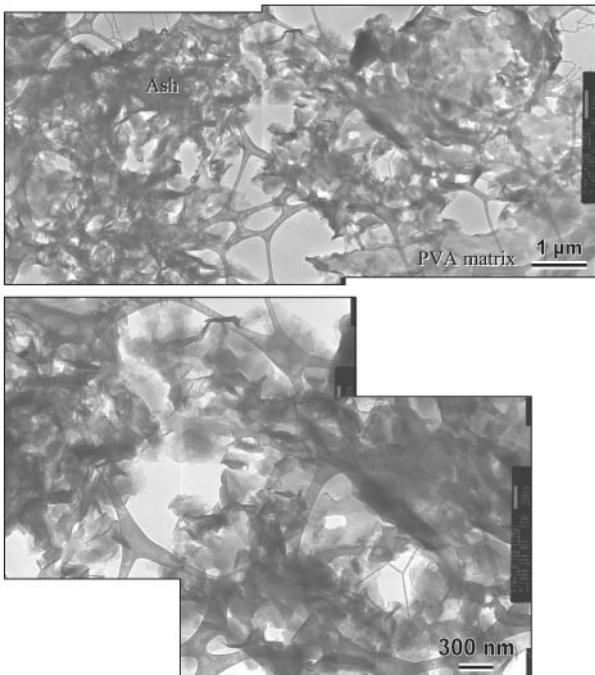


Figure 7.19 Transmission electron micrographs of posttest specimens of PVA-30% clay at progressive magnifications.

ammonium polyphosphate, supplied by StanChem) was observed. With only 5 percent conventional intumescent FR additives, PHRR has been significantly reduced, whereas the sustained ignition time and time to first PHRR have been greatly extended. This result clearly demonstrated a synergistic effect. Figure 7.20 summarizes the heat release rates (HRR) of the PVA-clay-intumescent hybrid coating systems studied. With 5 percent conventional intumescent FR additives, the HRR was significantly reduced. However, it is interesting to note that with 10 percent loading of intumescent FR additives, the first peak of HRR showed up at the very beginning of the test, i.e., only approximately 25 seconds to sustained ignition, and then the flame self-extinguished. This could be attributed to the excessive expansion of the intumescent FR additives under heat, which ruptured the protective ceramic layer. Figure 7.20 also shows the HRR of a PVA-clay nanocomposite coating system that had a 30 percent clay loading but was prepared via a revised procedure, i.e., at a higher shearing speed and higher viscosity (better exfoliation of clay in the system). As can be seen in Fig. 7.20, compared with its old version (PVA-Clay30), the new version (PVA-Clay30New) has a lower HRR throughout the test. Similarly, better fire-retardant properties have also been obtained with this revised procedure for the PVA coating system with 30 percent clay and 5 percent conventional intumescent FR additives. This improved fire-retardant property has resulted from better exfoliation of clay in the system. A high-shear IKA mixer was used to mix 50% PVA+25% Na+25% water. The progressive TEM micrographs (Fig. 7.21) indicate that an excellent dispersion and exfoliation was achieved in such a high level of Cloisite Na⁺ using this type of equipment.

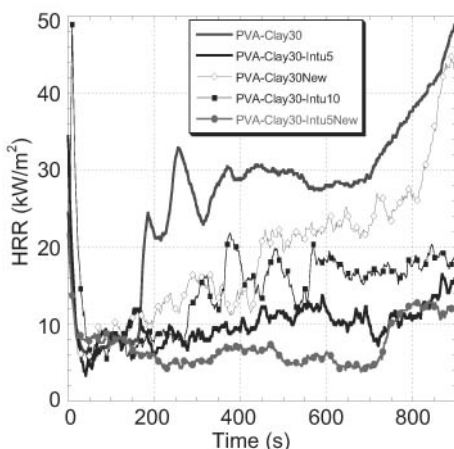


Figure 7.20 The effect of intumescent fire-retardant additives on HRR of PVA-clay coatings at 50 kW/m².

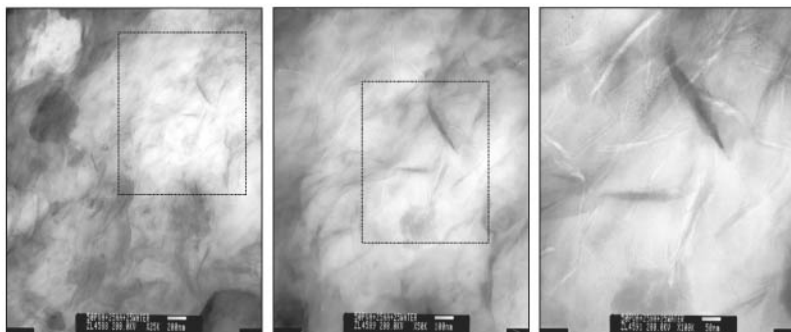


Figure 7.21 Progressive transmission electron micrographs of 50% PVA + 25% Na⁺ + 25% water using IKA high-shear mixing.

Summary and conclusions. The mass loss cone calorimeter is a useful device for screening FR coating systems. The PVA-MMT Cloisite Na⁺ clay, water-based FR coating system shows promise as a vital commercial system. Peak heat release rate and residual mass performance increase with clay loading. A synergistic effect of MMT clay and conventional FR additives in PVA was observed. Enhanced processing procedures and equipment will enhance dispersion and exfoliation of clay in the polymer system thus reduce the flammability of FR coating.

7.1.3 Flame-retardant polymer nanocomposites for rapid manufacturing¹⁰⁻¹⁵

Rapid prototyping (RP) has been embraced as a preferred tool, not only for product development but also, in many cases, for “just-in-time manufacturing.” The use of recently developed additive layered-build fabrication methods of RP, particularly selective laser sintering (SLS), have the potential to facilitate true flexible manufacturing of a small batch of parts “on demand” while avoiding product-line tooling, under-utilization of skilled labor, and the need to maintain high overhead facilities costs.

The automated, layered fabrication of plastic parts, for models, patterns and non-operational prototypes, using sliced computer aided design (CAD) files was first conceived and commercialized in the United States with the method known as stereolithography. This was followed by variations of the “rapid prototyping” method such as SLS, laminated object manufacturing, fused deposition modeling and 3-D printing. There have been many efforts to extend the layered fabrication technologies from purely “mold or prototype” components to functional (structural) build materials by using high strength polymeric powders. The SLS process builds parts layer-by-layer from laser-sintered polymer powder in an automated system that replicates the part

directly from a 3D CAD file. One of the reasons for choosing the SLS technology is its inherent ability to use a wide range of powdered build materials to manufacture few or many parts without costly tooling, labor, or intermediates inventory.

Materials that are commonly used to fabricate polymeric SLS parts are high-strength thermoplastics such as nylon (polyamide) 11 (PA11) and nylon (polyamide) 12 (PA12), as well as polycarbonate and polystyrene. All of these polymeric materials lack flame retardancy. This is a critical safety requirement, especially for the manufacture of finished products that invariably require some fire retardancy. Methods to flame-retard or modify flammable thermoplastic materials to flame-retardant products consist of the introduction of flame-retardant additives such as inorganic metal oxides and hydroxides (aluminum trihydrate, magnesium hydroxide) or halogens with or without phosphorous and nitrogen-containing materials.¹⁶ Large amounts of metal oxides (>30%) are necessary to flame-retard thermoplastics, and in many cases they compromise some mechanical properties, such as reduced toughness, melt flow, etc., of the thermoplastic. Similarly, the use of halogens and/or phosphorous and nitrogen compounds also involves the addition of large amounts of additive(s), resulting in the release of smoke and toxic emissions when the modified thermoplastic is subjected to fire conditions.

A new procedure for developing flame-retardant thermoplastic polymers involves the use of nanotechnology, whereby nanoparticles are incorporated into the thermoplastic by a melt blending process (extruder) that requires small amounts (<7%).¹⁷⁻²⁷ A nanophase is formed within the nanomodified thermoplastic material, resulting in the formation of a nanocomposite system that forms a char barrier or insulative shield for flame retardancy. These novel nanocomposites exhibit not only improved flame retardancy, but also enhanced mechanical properties such as high strength and modulus, moisture resistance, and a higher heat distortion temperature, thereby meeting the objectives of improved, high-strength polymer powdered materials to manufacture “net shape” replacement parts by the SLS method.

Selection of materials. Arkema’s RILSAN® PA11 thermoplastic was selected for this study, because this is the industrial standard polymer system used by the SLS technique. RILSAN PA11 thermoplastic²⁸ is a high-performance technical polymer developed by Arkema Chemicals, Inc. in 1942. Derived from a series of complex chemical operations, RILSAN PA11 is one of the few polymers in existence produced from “green” raw materials—castor beans. RILSAN PA11 resin has earned a preferred material status in the most demanding applications, owing largely to its unique combination of thermal, physical, chemical, and

mechanical properties. This combination of properties results in an outstanding cost performance ratio. Processing ease is another major benefit of RILSAN PA11 resin. Supplied in powder or pellet form, RILSAN PA11 resin can be processed by injection molding, extrusion, blown-film extrusion, extrusion blow molding, or rotomolding. RILSAN PA11 PCGLV pellets were used in this study.

RILSAN PA11 resin has a unique combination of properties. Its ease of processing has led designers to select it for industries as diverse as aerospace, offshore drilling, electrical cables, and automotive, pneumatic, and hydraulic hoses.

Three types of nanoparticles were used, namely montmorillonite (MMT) nanoclays from Southern Clay Products, Degussa's nanosilicas, and carbon nanofibers (CNFs) from Applied Sciences (Chap. 2). These nanoparticles are known to reinforce the polymer in the nanoscale and lead to enhancement of the dimensional stability and mechanical properties of the resulting polymer nanocomposites.

Processing and characterization of resin/nanoparticle systems. Processing and morphological characterization of PA11-nanoclay, PA11-nanosilica, and PA11-carbon nanofibers are discussed in this section.

Blending PA11-nanoclay polymer. A 30-mm Werner Pfleider corotating, twin-screw extruder was used and was configured for a wide variety of materials. Table 7.2 shows the two nanoclays (Cloisite 30B and 93A) selected at 2.5, 5, 7.5, and 10 wt% loading levels with the PA11 resin. Approximately 10 lb of each formulation were produced. The PA11 was dried in a desiccant drier before compounding. Injection-molded

TABLE 7.2 Material Matrix for Resin/Nanoparticles

Sample number	Resin (wt%)	Nanoparticles (wt%)	Nanoparticle type
1	PA11 100%	0%	None
2	PA11 97.5%	2.5%	Cloisite 30B
3	PA11 95%	5%	Cloisite 30B
4	PA11 92.5%	7.5%	Cloisite 30B
5	PA11 90%	10%	Cloisite 30B
6	PA11 97.5%	2.5%	Cloisite 93A
7	PA11 95%	5%	Cloisite 93A
8	PA11 92.5%	7.5%	Cloisite 93A
9	PA11 90%	10%	Cloisite 93A
10	PA11 99%	1%	PR-19-PS CNF
11	PA11 97%	3%	PR-19-PS CNF
12	PA11 95%	5%	PR-19-PS CNF
13	PA11 93%	7%	PR-19-PS CNF
14	PA11 97.5%	2.5%	AEROSIL 300
15	PA11 95%	5%	AEROSIL 300
16	PA11 92.5%	7.5%	AEROSIL 300

specimens of each blend were prepared and examined by WAXD and TEM. Figure 7.22 shows the TEM micrographs of the 90 percent PA11:10 percent Cloisite 30B. It is evident that exfoliation of Cloisite 30B in PA11 polymer was achieved.

Blending PA11-carbon nanofiber polymer. Carbon nanofiber PR-19-PS is about 130 nm in diameter and several micrometers in length, and can be classified as MWNT. It was blended with PA11 polymer in four different loading levels via twin-screw extrusion. Table 7.2 shows that the CNFs were selected at 1, 3, 5, and 7 wt% loading levels with the PA11 resin. Approximately 10 lbs of each formulation were produced. Injection-molded specimens of each blend were prepared and examined by TEM, as shown in Fig. 7.23. It is evident that good dispersion of PR-19-PS CNFs in PA11 was achieved.

Blending PA11-nanosilica polymer. Nanosilica AEROSIL 300 was blended with PA11 polymer in three different loading levels. Table 7.2 shows

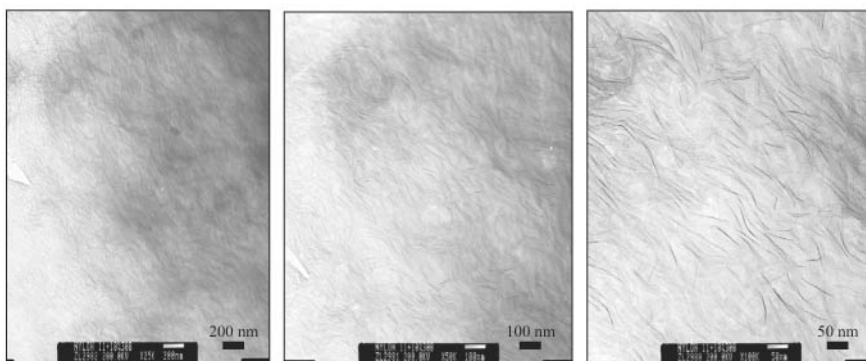


Figure 7.22 Transmission electron micrographs of the 90% PA11:10% Cloisite 30B polymer showing that exfoliation of nanoclay in PA11 was achieved.

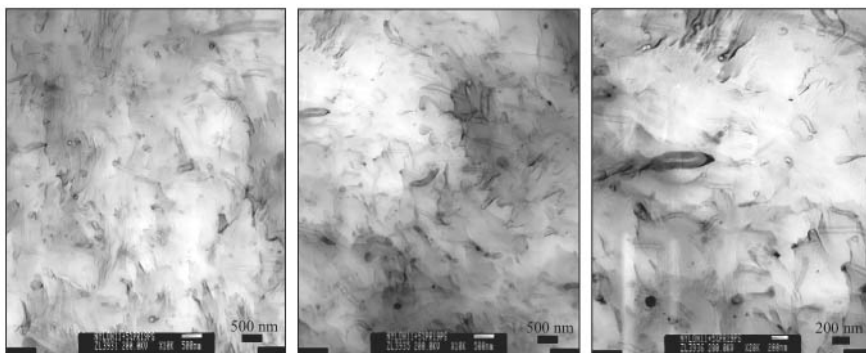


Figure 7.23 Transmission electron micrographs of the 95% PA11:5% PR-19-PS polymer showing that good dispersion of CNF in PA11 was achieved.

that the nanosilica was selected at 2.5, 5, and 7.5 wt% loading levels with the PA11 resin. Approximately 10 lbs of each formulation were produced. Injection-molded specimens of each blend were prepared and examined by TEM, as shown in Fig. 7.24. It is evident that nanosilicas formed very large (micron-sized) aggregates.

Discussion of results

Flammability properties. The fifteen PA11 polymer blends and PA11 control in Table 7.2 were exposed to a radiant heat flux of 50 kW/m^2 within the cone calorimeter, according to ASTM E 1354 (see Chap. 5).²⁹ Each blend was tested in duplicate. The detailed average flammability properties are shown in Table 7.3 and Ref. 10. Figures 7.25 through 7.28 show the heat release rate, residual mass, carbon monoxide yield, and smoke extinction coefficient of the 2.5, 5, 7.5, and 10 percent Cloisite 30B/97.5, 95.0, 92.5, and 90 percent PA11, respectively. It is evident from Table 7.3 that the most effective nanofiller for the PA11 polymer is Cloisite 30B. A reduction of 73 percent peak HRR was observed with 10 percent Cloisite 30B in PA11. A reduction of the average HRR at 180 s and of the mean CO yield were also exhibited. The second best nanofiller for the PA11 polymer was PR-19-PS CNF. A reduction of 71 percent peak HRR was observed with 7 percent PR-19-PS CNF. Peak

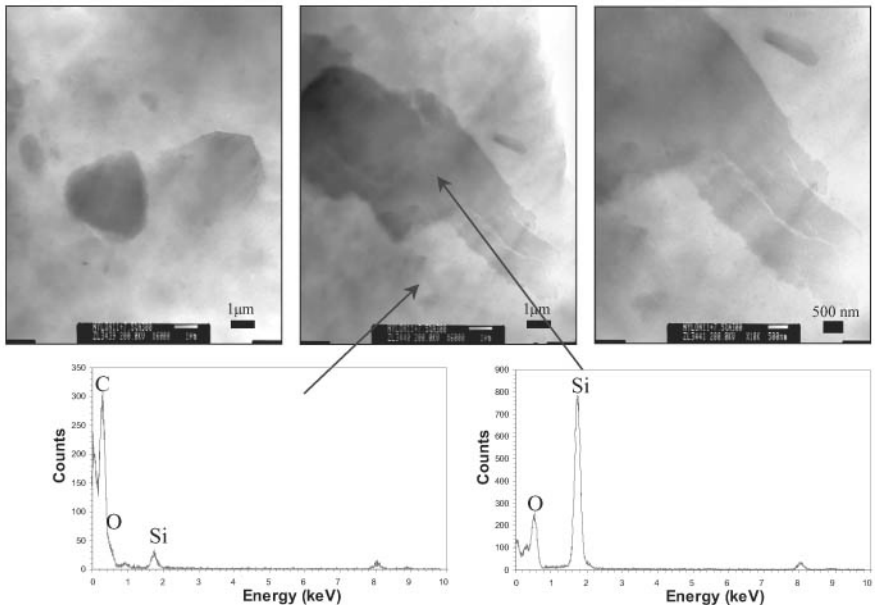


Figure 7.24 Transmission electron micrographs of the 92.5% PA11:7.5% AEROSIL 300 nanosilica polymer showing that very large nanosilica aggregates were formed in the PA11 polymer.

TABLE 7.3 Cone Calorimeter Data of the Different Nylon 11 Nanocomposites (PA11N)

Sample	Peak HRR ($\Delta\%$) (kW/ m ²)	Avg. HRR at 180 s (Δ %) (kW/ m ²)	Mean H _c (MJ/kg)	Mean SEA (m ² /kg)	Mean CO yield (kg/ kg)
Nylon 11 (PA11)	1866	658	33.4	201	0.0245
PA11/2.5% Cloisite 30B	1437 (23%)	657 (0.1%)	35.8	184	0.0145
PA11/5% Cloisite 30B	784 (58%)	621 (6%)	32.1	212	0.0135
PA11/7.5% Cloisite 30B	606 (68%)	519 (21%)	33.5	235	0.007
PA11/10% Cloisite 30B	509 (73%)	435 (34%)	33.3	241	0.0075
PA11/2.5% Cloisite 93A	1484 (21%)	646 (2%)	35.4	163	0.019
PA11/5% Cloisite 93A	1349 (28%)	661 (0.4%)	35.6	187	0.018
PA11/7.5% Cloisite 93A	1084 (42%)	642 (3%)	34.9	195	0.019
PA11/10% Cloisite 93A	873 (53%)	623 (5%)	34.2	223	0.0205
PA11/1% PR-19PS CNF	1294 (31%)	651 (1%)	34.9	243	0.0325
PA11/3% PR-19PS CNF	1213 (35%)	645 (2%)	37.3	286	0.0415
PA11/5% PR-19PS CNF	752 (60%)	569 (14%)	32.5	303	0.047
PA11/2.5% AEROSIL 300	1597 (14%)	613 (7%)	35.3	237	0.03
PA11/5% AEROSIL 300	1560 (16%)	612 (7%)	34.7	210	0.0285
PA11/7.5% AEROSIL 300	1553 (17%)	626 (5%)	34.0	188	0.0245

HRR data for Cloisite 93A followed CNF data. The AEROSIL 300 nanosilica FR data indicated it was not an effective FR nanoparticle. Figures 7.29 to 7.31 show the HRR of PA11-Cloisite 93A, PA11-PR-19-PS CNF, and PA11-A300, respectively. Table 7.3 summarizes the flammability properties of all the PA11N and PA11 materials.

Mechanical properties. Tensile strength, flexural strength, Young’s modulus, and elongation at break of all the PA11N materials are shown in detail in Ref. 24. Table 7.4 summarizes the flammability and mechanical properties of all the PA11N and PA11 materials. Figures 7.32 through 7.35 show, respectively, the tensile yield strength, flexural strength, Young’s modulus, and elongation at break of all the materials.

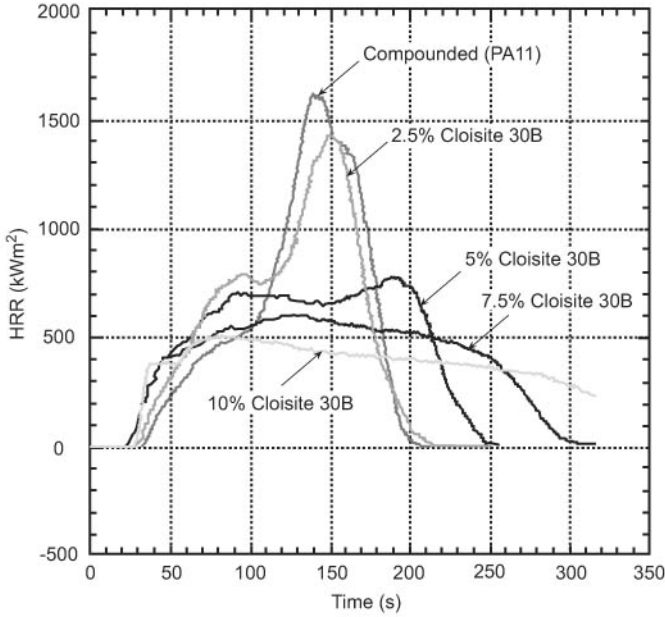


Figure 7.25 Comparison of heat release rate for 2.5, 5, 7.5, and 10 wt% of Cloisite 30B PA11N at 50 kW/m² heat flux.

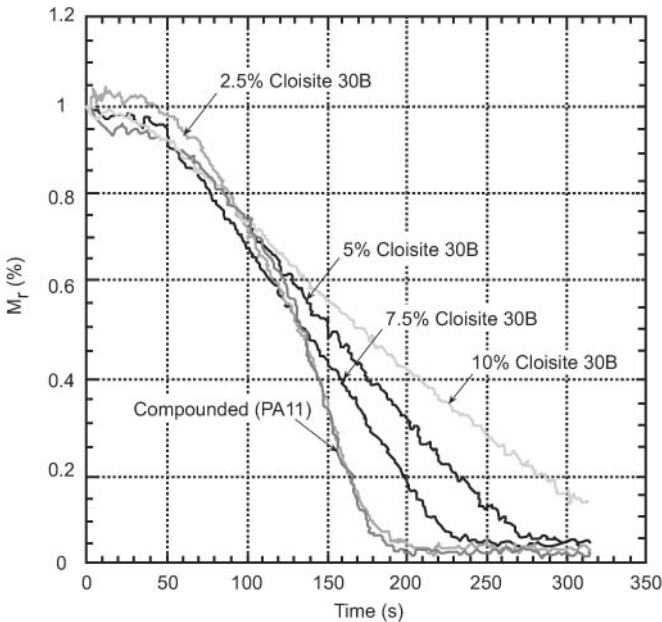


Figure 7.26 Comparison of residual mass for 2.5, 5, 7.5, and 10 wt% of Cloisite 30B PA11N at 50 kW/m² heat flux.

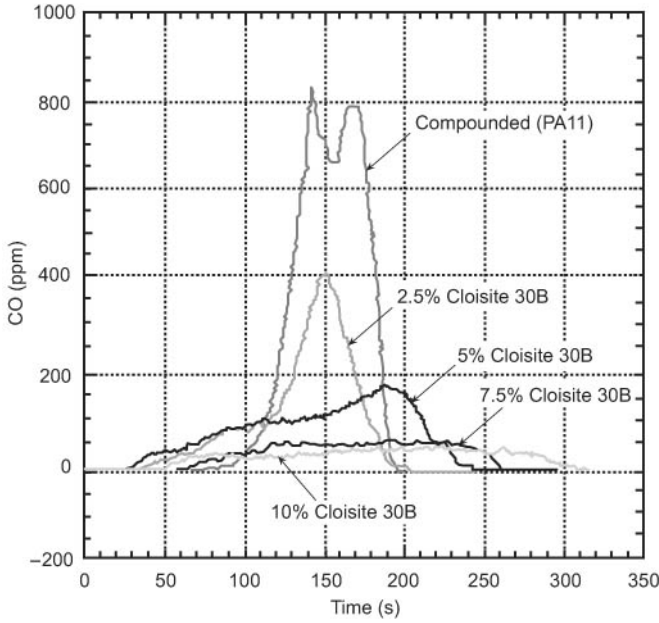


Figure 7.27 Comparison of carbon monoxide yield for 2.5, 5, 7.5, and 10 wt% of Cloisite 30B PA11N at 50 kW/m² heat flux.

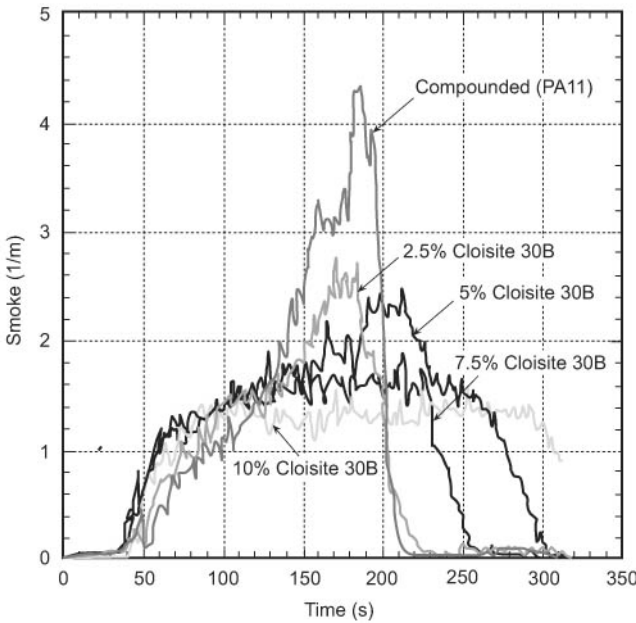


Figure 7.28 Comparison of smoke extinction coefficient for 2.5, 5, 7.5, and 10 wt% of Cloisite 30B PA11N at 50 kW/m² heat flux.

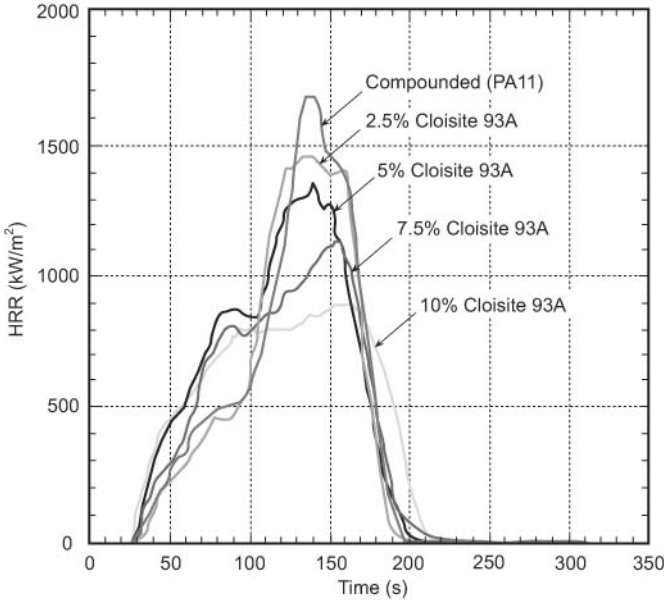


Figure 7.29 Comparison of heat release rate for 2.5, 5, 7.5, and 10 wt% of Cloisite 93A PA11N at 50 kW/m² heat flux.

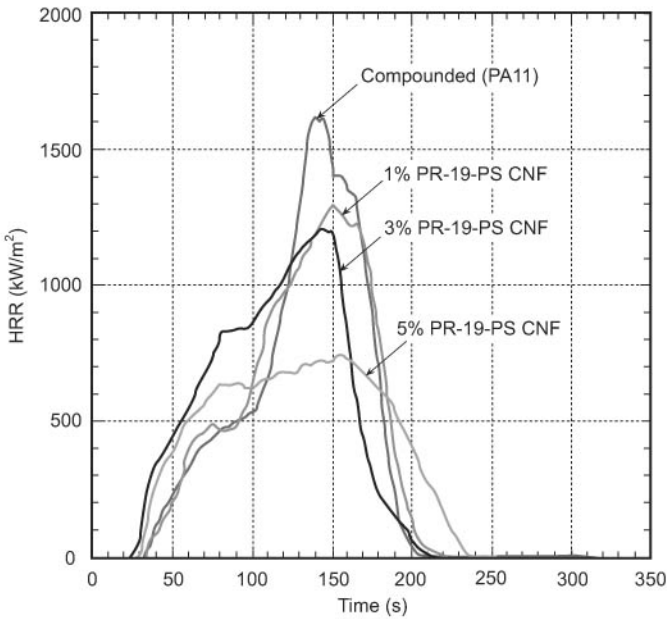


Figure 7.30 Comparison of heat release rate for 1, 3, 5, and 7 wt% of PR-19-PS CNFs PA11N at 50 kW/m² heat flux.

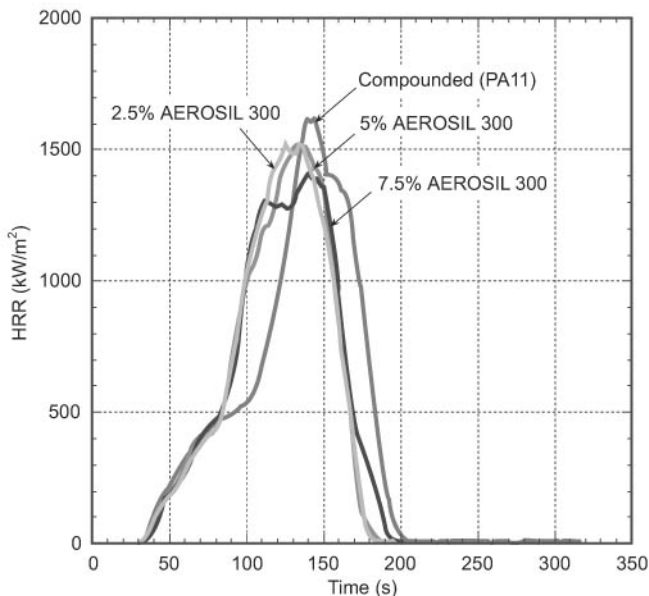


Figure 7.31 Comparison of heat release rate for 2.5, 5, and 7.5 wt% of AEROSIL 300 nanosilica PA11N at 50 kW/m² heat flux.

In summary, the 5% PR-19-PS CNF/95% PA11 polymer has the highest tensile strength. The tensile strength of all AEROSIL 300 PA11 polymer blends was lower than the control. The flexural strength of 7% PR-19-PS CNF/95% PA11 polymer is the highest among all PR-19-PS CNF formulations. Modulus was significantly increased for both PA11N-containing nanoclays, with 10 percent 30B exhibiting the highest modulus, indicative of excellent dispersion and exfoliation of nanoclay in the PA11 matrix. Only low (2.5%) amounts of nanoclays showed higher elongation at break than the control. As the level of nanoclay was increased to 10 percent, a corresponding decrease in elongation was observed.

Microstructural analyses of fracture surface. The fracture surfaces of tensile specimens were studied by scanning electron microscopy (SEM).¹⁴ The SEM micrographs of two different types of nanofillers were compared with the baseline material. The nanofillers were Cloisite 30B nanoclay and PR-19-PS CNF. At low magnification (Fig. 7.36), the fracture surface of the polyamide 11-Cloisite 30B nanoclay is noticeably smoother than that of polyamide 11-CNF. At higher magnification (Fig. 7.37), the differences between Cloisite 30B and PR-19-PS CNF specimens were more pronounced. The polyamide-nanoclay had a considerably smoother fracture surface topography relative to the baseline and the polyamide-CNF. The clean shear surface indicates a fast fracture mechanism.

TABLE 7.4 Summary of Mechanical and Flammability Properties of PA11 and PA11N

Specimen ID	PHRR (kW/m ²)	Avg. HRR, 60 s (kW/m ²)	Avg. HRR, 180 s (kW/m ²)	Avg. elong. (strain %)	Avg. flex. (MPa)	Avg. tens. (MPa)
PA11 Compounded	1866	365	658	26.7	5526	7203
2.5% Cloisite 30B	1437	510	657	52.0	6486	7499
5.0% Cloisite 30B	784	480	621	5.4	7323	7343
7.5% Cloisite 30B	606	441	519	3.4	7344	7344
10% Cloisite 30B	509	430	435	1.8	6447	6549
2.5% Cloisite 93A	1485	310	646	58.2	6179	7256
5.0% Cloisite 93A	1349	399	661	35.1	6116	7379
7.5% Cloisite 93A	1084	548	642	9.2	6992	6994
10% Cloisite 93A	873	485	623	3.1	6799	6799
1.0% PR-19-PS CNF	1294	373	651	25.5	5880	7255
3.0% PR-19-PS CNF	1214	562	645	25.2	6810	7857
5.0% PR-19-PS CNF	754	497	569	23.4	7645	8294
7.0% PR-19-PS CNF	545	481	419	13.1	8249	7929
2.5% AEROSIL 300	1597	419	612	8.0	6208	6208
5.0% AEROSIL 300	1560	429	612	5.3	6090	6090
7.5% AEROSIL 300	1553	429	626	4.3	5712	5712

PHRR = peak heat release rate, Avg. HRR = average heat release rate, Avg. Elong. = average elongation, Avg. Flex. = average flexural strength, Avg. Tens. = average tensile strength.

However, because the fracture surface is severely sheared, nanoclay particles could not be identified, and thus future studies on its exact

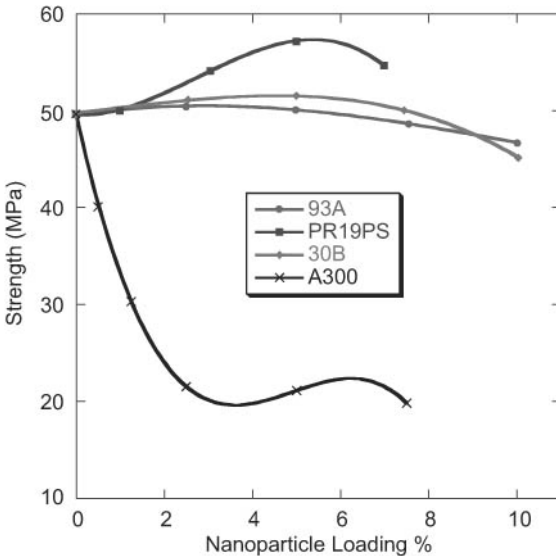


Figure 7.32 Tensile yield strength of PA11 and PA11Ns.

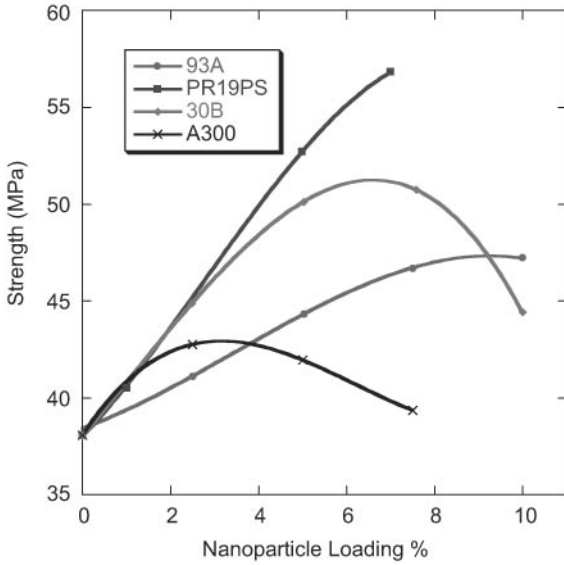


Figure 7.33 Flexural strength of PA11 and PA11Ns.

fracture mechanism are needed. On the other hand, the carbon nanofibers were observed at 1.5k magnification. When the tensile specimens were fractured, the shear-directed CNFs were also fractured as expected. The micrograph on the right of Fig. 7.38 shows the broken

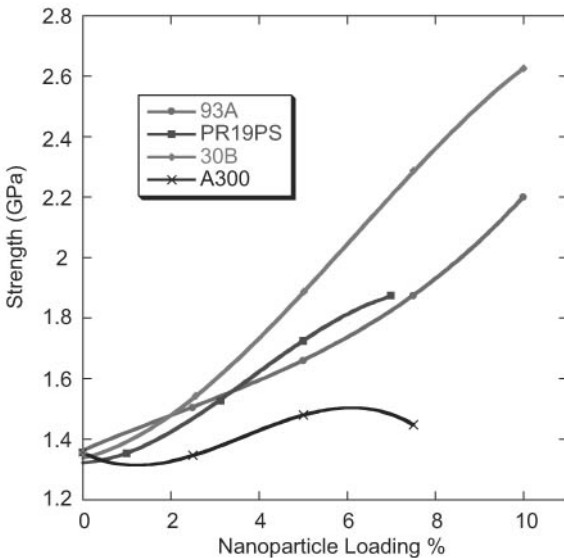


Figure 7.34 Young's modulus of PA11 and PA11Ns.

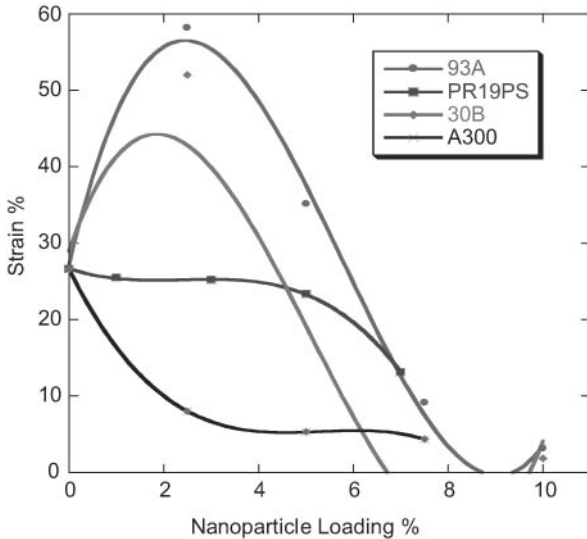


Figure 7.35 Elongation at break of PA11 and PA11Ns.

CNF protruding from the fractural surface. Relative to polyamide-Cloisite 30B nanoclay and the baseline, the polyamide-CNF showed a much rougher fracture surface topography and an impediment to clean shearing that possibly resulted from the intertwining networks of CNF, as shown in Fig. 7.38.

Microstructural analyses of flammability specimens. Microstructural analyses of pre- and posttest PA11N specimens were conducted on injection-molded and SLS specimens to gain a fundamental understanding of material behavior.¹⁴ In particular, PA11-5% Cloisite 30B and PA11-5% PR-19-PS CNF for cone calorimetry experiments were selected. However, the experiments were terminated at times during both the first and second peaked heat release rates, 74 and 150 seconds, respectively, as shown in Fig. 7.39, for microstructural analyses.

The surface and cross-section of the charred specimens were investigated by studying the mechanisms of flame retardancy. A thin layer of coating was applied during SEM analyses to prevent charging of the nanoparticles. At 74 seconds or the first peak heat release rate (the images of the charred sample of PA11-Cloisite 30B), large portions of char yielded in the polymer matrix, and the matrix remained uniform (Fig. 7.40). The nanoparticles reinforced the fragile polymer char and formed a protective layer on the surface that blocked the thermal wave from penetrating down the surface. On the other hand, the sample with CNF exhibited voids and discontinuous char formation on the surface (Fig. 7.41). The char was fragile and appeared to burn throughout the

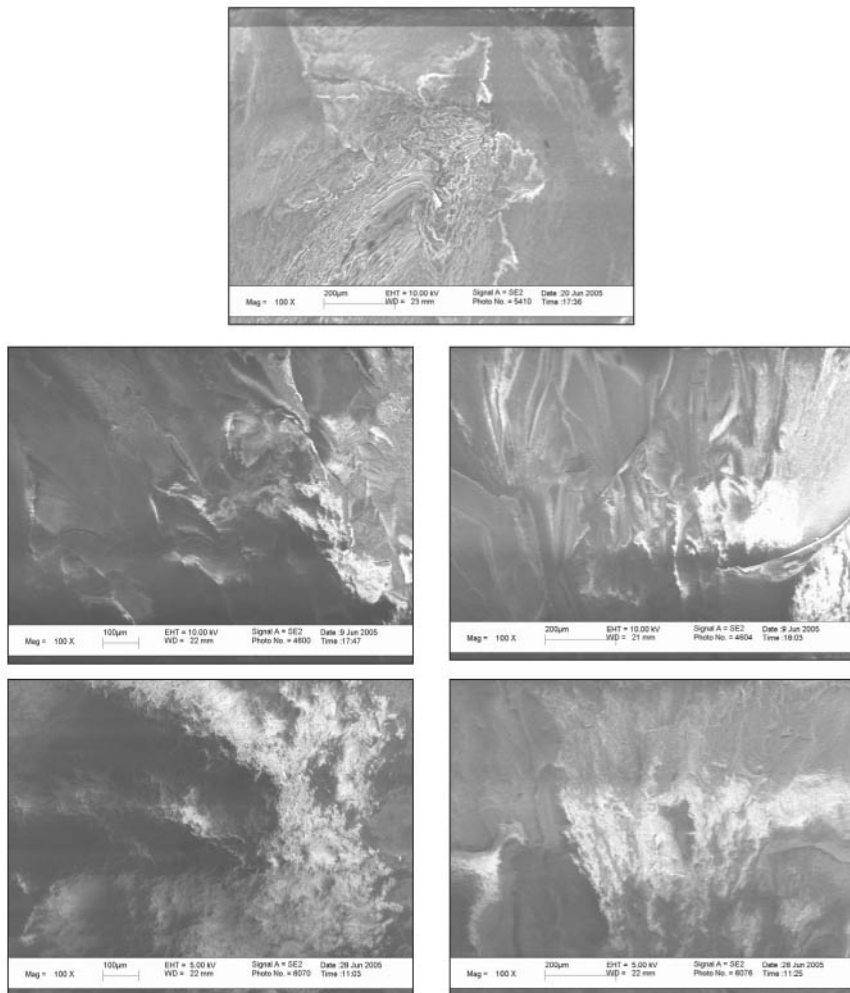


Figure 7.36 SEM micrographs of PA11 at low magnification. The top micrograph is the baseline without any nanoparticles. The second row shows the micrographs for PA11 with Cloisite 30B nanoparticles (95/5) and (93/7), respectively. The third row shows the micrographs for PA11 with PR-19-PS CNF nanoparticles (95/5) and (93/7), respectively.

matrix. The white spots on the images are presumed to be the remaining polymer matrix and suggest that the sample burned randomly at different locations. As the length of the CNF was measured under higher magnification, the results clearly show that the usual lengths of CNF are about $0.2 \mu\text{m}$ in length. The CNF was reduced in length during extrusion.

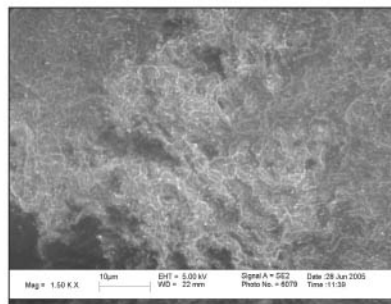
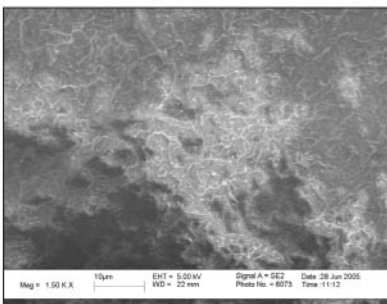
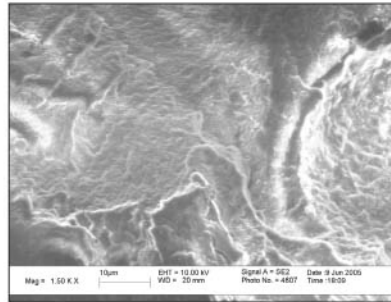
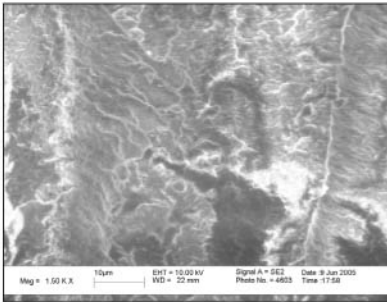
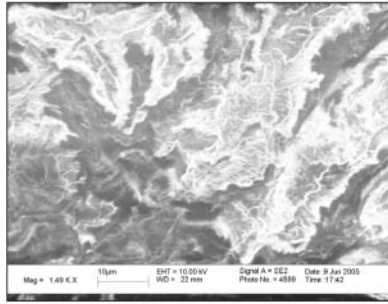


Figure 7.37 SEM micrographs of PA11 at higher magnification. The top micrograph is the baseline without any nanoparticles. The second row shows the micrographs for PA11 with Cloisite 30B nanoparticles (95/5) and (93/7), respectively. The third row shows the micrographs for PA11 with PR-19-PS CNF nanoparticles (95/5) and (93/7), respectively.

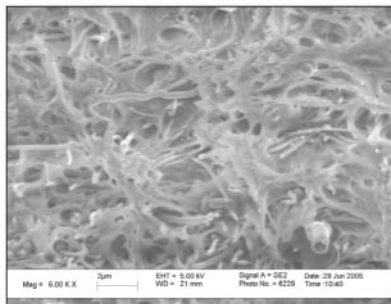
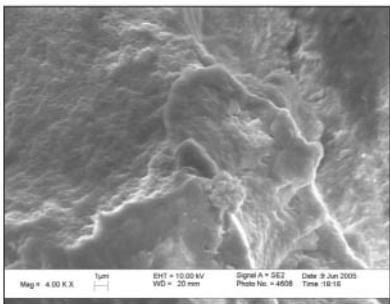


Figure 7.38 Higher magnification of PA11 with Cloisite 30B (93/7) on the left and PR-19-PS CNF (93/7) on the right.

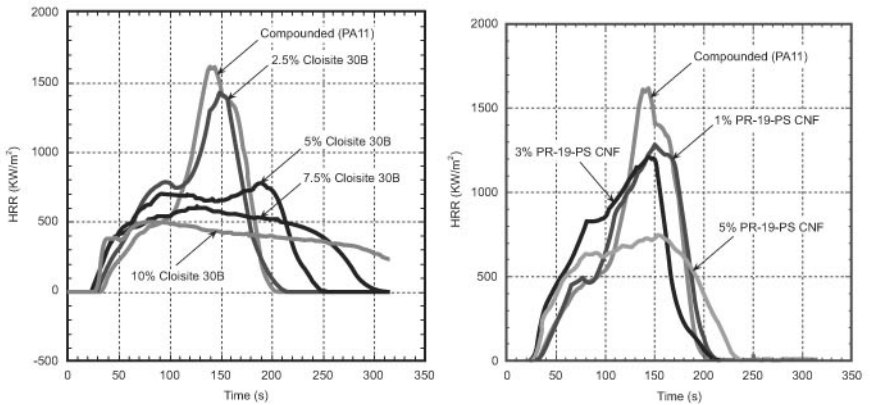


Figure 7.39 Plots of heat release rate for polyamide 11 with nanoparticles of Cloisite 30B (left) and of PR-19-PS CNF (right).

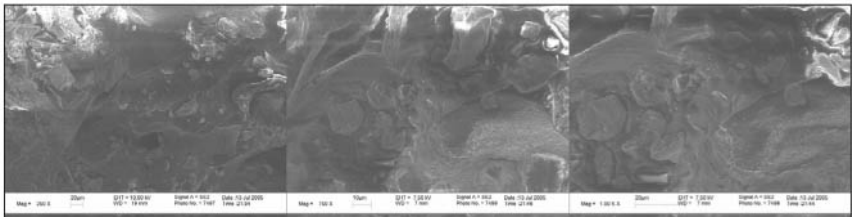


Figure 7.40 Scanning electron microscopy images of posttest cone calorimeter PA11/5% Cloisite 30B surface at the first peaked heat release rate (74 seconds) at magnifications of 250 \times (left), 750 \times (middle), and 1000 \times (right).

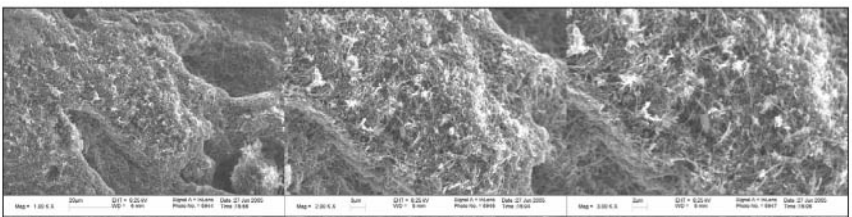


Figure 7.41 Scanning electron microscopy images of posttest cone calorimeter PA11/5% PR-19-PS CNF surface at the first peak heat release rate (74 seconds) at magnifications of 1000 \times (left), 2000 \times (middle), and 3000 \times (right).

At the second peak heat release rate (150 s), the surface of the Cloisite 30B sample was mainly covered with char. The polymer matrix was reduced in thickness due to the loss in mass but remained uniform as opposed to the sample with carbon nanofibers, which in the matrix could not be observed under SEM. Only nanofibers remained (Figs. 7.42 and 7.43). It is proposed that the role of the nanoclay is to reduce the heat release rate by forming an insulating char structure on

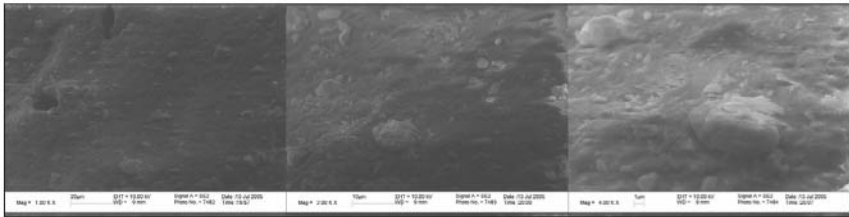


Figure 7.42 Scanning electron images of posttest cone calorimeter PA11/5% Cloisite 30B surface at the second peak heat release rate (150 seconds) at magnifications of 1000 \times (left), 2000 \times (middle), and 4000 \times (right).

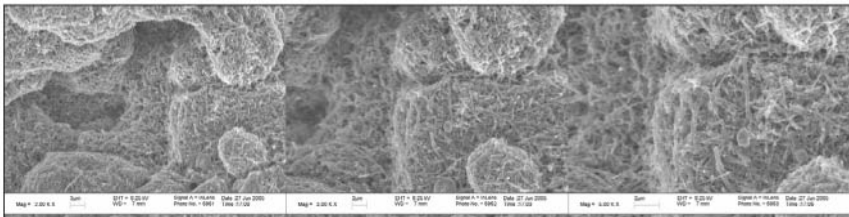


Figure 7.43 Scanning electron microscopy images of posttest cone calorimeter PA11/5% PR-19-PS CNF surface at the second peak heat release rate (150 seconds) at magnifications of 2000 \times (left), 3000 \times (middle), and 5000 \times (right).

the surface of the polymer matrix. The nanoclay facilitated the formation of a heat shield to prevent the polymer matrix from burning, as it was below the char surface.

From the cross sections of the charred samples at 74 seconds (Fig. 7.44), the nylon-nanoclay specimen displayed micron-sized char formation in the matrix in addition to the layers of observed matrix (Fig. 7.44). During the burning process timeframe, some polymer matrix adhering to the carbon nanofibers can be observed (Fig. 7.45). Despite the cross-section being sheared, some CNF protruding out of the matrix can also be observed. Even in cross-sectional view, the burning of the nylon with carbon nanofibers behaved as if the burned locations were randomly selected.

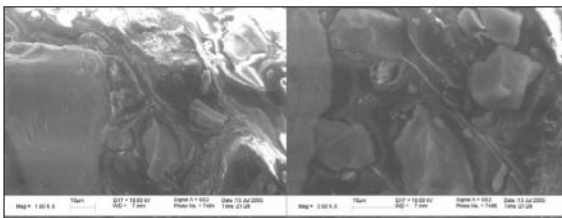


Figure 7.44 Scanning electron microscopy images of posttest cone calorimeter PA11/5% Cloisite 30B cross-section at the first peak heat release rate (74 seconds) at magnifications of 1000 \times (left) and 2000 \times (right).

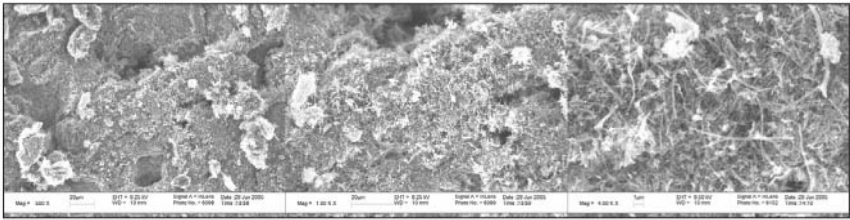


Figure 7.45 Scanning electron microscopy images of posttest cone calorimeter PA11/5% PR-19-PS CNF cross-section at the first peak heat release rate (74 seconds) at magnifications of 500× (left), 1000× (middle), and 4000× (right).

During the second peak heat release rate (Figs. 7.46 and 7.47), the layers of collapsing matrix in the sample with nanoclay were more easily seen. The polymer matrix was still uniform and intact, and no matrix remained in the sample with carbon nanofibers.

Processing and characterization of SLS candidates. Based on flammability and mechanical properties of the injection-molded PA11N candidates (Table 7.4), five materials were cryogenically ground into fine powders (about 50 μm in diameter) for SLS processing:

- Polyamide 11 (control)
- Polyamide 11/5% Cloisite 30B

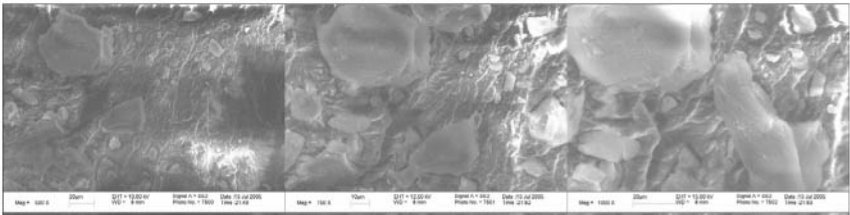


Figure 7.46 Scanning electron microscopy images of posttest cone calorimeter PA11/5% Cloisite 30B cross-section at the second peak heat release rate (150 seconds) at magnifications of 500× (left), 750× (middle), and 1000× (right).

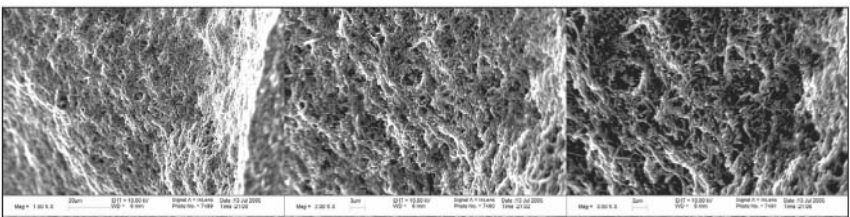


Figure 7.47 Scanning electron microscopy images of posttest cone calorimeter PA11/5% PR-19-PS CNF cross-section at the second peak heat release rate (150 seconds) at magnifications of 1000× (left), 2000× (middle), and 3000× (right).

- Polyamide 11/5% Cloisite 93A
- Polyamide 11/5% PR-19-PS CNF
- Polyamide 11/7% PR-19-PS CNF

Fabricated SLS specimens were obtained to measure mechanical, HDT, and thermal conductivity properties, as well as flammability, using the 3D Systems Vanguard HS machine. The SLS process was shown to be successful for polyamide 11-clay and polyamide 11-CNF nanocomposites. It was noted that polyamide 11-clay nanocomposites are more difficult to process. The observed reason for the difficulties is that the process is inhibited by powder mechanics. The poor powder flow for the polyamide 11-clay nanocomposites led to poor powder deposition and subsequent SLS processing difficulties. The difference in powder mechanics is clearly visible: the polyamide 11-clay nanocomposites flow like flour, whereas the polyamide 11-CNF nanocomposites flow like fine particles. Yet there is no quantitative measurement technique in the existing SLS technology area to characterize powder flow behavior, which makes it very difficult to predict the processibility of a new material. It is suggested that quantitative powder mechanics characterization methodology be developed to facilitate SLS processing.³⁰

For more efficient SLS processes, it was also suggested that a very small amount (~ 0.5 wt%) of fumed silica additive can be introduced to enhance powder flow and facilitate the SLS process. Further studies are needed to optimize the SLS processing of the polyamide 11-clay and polyamide 11-CNF nanocomposites.

During the processing of the polyamide 11-5% CNF nanocomposites, a unique phenomenon was observed during the sintering process. Upon laser impact, the nanocomposite powder emits a consistent white light. This phenomenon was not observed in any other nylon-based material, and it should be investigated further. Also, the sintering of polyamide 11-CNF nanocomposites appeared to produce a substantially higher amount of smoke than the baseline polyamide 11. An understanding of white light emission and excess smoke with polyamide 11-CNF requires additional study.

At present, all five SLS candidates were successfully fabricated, and limited flammability and mechanical properties were obtained, as shown in Tables 7.5 and 7.6, respectively. Preliminary data indicated that the density of polyamide 11 plays an important role in material properties. Optimal SLS processing conditions need to be determined to fabricate denser parts and thus to obtain enhanced material properties.

Thermal conductivity data for the polyamide 11-CNF are reported elsewhere.^{15,31} Additional processing and characterization of SLS

TABLE 7.5 Summary of Flammability Properties of Injection-Molded and SLS PA11N Specimens

Sample	Peak HRR ($\Delta\%$) (kW/m ²)	Avg. HRR at 180 s ($\Delta\%$) (kW/m ²)	Mean H _c (MJ/kg)	Mean SEA (m ² /kg)	Mean CO yield (kg/kg)
Nylon 11 (PA11), Injection-Molded	1,866	658	33.4	201	0.025
PA11/5% PR-19-PS CNF, Injection-Molded	752 (60%)	569 (14%)	32.5	303	0.047
Nylon 11 (PA11) SLS	1,256	764	32.5	N/A	0.025
PA11/5% PR-19- PS CNF SLS	1,027 (18%)	775 (-1%)	32.6	N/A	0.043

TABLE 7.6 Summary of Mechanical Properties of Injection-Molded and SLS PA11N Specimens

Sample	Tensile yield strength (MPa)	Flexural strength (MPa)	Young's modulus (GPa)	Elongation at break (strain %)
Nylon 11 (PA11), Injection-Molded	49.7	37.6	1.36	25.1
PA11/5% PR-19-PS CNF, Injection- Molded	57.1	55.1	1.68	22.3
Nylon 11 (PA11) SLS	43.9	43.9	1.84	4.6
PA11/5% PR-19-PS CNF SLS	In progress	In progress	In progress	In progress

polyamide 11 nanocomposites are still in progress to determine whether SLS-processed polyamide 11 nanocomposites are comparable to injection molded polyamide 11 nanocomposites.

Summary and conclusions. The nylon 11 (polyamide 11 PA11) polymer and three types of nanoparticles (MMT nanoclay, nanosilica, and CNF) were selected for this study. Fifteen polymer blends were compounded via twin-screw extrusion and compared with the control PA11. Transmission electron microscopy analysis was used to study the morphology of all the polymer blends. Physical properties such as specific gravity and hardness were measured. Mechanical properties such as tensile strength, flexural strength, elongation at break, and Young's modulus were measured. Thermal properties such as thermal conductivity were measured.^{15,31} Flammability properties were measured by cone calorimeter at a radiant heat flux of 50 kW/m². Five polymers were cryogenically ground into fine powders (50 μm in diameter) for SLS

processing. Mechanical, flammability, and thermal properties were characterized for these SLS specimens.

The following conclusions were drawn from this study:

- The peak release rate of the injection-molded PA11-nanoclay polymers decreases as the amount of nanoclay increases with PA11-10% Cloisite 30B (which had a PHRR of 509 kW/m², a reduction of 73%, as compared to PA11, which had a PHRR of 1866 kW/m²).
- The peak heat release rate of injection-molded PA11-CNF polymers also decreases as the amount of CNF increases with PA11-7% PR-19-PS CNF (which had a PHRR of 545 kW/m², a reduction of 71%).
- Cloisite 30B has better flame retardant properties than Cloisite 93A.
- Nanosilica does not enhance neither the flammability nor the mechanical properties of PA11 because of the poor dispersion of nanosilica in the PA11 polymer.
- For the injection-molded specimens, subtle features of using nanoclay or CNF as the nanomaterial in PA11N indicate that CNF provided the highest tensile yield strength and flexural strength, whereas the nanoclays provided enhanced modulus with increasing amounts of nanoclay. The benefit of improved elongation at break occurred only at low amounts of nanoclay (2.5%), with elongation decreasing as the amount of nanoclay was increased above 2.5 percent. Little or no benefit was observed with nanosilica, a finding that is attributable to poor dispersion.
- The technical objective of transforming nanomodified nylon 11 (PA11/5% PR-19-PS CNF) by SLS into an SLS component for characterization for flammability behavior (cone calorimeter) and mechanical properties was achieved.
- All five planned SLS candidates were successfully fabricated, and limited mechanical and flammability properties were determined. We are in the process of translating the successes of the injection-molded polyamide 11 nanocomposites to their SLS counterparts. Preliminary data indicated that the density of polyamide 11 plays an important role in flammability and mechanical properties. Optimal SLS processing conditions are needed to identify the procedure to fabricate denser parts to enhance material properties. Studies are continuing.
- Powder mechanics and powder flow behavior characterization are suggested to assist in obtaining optimum SLS components.
- To gain a fundamental understanding of material behavior, microstructure analyses of pre- and posttest PA11N specimens were

conducted on injection-molded and SLS specimens and differences were noted.

- Processing and characterization of SLS polyamide 11 nanocomposites are reported elsewhere¹² and indicate our success in the injection-molded nylon 11 nanocomposites to SLS-processed nylon 11 nanocomposites. Additional research is in progress.

7.2 Thermoset Nanocomposites

Four applications are selected as examples for this section: (a) nanocomposite rocket ablative materials (NRAMs), (b) flammability properties of polymer nanostructured materials, (c) nanomodified carbon/carbon composites (NCCCs), and (d) nanocomposites for carbon fiber-reinforced polymer matrix composites (NCPMCs). These examples were used to illustrate the processing techniques to form the desired polymer nanocomposites and to transform them into polymer nanostructured materials for the intended applications. Flammability properties, mechanical properties, and performance characteristics for their specific applications are included.

7.2.1 Nanocomposites for rocket ablative materials (NRAMs)³²⁻³⁸

Ablative materials are required to protect aerospace propulsion systems against rocket exhaust plumes. The flow environment of solid rocket exhaust is particularly hostile. System components need to be protected from extreme flow temperatures of 1000 to 4000°C and from highly abrasive particles ejecting at velocities greater than 1000 m/s. Phenolic matrix composites have been used extensively for ablative materials. Current rocket nozzle assemblies are made of carbon phenolic composites such as MX-4926 from Cytec Engineered Materials (CEM). Three versions of carbon phenolic ablative MX-4926 laminates were fabricated by CEM as controls for this study. The three versions of MX-4926 laminates were fabricated based on fiber orientation: (a) 60° shingle, (b) molding compound, and (c) two-dimensional fabric.

Vaia et al.³⁹ examined the ablative performance of poly(caprolactam) (nylon 6) nanocomposites. A relatively tough, inorganic char forms during the ablation of these nanocomposites, resulting in at least an order-of-magnitude decrease in the mass loss (erosion) rate relative to the neat polymer. This effect occurs for as little as 2 wt% (\approx 0.8 vol%) exfoliated mica-type layered silicate. The presence of the layers does not alter the first-order decomposition kinetics of the polymer matrix. Instead, the nanoscopic distribution of silicate layers leads to a uniform char layer that enhances the ablative performance. The formation of

this char is only minutely influenced by the type of organic modification on the silicate surface of specific interactions between the polymer and the aluminosilicate surface, such as end-tethering of a fraction of the polymer chains through ionic interaction to the layer surface.

Our previous studies³²⁻³⁴ have allowed us to explore other nanoparticles besides MMT nanoclays with phenolic for ablative application. The NRAMs exploit the ablation resistance of both phenolic and nanoparticles. The objective of this material development program is a new class of nanostructured materials that is lighter and has better erosion and insulation characteristics than current ablatives. Borden Chemical's SC-1008, a resole phenolic, was selected as the resin for this investigation. Several nanoparticles such as Southern Clay Products (SCP) nanoclay, Applied Sciences CNFs, and Hybrid Plastics POSS have been evaluated with the SC-1008 phenolic resin. Based on WAXD and TEM, several nanoparticles were selected for further study. Cytec Engineered Materials fabricated several MX-4926 alternates by replacing the carbon black filler with selected nanoparticles for ablation testing.

A small-scale, supersonic, liquid-fueled rocket motor burning kerosene and oxygen was used to study the ablation and insulation characteristics of the ablatives. Testing ablative materials in full-scale firings is not only expensive, but also requires lengthy planning and limited exposure time, thus reducing the number of samples and the variety of test conditions available. The simulated solid rocket motor (SSRM) has been demonstrated as a cost-effective laboratory device to evaluate different ablatives under identical conditions for initial material screening and development.⁴⁰

Experimental approach

Simulated solid rocket motor (SSRM). The SSRM⁴⁰ was used to evaluate the candidate materials. The SSRM is an established testing approach developed earlier that has been used extensively in our previous studies.⁴¹⁻⁴⁵ It is a small-scale, liquid-fueled rocket motor burning a mixture of kerosene and oxygen as shown in Figs. 7.48 and 7.49. Aluminum oxide particles are injected into the plume to simulate the particle-laden flow of solid rocket exhaust plumes. The SSRM is a controlled laboratory device capable of producing a particle-laden exhaust environment with measured heat fluxes from 40 to 1250 Btu/ft²-s (454 to 14,200 kW/m²). The flame temperature is approximately 3992°F (2200°C), and the velocity of the particle-laden exhaust is approximately 2000 m/s. Figure 7.49 shows a close-up picture of a SSRM post-test ablative specimen. Calibration of the SSRM was performed using a Medtherm water-cooled heat flux gauge. The total heat

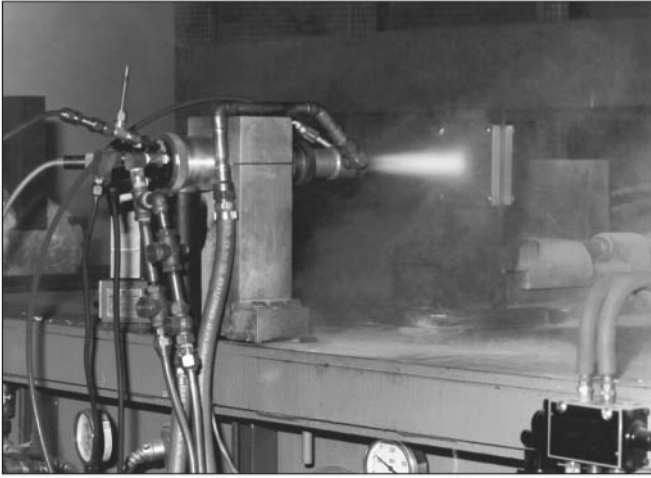


Figure 7.48 Ablative material testing using SSRM.

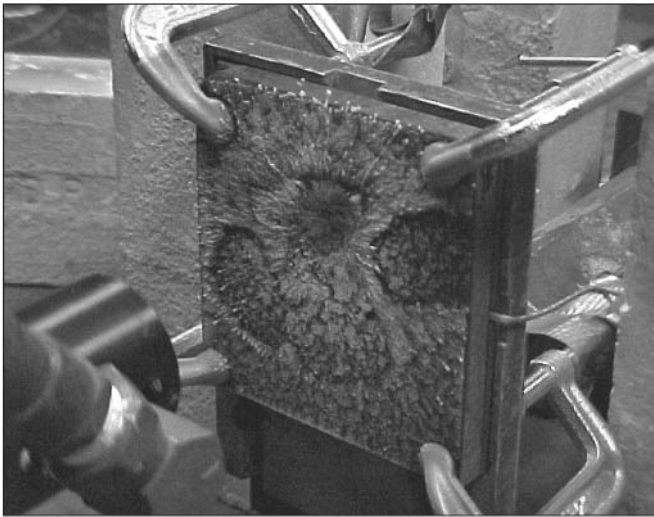


Figure 7.49 Close-up of ablative material after SSRM testing.

flux calibration of the SSRM is shown in Fig. 7.50. The highest heat flux is 1250 Btu/ft²-s at 2 inches from the nozzle exit, and the lowest heat flux is about 40 Btu/ft²-s at 14 inches from the nozzle exit.

The standard sample size was 4 by 4 by 1/4- or 1/2-inch thick (10.2 by 10.2 by 0.64- or 1.28-cm thick). The composite materials were bonded to 4 by 4 by 1/8-inch (10.2 by 10.2 by 0.32-cm) steel substrate. A narrow slot was machined into the bondline side of the steel substrate. The thermocouple was embedded into this slot. The bead of the

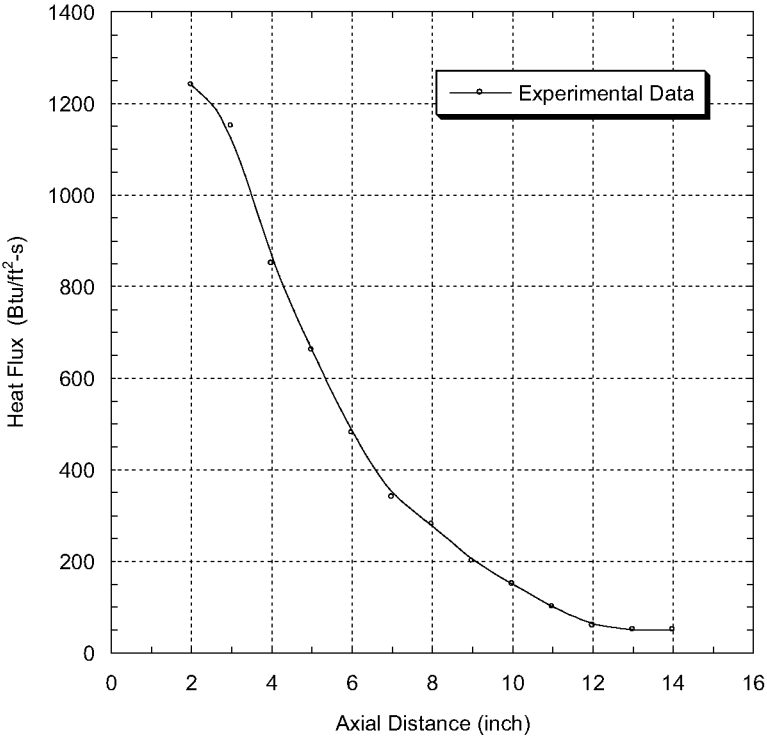


Figure 7.50 Calibration of SSRM in heat flux.

thermocouple was placed at the center point of the plate. The temperature history of the bondline was recorded with this thermocouple. C-clamps were used to clamp the ablatives to the steel substrate during testing. The test samples were placed in a fixture downstream from the SSRM nozzle exit. The fixture had adjustments in axial distance and impingement angle with reference to the plume centerline. A normal 90° impingement was used for this study.

Three axial distances were used to correspond with heat fluxes of 250, 625, and 1000 Btu/ft²-s (2838, 7094, and 11,345 kW/m²). These distances were selected to simulate low, medium, and high heating conditions. Prior to the motor burn, the bondline temperature was recorded. Peak erosion was determined by pre- and posttest measurements using a pencil-point dial indicator. Mass loss was determined by pre- and posttest weight loss measurements. Consistent data sets were averaged for this study. The following data were acquired during the experiment:

- Peak erosion (mm)
- Residual mass (%)

- Maximum backside heat-soaked temperature (°C)
- Time to reach maximum heat-soaked temperature (min.)
- Surface temperature (°C)

Selection of materials

Polymer matrix composites. MX-4926 is a rayon-based, eight-harness weave carbon fabric impregnated with a Mil R-9299 phenolic resin that contains a carbon black filler.⁴⁶ The approximate ratio of ingredients of MX-4926 is 50 wt% carbon reinforcements, 35 wt% phenolic resin, and 15 wt% carbon black. Figure 7.51 shows how MX-4926 is currently used in a typical solid rocket motor nozzle assembly.⁴⁷ As noted in the figure, MX-4926 (shaded areas) is mainly used in the entrance region and nozzle exit cone of the rocket nozzle assembly. The phenolic char formed at high temperature is usually not very strong. The carbon black filler in the phenolic resin was replaced by different nanoparticles, so that the nanoparticles will reinforce the phenolic in the nanometer scale and strengthen the char. Borden Chemical SC-1008⁴⁸ is the phenolic resin used in the MX-4926. This was the phenolic resin of choice for this investigation.

Phenolic resin. The phenolic resin used in the rocket nozzle ablative (MX-4926) was a solvent (isopropanol)-based resole, SC-1008. Table 7.7 shows some properties of the phenolic resin.⁴⁸

MMT nanoclays. Cloisite 30B, in loadings of 5, 10, and 15 wt%, was dispersed in a phenolic resole (SC-1008). The TEM analyses allowed us to determine the degree of dispersion and exfoliation of the nanoclay before committing to a 20-lb run at Cytec Engineered Materials of these nanoparticle-resin mixtures to make prepreps. This proved to be a

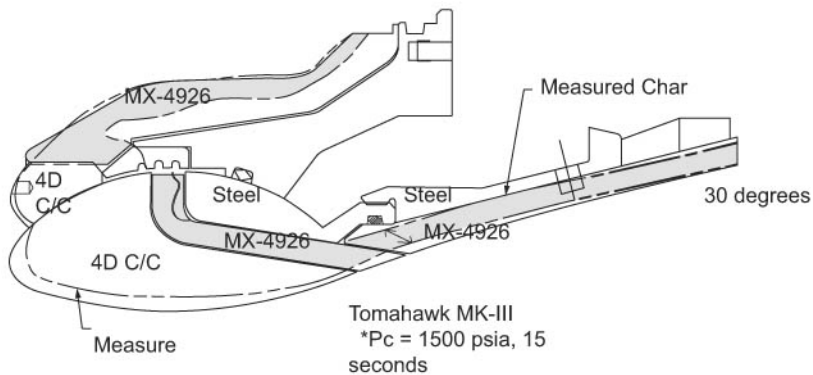


Figure 7.51 Schematic of a typical solid rocket motor assembly showing the usage of MX-4926.

TABLE 7.7 Phenolic Resin Properties⁴⁸

Resin	Supplier	Formulation	Final cure temp (°C)	T_g (°C) by DMTA	Specific gravity
SC-1008	Borden Chemical	60–64% solids isopropanol solvent	140	110	1.28

very cost-effective and efficient technique for screening different formulations. This nanoclay has been used with other resin systems, such as cyanate ester,^{49–51} thermoplastic elastomer,^{52–54} epoxy,^{55–57} and polyamide,^{10–15} in our research. More details can be found in Chap. 2.

Carbon nanofibers (CNFs). CNFs are a form of vapor-grown carbon fiber, which is a discontinuous graphitic filament produced in the gas phase from the pyrolysis of hydrocarbons. The CNFs PR-19-PS and PR-24-PS were used in this study. More details can be found in Chap. 2.

Polyhedral oligomeric silsesquioxane (POSS). Representing a merger between chemical and filler technologies, POSS nanostructured materials can be used as multifunctional polymer additives, acting simultaneously as molecular-level reinforcements, processing aids, and flame retardants. More details can be found in Chap. 2. Trisilanolphenyl-POSS was selected for this study.

Discussion of results. The candidate materials were evaluated for degree of dispersion using WAXD and TEM prior to full ablation testing using the SSRM. Borden SC-1008 resole phenolic in isopropanol alcohol (IPA) was used. Our first attempts were to modify this resin by the incorporation of MMT organoclays. These blends were dispersed using high-shear, nonsparking paint-mixing equipment. Neat resin castings (no fiber reinforcement) were made for WAXD and TEM analyses.

Transmission electron microscopy analyses and blending experiments. Each type of nanoparticle was dissolved in 0.5 percent IPA solvent over-night to create specimens for TEM analyses. The TEM image in Fig. 7.52(a) shows the carbon black particles agglomerated in the IPA. The TEM image in Fig. 7.52(b) shows that the Cloisite 30B nanoclay layers are in an intercalated state. Figure 7.52(c) shows the PR-24-PS CNFs are entangled. Figures 7.53(a) and 7.53(b) show the TEM images of Trisilanolphenyl-POSS-SO1458 ($C_{48}H_{38}O_{12}Si_7$) and polyvinyl silsesquioxane uncured (PVSQ)-PM1285 ($(C_2H_3O_{1.5}Si)_n$) dissolved in the IPA solvent. The scale bar is 1 μm .

Based on TEM analyses, it was concluded that carbon black (CB) particles caused interference of the dispersions of all nanoparticles in the SC-1008. As a result, CB was eliminated in subsequent blending.

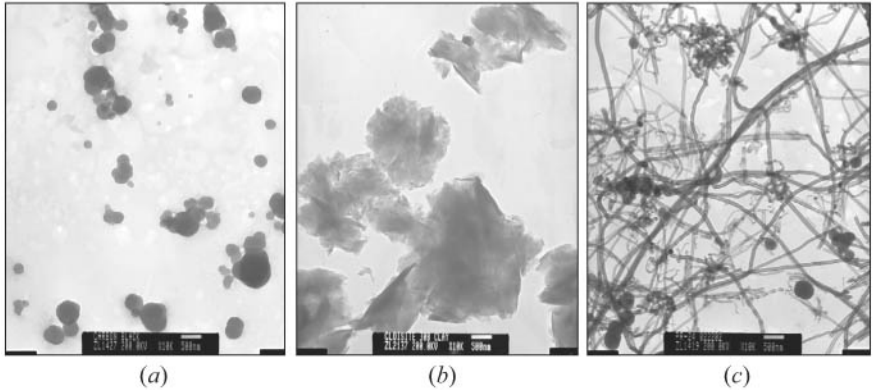


Figure 7.52 Transmission electron microscopy images of: (a) carbon black, (b) Cloisite 30B, and (c) PR-24-PS CNF dissolved in the IPA solvent (scale bar is 500 nm).

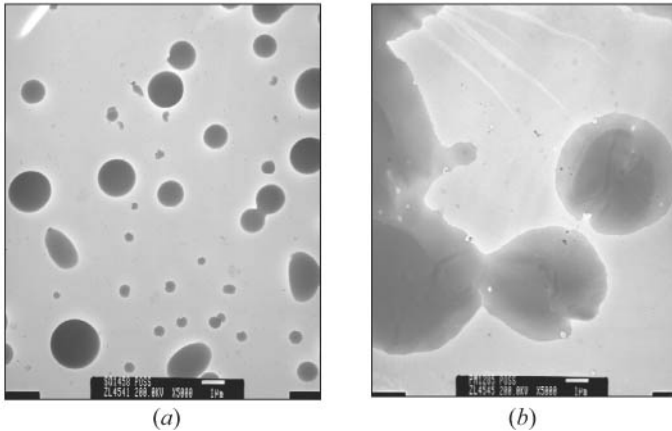


Figure 7.53 Transmission electron microscopy images of (a) Trisilanophenyl-POSS-SO1458 ($C_{48}H_{38}O_{12}Si_7$) and (b) polyvinyl silsesquioxane uncured (PVSQ)-PM1285 ($C_2H_3O_{1.5}Si_n$) dissolved in the IPA solvent (scale bar is 1 μ m).

Cloisite 30B, in loadings of 5, 10, and 15 wt%, was dispersed in the SC-1008. Figures 7.54 to 7.56 show the TEM images of the 5 wt% Cloisite 30B:95 wt% SC-1008 (Fig. 7.54), 10 wt% Cloisite 30B:90 wt% SC-1008 (Fig. 7.55), and 15 wt% Cloisite 30B:85 wt% SC-1008 (Fig. 7.56). The TEM images indicated intercalation, and not exfoliation, of the nanoclay in the resin system. The TEM analyses provided guidance to determine the degree of dispersion and exfoliation of the nanoclay before committing to a 20-lb run at CEM of these nanoparticle-resin mixtures for the preparation prepreps. This proved to be a very cost-effective and efficient technique for screening different formulations on a small scale.

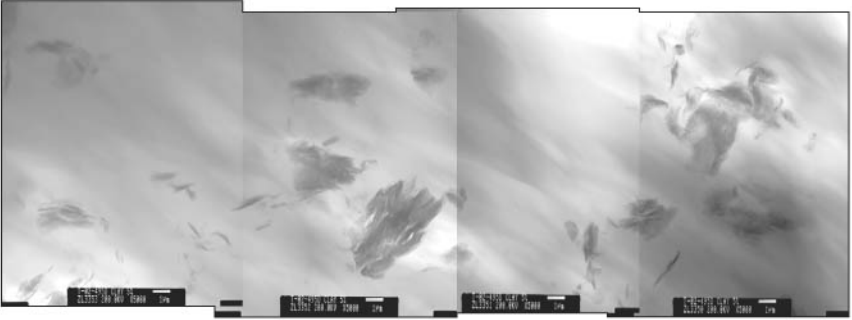


Figure 7.54 Transmission electron microscopy images of 5 wt% Cloisite 30B in 95 wt% SC-1008 (scale bar is 1 μ m).

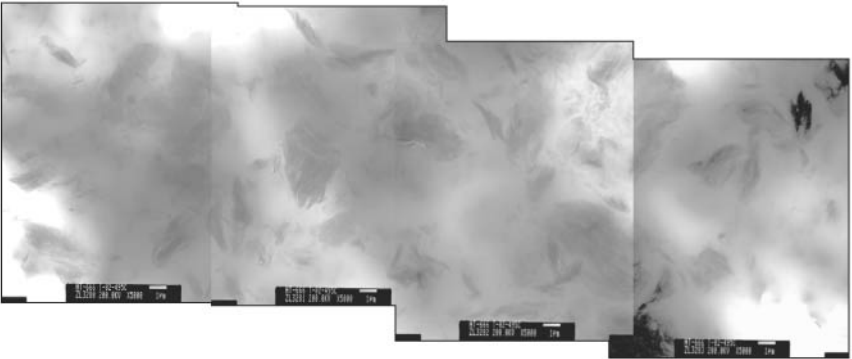


Figure 7.55 Transmission electron microscopy images of 10 wt% Cloisite 30B in 90 wt% SC-1008 (scale bar is 1 μ m).

Ablation test: SSRM test conditions. Three test conditions to simulate thermal effect of the exhaust plumes using low, medium, and high heat flux

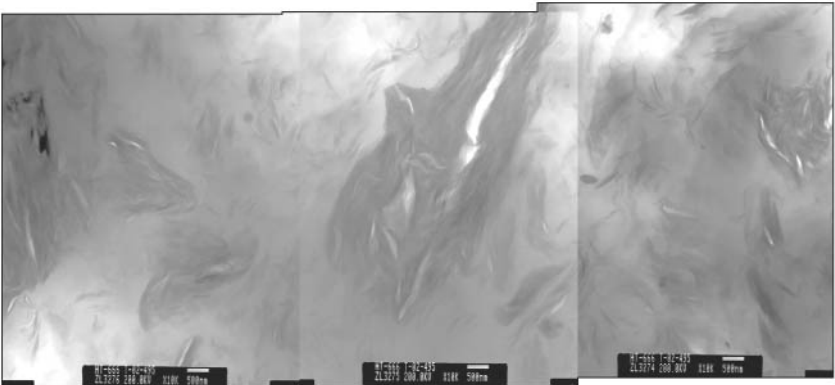


Figure 7.56 Transmission electron microscopy images of 15 wt% Cloisite 30B in 85 wt% SC-1008 (scale bar is 500 nm).

were selected. These different conditions represent different regions in a rocket nozzle assembly. Alumina (Al_2O_3) particles were added to the exhaust stream to simulate the particle impingement effect of the solid rocket exhaust plumes from the aluminized solid propellants. The following six test conditions used are listed in the order of their severity:

- 1000 Btu/ft²-s (11,345 kW/m²) with Al_2O_3 particles
- 625 Btu/ft²-s (7094 kW/m²) with Al_2O_3 particles
- 250 Btu/ft²-s (2838 kW/m²) with Al_2O_3 particles
- 1000 Btu/ft²-s without Al_2O_3 particles
- 625 Btu/ft²-s without Al_2O_3 particles
- 250 Btu/ft²-s without Al_2O_3 particles

MX-4926 as controls. Cytec Engineered Materials fabricated three sets of carbon phenolic laminates (MX-4926) based on the SC-1008 resin system. Three versions of MX-4926 were used as controls for this investigation. They were made based on fiber orientation:

- Molding compound (1/4-inch squares of chopped fabric, designated by MX-4926 MC)
- Two-dimensional fabric (designated by MX-4926 2D)
- 60° shingle (the most effective orientation for rocket nozzle application, designated by MX-4926 SH)

Samples of MX-4926 MC were tested at six conditions, as listed above, with an Al_2O_3 particle flow rate of 15 g/min for a test duration of 15 s. Table 7.8 shows a summary of the ablation data for MX-4926 MC specimens. Figure 7.57 shows the peak erosion of MX-4926 MC exposed to the six test conditions. As shown in Fig. 7.57, the peak erosion with Al_2O_3 was significantly higher than those specimens without particles. The residual mass increased with the decrease of heat flux for test cases with and without particles. The maximum backside heat-soaked (MBHS) temperature rise also decreased with the decrease of heat flux.

Figure 7.58 shows that MX-4926 SH has the lowest peak erosion, followed by MX-4926 2D, and that MX-4926 MC has the highest peak erosion. The residual mass of the three versions of MX-4926 specimens is very much the same at the three different heat fluxes. This is an insensitive criterion for comparing material candidates. The data indicated that MX-4926 MC has the best insulative property, followed by MX-4926 2D, and that MX-4926 SH has the worst insulative property.

TABLE 7.8 Summary of Ablation Data for MX-4926 MC

Ablation data/heat flux	1000 Btu/ft ² -s with particles	625 Btu/ft ² -s with particles	250 Btu/ft ² -s with particles	1000 Btu/ft ² -s without particles	625 Btu/ft ² -s without particles	250 Btu/ft ² -s without particles
Peak erosion (inch)	0.235*	0.234	0.073	0.03	0.029	0
Residual mass (%)	85.0	86.3	90.2	88.2	88.9	91.6
MBHS temperature rise (°C)	315	159	133	175	164	133
Time to MBHS temperature rise (min)	0.3	0.5	1	1	0.9	0.9

*Bold entry stands for total erosion (burned through)

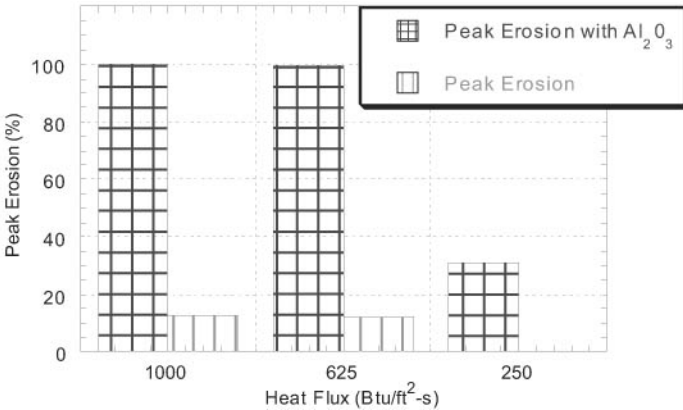


Figure 7.57 Peak erosion of MX-4926 MC exposed to six test conditions.

In summary, MX-4926 SH has the most erosion-resistant (lowest peak erosion) characteristic and the worst insulative property (highest MBHS temperature rise); MX-4926 MC has the worst erosion-resistant characteristic and the best insulative property; and MX-4926 2D has moderate peak erosion and insulative properties. For ease of manufacturing, MX-4926 SH is the most difficult and MX-4926 2D is the easiest. MX-4926 MC is more representative than MX-4926 2D. The molding compound specimens were selected for this study.

Scale ablation test. SC-1008 with 5, 10, and 15 wt% Cloisite 30B were selected to replace 15 wt% of carbon black in the original MX-4926 formulation. Cytec Engineered Materials prepared three versions of MX-4926 alternates, designated MX-4926 ALT 5 %, MX-4926 ALT 10%, and MX-4926 ALT 15%. Three loadings of PR-24-PS in 20, 24, and

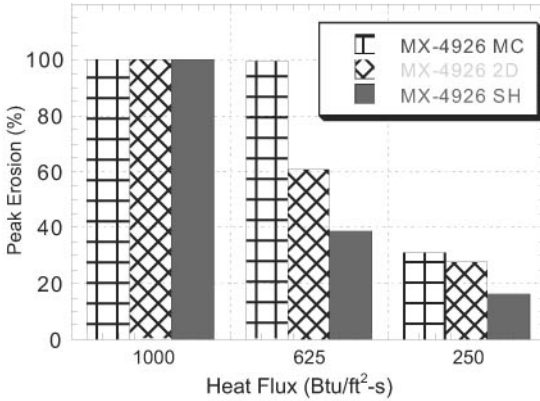


Figure 7.58 Peak erosion of MX-4926 MC, 2D, and SH with Al₂O₃ particles.

28 wt% were dispersed in SC-1008 without the rayon-carbon fiber reinforcement. Three loadings of Trisilanolphenyl-POSS in 2, 6, and 10 wt% were also dispersed in SC-1008. The POSS/SC-1008 mixture was used with the rayon-carbon fabric to produce prepreps in a manner similar to the nanoclay mixture. Table 7.9 shows the chemical compositions of the laminates used for ablation testing. Figure 7.59 compares the densities of three types of NRAMs with nanoclay, CNF, and POSS at various loading levels of nanoparticles. All clay-NRAMs, CNF-NRAMs, and POSS-NRAMs have densities lower than MX-4926.

TABLE 7.9 Specimen Configuration for SSRM Laminate Fabrication

Material ID	Density (g/cc)	Rayon carbon fiber reinforcement (wt%)	Resin SC-1008 phenolic (wt%)	Filler (wt%)
MX-4926 (Control)	1.44	50	35	15 carbon black (CB)
MX-4926 ALT Clay 5%	1.42	50	47.5	2.5 Cloisite 30B
MX-4926 ALT Clay 10%	1.43	50	45	5 Cloisite 30B
MX-4926 ALT Clay 15%	1.43	50	42.5	7.5 Cloisite 30B
PR-24-PS 20%/SC-1008	1.35	None	80	20 PR-24-PS CNF
PR-24-PS 24%/SC-1008	1.38	None	76	24 PR-24-PS CNF
PR-24-PS 28%/SC-1008	1.41	None	72	28 PR-24-PS CNF
MX4926 ALT SO-1458 2%	1.41	50	49	1 Trisilanolphenyl-POSS
MX4926 ALT SO-1458 6%	1.38	50	47	3 Trisilanolphenyl-POSS
MX4926 ALT SO-1458 10%	1.40	50	45	5 Trisilanolphenyl-POSS

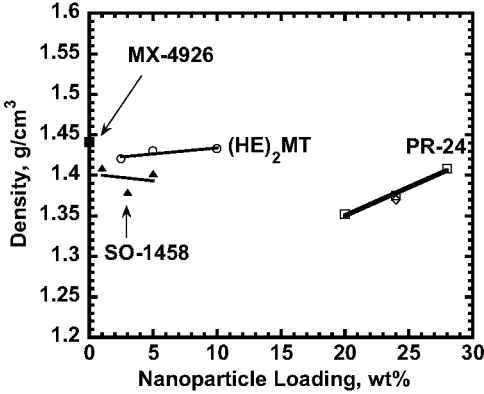


Figure 7.59 Density of MX-4926 and NRAMs with different nanoparticle loadings.

At the suggestion of W. Luehmann⁴⁷ of Pratt & Whitney Space Propulsion/Chemical Systems Division (P&WSP/CSD), a lower flow rate of Al₂O₃ particles in the SSRM to simulate a total erosion of 200 mils (0.20 inch) of MX-4926 SH at 1000 Btu/ft²-s was adopted. Several MX-4926 SH and MX-4926 2D were tested under this new test condition, using a flow rate of 4 g/min Al₂O₃ particles.³⁵ For this study, test conditions of 1000 Btu/ft²-s heat flux with a flow rate of 4 g/min Al₂O₃ particles for a test duration of 15 s were adopted.

Figure 7.60 shows the ablation rates of MX-4926 and all three groups of NRAMs: clay-NRAM [(HE)₂MT nanoclay], CNF-NRAM (PR-24), and POSS-NRAM (SO-1458). The ablation rate of MX-4926 was about 0.4 mm/s. For the clay-NRAM group, only the 7.5 wt% clay-NRAM had a lower ablation rate than MX-4926. The 15 wt% clay and 85 wt% phenolic becomes 7.5 wt% clay-NRAM when it is transformed into

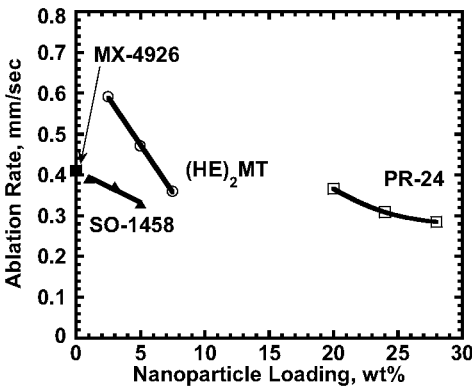


Figure 7.60 Ablation rate of MX-4926 and NRAMs with different types of nanoparticles at various loading levels.

laminate, since all clay-NRAM contains 50 wt% carbon fiber reinforcements (Table 7.9). For the CNF-NRAM group, all three loadings had lower ablation rates than MX-4926, with 28% CNF-NRAM being the lowest. For the POSS-NRAM group, all three loadings had lower ablation rates than MX-4926, with 5% POSS-NRAM being the lowest. The loadings of POSS were 1, 3, and 5 wt%, the lowest of the three NRAM groups. The loadings of clay were 2.5, 5, and 7.5 wt%, the medium values of the three NRAM groups. The loadings of CNF were 20, 24, and 28 wt% without the rayon-carbon reinforcements, the highest of the three NRAM groups.

Figure 7.61 shows the residual masses of MX-4926 and all the NRAMs. The residual mass of MX-4926 was about 92 percent. The POSS-NRAM group had the most residual mass, about 93 percent for all three loadings. The clay-NRAM group had about the same residual mass as the MX-4926. The CNF-NRAM group had about 86 to 88 wt% residual mass, the lowest of all materials, control and NRAMs.

Figure 7.62 shows the maximum backside heat-soaked temperature rise of MX-4926 and the NRAMs. All NRAMs had lower maximum backside heat-soaked temperature rises than MX-4926. The backside heat-soaked temperature rise of MX-4926 was about 106°C. It is obvious that the CNF-NRAM group had a substantially lower maximum backside heat-soaked temperature rise than MX-4926. It was from 54° to 72°C. The result for the POSS-NRAM group was from 75° to 86°C, the second lowest. The clay-NRAM group had the third lowest, from 82° to 98°C.

An IR pyrometer was used to measure the surface temperatures of all materials during SSRM firings. Figure 7.63 shows the surface temperatures of MX-4926 and the NRAMs. The surface temperature of

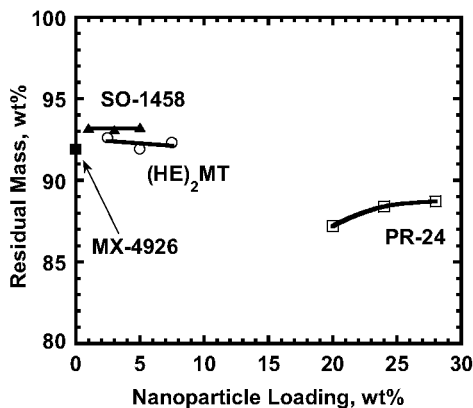


Figure 7.61 Residual mass of MX-4926 and NRAMs with different types of nanoparticles at various loading levels.

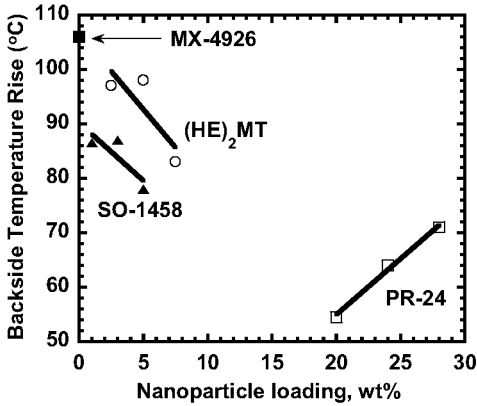


Figure 7.62 Backside temperature rise of MX-4926 and NRAMs with different types of nanoparticles, at various loading levels.

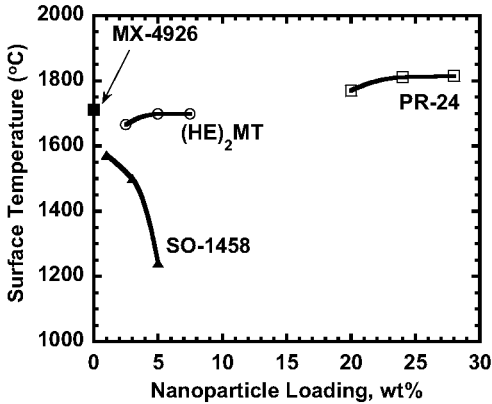


Figure 7.63 Surface temperature of MX-4926 and NRAMs with different types of nanoparticles, at various loading levels.

MX-4926 was about 1700°C. Surface temperatures of the CNF-NRAM samples were higher than those of MX-4926, the clay-NRAMs, and the POSS-NRAMs. This finding suggests that we may have better radial heat transfer than axial heat transfer, supported by the glowing heat of the surface observed during material testing. This phenomenon was observed by other researchers⁵⁸ and needs further study. The surface temperatures of clay-NRAMs and POSS-NRAMs were lower than that of MX-4926. The amount of nanoclay in the clay-NRAMs had essentially no effect. The amount of POSS in the POSS-NRAMs had a significant effect on the surface temperature of the POSS-NRAMs.

Air Force Research Laboratory Pi-K solid rocket motor ablation test. Based on the SSRM test data, selective NRAMs were scaled to 20-lb quantities

at CEM. These nanoparticle-resin mixtures were to transform into prepregs using T300 carbon fabric in a semiproduction R&D facility in Winona, MN. These prepregs were fabricated into molding compound and compression-molded into cylindrical billets (about 4.25 inches in diameter and 4 inches in length). The billet was machined into a nozzle assembly similar to the ones shown in Figs. 7.64 to 7.67. Figures 7.64 to 7.67 show an MX-4926 with SC-1008 phenolic resin, clay-NRAM with SC-1008 phenolic resin, a CNF-NRAM with SC-1008 phenolic resin, and an SM-8029 (quartz fabric-silicone resin composite) machined nozzle assembly of the AFRL/Edwards Pi-K SRM, respectively. The nozzle throat area is replaced by a graphite insert to avoid excess throat erosion during the motor firing. Using this experimental setup, reasonably accurate testing of materials designed to be used for the entrance region and the exit cone of the solid rocket nozzle assembly was anticipated.

At Edwards AFB, CA, AFRL/PRSM has developed a very cost-effective char motor to screen SRM insulation materials.⁵²⁻⁵⁴ A schematic of the Pi-K SRM experimental setup is illustrated in Fig. 7.68. The motor is operated and fired in the upward direction. It usually contains up to 2 lbs of solid rocket propellant in an end-grain burning configuration.



MX-4926 (Fig. 7.64)



Clay-NRAM (Fig. 7.65)

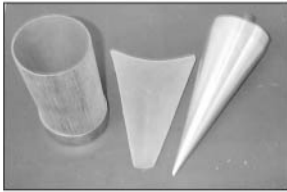


CNF-NRAM (Fig. 7.66)



SM-8029 (Fig. 7.67)

Figures 7.64 to 7.67 Prefired Pi-K rocket motor nozzle assemblies fabricated from MX-4926, clay-NRAM, CNF-NRAM, and SM-8029 materials. This nozzle assembly is shown as the nozzle part in Fig. 7.68 slides into the back end of the heavy-walled Pi-K rocket motor.



- 4-inch char motor
- Only 100 g of insulation material needed (clear POSS sample shown on the left)
- Very cost-effective tool
- Rapid testing of 6 samples/day (or more)

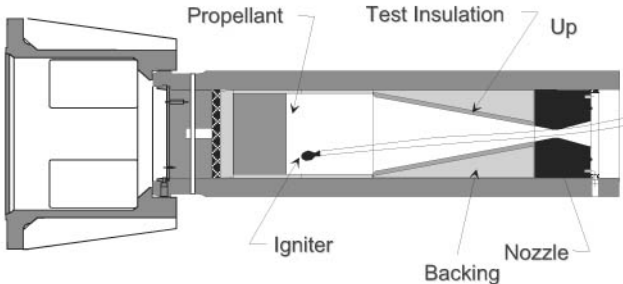


Figure 7.68 Schematic of the AFRL/Pi-K SRM experimental setup for ablation testing. Both nonaluminized and aluminized propellants can be used. Average chamber pressure is about 800 psia and test duration is about 8 seconds when an end-burning propellant grain is used. Nanocomposite rocket ablative materials is tested at the nozzle section.

Both nonaluminized and aluminized propellants have been used for insulation material testing. The average chamber pressure is typically about 800 psia, and the test duration is about 8 seconds. For insulation material testing, a cylindrical cone made of glass phenolic material of different area ratio is used inside the motor. This configuration is used to simulate a range of Mach numbers that the insulation materials are exposed during to the combustion of gaseous products. Rapid testing of 6 samples or more per day can be achieved.

For nozzle material testing, the cylindrical cone is removed, and the whole nozzle assembly at the back end of Pi-K SRM is replaced by NRAM candidate materials. The whole assembly is a convergent/divergent nozzle, and the nozzle throat is a machined graphite nozzle insert, as shown in Fig. 7.69. The graphite nozzle insert piece prevents excess erosion in the nozzle throat area. This configuration enables the evaluation of candidate materials in the entrance region and exit cone of the nozzle. Four successful firings were conducted recently, and erosion data are being analyzed. Erosion data at different area ratios were collected. Posttest specimens of selective regions of the nozzle assembly were sectioned and analyzed using SEM.

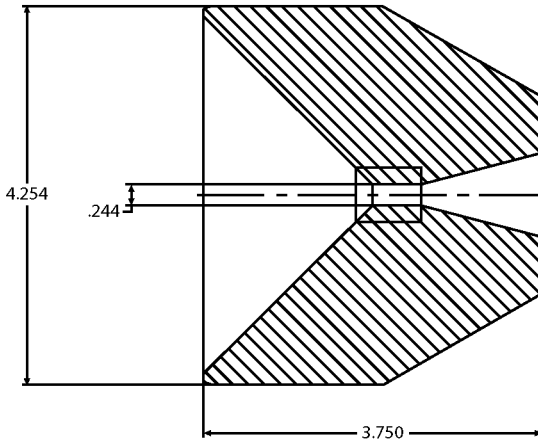


Figure 7.69 Cross-sectional diagram of the motor nozzle assembly showing the graphite insert at the nozzle throat of the NRAM material. This nozzle assembly fits into the back end of the Pi-K motor. The direction of the combustion of gaseous products from the rocket chamber is from right to left.

Summary and conclusions. From this study, the following conclusions were drawn:

- The feasibility of using nanocomposite rocket ablative materials (NRAMs) in rocket nozzle assemblies was clearly demonstrated using SSRM subscale ablation testing.
- MMT organoclays, CNF, and POSS can be implemented into the existing semiproduction line at Cytex Engineered Materials to manufacture fiber-reinforced prepregs and compression molded into laminates.
- Higher loadings of MMT, POSS, and CNF improve erosion resistance, and 28 percent CNF has the lowest erosion rate in the absence of carbon fiber reinforcements.
- Backside temperatures of all NRAMs were lower than that of baseline MX-4926, and CNF-NRAM as a group had lower temperatures than the MMT-NRAM and POSS-NRAM groups.
- Backside temperature trends were reversed for MMT and CNF, whereas higher loadings of CNF appeared to conduct heat better.
- Peak erosion of POSS-NRAM is 20 percent lower than MX-4926 at very low loadings.
- Peak erosion of CNF-NRAM (28% CNF) without rayon fabric is 42 percent lower than MX-4926.
- Backside temperatures of CNF-NRAM are 68 percent lower.

- Backside temperatures of MMT-NRAM are 28 percent lower.
- Backside temperatures of POSS-NRAM are 26 percent lower.

The following topics should be investigated:

- SEM analyses of posttest specimens of MX-4926 and all NRAMs.
- Fabrication of the following NRAMs was scheduled at Cytec for SSRM tests:
 - (a) SM-8029 (S-826 rigid silicone with quartz fibers)
 - (b) S-826 rigid silicone with PR-24-PS CNFs
 - (c) SM-8029 ALT nanoclay
 - (d) SM-8029 ALT POSS
- Additional solid rocket motor firings are being scheduled at the Air Force Research Laboratory/Edwards AFB (AFRL/PRSM) to test the best candidates from SSRM firings.⁵⁹
- Physical, mechanical, and thermophysical properties of selective NRAMs need to be measured.
- Optimal nanoclay dispersion needs further study.
- Synergism between CNF and other nanoparticles needs further study.

7.2.2 Flammability properties of polymer nanostructured materials³⁸

Flammability of organic polymeric materials is a major problem, especially in those applications where the safety of the general public is of concern. Advanced fire-resistant polymeric material systems are used in vehicles, aircraft, aerospace and shipboard applications, and portable or prefabricated buildings.

Previous studies⁶⁰ have shown that fire-retardant additives can reduce the flammability of polymeric materials and enhance the ability of the material systems to endure a small fire. Koo et al.^{61,62} have reported the development of thermally resistant polymers for airplane interiors using the cone calorimeter method (ASTM E1354/ISO 5660).²⁹ Based on the review of technical and commercial literature, several categories of polymers were selected for testing. Cone calorimeter tests were performed at a heat flux of 50 kW/m² on these polymers without any reinforcements.^{61,62}

Koo et al.⁶³⁻⁶⁵ are also involved with the research and development of advanced fire-safe polymeric materials for structural applications inside the pressure hulls of Navy submarines. This work consists of

addressing serious technical issues that have limited the use of composites inside submarines. These issues are flammability, smoke, toxic gas emissions, and mechanical properties of polymer matrix composites. Nine glass-reinforced composite and one carbon-reinforced composite were fabricated. They were tested under the cone calorimeter test according to MIL-STD-2031: "Fire and Toxicity Test Methods and Qualification Procedure for Composite Material Systems Used in Hull, Machinery, and Structural Applications Inside Naval Submarines."⁶⁶ The characterization of flammability and mechanical properties of these fiber-reinforced composites is included in this work.

Gilman et al. of the National Institute of Standards and Technology (NIST) have reported the flammability properties of several thermoplastic and thermosetting polymer nanocomposites: delaminated nylon 6 and nylon 12 layered silicate nanocomposites and intercalated polymer layered-silicate nanocomposites prepared from PS, PP-g-MA, and vinyl esters.^{67,68} The cone calorimeter results at a 35 kW/m² heat flux of the two vinyl esters and their respective nanocomposites showed the peak and average heat release rates (HRR) were significantly improved with a low percentage (6%) of silicate. Reductions of 25 percent and 39 percent in peak HRR and reductions of 39 percent and 44 percent in mean HRR were reported.⁶⁸ Mean mass loss rates (MLR) reduction of 30 percent and 39 percent were also reported.⁶⁸ The mean heat of combustion (H_c), mean soot (SEA), and mean carbon monoxide yields were unchanged.

Of all the above work consisting of (a) fire-resistant polymer only,⁶⁰⁻⁶² (b) fire-resistant resin reinforced with conventional fibers,⁶³⁻⁶⁵ and (c) polymer nanocomposites without conventional fiber reinforcement,^{67,68} none involved the use of polymer nanocomposites combined with conventional fiber reinforcements to form polymer matrix composites. Recently, the impregnation of polymer nanocomposites (phenolic resin with nanoparticles) into carbon fabric to form polymer matrix composites (PMCs) was initiated through an AFOSR research program for ablation and flammability studies. This study deals with the flammability studies of these PMCs, whereas the ablation studies are described elsewhere.³²⁻³⁷

Materials testing. The potential fire hazard of any material depends on many factors, including ignitability, rate of surface flame spread, heat release rate (peak, average, and total), mass loss rate, smoke evolution, and evolution of toxic gases (e.g., CO). Cone calorimeter data address most of these factors, either directly [e.g., heat release rate (HRR)] or indirectly (e.g., time to ignition and HRR as functions of external heat flux, as indicators of flame spread potential). The data obtained from the cone calorimeter test are available in engineering units that are

conductive to extrapolation to other fire sizes and scenarios. More detailed discussions of Cone calorimeter data are described in Chap. 5.

The Cone calorimeter data are grouped into three areas of discussion: (a) ignition and heat release, (b) mass loss, and (c) gas generation. All polymer nanostructured materials were tested at a heat flux of 75 kW/m^2 for an interval of 20 minutes.

Selection of materials

Polymer matrix composites. MX-4926 is a rayon-based, eight-harness weave carbon fabric impregnated with a Mil R-9299 phenolic resin that contains a carbon black filler.⁴⁶ The approximate composition of MX-4926 is 50 wt% carbon reinforcements, 35 wt% phenolic resin, and 15 wt% carbon black. MX-4926 is currently used in a typical solid rocket motor nozzle assembly (see Sec. 7.2.1). The phenolic char formed at high temperature is usually not very strong. Our approach is to replace the carbon black filler in the phenolic resin with different nanoparticles, so that the nanoparticles will reinforce the phenolic in the nanometer scale.

The phenolic used in the rocket nozzle ablative (MX-4926) was a solvent (isopropanol)-based resole, SC-1008, manufactured by Borden Chemical. The Cloisite 30B used was a natural montmorillonite nanoclay [Tallow bishydroxyethyl methyl, T(EOH)₂M], manufactured by SCP. Carbon nanofibers (CNF) are a form of vapor-grown carbon fiber, which is a discontinuous graphitic filament produced in the gas phase from the pyrolysis of hydrocarbons. PR-19-PS CNF was used in this study. More detailed descriptions of these materials can be found in Chap. 2 and Sect. 7.2.1.

Nanostructured materials. SC-1008 with 5, 10, and 15 wt% Cloisite 30B were selected to replace 15 wt% of carbon black in the original MX-4926 formulation. Cytac Engineered Materials prepared three versions of MX-4926 alternates, designated MX-4926 ALT 5%, MX-4926 ALT 10%, and MX-4926 ALT 15%. Two CNFs in SC-1008 without the rayon-carbon fiber reinforcement materials were also included. Table 7.10 shows the chemical compositions for the laminates.

Discussion of results. Fire testing was performed using the cone calorimeter. All nanostructured materials in Table 7.10 were tested at 75 kW/m^2 heat flux. We will briefly summarize the cone calorimeter results in the areas of ignitability, peak heat release rate, and average heat release rate for 300 s, mass remaining, smoke ratio, CO, and CO₂. Table 7.11 summarizes the time to ignition, peak heat release (PHRR), and average heat release rate (HRR) for 300 s for the tested materials.

TABLE 7.10 Specimen Configuration for Laminate Fabrication

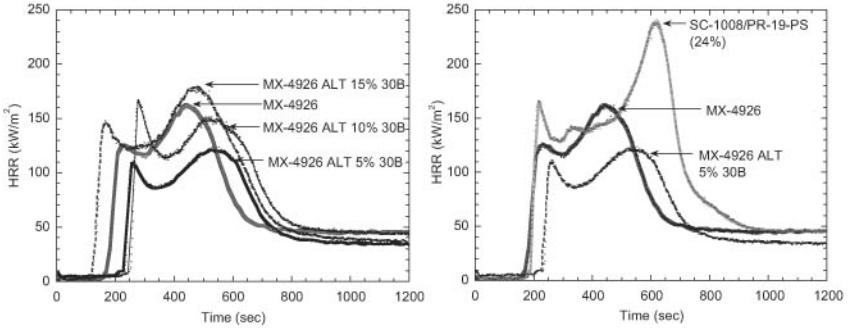
Material	Density (g/cc)	Rayon-carbon-fiber reinforcement (wt%)	Resin SC-1008 phenolic (wt%)	Filler (wt%)
MX-4926 (Control)	1.40	50%	35%	15% carbon black (CB)
MX-4926 ALT 5%	1.42	50%	47.5%	2.5% Cloisite 30B
MX-4926 ALT 10%	1.43	50%	45%	5% Cloisite 30B
MX-4926 ALT 15%	1.35	50%	42.5%	7.5% Cloisite 30B
PR-19-PS/SC-1008	1.37	None	76%	24% PR-19-PS CNF
PR-24-PS/SC-1008	1.26	None	76%	24% PR-24-PS CNF

TABLE 7.11 Flammability Properties of MX4926 and MX-4926 ALTs at 75 kW/m² Heat Flux

Material	Time to ignition (s)	PHRR (kW/m ²)	Avg. HRR for 300 s (kW/m ²)
MX-4926	188	163	134
MX-4926 ALT 5	233 (24% longer)	123 (25% lower)	97 (28% lower)
MX-4926 ALT 10	252 (34% longer)	167 (1st) 150 (2nd)	131
MX-4926 ALT 15	140	180	147
SC-1008/PR-19-PS	185	241	137

Ignitability. Figure 7.70 shows a comparison of the HRR of MX-4926, MX-4926 ALT 5% 30B, MX-4926 ALT 10% 30B, and MX-4926 ALT 15% 30B materials. As shown in Table 7.11 and Fig. 7.70, a 24 percent longer time to ignition (TTI) for the MX-4926 ALT 5% 30B (233 s) and a 34 percent longer TTI for MX-4926 ALT 10% 30B (252 s) than for the baseline MX-4926 (188 s) material was achieved. Figure 7.71 shows a comparison of the HRR of MX-4926, MX-4926 ALT 5% 30B, and SC-1008/PR-19-PS CNF materials. The time to ignition of SC-1008/PR-19-PS CNF material (185 s) was similar to that of MX-4916 (188 s).

Heat release. Figures 7.70 and 7.71 show the peak heat release rates (PHRR) for the candidate materials at 75 kW/m² heat flux. As shown in Table 7.11 and Figs. 7.70 and 7.71, the PHRR of MX-4926 ALT 5% 30B is 123 kW/m², about 25 percent lower than MX-4926 at 163 kW/m². Two PHRRs were observed with the MX-4926 ALT 10% 30B material at 167 and 150 kW/m². The first PHRR is higher than the second PHRR, which is different from the behavior of other nanostructured materials. This behavior needs further study.



Figures 7.70 and 7.71 Comparison of HRR of MX-4926 with MX-4926 ALTs (left) and with PR-19-PS CNF (right) materials at 75 kW/m^2 heat flux.

Average heat release rates. Table 7.11 shows the average HRR for 300 s for all the nanostructured and MX-4926 materials. The MX-4926 ALT 5% 30B material has a 28 percent lower average HRR for 300 s than the MX-4926 material.

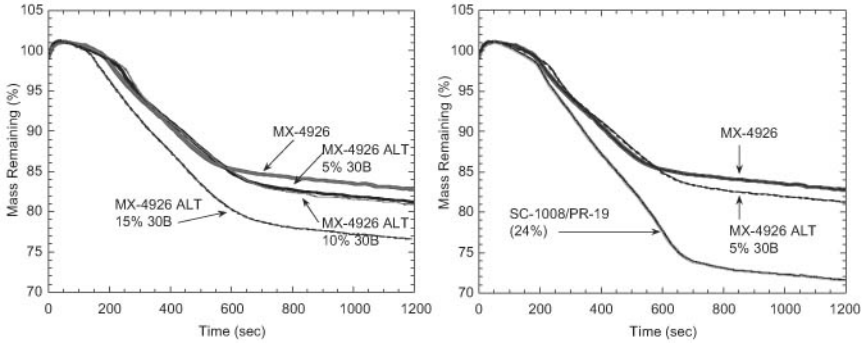
Based on the three criteria of sustained time to ignition, peak HRR, and average HRR for 300 s, MX-4926 ALT 5% 30B is the only candidate material that performed better than the MX-4926 material, and the result is summarized below:

- Time of ignition of MX-4926 ALT 5% 30B is 24 percent longer than that of MX-4926
- Peak heat release rate of MX-4926 ALT 5% 30B is 25 percent lower than that of MX-4926
- Average heat release rate for 300 s of MX-4926 ALT 5% 30B is 28 percent lower than that of MX-4926

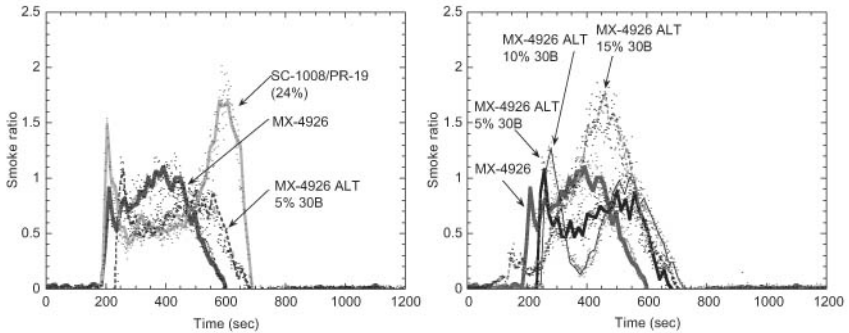
Mass remaining. Figures 7.72 and 7.73 show the comparison of mass remaining (%) for MX-4926 ALTs and for SC-1008/PR-19-PS materials with MX-4926, respectively. All MX-4926 ALTs showed a lower mass remaining than MX-4926. SC-1008/PR-19-PS CNF showed a substantially lower mass remaining value than MX-4926, because there were no rayon-based carbon fibers in it.

Smoke ratio, carbon monoxide, and carbon dioxide. Additional cone data related to smoke and gas generation were investigated during the experiment and are shown in Figs. 7.74 and 7.75.

Figures 7.74 and 7.75 show the smoke ratio of MX-4926 ALTs and SC-1008/PR-PS-19 as compared to MX-4926, respectively. MX-4926 ALT 5% 30B has a comparable smoke ratio to MX-4926, whereas SC-1008/PR-19-PS CNF has a higher smoke ratio. Figures 7.76 and 7.77 show the carbon monoxide (CO) in ppm. MX-4926 ALT 5% 30B has

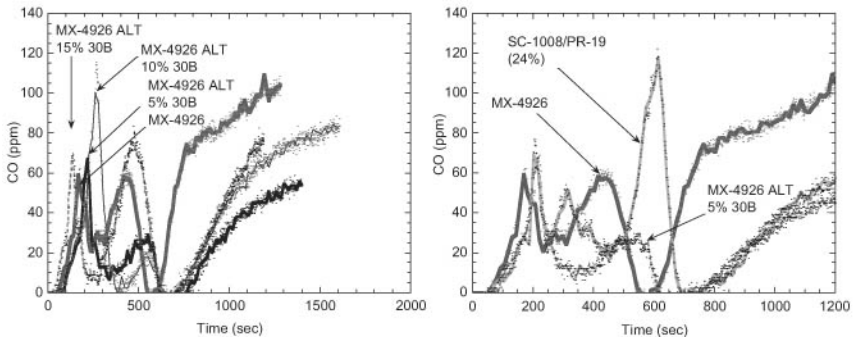


Figures 7.72 and 7.73 Comparison of mass remaining of MX-4926 with MX-4926 ALTs (left) and with PR-19-PS CNF (right) materials at 75 kW/m² heat flux.

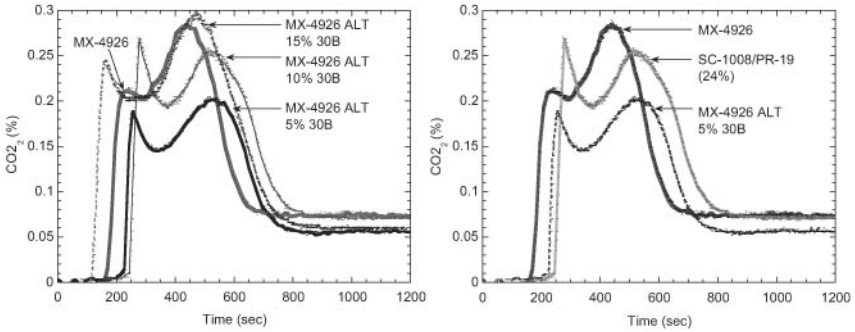


Figures 7.74 and 7.75 Comparison of smoke ratio of MX-4926 with MX-4926 ALTs (left) and with PR-19-PS CNF (right) materials at 75 kW/m² heat flux.

a comparable CO in ppm to MX-4926, whereas SC-1008/PR-19-PS CNF has a higher CO content. Figures 7.78 and 7.79 show the carbon dioxide as a percentage. MX-4926 ALT 5% 30B has lower CO₂ yields than



Figures 7.76 and 7.77 Comparison of carbon monoxide (ppm) of MX-4926 with MX-4926 ALTs (left) and with PR-19-PS CNF (right) materials at 75 kW/m² heat flux.



Figures 7.78 and 7.79 Comparison of carbon dioxide (%) of MX-4926 with MX-4926 ALTs (left) and with PR-19-PS CNF (right) materials at 75 kW/m² heat flux.

MX-4926, and MX-4926 has the highest CO₂ yields of all other materials tested.

Conclusions. The following conclusions have been reached from this study:

- The feasibility of using polymer nanostructured carbon-reinforced materials as fire-safe composites has been successfully demonstrated.
- Five polymer nanostructured materials were compared with baseline MX-4926 phenolic carbon-reinforced composites with the cone calorimeter at 75 kW/m².
- The most promising material was the MX-4926 ALT 5% 30B material, which had substantial improvements in time to ignition (24% lower), peak heat release rate (25% lower), and average heat release rate (28% lower) over the baseline MX-4926 material.

7.2.3 Nanomodified carbon/carbon composites (NCCCs)^{7,49-51}

Carbon/carbon (C/C) structures are traditionally designed and optimized for high-temperature applications. They have very high temperature capabilities under inert atmospheric conditions, but without oxidation protection, they suffer from thermo-oxidative instability above ~700°F and result in poor mechanical strength. Oxidation protection technologies developed to be used above ~1800°F in thermo-oxidative environments have had limited success. Carbon/carbon composites (CCCs) would be ideal materials to extend organic-based material systems beyond the 700°F limit if their mechanical strength can be improved and maintained by preventing oxidation of the composite.

The major objective of this material program is to develop a better CCC with enhanced thermo-oxidative resistant performance at intermediate temperatures (700° to 1200°F). We proposed that a nanophase be introduced into the CCC prior to cure, to provide improved and maintained mechanical strength by preventing oxidation of the composites. In this study, (a) three resin systems: Lonza low- and medium-viscosity cyanate esters, PT-15 and PT-30, and Hitco phenolic, 134A and (b) three types of nanoparticles: chemically modified montmorillonite (MMT) organoclays, polyhedral oligomeric silsesquioxanes (POSS), and carbon nanofibers (CNF) were used to create new types of nanomodified CCCs.

The minor objectives of this investigation are to: (a) develop *processes* to disperse these nanoparticles uniformly in the cyanate esters and the phenolic resin prior to curing, (b) use wide-angle x-ray diffraction (WAXD), transmission electron microscopy (TEM), and scanning electron microscopy (SEM) to characterize polymer nanocomposite *structures* after curing, (c) study the *structure-property* relationship of these types of new materials, and (d) evaluate the *performance* (mechanical properties) of these materials in the intermediate temperature range (700° to 1200°F) after carbonization.

Six resin/nanoparticle material systems were selected to produce prepregs at Hitco Carbon Composites. The prepregs were fabricated into composites for carbonization and densification to produce C/C composites. Heat aging of CCCs was conducted for 24 hrs at 700° and 1200°F for the six candidates and the baseline Hitco CC139 materials. Mechanical properties such as the tensile strength and modulus and interlaminar shear strength were determined on the C/C nanomaterials and are compared with the baseline CCC.

Selection of materials

Resin systems and CCC. Three resin systems were selected for this study: Lonza's Primaset® PT-15 and PT-30 cyanate esters, and Hitco's 134A phenolic resin system. For a baseline CCC, Hitco's CC139 was selected.

Cyanate ester resin. The polymer system is the most important component of the CCC materials. Lonza Corporation's Primaset PT-15 and PT-30 multifunctional cyanate ester⁶⁹ were selected for this study. These polymer systems have 65 percent char yield, less than 0.5 percent volatiles, and no decomposition byproducts during curing, and low viscosity (80cP) at 120°C. Shivakumar et al. successfully used PT-30 resin for the fabrication of CCC.^{70,71} PT-15 is a multifunctional, low-viscosity liquid cyanate ester resin,⁷² similar to PT-30.

Phenolic resin. The Hitco-specific resin, 134A, a resole amine-containing phenolic, was used as the baseline resin material.⁷³ The resin is a phenol-formaldehyde system made specifically for Hitco, but it is similar in many ways to other commercial phenol-formaldehyde resins such as Borden Chemical SC-1008. The main properties relevant to the formation of a carbon/carbon composite are its char yield and the type of crack structure generated to be favorable to infiltration during the chemical vapor infiltration (CVI) process.

Carbon/carbon composite. Hitco's CC139 material (baseline CCC for this study) is a standard commercial material that has been manufactured by Hitco for a number of applications for several years.⁷⁴ Its basic construction is a PAN fiber fabric lay-up with a Hitco-specific phenolic resin (134A), carbonized and processed using CVI to a density of 1.75 g/cc. The 134A resin is mixed with a fill material of carbon black to help tailor the shrinkage and porosity for the CVI.

Nanoparticles. Three types of nanoparticles were used, namely Southern Clay Products' and Nanocor's montmorillonite (MMT) nanoclays, Hybrid Plastics' polyhedral oligomeric silsesquioxanes (POSS) materials, and Applied Sciences' carbon nanofibers (CNF).

Nanoclays. Six MMT nanoclays including Southern Clay Products' (a) Cloisite 10A (a natural MMT modified with a quaternary ammonium salt), (b) Cloisite 30B (a natural MMT modified with a ternary ammonium salt) and (c) Cloisite Na⁺ (a natural MMT); Nanocor's (d) Nanomer[®] I.28E (an onium ion surface modified MMT mineral), (e) Nanomer I.30E (an onium ion surface modified MMT mineral), and (f) PGW (Na⁺, no organic pillaring) were selected.

POSS. The lab-scale dispersion of these materials involved the examination of seven POSS chemicals, including (a) Trisilanolphenyl-POSS (SO1458), (b) cyanopropyl cyclopentyl POSS (NI0910), (c) a tetra- β -substituted styryl POSS with four epoxy groups [POSS(1)], (d) epoxy cyclohexyl dimethylsilyl POSS, (e) octaisobutyl POSS, (f) poly(phenyl silsesquioxane) (PPSQ) (PM1270), and (g) dichloromethylsilylethyl isobutyl POSS (CS0335) to prepare nanocomposites.

CNF. Two Applied Sciences Pyrograf III carbon nanofibers (CNF), (a) PR-19-PS (128 nm in diameter) and (b) PR-24-PS (65 nm in diameter), were selected for this study. The TEM analyses were conducted on selective specimens.

These TEM images facilitated screening various formulations for desirable nanolevel dispersion of the clay, POSS, or CNF within the cure resin/inorganic composites. Desirable features included higher

levels of clay exfoliation, molecular dispersion of POSS, and uniform dispersion of CNF within the resin both before and after curing.

Discussion of results. The candidate materials developed were screened for dispersion using WAXD and TEM prior to full scale-up. Lab scale dispersion of (a) PT-30 with different weight percent POSS, nanoclays, and CNF; (b) PT-15 with different weight percent of POSS and nanoclays; and (c) 134A with different weight percent POSS and nanoclays were conducted. The morphology of selective resin/nanoparticle systems were characterized using TEM and SEM analyses.

Processing and characterization of resin/nanoparticle systems. Detailed processing and characterization of PT-30/nanoparticle, PT-15/nanoparticle, and 134A/nanoparticle systems are reported elsewhere,⁴⁹⁻⁵¹ and a brief discussion is included in this section.

PT-30 CE resin. Cloisite 30B was first dispersed in THF before blending with the PT-30 resin. Cloisite 30B is uniformly dispersed in a PT-30/30B THF system. Under higher magnification, Cloisite 30B was seen in an intercalated state in the PT-30 resin, and clay tactoids were observed that were larger than when PT-15 was mixed with Cloisite 30B and cured in the same manner (Fig. 7.80).

Weight percent (wt%) of seven POSS chemicals were blended with PT-30 for a total of 15 blends using a lab-scale, high-shear mixer. Appearance, in terms of transparency, translucency, or opaqueness, was examined during mixing and before and after curing for all blends, and densities were recorded. Based on visual observations, Trisilanophenyl-POSS was the only potential POSS compound that was satisfactory with PT-30 using the direct melt blending process. All

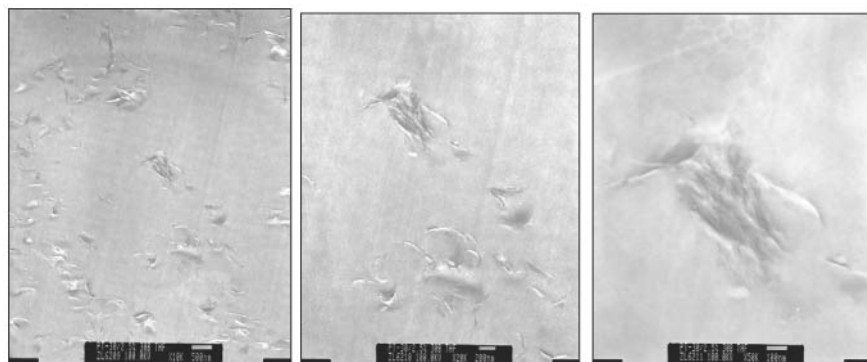


Figure 7.80 Higher magnification of PT-30/Cloisite 30B (97.5/2.5) THF showing nanoclay in an intercalated state in the PT-30 cyanate ester resin, where scale bars are 500 nm (left), 200 nm (center), and 100 nm (right).

other blends were either opaque or translucent, and agglomerated particles were observed. Clearly, phase separation had taken place. Selective candidates were cured for TEM analyses. PT-15 and PT-30 were cured thermally. Figure 7.81 shows very few undissolved SO1458 POSS particles, when directly blended into PT-30 resin matrix. Some molecular dispersion in the PT-30/SO1458 POSS (95/5) was achieved, as shown in Fig. 7.81. Significant Si is detected in the resin matrix, where no phase separation can be detected. SO1458 was the preferred POSS system for PT-30 resin. PT-30/PR-19-PS and PT-30/PR-24-PS were blended in (99.5/0.5) and (99/1) wt%, and a total of four CNF blends were prepared.

PT-15 CE resin. When PT-15 was blended with several clays (Nanomer I.28E, Nanomer I.30E, PWG, Cloisite 10A, and Cloisite 30B, see Chap. 2) using different mixing methods, 34 blends were recorded. Resulting samples were either opaque or translucent. The PT-15/30B (97.5/2.5) THF, PT-15/10A (97.5/2.5) THF, and PT-15/I.30E (97.5/2.5) THF blends were prepared using THF as a carrier medium to facilitate clay dispersion. When Cloisite 30B, Cloisite 10A, and Nanomer I.30E were compared in higher magnification TEM micrographs, Cloisite 30B was shown to be dispersed slightly more uniformly than the other two clays. Cloisite 30B is in a partial exfoliated state in PT-15, as shown in Fig. 7.82. Small tactoids were present in this nanodispersion. Figure 7.83 shows higher magnification TEM micrographs of PT-15/Cloisite 30B (97.5/2.5) THF, showing that Cloisite 30B clays are exfoliated in PT-15 cyanate ester. Cloisite 30B was our preferred clay for the PT-15 resin.

PT-15 was blended with PPSQ in THF and Trisilanolphenyl-POSS in different weight percent, and a total of 13 blends were recorded. Only PT-15/Trisilanolphenyl-POSS in (99/1) and (97/3) were completely

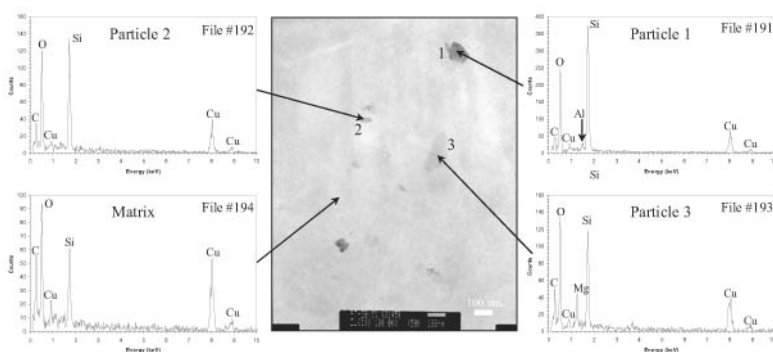


Figure 7.81 Transmission electron micrographs of PT-30/SO1458 POSS (95/5) in high magnification, showing molecular dispersion of SO1458 POSS with some POSS particles in the PT-30 cyanate ester. Significant Si is detected in the resin matrix.

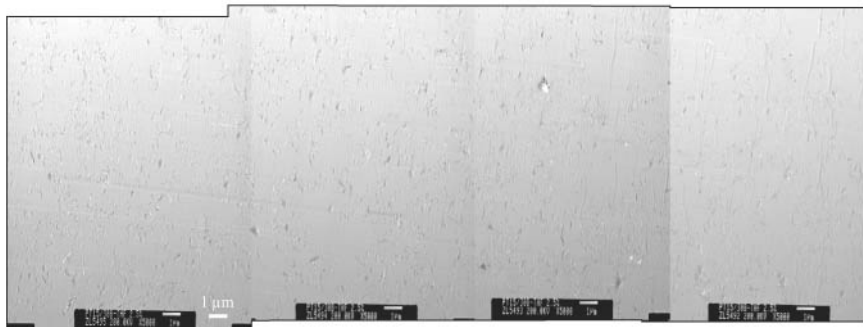


Figure 7.82 Transmission electron micrographs of PT-15/Cloisite 30B (97.5/2.5) THF showing uniform dispersion of Cloisite 30B in the PT-15 cyanate ester, where the scale bar is 1 μm .

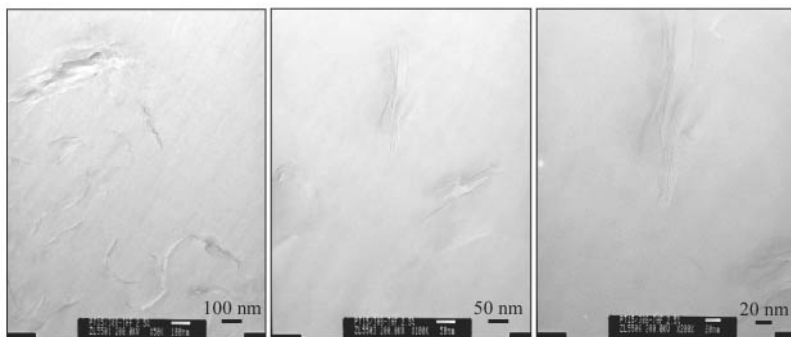


Figure 7.83 Higher magnification TEM micrographs of PT-15/Cloisite 30B (97.5/2.5) THF showing Cloisite 30B clays are exfoliated in PT-15 cyanate ester.

transparent. Transmission electron microscopy of PT-15/SO1458 (97/3), & PT-15/SO1458 (95/5) blends was performed. Figure 7.84 shows molecular dispersion of SO1458 POSS in the PT-15/SO1458 (97/3) system. Where particles are noted, one finds their Si content is higher than in the open resin matrix. Significant Si is detected in the resin matrix in regions where no particles are observed. Clearly, the POSS is partially dissolved in the matrix and partially nanodispersed. This was a good candidate system for a conversion to CCC. SO1458 POSS was the preferred POSS system for the PT-15 resin.

134A phenolic resin. The 134A/Trisilanophenyl-POSS in THF in (99/1), (97/3), and (90/10) were examined. 134A/Cloisite 10A IPA were blended in compositions of (98/2), (95/5), and (90/10). Wide-angle x-ray diffraction analyses showed that a portion of the clay appeared very similar to the pure, as-received Cloisite 10A, and another portion had contracted to a smaller d-spacing than that of the original, as-received clay. Based on previous studies on SC 1008 phenolic resin,³²⁻³⁸ Cloisite 30B

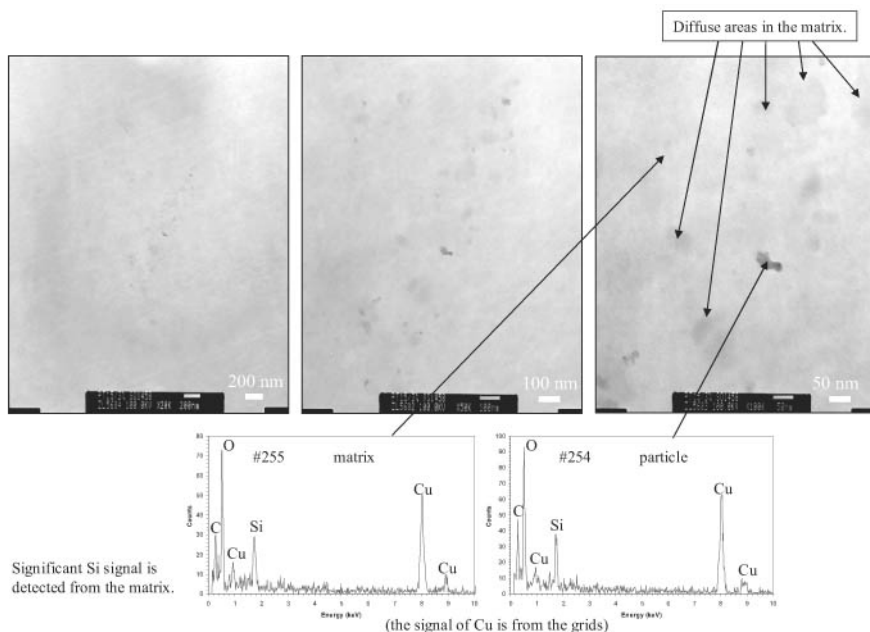


Figure 7.84 Progressive magnification TEM micrographs of PT-15/SO1458 POSS (97/3) showing molecular dispersion of SO1458 POSS in PT-15 cyanate ester. Silicon from POSS molecules is dispersed in the resin matrix. The dark particle has the same Si/O/C composition as the resin matrix.

was selected as the preferred nanoclay for the 134A phenolic. Hitco 134A/dichloromethylsilylethyl isobutyl POSS in THF in (97/3) and (90/10) were examined using TEM analysis. Micron- and nanosized POSS particles were observed in the 134A resin matrix, indicating this POSS chemical is not compatible with the phenolic. Apparently, the two Si-Cl bonds react with IPA faster than with phenolic resin hydroxyl groups. The resulting POSS molecule is not highly soluble in the resin. Based on previous studies on the SC 1008 phenolic resin,³²⁻³⁸ SO1458 POSS was selected as the preferred POSS for the 134A phenolic.

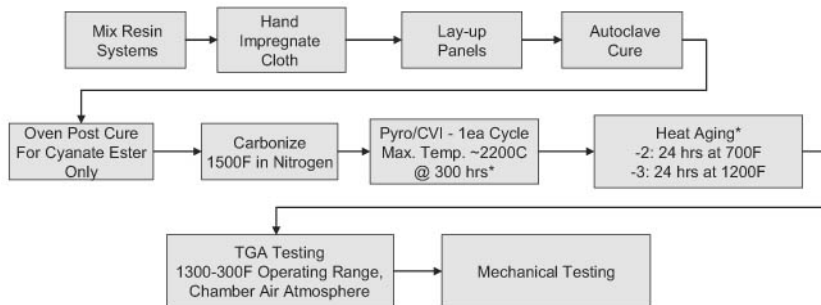
Fabrication of carbon/carbon composites. Based on TEM analyses and scale up studies, the final compositions of the six candidates to produce prepreps at Hitco were:

- 134A/Cloisite 30B in (97/3) wt%
- 134A/SO1458 POSS in (97/3) wt%
- PT-15/Cloisite 30B in (95/5) wt%
- PT-15/SO1458 POSS in (95/5) wt%

- PT-30/PR-24-PS in (99/1) wt%
- PT-30/Cloisite 30B in (95/5) wt%

An overall procedure of processing, fabrication, thermo-oxidative, and mechanical properties testing of all the NCCCs and CC139 is outlined in Fig. 7.85.

Processing procedures. Hitco used the same T-300 carbon fiber fabric for all six CCC candidates that is used for CC139. The fabric was prepregged by hand in Hitco’s research and development lab using the predetermined resin/filler compositions. All panels are consolidated by vacuum bagging and autoclave-cured at appropriate temperature cycles. Panels are physically characterized for dimensions and weight. The cured panel is carbonized in inert gas (nitrogen) to 1500°F, cooled and characterized for density and porosity. All panels are coprocessed in Hitco’s proprietary carbon CVI process to achieve a target density of 1.7 g/cc within two cycles. At the completion of the processing, all panels are given a final characterization for density and porosity. One witness panel of each type is processed, with samples removed for archiving at the cure, carbonized, and fully infiltrated stages. A set of four 12.25- by 12.25- by 0.15-inch CCC panels is fabricated for each candidate and CC139, so 28 panels are manufactured. Figure 7.86 shows the nanomodified C/C composite (NCCC) panels.



Notes:

134A systems mixed mechanically in IPA for 1 hr then allowed to stand 24 hrs. Remixed for 1 hr prior to use. IPA added as required to maintain wt. ratios.

PT-15 and PT-30 systems mixed mechanically on hot plate at 160F for 1 hr then allowed to stand 24 hrs. Remixed for 1 hr prior to use with hot plate assist.

Panel dimensions 12.25"X12.25"X0.150"

*Furnace vented with positive exhaust pressure nitrogen for heat aging.

Panels piggybacked with brake CVI. Typically yields smooth laminar carbon structure.

Figure 7.85 Overall procedures for processing, fabrication, thermo-oxidative, and mechanical testing of NCCCs and CC139.

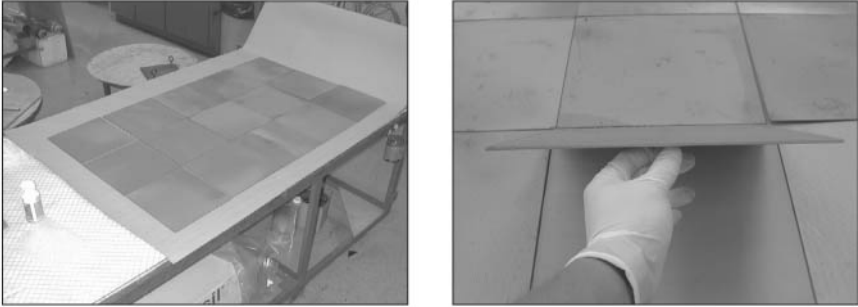


Figure 7.86 Nanomodified C/C composite (NCCC) 12.25- by 12.25- by 0.15-inch panels (left) and close-up of NCCC panels (right).

Thermo-oxidative studies of CCC. Hitco conducted exposure testing of panels to determine the magnitude of the benefit of each material's variation. Hitco provided QA testing for heat exposure for a number of its current products using several small-capacity, air-muffle furnaces. The four panels of the seven C/C composites were tested in the following manner:

- One panel was heat-aged for 24 hrs at 1200°F
- One panel was heat-aged for 24 hrs at 700°F
- One panel was reserved for room temperature (RT)
- One panel was a spare

Samples were removed from the furnace for brief periods for spot measurement of weight loss. At the completion of the 24-hour exposure, mechanical test coupons were machined for the panels and tested for tensile and shear strengths and modulus. Data for physical properties, such as averaged bulk density, skeletal density, and porosity, of NCCC materials were recorded as shown in Table 7.12. Porosity is a measure of how much pyrocarbon could be added to the CCC. One panel from each candidate was subjected to 24 hours at 700°F and 1200°F in nitrogen. Samples were removed from the furnace for brief periods for spot measurement of weight loss. After the 24 hours of exposure, TGA furnaces were used to record weight loss using a set volume of air flow to simulate oxidation on the RT, 700°F, and 1200°F specimens designated as -1, -2, and -3, respectively. Air flow was set at 2 L/min and approximately 10°C/hr ramp rate to 1300°F. All specimens were exposed for 8 hours. Figures 7.87 and 7.88 show typical temperature and weight loss data of the thermo-oxidative studies for PT30/CLO/5 NCCC specimens that were RT, heat-aged at 700°F, and heat-aged at 1200°F.

A summary of all the NCCC candidates and CC139 (control) with their weight-loss percentage, density, and ranking based on weight-loss

TABLE 7.12 Summary of Physical Data of NCCCs

P/N	Bulk density (g/cc)	Skeletal density (g/cc)	Porosity (%)	Conditions	Rank
134A/CLO/3-1	1.619	1.816	10.8	-1 RT	
134A/CLO/3-2	1.581	1.831	13.7	-2 700°F	
134A/CLO/3-3	1.567	1.815	13.7	-3 1200°F	
134A/CLO/3-4	1.585	1.816	12.7	-4 Spare	5
134A/POSS/3-1	1.616	1.814	10.9	-1 RT	
134A/POSS/3-2	1.575	1.804	12.7	-2 700°F	
134A/POSS/3-3	1.611	1.813	11.1	-3 1200°F	
134A/POSS/3-4	1.603	1.801	11.0	-4 Spare	4
PT15/POSS/5-1	1.651	1.797	8.1	-1 RT	
PT15/POSS/5-2	1.595	1.804	11.6	-2 700°F	
PT15/POSS/5-3	1.626	1.804	9.8	-3 1200°F	
PT15/POSS/5-4	<i>Lost</i>			-4 Spare	
PT15/CLO/5-1	NA	NA	NA	-1 RT	
PT15/CLO/5-2	NA	NA	NA	-2 700°F	
PT15/CLO/5-3	NA	NA	NA	-3 1200°F	
PT15/CLO/5-4	NA	NA	NA	-4 Spare	
PT30/PR24PS/1-1	1.630	1.773	8.1	-1 RT	
PT30/PR24PS/1-2	1.643	1.775	7.4	-2 700°F	
PT30/PR24PS/1-3	1.684	1.889	10.8	-3 1200°F	
PT30/PR24PS/1-4	1.667	1.876	11.1	-4 Spare	2
PT30/CLO/5-1	1.653	1.906	13.3	-1 RT	1
PT30/CLO/5-2	1.656	1.913	13.4	-2 700°F	1
PT30/CLO/5-3	1.618	1.917	15.6	-3 1200°F	1
PT30/CLO/5-4	1.653	1.898	12.9	-4 Spare	1
CC139-1	1.627	1.801	9.7	-1 RT	3
CC139-2	1.638	1.801	9.1	-2 700°F	3
CC139-3	1.630	1.799	9.4	-3 1200°F	3
CC139-4	1.644	1.801	8.7	-4 Spare	3

* RT, 700°F, and 1200°F specimens were designated as -1, -2, and -3, respectively.

data is shown in Table 7.13. An air leakage was detected in our first set of experiments; as a result, the 134A/CLO/3-1A, 134A/CLO/3-2A, 134A/CLO/3-3A, 134A/POSS/3-1A, 134A/POSS/3-2A, 134A/POSS/3-3A, PT15/POSS/5/-1B, PT15/POSS/5/-2A, and PT15/POSS/5/-3A specimens were overexposed to unrealistic thermo-oxidative conditions. They are denoted with an * in Table 7.13. The 134A/CLO/3-4B and 134A/POSS/3-4D specimens were retested for the 1200°F condition using the fourth spare panels of the 134A/CLO/3 and 134A/POSS/5 candidates marked

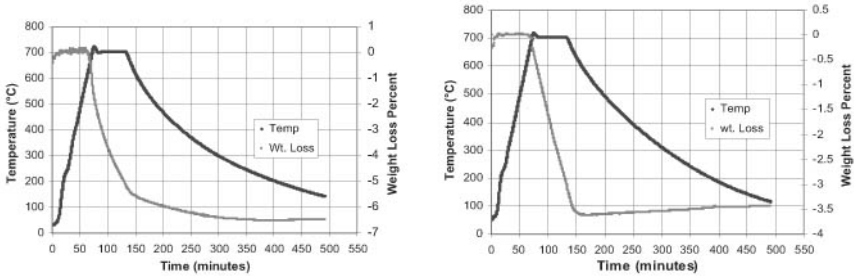


Figure 7.87 Thermo-oxidative study of PT30/CLO/5-1B RT specimen (left) and PT30/CLO/5-2B 700°F specimen (right) heat-aged in air for 8 hours.

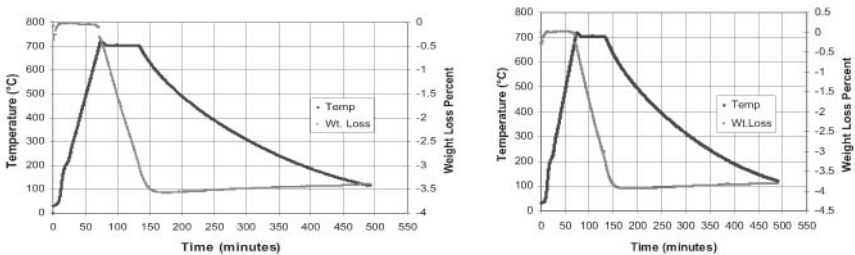


Figure 7.88 Thermo-oxidative study of PT30/CLO/5-3B 1200°F specimen (left) and PT30/CLO/5-3C 1200°F specimen (right) heat-aged in air for 8 hours.

as “-4.” The PT15/POSS/5-4 spare specimen was lost, and as a result the PT15/POSS/5 candidate was not retested for the 1200°F condition for this project. Regrettably, the behavior of molecularly dispersed POSS into PT-15 (Table 7.13, entries 9 to 12) could not be assessed for improved thermo-oxidative stability because of the overexposed or lost specimens.

Based on the thermo-oxidative analyses, the PT30/CLO/5 candidate is the most thermo-oxidative resistant; weight losses were 5.2 percent, 5.1 percent, and 3.7 percent at room temperature (RT), 700°F, and 1200°F, respectively. The PT15/CLO/5 candidate is the second-best thermo-oxidative resistant, and weight losses were 6.5 percent, 5.1 percent, and 3.7 percent at RT, 700°F, and 1200°F, respectively. The PT30/PR24PS/1 NCCC, which had a 6.8 percent weight loss, is the third-best thermo-oxidative resistant NCCC candidate. The standard CC139 is the fourth-best material, with a weight loss of 8.9 percent, 9.0 percent, and 13.6 percent for RT, 700°F, and 1200°F, respectively. The 134A/CLO/3-4B and 134A/POSS/3 had high weight losses of 30.5 percent and 23.3 percent, respectively.

Weight losses of different NCCCs were compared as shown in Fig. 7.89. It is evident that the cyanate ester resin-based PT30/PR24PS/1 and PT30/CLO/5 specimens have better thermo-oxidative resistance

TABLE 7.13 Summary of Thermo-Oxidative Data and Ranking

P/N	Initial wt (g)	TGA recorded wt. (g)	Weight loss (%)	Sample density (g/cc)	Rank
134A/CLO/3-1A*	2.053	1.728	-15.8	1.619	
134A/CLO/3-2A*	2.145	1.772	-17.4	1.581	
134A/CLO/3-3A*	2.056	1.152	-44.0	1.567	
134A/CLO/3-4B	2.036	1.414	-30.5	1.585	6
134A/POSS/3-1A*	1.958	1.441	-26.4	1.616	
134A/POSS/3-2A*	1.989	1.216	-38.9	1.575	
134A/POSS/3-3A*	1.933	1.666	-13.8	1.611	
134A/POSS/3-4D	2.055	1.573	-23.2	1.603	5
PT15/POSS/5-1B*	2.469	2.178	-11.8	1.650	
PT15/POSS/5-2A*	2.462	2.146	-12.9	1.595	
PT15/POSS/5-3A*	2.577	1.782	-30.8	1.651	
PT15/POSS/5-4	Lost				
PT15/CLO/5-1	2.52	2.36	-6.5	NA	2
PT15/CLO/5-2B	2.36	2.28	-3.4	NA	2
PT15/CLO/5-2C	2.40	2.24	-6.8	NA	2
PT15/CLO/5-3B	2.34	2.26	-3.5	NA	2
PT15/CLO/5-3C	2.38	2.29	-3.8	NA	2
PT30/PR24PS/1-1A*	2.586	1.244	-51.9	1.630	
PT30/PR24PS/1-2A*	2.574	1.406	-45.4	1.643	
PT30/PR24PS/1-3B,C	2.573	2.399	-6.8	1.684	3
PT30/CLO/5-1B,C	2.522	2.358	-5.2	1.653	1
PT30/CLO/5-2B,C	2.383	2.261	-5.1	1.656	1
PT30/CLO/5-3B,C	2.363	2.265	-3.7	1.618	1
CC139-1A	2.673	2.436	-8.9	1.627	4
CC139-2A	2.506	2.881	-9.0	1.638	4
CC139-3A	2.536	2.191	-13.6	1.630	4

*An air leakage was detected in these experiments. RT, 700°F, and 1200°F specimens were designated as -1, -2, and -3, respectively.

than the phenolic resin-based CC139 standard CCCs. The phenolic resin-based 134A/CLO/3 and 134A/POSS/3 specimens have worse thermo-oxidative resistant characteristics than the CC139 standard. From our TEM analyses, we concluded that the nanoparticles were dispersed very well in the PT30 and PT15 cyanate resin systems and poorly in the 134A phenolic resin system. Figure 7.90 shows a comparison of the density of the different NCCCs. It is also evident that PT30/PR24PS/1-3B,C has the highest density (1.684 g/cc), followed by

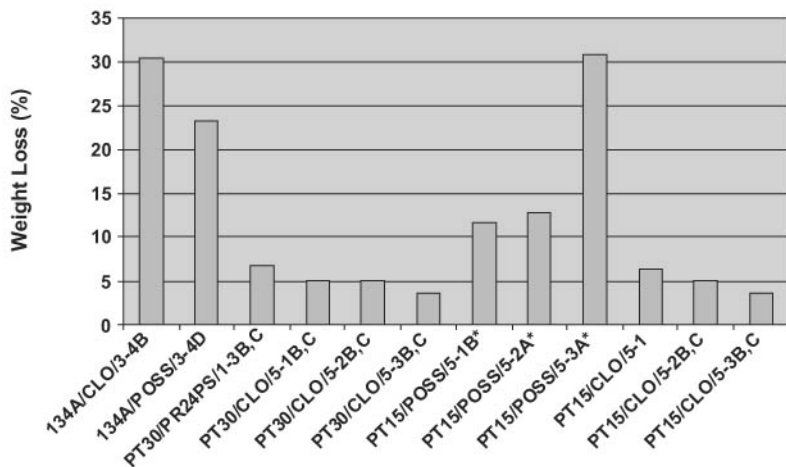


Figure 7.89 Comparison of weight loss with different NCCCs.

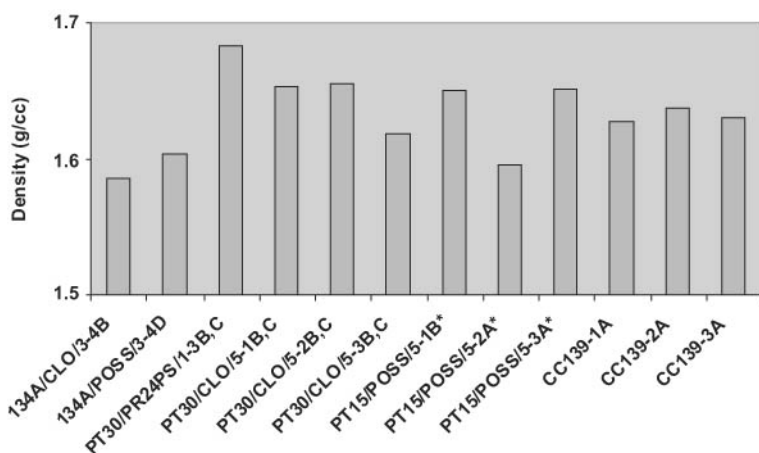


Figure 7.90 Comparison of density of different NCCCs.

PT30/CLO/5-2B,C (1.656 g/cc) and PT30/CLO/5-1B,C (1.653 g/cc), then the CC139 specimens (1.627 to 1.638 g/cc), whereas the densities of 134A/POSS/3-4D and 134A/CLO/3-4B were 1.603 g/cc and 1.585 g/cc, respectively. Figure 7.91 shows a comparison of densities versus weight loss of the different NCCCs. A trend of higher density NCCCs exhibiting lower weight loss and lower density NCCCs showing higher weight loss is proposed. Lower weight loss for NCCC from cyanate ester resin systems is expected, owing to little or no volatiles from cured cyanate esters, as well as proposed improved thermo-oxidative stability attributable to the presence of a nanophase in the NCCC cyanate ester materials.

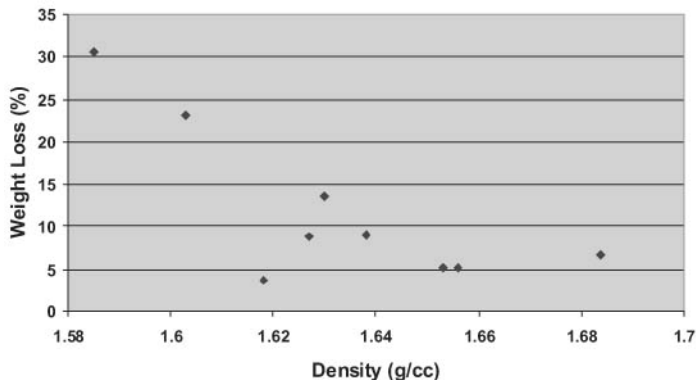


Figure 7.91 Comparison of density and weight loss of NCCCs.

Mechanical properties of CCC. All four NCCCs (134A/CLO/3, 134A/POSS/3, PT30/CLO/5, PT30/PR24PS/1) and CC139 panels were visually inspected and tap tested to identify blisters (delamination defects), and the data were recorded. Specimens were extracted from defect-free (as much as possible) areas. All interlaminar test specimens were visually defect-free areas, but some tensile specimens had to be cut from the blistered areas. No blisters or delaminations were found in 134A-based panels. PT30-based panels had delaminations, blisters, and microcracks within the layer. PT30/CLO/5 panels had the greatest number of defects. Blister diameters in PT30-based panels ranged from 2 to 5 inches in diameter. Blisters were located under the surface plies and near the midplane of the panel. All panels showed a lack of or uneven densification. Macro- or microcracks or voids were apparent from 10 \times and 20 \times microscopy study. This finding is predominant in PT30-based panels. It was concluded that the blisters and delaminations were the result of an improper heating cycle of the as-cured composite part. Tensile specimens were selected from areas of each panel where little or no delamination was visually detected. Tensile specimen length in the delaminated panels was increased to 12 inches to prevent splitting open the laminate at the grip-ends of the coupons. Interlaminar shear strength (ILSS) specimens were selected from areas of each panel where no delamination was visually detected and the thickness was uniform.

Tension and interlaminar shear (4-point, short-beam shear) tests were conducted following ASTM using at least three specimens. All ILSS tests were successful, and the failure modes were delaminations near the midplane, as expected. The average ILSS of CC139-4, 134A/CLO/3-4, 134A/POSS/3-4, PT30/CLO/5-4, and PT30/PR24PS/1-4 panels at room temperature was 2.8, 1.7, 1.9, 2.1, and 2.2 ksi, respectively.⁴⁹⁻⁵¹

The heat-treated (1200°F) CC139-3, PT30/CLO/5-3, PT30/PR24PS/1-3 panels lost 3 percent, 9 percent, and 13 percent of the ILSS, respectively. The room-temperature ILSS of CC139, about 2.5 ksi, agreed well with North Carolina A&T State University manufactured PT30/T300-based C/C composite panels.^{70,71} Tensile modulus, tensile strength, and Poisson's ratio were measured for all five material systems. Variable tensile testing of some of the panels may be attributable to tab slippage problems or poor interfacial bonding between the base material and the CVI deposited carbon. The tab slippage problem was resolved by abrading the tabbing surfaces. The room-temperature elastic moduli of CC139-4, 134A/CLO/3-4, 134A/POSS/3-4, PT30/CLO/5-4, and PT30/PR24PS/1-4 were 13.0, 17.0, 16.8, 13.8, and 14.3 msi, respectively. An increase in elastic modulus for NCCCs as compared to baseline CC139 is attributed to nanophase formation. The heat-treated panels lost 3 percent, 2 percent, and 6 percent of the modulus, respectively.

The PT30/PR24PS/1-3, -4 specimens had the highest ultimate tensile strength (UTS). This material exhibited the largest maximum failure load (both RT and 1200°F heat-aged specimens) and gradually fell off to 75 percent load until complete fracture. This finding indicated that the CNF would enhance ductility while increasing the ultimate strength of the NCCC. The nanoclay specimens were significantly weaker and also had excessive blisters. Nanoclay may adversely affect the CCC if proper heat-cycling is not used in the pyrolysis of the as-cured panels. All of the PT30 materials fracture inside the tab area, with the greatest tendency to fail at the actuator end. All PT30 materials had microcracking as well as some blistering, particularly the PT30/CLO/5-3 and -4 specimens, which had blistering near the midplane and surface plies. The strength of CC139 panels without and with heat treatment was 46.5 and 47.8 ksi; the difference is less than the one STD of the data. All nanomodified samples except PT30/CLO/5-4 exhibited higher room temperature strength and modulus when compared to control CC139-4. Table 7.14 summarizes all the mechanical properties for the five materials at RT and under heat-aged conditions.⁴⁹⁻⁵¹

Summary and conclusions. Three resin systems (134A phenolic, PT-15 and PT-30 cyanate esters) and three types of nanoparticles (MMT nanoclay, POSS, and CNF) were selected for this study. Transmission electron microscopy analysis was used to characterize and screen candidates based on their degree of dispersion. Six candidates and one baseline (CC139) carbon/carbon composites were selected to produce prepregs and cured composites. A set of four 12.25- by 12.25- by 0.15-inch CCC panels was fabricated for each candidate and for the

TABLE 7.14 Comparison of Mechanical Properties of the Five Materials in RT and Heat-Aged Conditions

Material	UTS (ksi)	Modulus (msi)	Poisson's ratio	ILSS (ksi)
CC139-4	46.5	13.0	0.074	2.83
134A/CLO/3-4	53.2	17.0	0.026	1.7
134A/POSS/3-4	51.2	16.8	0.020	1.92
PT30/CLO/5-4	43.4	13.8	0.036	2.09
PT30/PR24PS/1-4	59.2	14.3	0.025	1.94
CC139-3	47.8	12.8	0.111	2.76
PT30/CLO/5-3	33.5	14.7	0.028	1.94
PT30/PR24PS/1-3	60.4	13.9	0.033	1.94

baseline materials. Heat aging of the NCCCs was conducted at 700° and 1200°F in nitrogen for 24 hours, and the NCCCs were then exposed to heated air for 8 hours under simulated thermo-oxidative conditions. Mechanical properties such as tensile strength, tensile modulus, Poisson's ratio, and interlaminar shear strength were measured and compared with CC139 at room temperature and at 1200°F.

The following conclusions were drawn from this study:

- MMT clay, POSS, and CNF dispersed very well in the PT-30 and PT-15 CE resins but poorly in the 134A phenolic resin, which identified the CE nanocomposites as more desirable than the phenolic nanocomposites. Transmission electron microscopy evidence of molecular dispersion of POSS into PT-15 could not be translated into improved thermo-oxidative stability (less weight loss) because of specimen overexposure or loss.
- The nanomodified CE CCCs (PT15/CLO/5, PT30/PR24PS/1 and PT30/CLO/5) are more thermo-oxidative resistant than the baseline CCC (CC139). The nanomodified phenolic CCCs (134A/CLO/3 and 134A/POSS/3) are less thermo-oxidative resistant than the baseline CC139 material.
- The densities of nanomodified CE CCCs (PT30/PR24PS/1, PT30/CLO/5, PT15/POSS/5, and PT15/CLO/5) were higher than that of the baseline CCC (CC139), whereas the densities of the nanomodified phenolic CCCs (134A/CLO/3 and 134A/POSS/3) were lower than that of CC139.
- The higher-density NCCCs (based on nanomodified CE) have less weight loss than the lower-density phenolic-modified NCCC and CC139, which makes them more thermo-oxidative resistant.
- Blisters and delaminations of NCCCs were the result of an improper heating cycle of the as-cured composite part. The use of differential scanning calorimetry (DSC) during the curing of cyanate

ester resin to determine optimum cure conditions is proposed to reduce or eliminate blisters and delaminations through better cure conditions.

- The ultimate tensile strength (UTS) of CC139-4, 134A/CLO/3-4, 134A/POSS/3-4, PT30/CLO/5-4, and PT30/PR24PS/1-4 panels at room temperature were 46.5, 53.2, 51.2, 43.4, 59.2 ksi, respectively. Increases in the UTS of NCCCs over baseline may be attributable to nanophase formation.
- Elastic moduli of CC139-4, 134A/CLO/3-4, 134A/POSS/3-4, PT30/CLO/5-4, and PT30/PR24PS/1-4 were 13.0, 17.0, 16.8, 13.8, and 14.3 msi, respectively. Increased elastic modulus of NCCCs over baseline may be caused by nanophase formation.
- The average ILSS of CC139-4, 134A/CLO/3-4, 134A/POSS/3-4, PT30/CLO/5-4, and PT30/PR24PS/1-4 panels at RT were 2.8, 1.7, 1.9, 2.1, and 2.2 ksi, respectively. The heat-aged (1200°F) CC139-3, PT30/CLO/5-3, PT30/PR24PS/1-3 panels lost 3 percent, 9 percent, and 13 percent of the ILSS, respectively.
- The PT30/PR24PS/1-3, -4 specimens had the highest UTS. They exhibited the largest maximum failure load (for both RT and 1200°F heat-aged specimens), and then gradually fell off to 75 percent load until complete fracture. It appears that CNF would enhance the ductility as well as increase the ultimate strength.
- All nanoclay NCCCs were significantly weaker and also had excessive blisters. Nanoclay may compromise the CCC if proper heating cycling is not used in the pyrolysis of the as-cured panels. Improved thermal stability in surface-modified clays with alkyl imidazole surfacing agents and controlled cure (using DSC) are proposed to eliminate blisters and improve cured panel appearance and performance of nanoclay CE panels.
- All the PT-30 CE materials had microcracking as well as some blistering, particularly the nanoclay specimens, which had blistering near midplane and surface plies.
- Microstructure analyses of pre- and posttest NCCC specimens would provide a more fundamental understanding of material behavior. Additional research is ongoing.

7.2.4 Nanocomposites for carbon fiber-reinforced polymer matrix composites (NCPMCs)⁵⁵⁻⁵⁷

Carbon fiber-reinforced polymer matrix composites (CPMCs) are preferred high-performance and advanced composite systems that are used

in a multitude of applications encompassing aerospace and aircraft structures, advanced marine vessels, oil field drilling risers, fuel cell components, natural gas fuel tanks, sports equipment, satellites, and others. These CPMC materials are based on high-strength, high- T_g resin systems such as epoxies, BMI, cyanate esters, and polyimides. These resins are well-established material systems for high performance and advanced CPMCs that are currently qualified and specified in most of these critical applications. Yet there are occasions when further improvements in CPMCs are desired or mandated. Areas of improvement include higher temperature performance capability, mechanical performance, damage resistance, extreme environment corrosion resistance, and improved wet strength/dimensional control.

The use of nanocomposite concepts for improving CPMCs by incorporating nanoparticles within a matrix resin is the objective of this study. The nanomodified matrix resin is then combined with carbon fiber into the resulting nanocomposite CPMC. It is anticipated that the nanocomposite CPMC would exhibit many of desired improvements mentioned earlier.

Epoxy resins are one type of matrix resin used in many high-performance and advanced carbon fiber composites today. Epoxies are reasonably priced and possess an outstanding combination of characteristics. These characteristics include a wide choice of compositions, from low-viscosity liquids to solids, a variety of curing systems (amine or anhydride), latitude in processing conditions, low shrinkage, no volatiles emitted, good mechanical properties, good chemical resistance, good adhesion to fiber reinforcement, thermal stability over a wide temperature range, and good resistance to moisture. The versatility and ease of epoxy processing in all composite fabrication methods, such as prepreg/tape placement, pultrusion, filament winding, SMC, RTM, and hand lay-up, is also an attractive feature. Limited ductility and reduced hot and wet strength performance are areas requiring improvement and may be enhanced by the development of the nanocomposite phase within the CPMC. Within the family of epoxy resins, there are general-purpose, intermediate T_g ($< 150^\circ\text{C}$) epoxies and high-performance, high T_g ($> 200^\circ\text{C}$) epoxy resins. Of particular importance are high-performance epoxy resins that are well established in many aerospace and aircraft CPMC components. Thus the nanophase modification of these epoxy resins contained within the CPMC would generate the desirable improvements.

The presence of *nanophase* in many polymeric systems, either thermoplastic or thermoset, leads to improved mechanical properties and performance characteristics, as demonstrated by Vaia,⁷⁵ Giannelis,⁷⁶ Koo,⁷ Lichtenhan,⁷⁷ Lake,⁷⁸ and Gilman.⁷⁹ Many different types of nanoparticles have been introduced into epoxy resins, resulting

in enhanced mechanical properties of the cured epoxy resin systems, as demonstrated by Barron,⁸⁰ Zilg,⁸¹ Tie Lan,⁸² Seferis,⁸³ Bakis,⁸⁴ Curliss,⁸⁵⁻⁸⁷ Becker,^{88,89} Lee,⁹⁰ and Pittman.⁹¹ (See Sec. 6.3.1)

In virtually all nanomodified epoxy resin systems, enhanced mechanical properties are observed. Yet these results using nanoparticles for increased thermal resistance or increased T_g are variable. Tie Lan⁸² reported higher T_g values in anhydride-cured epoxy when both epoxy components (epoxy resin and anhydride) were intercalated with nanoclay prior to cure. Zilg⁸¹ and Becker^{88,89} intercalated only the epoxy resin with nanoclay and not the amine hardener. Recent studies by Vaia and coworkers⁹² indicate that there are subtle considerations in using surface-treated clay with each epoxy component, i.e., epoxy resin with clay and amine hardener with clay (Chap. 6). These considerations include viscosity increases within each component, and then combining these nanoclay-modified components for reaction and crosslinking into the cured epoxy. A facile intergallery transfer of epoxy and amine must occur to facilitate cure and obtain the desired nanophase within the cured epoxy. Pinnavaia and coworkers^{93,94} have remedied the intercalation and exfoliation of amine hardener by employing a concomitant use of the amine as the clay surface modifier and epoxy curing agent.

However, the use of the nanomodified epoxy resin systems as matrix resin systems for fiber-reinforced composite materials has been a challenge. The introduction of nanoparticles into the epoxy resin system is sensitive to the amount of nanoparticles that is introduced into the epoxy. Resin viscosity increases exponentially as weight percent of nanoparticles is increased from 1 percent to 5 to 7 percent. With a manageable resin viscosity when 1 percent nanoparticles is added, little or no benefit in mechanical properties occurs. Mechanical properties enhancement usually occurs when nanoparticle loadings are 5 to 7 percent, resulting in excessive resin viscosity behavior and erratic, nonuniform fiber *wet-out* during impregnation of fibers or fabric in the fabrication of the fiber-reinforced composite.

The major objective of this material program is to develop an improved epoxy nanocomposite carbon fiber-reinforced polymer matrix composite with enhanced mechanical properties. We proposed that a nanophase be introduced into the epoxy resin system, prior to cure, to provide improved and maintained mechanical strength of the composites. In this study, the following components: (a) CYCOM[®] 977-3 epoxy system from Cytec Engineered Materials; and (b) three types of nanoparticles: chemically modified montmorillonite (MMT) organoclays, nanosilica, and carbon nanofibers (CNF) were used to create new types of NCPMCs.

The minor objectives of this investigation were to: (a) develop *processes* to disperse these nanoparticles uniformly in the epoxy resin

prior to curing, (b) use wide-angle x-ray diffraction (WAXD), transmission electron microscopy (TEM), and scanning electron microscopy (SEM) to characterize polymer nanocomposite *morphological behavior* after curing, (c) study the *structure-property* relationship of these types of new materials, (d) study the *rheology* of the polymer nanocomposites, and (e) evaluate the *performance* (mechanical properties) of these carbon fiber-reinforced composites.

Five resin/nanoparticle material systems were selected to produce carbon fiber-reinforced prepregs at Cytec Engineered Materials (CEM). The prepregs were produced using AS4-6K woven cloth [in a 5-harness satin weave with a nominal (warp) \times 11 (fill) construction with areal weight of 356 to 384 g/m²]. Polymer matrix composites were fabricated for the five candidates and the baseline 977-3/AS4-6K materials. Mechanical properties such as G_{1C} , G_{2C} , FWT, SBS, and flexural strength were determined on these nanomaterials and were compared with the baseline 977-3 material.

Selection of materials

Resin systems. CYCOM 977-3 toughened epoxy resin was selected for this study, because this is an industry standard.⁹⁵ CYCOM 977-3 is a 350°F (177°C) curing toughened epoxy resin with a 350°F (177°C) dry and 270°F (132°C) wet service capability. CYCOM 977-3 is formulated for autoclave or press-molding and can be cured at 350°F (177°C) for six hours. Typical applications for CYCOM 977-3 include aircraft primary and secondary structures or any application where impact resistance and excellent hot and wet performance are crucial. Typical cured neat resin properties of CYCOM 977-3 are shown in Table 7.15.⁹⁵

Polymer nanoparticles. Three types of nanoparticles were used in this study, namely montmorillonite nanoclays (MMT nanoclays) from Southern Clay Products, carbon nanofibers (CNF) from Applied Sciences, and Degussa's nanosilica materials.

Montmorillonite nanoclays. Exfoliation of montmorillonite (MMT) clays into polymer will increase mechanical properties, barrier performance, and application processing. The Cloisite 30B and Cloisite 10A used in this study are surface-modified MMT materials manufactured by SCP (see Chap. 2).

Carbon nanofibers (CNF). CNFs are a form of vapor-grown carbon fiber, which is a discontinuous graphitic filament produced in the gas phase from the pyrolysis of hydrocarbons. Several versions of Applied Sciences' PR-19-PS CNF were used in this study (see Chap. 2).

TABLE 7.15 Cured^a Neat Resin Properties of CYCOM 977-3

Property	RT	250°F(121°C)/Wet [†]
Compressive yield strength, ksi (MPa)	27.0 ± 0.3 (186 ± 2.1)	
Flexural strength [‡] , ksi (MPa)	21.0 ± 4.4 (144.7 ± 30.3)	10.14 ± 0.4 (69.9 ± 2.8)
Flexural modulus [‡] , Msi (GPa)	0.55 ± 0.01 (3.79 ± 0.07)	0.354 ± 0.3 (2.41 ± 2.1)
K _{1C} [§] , (MPa)·m ^{1/2}	0.90 ± 0.08	
G _{1C} [§] , (J/m ²)	217 ± 24	
RDS DMTA T _g , °C (tested at 5°C/min) G'		178,218
G''		189,226
Tan delta		190,240

^a Cured at 350°F (180°C) for 6 hours.

[†] Wet = 7-day water immersion at 160°F (71°C).

[‡] Flexural testing performed using a 3-point loading fixture and a 16:1 S/D ratio.

[§] K_{1C} and G_{1C} tested using 3-point bending mode.

Nanosilica. AEROSIL is highly dispersed, amorphous, very pure silica that is produced by high-temperature hydrolysis of silicon tetrachloride in an oxyhydrogen gas flame.⁹⁶ Two Degussa products were selected for this investigation. They are the hydrophobic AEROSIL R202 and AEROSIL R805 materials. AEROSIL R202 is fumed silica treated with a polydimethylsiloxane. AEROSIL R805 is fumed silica treated with an octylsilane based on AEROSIL 200 (see Chap. 2).

Discussion of results. Dispersibility of the nanoparticles into CYCOM 977-3 was determined by WAXD and TEM prior to full scale-up. Lab-scale dispersion of 977-3 resin system with different weight percent nanoclays, CNF, and nanosilica were conducted as shown in Table 7.16. The morphology of selective resin/nanoparticle systems was characterized using WAXD, TEM, and SEM analyses. Mixing procedures were designed to achieve full contact between the nanoparticles and the polymer matrix. There were two basic types of nanoparticles for this study, carbon nanofibers and particulate solids like the nanoclays and nanosilicas. In all cases, the mixing procedure must allow sufficient opportunity for the liquid resin to contact and fully wet out the surface of the nanoparticles. Mixing and curing procedures were developed for the preparation of the nanocomposites based on the mix/cure profile provided by CEM.

Fully cured (polymerized) samples were prepared for DMTA and TEM analyses. The TEM analyses were conducted on selective specimens. These TEM images facilitated the screening of various formulations for desirable nanolevel dispersion of the clay, CNF, or nanosilica within the cure resin/inorganic composites. Desirable features included

TABLE 7.16 Blending Matrix for 977-3/Nanoparticle Resin Systems

Candidate no.	Nanoparticle percentage in resin	Nanoparticle type
1	0%	None
2	1%	Cloisite 30B
3	2%	Cloisite 30B
4	5%	Cloisite 30B
5	1%	Cloisite 10A
6	2%	Cloisite 10A
7	5%	Cloisite 10A
8	1%	PR-19-PS amine treated CNF
9	2%	PR-19-PS amine treated CNF
10	1%	PR-19-PS CNF
11	2%	PR-19-PS CNF
12	5%	PR-19-PS CNF
13	1%	PR-19-PS-O _x CNF
14	2%	PR-19-PS-O _x CNF
15	5%	PR-19-PS-O _x CNF
16	1%	AEROSIL R202
17	2%	AEROSIL R202
18	5%	AEROSIL R202
19	1%	AEROSIL R805
20	2%	AEROSIL R805
21	5%	AEROSIL R805

higher levels of clay exfoliation and uniform dispersion of CNF or nanosilica within the resin both before and after curing.

Processing and characterization of 977-3/nanoclay systems. Weight percent (wt%) of 1 percent, 2 percent, and 5 percent of Cloisite 30B and 1 percent, 2 percent, and 5 percent of Cloisite 10A nanoclays were blended with the 977-3 resin system using the mixing procedures developed for this study.

Figure 7.92 shows a high magnification of 977-3/Cloisite 10A (scale bar is 50 nm), showing the nanoclay in an intercalated state in the 977-3 epoxy resin. Figure 7.93 shows a low magnification of 977-3/Cloisite 10A where the scale bar is 500 nm. Both surface-treated clays dispersed very well in the epoxy composition, as shown in TEM micrographs. In some cases, particularly in Cloisite 10A, a modest amount of cluster of clays is shown in Fig. 7.94, where the scale bar is 200 nm.

Figure 7.95 shows a comparison of the dynamic mechanical thermal analyses (DMTA) of 1 percent, 2 percent, and 5 percent Cloisite 10A. At a low loading of Cloisite 10A (1%), an increase in complex modulus and T_g were noted (Table 7.17).

Processing and characterization of 977-3/nanosilica systems. The 977-3 was blended with 1 percent, 2 percent, and 5 percent of AEROSIL R202 and

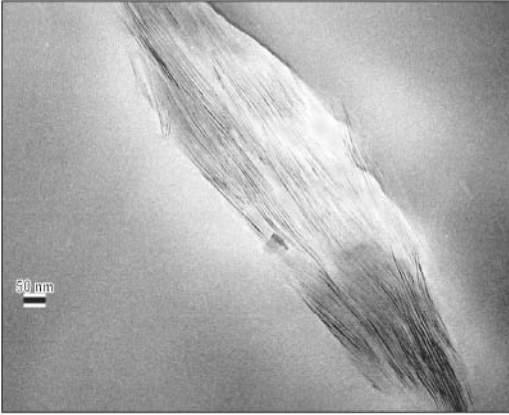


Figure 7.92 High-magnification TEM micrograph of 977-3/Cloisite 10A (2%) showing intercalated structure.

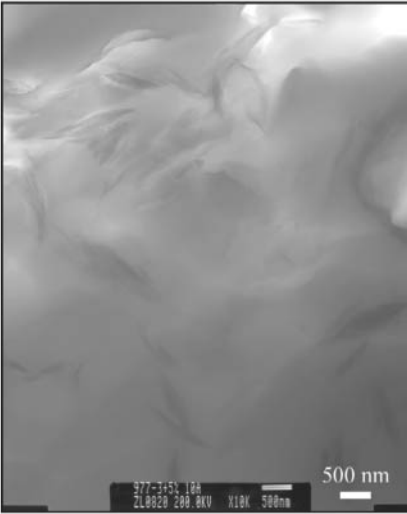


Figure 7.93 Low-magnification TEM micrographs of 977-3/Cloisite 10A (5%) showing uniform dispersion of nanoclay Cloisite 10A in 977-3 epoxy resin, where scale bar is 500 nm.

1 percent, 2 percent, and 5 percent of AEROSIL R805. Figure 7.96 shows the TEM micrographs of 977-3 epoxy with 2 percent of AEROSIL R202 nanosilicas. Dynamic mechanical thermal analysis data (Fig. 7.97) exhibited the highest T_g (258°C) and the highest complex modulus (964 MPa) for 2 percent AEROSIL R202. Figure 7.98 shows the TEM micrographs of 977-3 epoxy with 5% of AEROSIL R805. Dynamic mechanical thermal analysis data of 1 percent, 2 percent, and 5 percent AEROSIL R805 in 977-3 are shown in Fig. 7.99. The DMTA data (Table 7.17) for AEROSIL R805 indicated that a small increase in

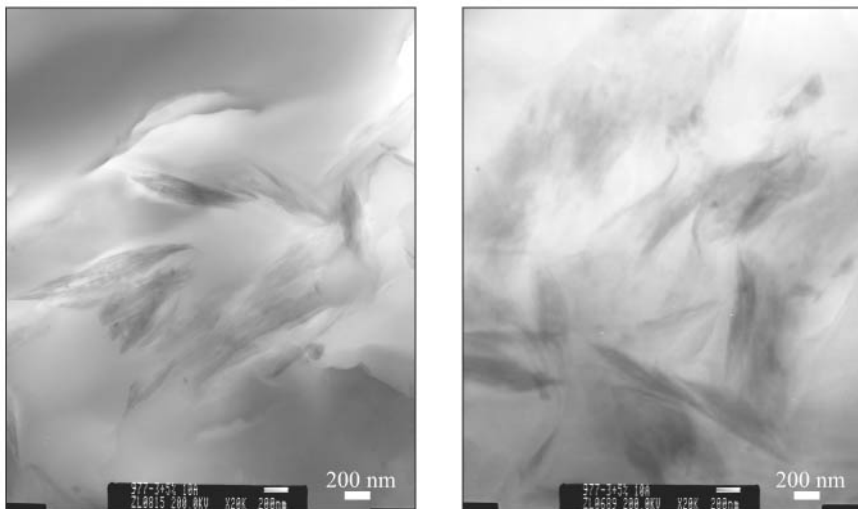


Figure 7.94 Transmission electron micrographs of 977-3/Cloisite 10A (5%) showing uniform dispersion of nanoclay Cloisite 10A in 977-3 epoxy resin, where scale bar is 200 nm.

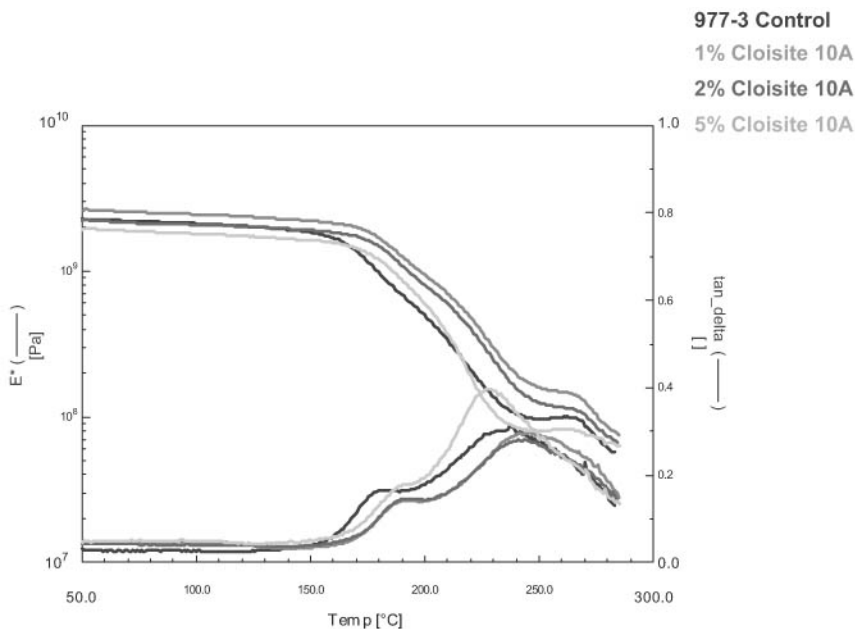


Figure 7.95 Dynamic mechanical thermal analyses of 1%, 2%, and 5% of Cloisite 10A in 977-3 epoxy resin.

T_g and complex modulus was observed, but this increase was not as dramatic as that of AEROSIL R202. It is possible that surface

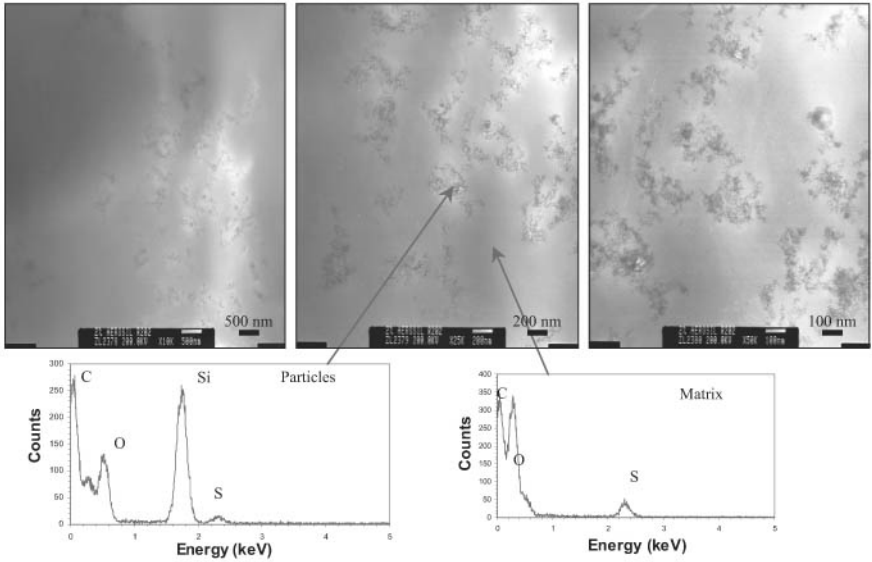


Figure 7.96 Transmission electron micrographs of 977-3/AEROSIL R202 (98/2) showing uniform dispersion of AEROSIL R202 aggregates in the 977-3 epoxy, where the scale bar is 500 nm (left), 200 nm (center), and 100 nm (right).

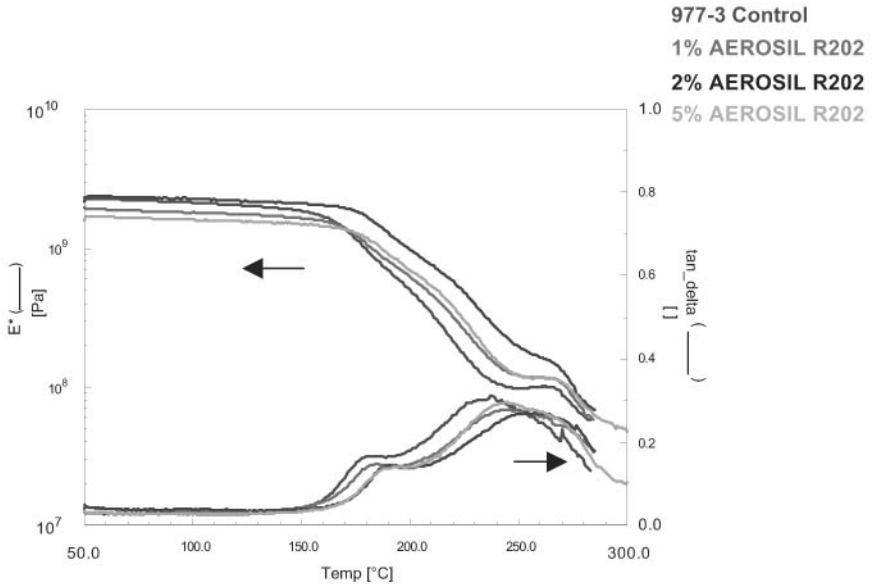


Figure 7.97 Dynamic mechanical thermal analyses of 1%, 2%, and 5% AEROSIL R202 in 977-3 epoxy resin.

treatment of the AEROSIL R805 by octylsilane resulted in more effective hydrophobic nanosilica and reduced interaction with the epoxy monomer.

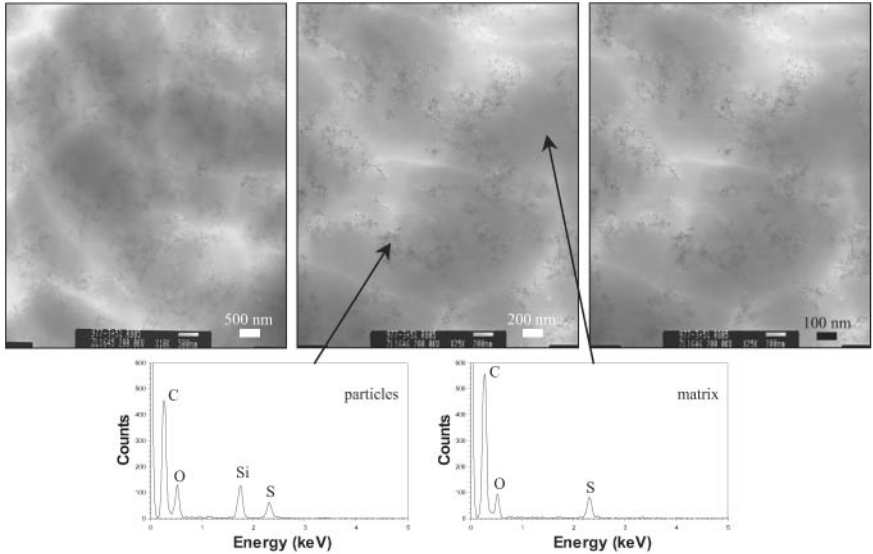


Figure 7.98 Transmission electron micrographs of 977-3/AEROSIL R805 (95/5) showing uniform dispersion of AEROSIL R805 aggregates in the 977-3 epoxy, where the scale bar is 500 nm (left), 200 nm (center), and 100 nm (right).

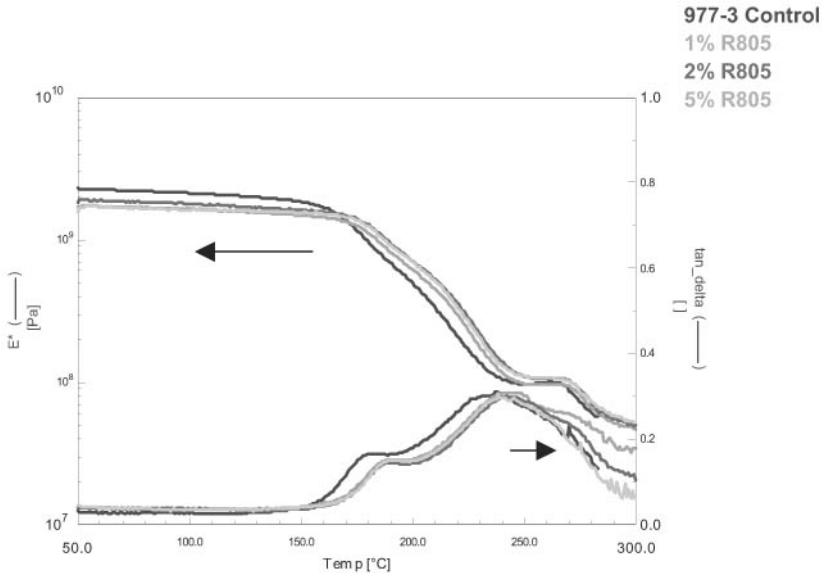


Figure 7.99 Dynamic mechanical thermal analyses of 1%, 2%, and 5% AEROSIL R805 in 977-3 epoxy resin.

Processing and characterization of 977-3/CNF nanoparticle. Figures 7.100 and 7.101 show the TEM micrograph of the 977-3/2% PR-19-PS-Ox CNF

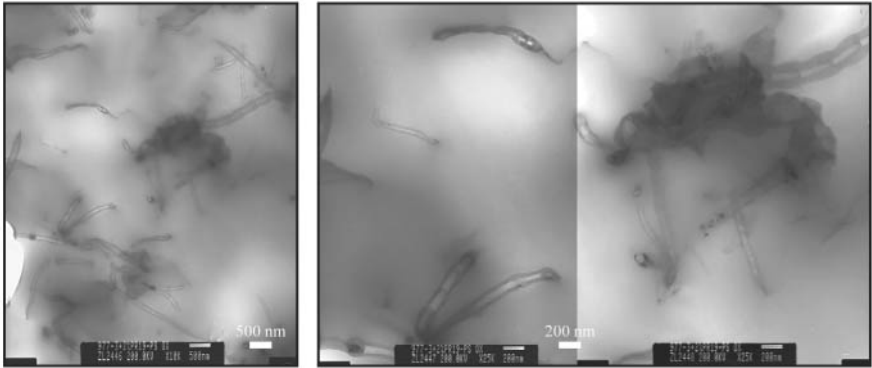


Figure 7.100 Transmission electron micrographs showing good dispersion of 2% PR-19-PS Ox CNF in the 977-3 resin.

and 977-3/5% PR-19-PS-Ox CNF. The DMTA analyses of the 977-3 1 percent, 2 percent, and 5 percent loadings of PR-19-PS-Ox CNF are shown in Fig.7.102 and Table 7.17. The T_g was barely increased with increased loading of PR-19-PS-Ox CNF (5%), yet the complex modulus doubled (961 MPa) with the 5% PR-19-PS-Ox CNF.

Table 7.17 summarizes the DMTA analyses for the neat epoxy nanocomposites as compared to the 977-3 control material. All the data are collected in three-point blending geometry with strain amplitude of 0.05 percent, frequency of 1 Hz, and heating rate of 5°C/min. Using 1 percent of Cloisite 10A nanoclay in the 977-3 resin system, a slight increase of 8°C in T_g and a substantial increase of complex modulus were detected. The Cloisite 30B nanoclay was not as effective as the

TABLE 7.17 Summary of DMTA Analyses of Epoxy Nanocomposites

Material	T_g from E' (°C)	T_g from E'' (°C)	T_g from $\tan\delta$ (°C)	E^* at 200°C (MPa)
977-3 Control	172	176	237	483
1% Cloisite 10A	183	186	245	923
2% Cloisite 10A	186	185	245	786
5% Cloisite 10A	183	185	228	572
5% Cloisite 30B	164	166	221	390
1% AEROSIL R202	178	178	242	609
2% AEROSIL R202	188	187	258	964
5% AEROSIL R202	186	184	245	702
1% AEROSIL R805	183	184	247	620
2% AEROSIL R805	182	186	243	711
5% AEROSIL R805	185	186	238	697
1% PR-19-PS-Ox	178	186	236	670
2% PR-19-PS-Ox	180	188	238	688
5% PR-19-PS-Ox	180	190	241	961

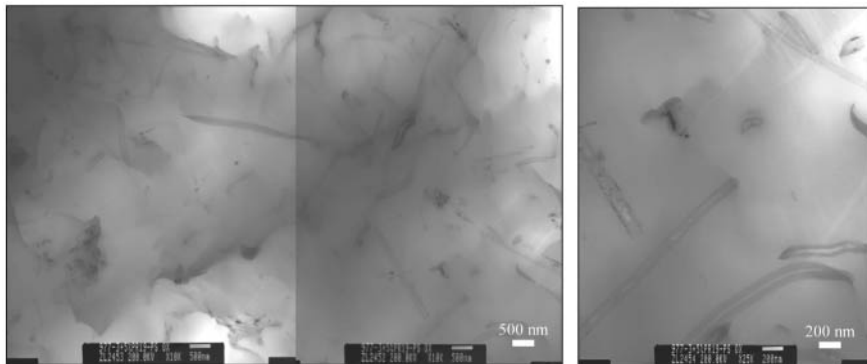


Figure 7.101 Transmission electron micrographs of 5% PR-19-PS CNF in 977-3 resin showing good dispersion of the CNFs in the resin.

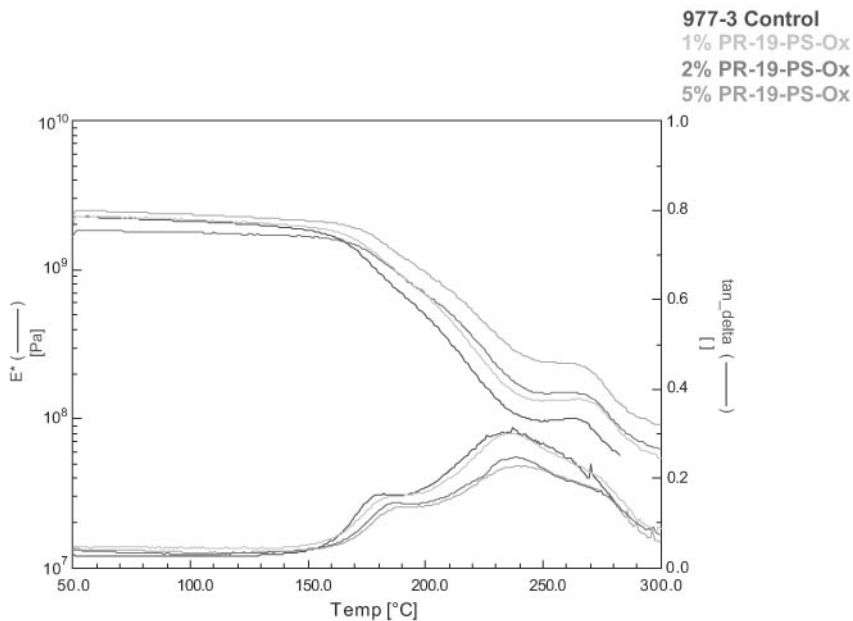


Figure 7.102 Dynamic mechanical thermal analyses of 1%, 2%, and 5% PR-19-PS-Ox in 977-3 epoxy resin.

Cloisite 10A nanoclay in the 977-3 resin system. Using 2 percent AEROSIL R202 nanosilica in the 977-3 resin system, a substantial increase of 21°C in T_g and a substantial increase of complex modulus were recorded. Using 1 percent of AEROSIL R805 nanosilica in the 977-3 resin system, a slight increase of 10°C in T_g and a small increase of complex modulus were also detected. In general, all samples

reinforced with nanosilica exhibit higher T_g . There was not much enhancement of T_g using PR-19-PS-Ox CNF in the 977-3 resin system.

Scaling up and processing of NCPMC. Based on the TEM and DMTA analyses, as well as literature data, five candidates and the control were selected for scaling up of 20 lbs of 977-3/nanoparticle resin systems to produce prepregs using AS4-6K carbon fiber fabric:

- Cloisite 10A nanoclay in 2 wt%
- AEROSIL R202 nanosilica in 2 wt%
- AEROSIL R805 nanosilica in 2 wt%
- PR-19-PS-Ox in CNF in 2 wt%
- AEROSIL R202 nanosilica in 3 wt%
- 977-3 in (100) wt% with no nanofillers

Mechanical properties of NCPMC. The following mechanical properties were obtained for each PMC material according to ASTM specifications and are summarized in Table 7.18 for the six materials:

- G_{1C}
- G_{2C}
- Flatwise tension strength (FWT)
- Short-beam interlaminar shear strength (SBS)
- Flexural strength

TABLE 7.18 Comparison of Mechanical Properties of the Six Materials

Material	G_{1C} (in-lb/in ²)	G_{2C} (in-lb/in ²)	FWT (psi)	Shear SBS (ksi)	Flexural strength (ksi)
977-3/2% Cloisite 10A PMC	1.10	6.02	5375	9.5	159
977-3/2% AEROSIL R202 PMC	1.69	11.26	5908	10.9	141
977-3/2% AEROSIL R805 PMC	1.93	12.02	5528	10.8	144
977-3/2% PR-19-PS-Ox CNF PMC	1.27	15.01	5932	12.7	142
977-3/3% AEROSIL R202 PMC	1.26	11.28	5631	13.7	155
977-3/AS4-6K baseline PMC	2.79	14.14	5823	11.7	150

Figures 7.103 to 7.107 show comparisons of G_{1C} , G_{2C} , FWT, SBS, and flexural strength of the five epoxy nanocomposite PMCs with the 977-3/AS4-6K baseline PMC, respectively. The short-beam shear values of all epoxy nanocomposites were slightly lower than the baseline with 3 percent AEROSIL R202 and 2 percent PR-19-PS-Ox CNF higher than the baseline. The flexural strength of all the epoxy nanocomposites was slightly lower than the baseline, with the 2 percent Cloisite 10A and 3 percent AEROSIL R202 materials higher than the baseline. Flatwise tension strength values of all the epoxy nanocomposites were slightly lower than the baseline, with 2 percent PR-19-PS-Ox and 2 percent AEROSIL R202 samples higher than the baseline material. The G_{1C} and G_{2C} values of all the epoxy nanocomposites were below the baseline, except for 2 percent AEROSIL R805 (G_{1C}) and 2 percent PR-19-PS-Ox (G_{2C}), which were higher than the baseline.

Summary and conclusions. The CEM 977-3 toughened epoxy resin system was modified by three types of nanoparticles (MMT nanoclay, CNF, and nanosilica) at several different weight percent loading levels (1%, 2%, and 5%) for this study. Transmission electron microscopy analysis was used to characterize the morphology of these resin systems and to screen candidates based on their degree of dispersion. Dynamic mechanical thermal analysis was also performed on selective neat epoxy nanocomposites. Based on the TEM and DMTA analyses, as well

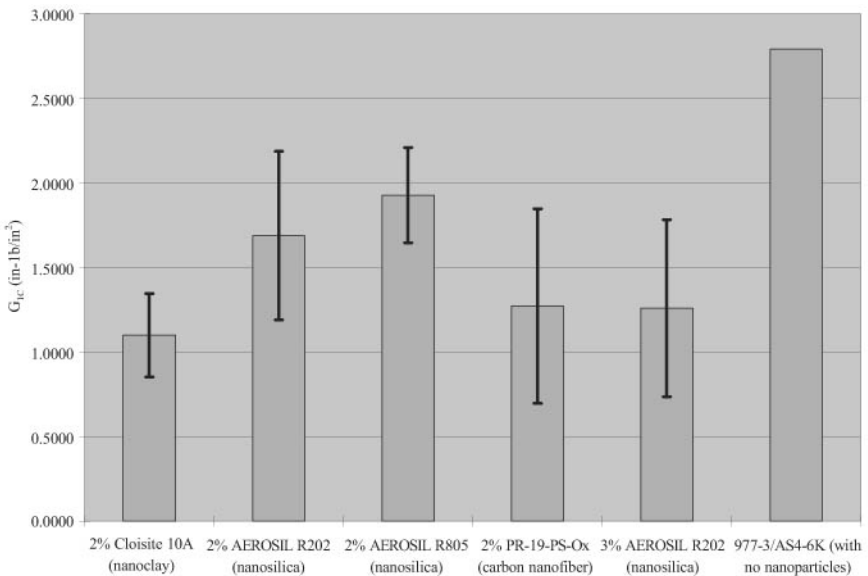


Figure 7.103 Comparison of G_{1C} values of the five nanomodified epoxy carbon fiber-reinforced PMCs with the 977-3/AS4-6K baseline composite.

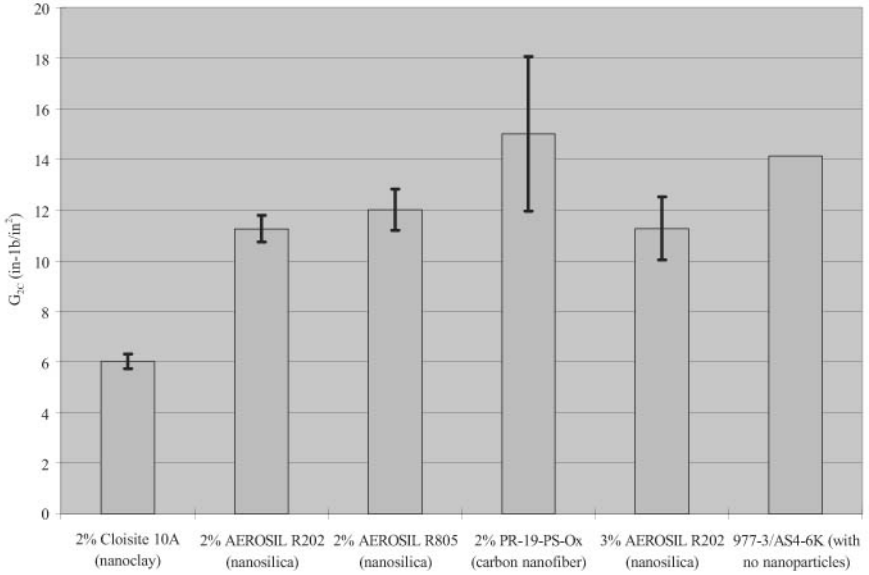


Figure 7.104 Comparison of G_{2C} values of the five nanomodified epoxy carbon fiber-reinforced PMCs with the 977-3/AS4-6K baseline composite.

as on literature data, six candidates were selected to produce AS4-6K carbon prepreps.

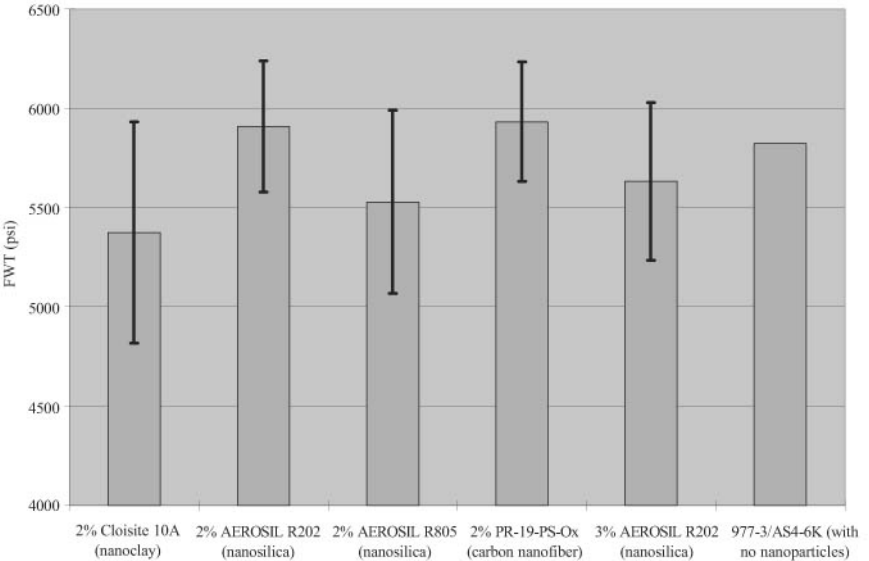


Figure 7.105 Comparison of FWT values of the five nanomodified epoxy carbon fiber-reinforced PMCs with the 977-3/AS4-6K baseline composite.

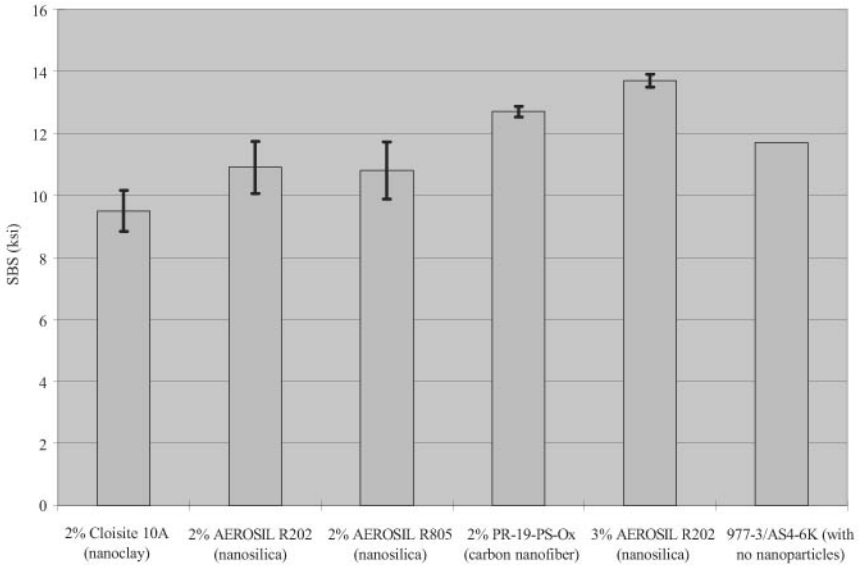


Figure 7.106 Comparison of SBS values of the five nanomodified epoxy carbon fiber-reinforced PMCs with the 977-3/AS4-6K baseline composite.

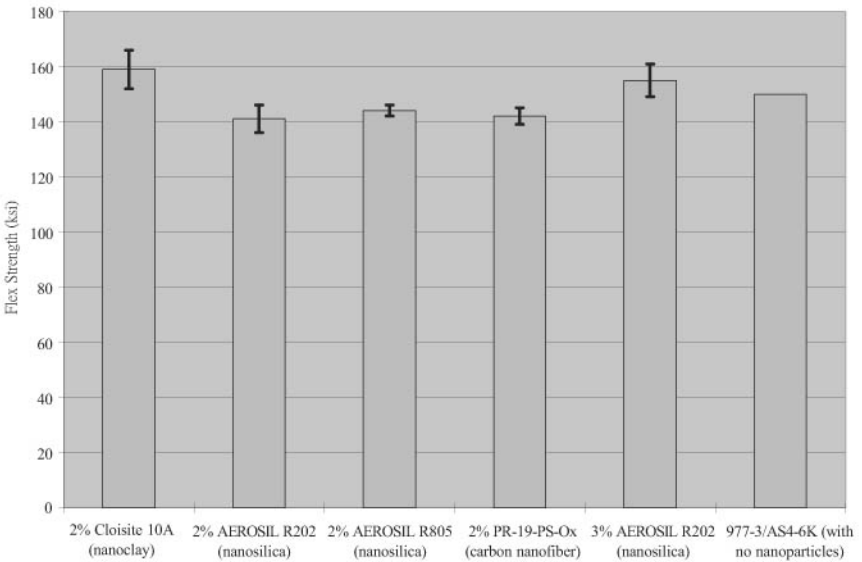


Figure 7.107 Comparison of flexural strength values of the five nanomodified epoxy carbon fiber-reinforced PMCs with the 977-3/AS4-6K baseline composite.

The following conclusions were drawn from this study:

- Dynamic mechanical thermal analysis data of the neat epoxy nanosilica nanocomposite (2% AEROSIL R202) show the highest T_g (258°C) and the highest complex modulus (964 MPa).
- Impressive values (T_g and complex modulus) of neat nanocomposite resin with 2% AEROSIL R202 did not carry over into the NCPMC.
- Transmission electron microscopy analysis has been demonstrated as an effective tool to characterize and screen candidates based on their degree of dispersion.
- Dynamic mechanical thermal analysis has also been demonstrated as an effective tool to characterize and screen candidates based on their mechanical properties.
- MMT clay, nanosilica, and CNF dispersed very well in the 977-3 resin system, forming epoxy nanocomposites.
- The G_{1C} values of all the epoxy nanocomposites were lower than the 977-3/AS4-K6 baseline material, with the least knockdown with the 2% AEROSIL R805 nanosilica sample. The G_{2C} values of all the epoxy nanocomposites were lower than the 977-3/AS4-K6 baseline material with the 2% PR-19-PS-Ox sample higher than the baseline material. The FWT values of all epoxy nanocomposites were slightly lower than the baseline, and 2% PR-19-PS-Ox and 2% AEROSIL R202 samples were higher than the baseline material. The SBS values of all epoxy nanocomposites were slightly lower than the baseline, and 3% AEROSIL R202 and 2% PR-19-PS-Ox CNF were higher than the baseline material. The flexural strength of all epoxy nanocomposites was slightly lower than the baseline, and the values for 2% Cloisite 10A and 3% AEROSIL R202 samples were higher than the baseline.

7.3 Thermoplastic Elastomer Nanocomposites

Three application examples are selected for this section: (a) elastomer nanocomposites for propulsion systems, (b) thermoplastic elastomer nanocomposites for propulsion systems, and (c) flame-retardant thermoplastic polyurethane nanocomposites. These examples are used to illustrate the processing and characterization techniques to form the resulting polymer nanocomposites. Flammability, thermal, and mechanical properties, and performance characteristics for their specific applications are included.

7.3.1 Elastomer nanocomposites for propulsion systems⁹⁷⁻⁹⁹

Polymer nanostructured ablatives have been prepared by blending an elastomer polymer system with carbon nanofibers. Thermal gravimetric analyses (TGA) and SEM analyses were used to characterize these materials in a laboratory and a scaled solid rocket motor heating environment. Kevlar[®]-filled, ethylene-propylene-diene rubber (EPDM) is used as motor insulation in solid rocket propulsion systems.¹⁰⁰ EPDM blends consisting of Kevlar fibers and carbon nanofibers are also included in this study. Results of various TGA tests at different heating rates and SEM analyses of virgin and charred samples will be shown.

Materials. Ethylene-propylene-diene rubber (EPDM) filled with silica or Kevlar has been used in propulsion systems for both thermal and ablation protection. Carbon nanofibers were blended with Kelvar-filled EPDM.

Thermal gravimetric analysis (TGA). The TGA data compiled in these studies were collected using a TA Instruments Model TGA 2050. Sample sizes of 15 to 20 mg of EPDM/CNF were used. The TGA samples were taken from the centers of the bulk samples for dispersion uniformity. Only one large piece was used, instead of grinding the material into a fine powder. All of the tests were conducted under an air environment, opposed to nitrogen, in order to best simulate the conditions inside solid rocket motors. A platinum pan was used to load the samples into the furnace. The instrument was tared before the blend was placed in the pan. The tare was executed inside of the furnace where the air is motionless. The TGA has a heating rate range of 0 to 200°C/min in 10°C/min increments. The maximum temperature that the furnace could achieve was 1000°C. The TGA was equilibrated at 30°C before ramping to 1000°C at the specified heating rate.

Discussion of results

TGA tests on EPDM/nanoparticles systems. Mathias and Johnson¹⁰¹ reported some high heating rate (100,000°C/min) material property data of carbon cloth phenolic used in space shuttle reusable solid rocket motor nozzles. This study prompted the examination of TGA and solid rocket motor insulation samples using SEM.⁹⁷⁻⁹⁹ Two types of materials were included in this study, Kevlar-filled EPDM (11% Kevlar) and Kevlar-filled EPDM blended with 15 wt% CNF. A low heating rate of 5°C/min, a high heating rate of 50°C/min from TGA tests, and a calculated heating rate of 150,000°C/min from AFRL's four-inch char motor were included. Figure 7.108 shows the TGA of the two samples at

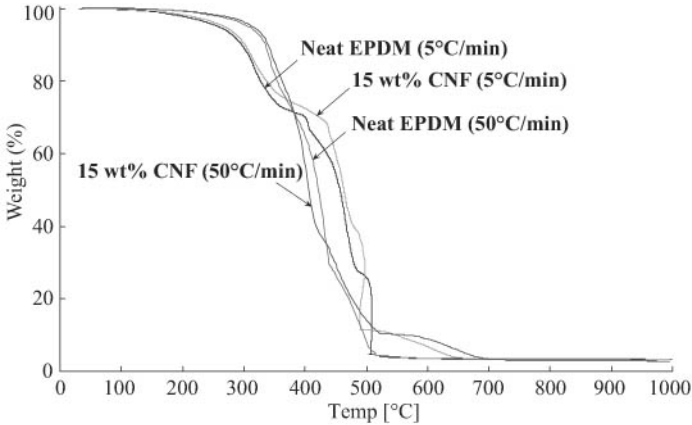
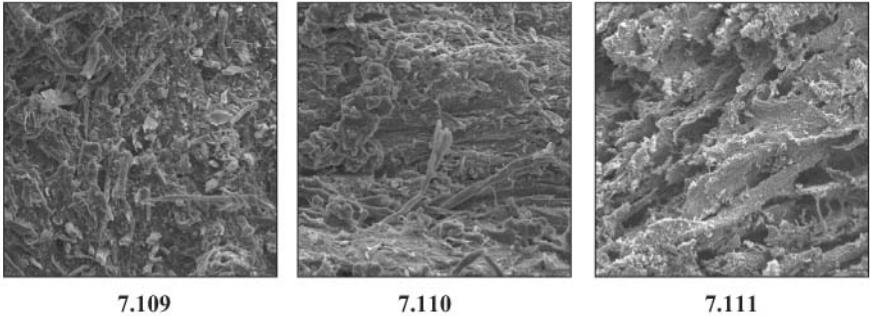


Figure 7.108 Mass loss of EPDM and EPDM/CNF nanocomposites at 5 and 50°C/min.

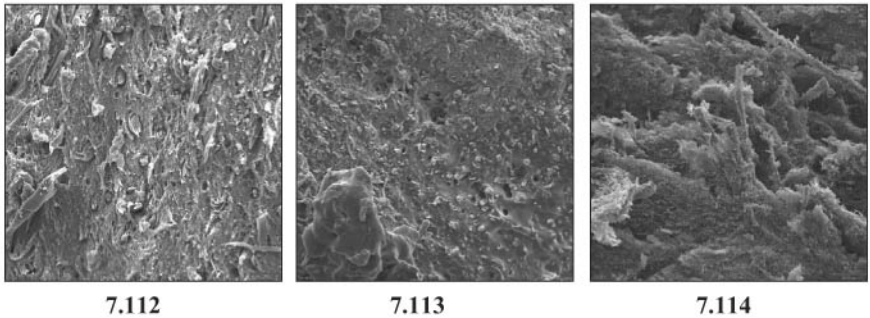
5°C/min and at 50°C/min. The EPDM-Kevlar-15 wt% CNF samples had less mass loss than the EPDM-Kevlar sample at both heating rates (5 and 50°C/min). The behavior of EPDM-Kevlar and EPDM-Kevlar-CNF exhibited a strong dependence on heating rate.

SEM analyses. Scanning electron microscopy (SEM) images were obtained to study the surface as well as the cross-sectional behavior of the nanostructured materials under thermal attack. Figures 7.109 to 7.111 show the samples at heating rates of 5°C/min (TGA), 50°C/min (TGA), and 150,000°C/min (four-inch char motor), respectively. At 5°C/min there was no EPDM charring observed in Fig. 7.109, and the Kevlar fibers were visible. Slight charring of the EPDM and Kevlar fibers was again quite visible in Fig. 7.110. In Fig. 7.111, severe EPDM charring was very visible in the rocket-motor-fired samples. The SEMs show substantial difference in material behavior under these three heating conditions. Figures 7.112 to 7.114 show the material behavior of the three samples at different heating rates of the EPDM-Kevlar-CNF samples. No EPDM charring was observed in Fig. 7.112. Melting of EPDM was visible in Fig. 7.113 when the sample was exposed to 50°C/min. In Fig. 7.114, very severe EPDM charring was noticeable in the rocket-motor-fired sample. Kevlar and CNF fibers were quite visible on the sample surface.

Conclusions. Thermal gravimetric analysis may not be a suitable method to study polymer nanostructured ablatives because of the extremely high heating rate that occurs inside the solid rocket motor combustion chamber. The SEM images also confirmed that the polymer nanostructured ablatives behave very differently for TGA and scaled rocket motor samples.



Figures 7.109 to 7.111 Scanning electron microscopy images of EPDM-Kevlar in Fig. 7.109 (5°C/min), Fig. 7.110 (50°C/min), and Fig. 7.111 (150,000°C/min), where the unit bar is 40 μm .



Figures 7.112 to 7.114 Scanning electron microscopy images of EPDM-Kevlar with carbon nanofiber in Fig. 7.112 (5°C/min), Fig. 7.113 (50°C/min), and Fig. 7.114 (150,000°C/min), where the unit bar is 40 μm .

7.3.2 Thermoplastic elastomer nanocomposites for propulsion systems^{7,97-99}

Polymer chopped-fiber-filled systems are used as insulative materials in rocket propulsion systems. This research program was aimed at developing new classes of polymer nanostructured materials that are lighter and have better erosion and insulation characteristics than current insulative materials (e.g., Kevlar-filled EPDM rubber).

Materials. The TPSiV™ X1180 thermoplastic elastomer (TPE) is a polyamide-based, vulcanized silicone thermoplastic resin manufactured by Dow Corning that was selected as a potential replacement material. Its typical uses include profiles for automotive, fuel and vapor line covers, brake hose covers, and industrial applications involving extruded profiles exposed to harsh environments. Table 7.19 shows the chemical compositions of three thermoplastic elastomer/nanoparticle blends that were produced by twin-screw extrusion.

TABLE 7.19 Thermoplastic Elastomer/Nanoparticle Blends

Material	TPE (wt%)	Nanoparticle (wt%)
1	TPSiV X1180 (90%)	Ph ₁₂ T ₁₂ -POSS (10%)
2	TPSiV X1180 (92.5%)	Cloisite 30B (7.5%)
3	TPSiV X1180 (85%)	PR-24-PS CNF (15%)

Characterization. Transmission electron microscopy analyses were conducted on the above three blends. Figure 7.115 shows the TEM images of the Dow Corning polyamide silicone TPSiV X1180 in two separate phases; the dark color is the silicone phase, and the light color is the polyamide phase. Figure 7.116 shows the TEM images of the 7.5 wt% Cloisite 30B/92.5 wt% TPSiV X1180 blend. We speculate that the Cloisite 30B nanoclays are dispersed only in the polyamide phase, because the silicone phase is already cross-linked. Transmission electron microscopy images of the 15 wt% PR-24-PS CNF/85 wt% TPSiV X1180 blend (Fig. 7.117) and 10% Ph₁₂T₁₂-POSS/90 wt% TPSiV X1180 blend (Fig. 7.118) showed similar results. It was determined that the TPSiV X1180 TPE is difficult to process with any of the three selected nanoparticles. None was compatible with the resin system.

Performance. The above three blends with the baseline Kevlar-filled EPDM rubber were tested for ablation resistance using a subscale solid rocket motor. Figure 7.119 shows the ablation rate of the materials at low, medium, and high Mach number regions inside the rocket motor. All three TPEs were out-performed by the baseline material. These observations clearly demonstrated that if the nanoparticles are poorly dispersed in the polymer matrix, no thermal performance improvement can be expected.

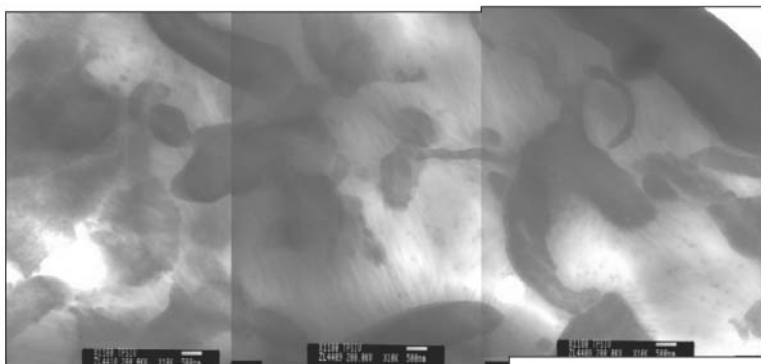


Figure 7.115 Transmission electron micrographs of polyamide silicone TPSiV X1180 (scale bar 500 nm).

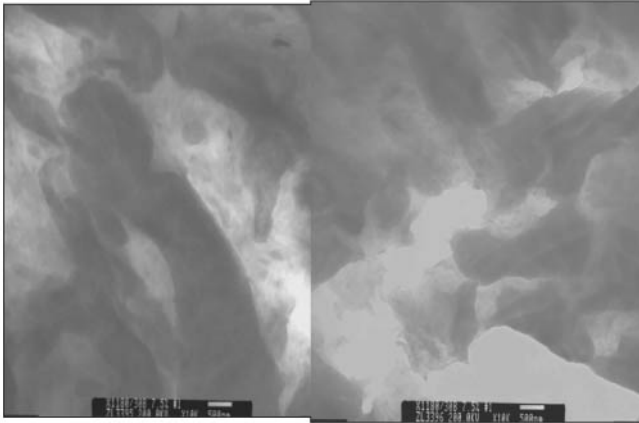


Figure 7.116 Transmission electron micrographs of 92.5% polyamide silicone TPSiV X1180 with 7.5% Cloisite 30B (scale bar 500 nm).

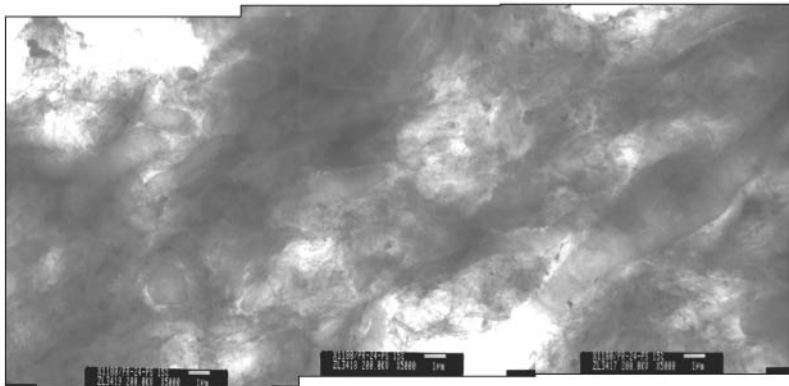


Figure 7.117 Transmission electron micrographs of 85% polyamide silicone TPSiV X1180 with 15% PR-24-PS CNF (scale bar 1 μm).

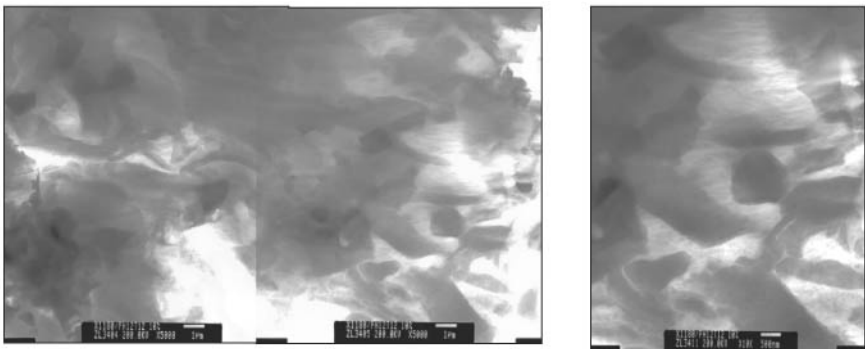


Figure 7.118 Transmission electron micrographs of 90% polyamide silicone TPSiV X1180 with 10% Ph₁₂T₁₂-POSS [scale bars are 1 μm (left) and 500 nm (right)].

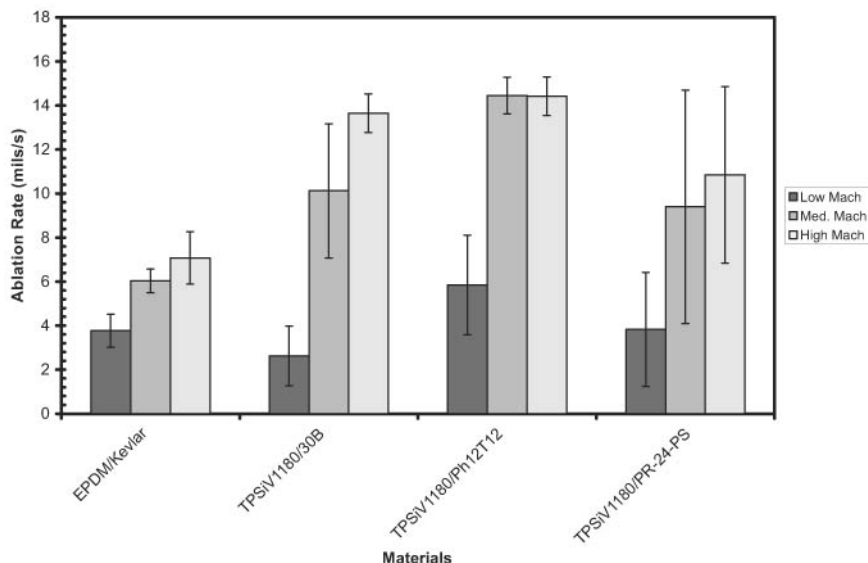


Figure 7.119 Ablation rate of polyamide silicone TPSiV X1180 with Cloisite 30B, Ph₁₂T₁₂-POSS, and PR-24-PS CNF as compared to EPDM/Kevlar in low, medium, and high Mach number regions inside the rocket motor.

7.3.3 Flame-retardant thermoplastic polyurethane nanocomposites¹⁰²

The introduction of inorganic nanomaterials as additives into polymer systems has resulted in polymer nanostructured materials exhibiting multifunctional, high-performance polymer characteristics beyond what traditional polymer composites possess. Selective thermoplastic elastomers have been used with montmorillonite organoclays, POSS, and carbon nanofibers to develop flame-retardant materials.¹⁰² Thermophysical and flammability properties of these polymer nanocomposites were determined.

Materials

Thermoplastic elastomers. PELLETHANE™ 2102-90A thermoplastic polyurethane elastomer (TPU) is a polyester polycaprolactone elastomer manufactured by Dow Chemical. Its typical applications include seals, gaskets, and belting, among others.

Montmorillonite nanoclays. Cloisite 30B is a surface-treated montmorillonite [tallow bishydroxyethyl methyl, T(EOH)2M] manufactured by Southern Clay Products (see Chap. 2).

Carbon nanofibers (CNFs). Carbon nanofibers, manufactured by Applied Sciences, are a form of vapor-grown carbon fibers, which are

discontinuous graphitic filaments produced in the gas phase from the pyrolysis of hydrocarbons. PR-19-PS CNF and PR-24-PS CNF were used (see Chap. 2).

Polyhedral oligomeric silsesquioxane (POSS). Representing a merger between chemical and filler technologies, POSS nanostructured materials can be used as multifunctional polymer additives, acting simultaneously as molecular-level reinforcements, processing aids, and flame retardants. SO1458 Trisilanolphenyl-POSS ($C_{42}H_{38}O_{12}Si_7$), manufactured by Hybrid Plastics, was used (see Chap. 2).

Processing and characterization. A 30-mm Werner Pfleider corotating, twin-screw extruder was used and can be configured for a wide variety of materials for polymer melt blending. The extruder length/diameter (L/D) ratio can be varied from 21 to 48, with options of multiple feeds and vents. The energy profile of the screw is optimized to meet the needs of the target products. Long residence time screw designs are available for reactive products. Several varieties of feeders are available to accommodate the material handling characteristics of the raw materials. Strand pelletization with low-temperature fluids allows the processing of very soft or rubbery materials. Approximately 5 lbs of each formulation were produced. Specimens were injection-molded in various configurations for measuring mechanical, flammability, and thermophysical properties. Table 7.20 shows the different TPU formulations made for this study.

Transmission electron microscopy analyses were conducted on all seven blends to examine the degree of dispersion of each type of nanoparticle in 2102-90A TPU. PR-24-PS CNFs and PR-19-PS CNFs dispersed very well in 2102-90A TPU, forming TPU nanocomposites (TPUNs), as shown in Figs. 7.120 to 7.123. In addition to TEM, the Cloisite 30B modified materials were analyzed using WAXD, as shown in Figs. 7.124 (a) to (d). No peaks were observed in all four specimens, an indication of exfoliated Cloisite 30B in 2102-90ATPU. TEM micrographs showed that the Cloisite 30B dispersed very well in 2102-90A TPU, forming intercalated/exfoliated TPUNs, as shown in Fig. 7.125.

TABLE 7.20 Material Matrix for Thermoplastic Elastomer Nanocomposites

Experiments	PELLETHANE TPU	Nanoparticles
1	2102-90A (100%)	None
2	2102-90A (95%)	5% Cloisite 30B
3	2102-90A (95%)	5% Trisilanolphenyl-POSS
4	2102-90A (95%)	5% PR-19-PS CNF
5	2102-90A (95%)	5% PR-24-PS CNF
6	2102-90A (85%)	15% PR-19-PS CNF
7	2102-90A (85%)	15% PR-24-PS CNF

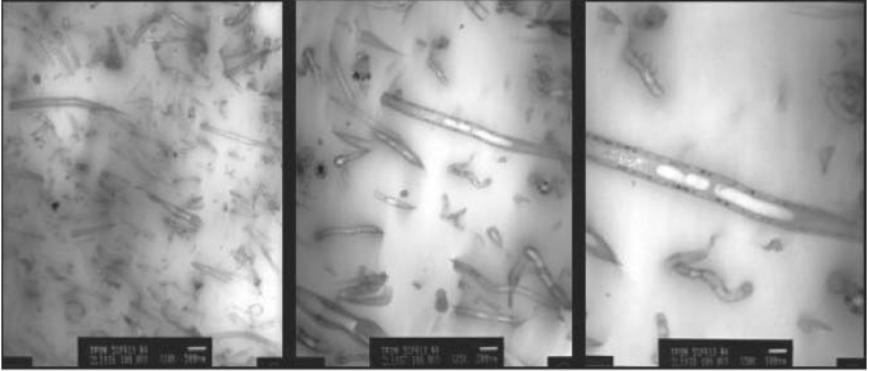


Figure 7.120 Transmission electron micrographs of TPUN: 5 wt% PR-19-PS CNF/ 95 wt% 2102-90A TPU.

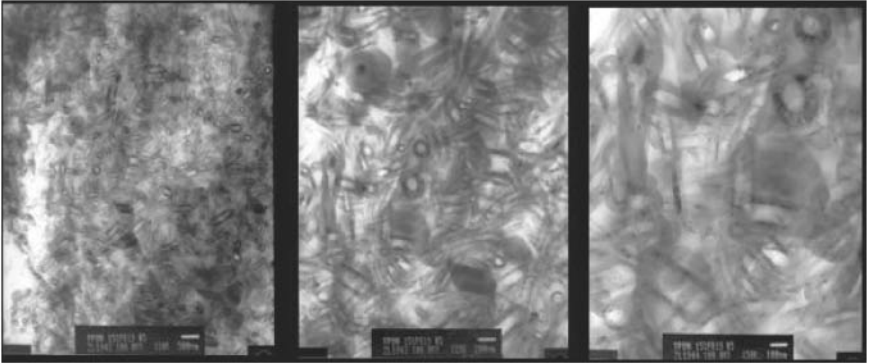


Figure 7.121 Transmission electron micrographs of TPUN: 15 wt% PR-19-PS CNF/ 85 wt% 2101-90A TPU.

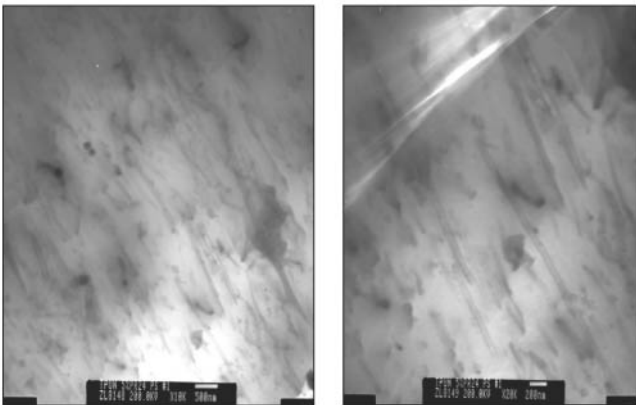


Figure 7.122 Transmission electron micrographs of TPUN: 5 wt% PR-24-PS CNF/95 wt% 2101-90A TPU.

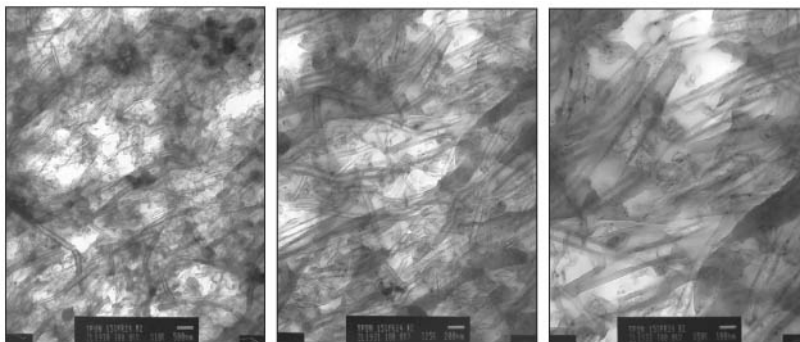
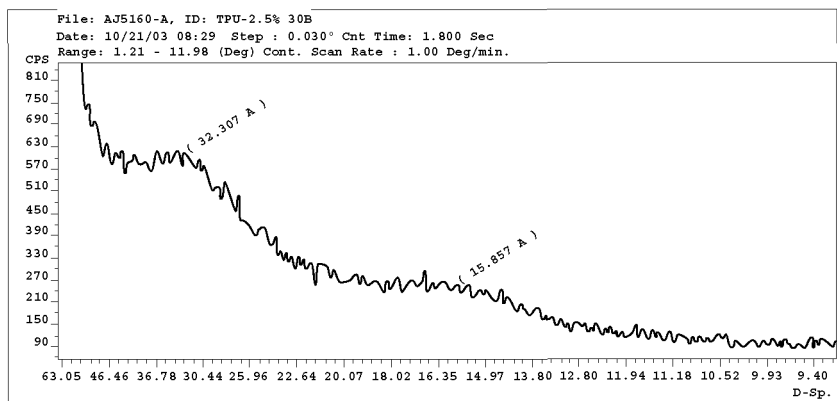
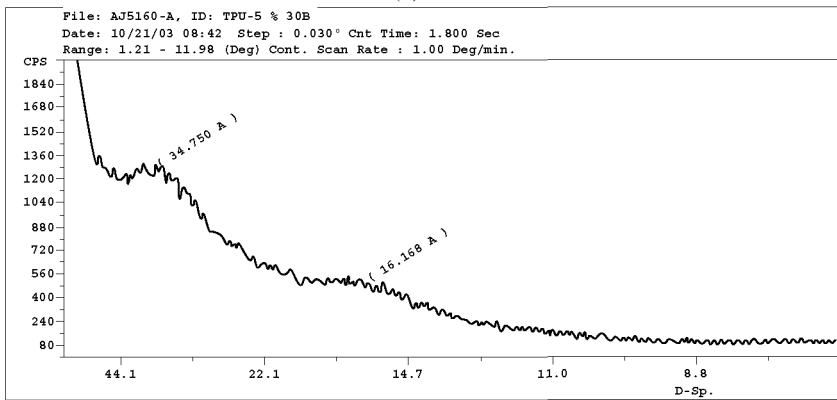


Figure 7.123 Transmission electron micrographs of TPUN: 15 wt% PR-24-PS CNF/85 wt% 2101-90A TPU.

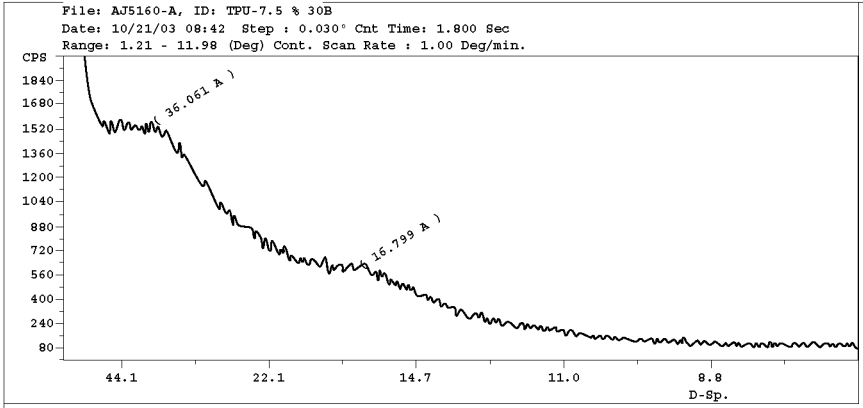


(a)

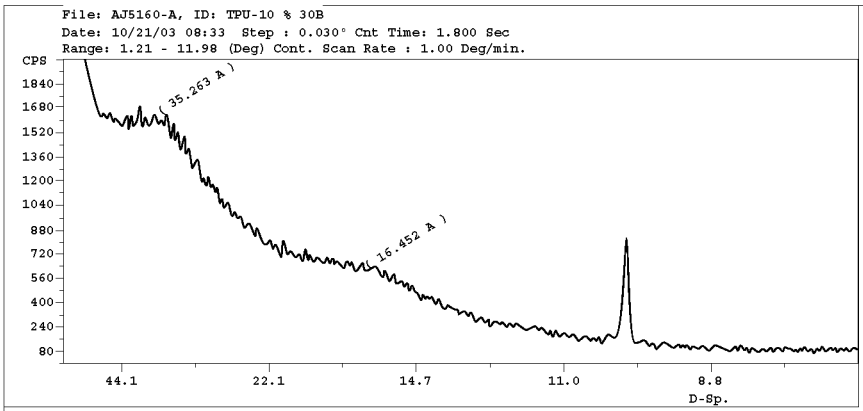


(b)

Figure 7.124 Wide-angle x-ray diffraction of (a) 2.5%, (b) 5%, (c) 7.5%, and (d) 10% Cloisite 30B in 2102-90A TPU.



(c)



(d)

Figure 7.124 Continued.

Thermophysical properties. Coefficient of thermal expansion (CTE), heat capacity, and thermal conductivity properties were measured. Figure 7.126 shows the correlations of CTE of CNF and nanoclay TPUNs with respect to their weight percent. PR-19-PS CNF TPUNs have lower CTE than PR-24-PS CNF and Cloisite 30B TPUNs. It was shown that nanoparticles (nanoclay and CNFs) increase the CTEs of the TPU. The heat capacity of all TPUNs was measured at 45° and 50°C, and the differences were insignificant (Fig. 7.127). The heat capacity of the 5 wt% PR-24-PS CNF TPUN is the highest among all TPUNs, as shown in Fig. 7.127. Heat capacity of all TPUNs was higher than the TPU (without nanofillers). When 15 wt% CNFs were added to the TPU, no increase in heat capacity was noted. This phenomenon needs to be further studied. Thermal conductivities of the 5 wt% and 15 wt% of all

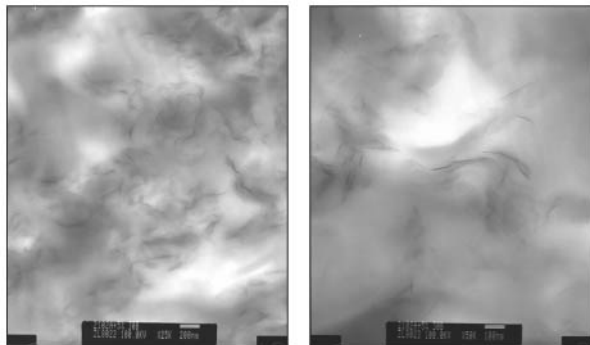


Figure 7.125 Transmission electron micrographs of TPUN: 5 wt% Cloisite 30B/95 wt% 2102-90A TPU.

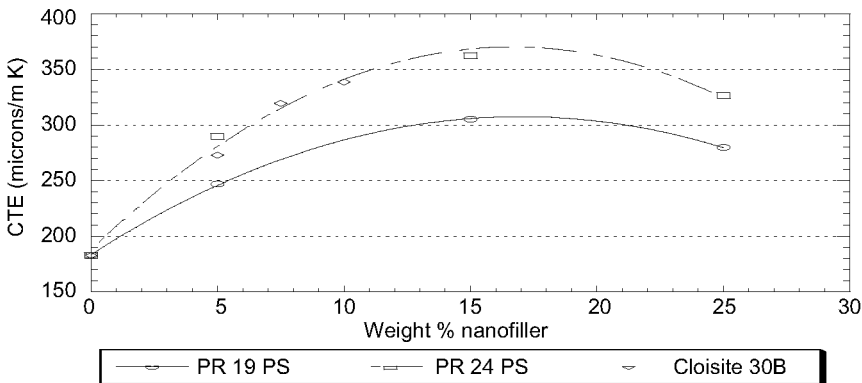


Figure 7.126 Correlations of CTE of CNF and nanoclay TPUNs.

TPUNs were compared with the baseline TPU (Fig. 7.128). The tests were conducted at 45° and 50°C. The 5% PR-24-PS CNF TPUN has the highest thermal conductivity.

Flammability properties. TPU and TPUNs were tested via cone calorimeter at an irradiance heat flux of 50 kW/m². Table 7.21 shows the flammability properties of the polymer nanocomposites. Reductions of peak heat release rate (PHRR) of 73 percent and 71 percent were recorded by the 5% PR-19-PS CNF TPUN and 5% Cloisite 30B TPUN, respectively. This is a significant improvement of the flammability property. The PHRRs for all TPUNs were less than that of the TPU. Figure 7.129 shows the HRR of TPUNs and TPUs. Posttest specimens are shown in Fig. 7.130. Both Cloisite 30B and PR-19-PS CNF TPUNs have residual chars, whereas TPU has no char formation at the end of the burn.

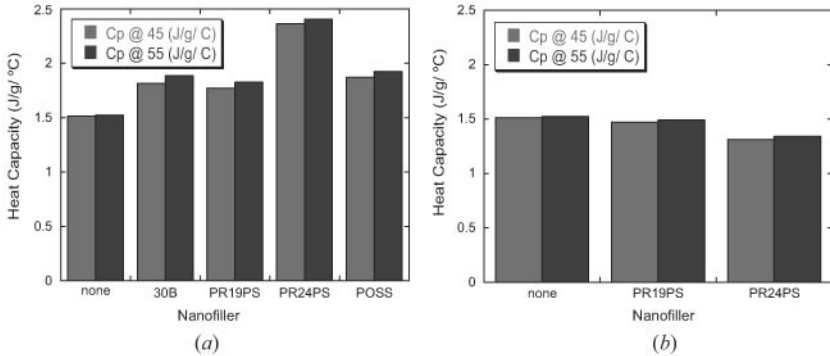


Figure 7.127 Heat capacity of TPUNs at 45° and 55°C with 5 wt% (left) and 15 wt% (right) of nanoparticles.

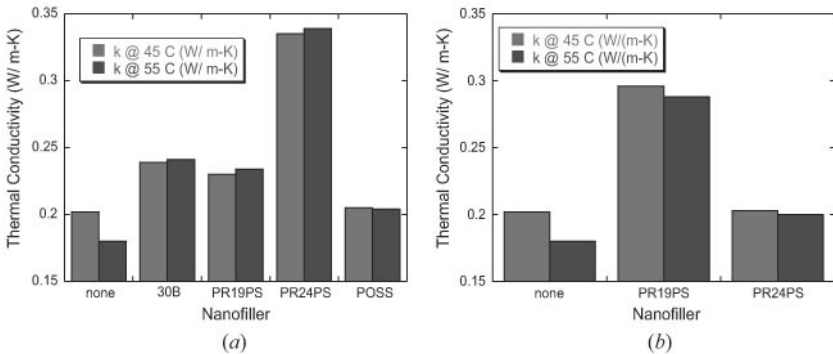


Figure 7.128 Thermal conductivity of TPUNs at 45° and 55°C with 5 wt% (left) and 15 wt% (right) nanoparticles.

Summary and conclusions

- Blending of 5 wt% of nanoclay, CNF, and POSS and 15 wt% of CNF in Dow's PELLETHANE 2102-90A TPU was conducted.
- Thermophysical and flammability properties of these TPUNs were measured.
- To obtain enhanced thermophysical and flammability properties, good dispersion of the nanoparticles in the polymer matrix is essential.
- Dow's polyester polycaprolactone elastomer disperses very well with Cloisite 30B nanoclay, PR-24-PS CNF, and PR-19-PS CNF, as shown by TEM.
- Trisilanolphenyl-POSS does not disperse readily with the PELLETHANE TPU and may actually degrade the material during the processing. Further investigation is underway.

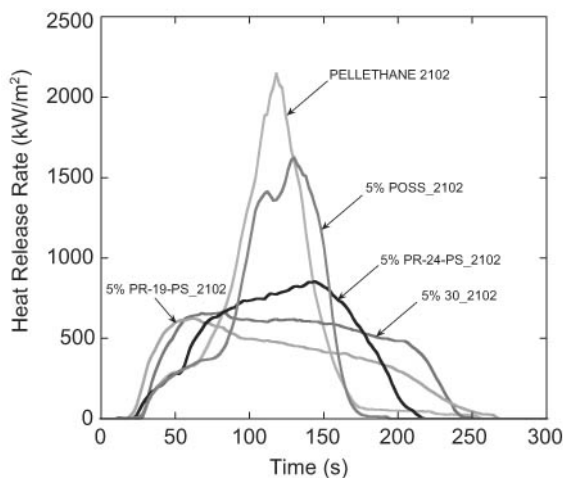


Figure 7.129 Heat release rate of TPUNs.

TABLE 7.21 Summary of Cone Calorimeter Data at Heat Flux of 50 kW/m²

Material	t_{ig} (s)	PHRR (kW/m ²)	Avg. HRR, 60s (kW/m ²)	Avg. HRR, 180s (kW/m ²)	Avg. Eff. H_c (MJ/kg)	Avg. SEA (m ² /kg)
PELLETHANE TPU	32	2,290	406	653	30	237
PELLETHANE-5% Cloisite 30B TPUN	34	664 (71% reduction)	560	562	25	303
PELLETHANE-5% PR-19-PS CNF TPUN	27	624 (73% reduction)	532	456	22	295
PELLETHANE-5% PR-24-PS CNF TPUN	30	911 (60% reduction)	407	554	25	283
PELLETHANE-5%-Trisilanophenyl-POSS TPUN	31	1,637 (29% reduction)	334	591	25	339

t_{ig} = time to sustained ignition

PHRR = peak heat release rate

Avg. HRR = average heat release rate after ignition

Avg. Eff. H_c = effective heat of combustion

Avg. SEA = average specific extinction area

- The CTE of nanoclay TPUN increases to greater than 2× for 10 wt% nanoclay, and the CTE of CNF TPUN goes through a maximum (~15 wt% loading).
- Correlations of CTE with Cloisite 30B, PR-24-PS CNFs, and PR-19-PS CNFs were obtained as a function of nanofiller loading.

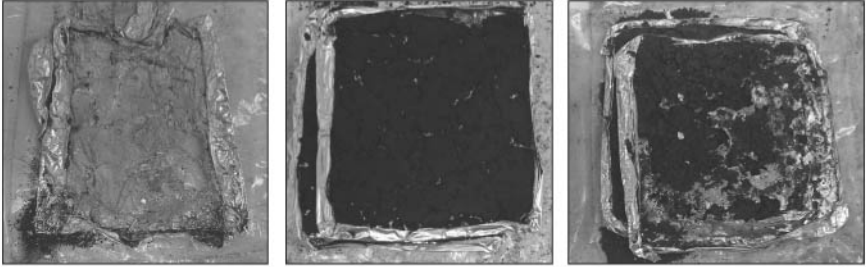


Figure 7.130 Posttest samples of cone calorimeter test: PELLETHANE (left), 5% Cloisite 30B TPUN (center), and 5% PR-19-PS CNF TPUN (right).

- Thermal conductivity increases with the addition of CNF nanoparticles and not with nanoclay and POSS.
- Significant reduction of PHRR was shown by 5 wt% PR-19-PS CNF (73%), 5 wt% Cloisite 30B (71%), and 5 wt% PR-24-PS CNF (60%) as compared to the baseline.
- Time to sustained ignition of PELLETHANE was 32 s, with a slight increase of t_{ig} of 34 s for 5% Cloisite 30B. All other TPUNs showed a slight decrease of t_{ig} .
- Average HRR (180 s) was lowered for all TPUNs.
- Average effective heat of combustion was lowered for all TPUNs.
- Average specific extinction area was slightly higher for all TPUNs.

7.4 Summary

This chapter provided some examples of thermoplastic-, thermoset-, and elastomer-based nanocomposites for high-temperature applications such as materials for fire protection, ablative and insulative materials for propulsion systems, carbon/carbon composite for thermo-oxidative resistance, and carbon fiber reinforced polymer matrix composites. It is apparent many more examples can be included in the discussion here, and many more are being or will be explored. Although it is uncertain which pathway nanotechnology will take, it is certain that nanomaterials can be developed for extreme conditions where conventional polymeric materials are deficient.

References

1. J. H. Koo, H. Stretz, R. Rushing, N. Burns, and W. Wootan, "Non-Halogenated Flame Retardant Polymers for Cabling Jackets," invited lecture at the *Nanocomposites 2001*, Baltimore, MD, June 4–5, 2001.
2. Specification for Cables, Fiber Optics, MIL-C-85045.

3. Standard Test Method for Fire and Smoke Characteristics of Cables Used in Air-Handling Spaces, UL-910, Underwriters Laboratories, Northbrook, IL.
4. V. Brabrauskas and S. J. Grayson, *Heat Release in Fires*, E & FN Spon, London, England, 1996, pp. 61–91.
5. Standard Test Method for Mass Loss Calorimeter, ASTM E 2102, ASTM, Philadelphia, PA.
6. X. Hu and J. H. Koo, “Flammability Studies of a Water Borne Fire Retardant Nanocomposite Coating on Wood,” presented at the Polymer Nanocomposites Symposium, ACS Southwest Regional Meeting, San Antonio, TX, Oct. 17–20, 2001.
7. J. H. Koo and L. A. Pilato, “Thermal Properties and Microstructures of Polymer Nanostructured Materials,” in *Nanoengineering of Structural, Functional, and Smart Materials*, Schulz, M. J., A. D. Kelkar, and M. J. Sundaresan (eds.), CRC Press, Boca Raton, FL, 2006, pp. 409–441.
8. Standard Test Method for Surface Burning Characteristics of Building Materials, ASTM E 84, ASTM, Philadelphia, PA.
9. J. H. Koo, W. K. Chow, W. Wootan, H. W. Au Yeung, and S. Venumbaka, “Flammability Studies of Fire Retardant Coatings on Wood,” ACS Symposium Series 797, *Fire and Polymers*, 2001, pp. 361–374.
10. J. H. Koo, L. Pilato, G. E. Wissler, and Z. P. Luo, “Flammability and Mechanical Properties of Nylon 11 Nanocomposites,” *Proc. Int’l SAMPE 2005 Symposium and Exhibition (ISSE)*, SAMPE, Covina, CA, 2005.
11. J. H. Koo, L. A. Pilato, and G. E. Wissler, “Fire Retardant Polymer Nanocomposites for Selective Laser Sintering Processing,” submitted patent application on 7/27/05.
12. J. Cheng, S. Lao, K. Nguyen, W. Ho, A. Cummings, and J. H. Koo, “SLS Processing of Nylon 11 Nanocomposites,” *Proc. 17th Solid Freeform Fabrication Symposium*, University of Texas at Austin, Austin, TX, Aug. 2005.
13. J. H. Koo, L. Pilato, et al., “Innovative Selective Laser Sintering Rapid Manufacturing Using Nanotechnology,” *Proc. 2005 Solid Freeform Fabrication Symposium*, University of Texas at Austin, Austin, TX, Aug. 2005.
14. S. Lao, W. Ho, K. Nguyen, J. Cheng, and J. H. Koo, “Microstructural Analyses of Nylon 11 Nanocomposites,” *Proc. 37th Int’l SAMPE Technical Conference (ISTC)*, Seattle, WA, Oct. 31–Nov. 3, 2005.
15. A. Cummings, L. Shi, and J. H. Koo, “Thermal Conductivity Measurements of Nylon 11-Carbon Nanofiber Nanocomposites,” *Proc. of IMECE 2005 (2005 ASME International Mechanical Engineering Congress and Exposition)*, Orlando, FL, Nov. 5–11, 2005.
16. E. D. Weil and S. Levchik, “Current Practice and Recent Commercial Developments in Flame Retardancy of Polyamides,” *J. Fire Sciences* **22**:251–264 (2004).
17. E. P. Giannelis, “Polymer Layered Silicate Nanocomposites,” *Adv. Mater.* **8**:29–35 (1996).
18. J. W. Gilman, T. Kashiwagi, and J. D. Lichtenhan, “Nanocomposites: A Revolutionary New Flame Retardant Approach,” *SAMPE J.*, **33**:40–46 (1997).
19. J. W. Gilman, “Flammability and Thermal Stability Studies of Polymer Layered-Silicate (Clay) Nanocomposites,” *Appl. Clay Sci.* **15**:31–49 (1999).
20. J. Zhu, A. B. Morgan, F. J. Lamelas, and C. A. Wilke, “Fire Properties of Polystyrene-Clay Nanocomposites,” *Chem. Mater.* **13**:3774–3780 (2001).
21. M. Zanetti, G. Camino, and R. Mulhaupt, “Combustion Behavior of EVA/Fluorohectorite Nanocomposites,” *Polym. Degrad. Stabil.* **74**:413–417 (2001).
22. J. W. Gilman, C. L. Jackson, A. B. Morgan, R. Harris, Jr., E. Manias, E. P. Giannelis, M. Wuthernow, D. Hilton, and S. H. Phillips, “Flammability Properties of Polymer-Layered Silicate Nanocomposites: Polypropylene and Polystyrene Nanocomposites,” *Chem. Mater.* **12**:1866–1873 (2000).

23. T. Kashiwagi, E. Grulke, J. Hilding, R. Harris, W. Awad, and J. Douglas, "Thermal Degradation and Flammability Properties of Polypropylene/Carbon Nanotube Composites," *Macromol. Rapid Commun.* **23**:761–765 (2002).
24. J. H. Koo and L. A. Pilato, "Polymer Nanostructured Materials for High Temperature Applications," *SAMPE J.* **41**:7 (2005).
25. F. Yang, R. A. Yngard, and G. L. Nelson, *Nanocomposites 2002*, San Diego, CA, Sept. 23–25, 2002.
26. T. Kashiwagi et al., *Nanocomposites 2002*, San Diego, CA, Sept. 23–25, 2002.
27. A. D. Pool and H. T. Hahn, "A Nanocomposite for Improved Stereolithography," *Proc. SAMPE 2003*, SAMPE, Covina, CA, 2003.
28. RILSAN polyamide 11 technical data sheet, Arkema Chemicals, Inc. Paris la Défense Cedex, France.
29. Standard Test Method for Heat and Visible Smoke Release Rates for Materials and Products Using an Oxygen Consumption Calorimeter, ASTM E 1354, ASTM, Philadelphia, PA.
30. R. S. Evans, "Indirect Rapid Manufacturing of Silicon Carbide Composites," PhD dissertation, The University of Texas at Austin, Dept. of Mechanical Engineering, Austin, TX, May 2005.
31. A. T. Cummings, "Thermal Conductivity Measurements of Nylon 11 Nanocomposites," M.S. thesis, The University of Texas at Austin, Dept. of Mechanical Engineering, Austin, TX, May 2005.
32. J. H. Koo, H. Stretz, A. Bray, and W. Wootan, "Next Generation Nanostructured Ablatives for Rocket Propulsion System," AFOSR Contract No. F49620-00-C-0045, STTR Phase I Final Report, Sept. 2001.
33. J. H. Koo, H. Stretz, A. Bray, W. Wootan, S. Mulich, B. Powell, T. Grupa, and J. Weispfenning, "Phenolic-Clay Nanocomposite for Rocket Propulsion Systems," *Int'l SAMPE Symposium and Exhibition* **47**:1085–1099 (2002).
34. J. H. Koo, H. Stretz, and A. Bray, "Nanocomposite Rocket Ablative Materials," AFOSR Contract No. F49620-00-C-0045, STTR Phase II Annual Report, Sept. 2002.
35. J. H. Koo, H. Stretz, A. Bray, J. Weispfenning, Z. P. Luo, and W. Wootan, "Nanocomposite Rocket Ablative Materials: Processing, Characterization, and Performance," *Int'l SAMPE Symposium and Exhibition* **48**:1156–1170 (2003).
36. J. H. Koo, H. Stretz, A. Bray, J. Weispfenning, Z. P. Luo, and W. Wootan, "Nanocomposite Rocket Ablative Materials: Processing, Microstructure, and Performance," AIAA-2004-1996 paper, *44th AIAA/ASME/ASCE/AHS Structures, Structural Dynamics, and Materials Conference*, Palms Springs, CA, Apr. 19–22, 2004.
37. J. H. Koo, H. Stretz, J. Weispfenning, Z. P. Luo, and W. Wootan, "Nanocomposite Rocket Ablative Materials: Subscale Ablation Test," *Int'l SAMPE Symposium and Exhibition* **49**:1000–1014 (2004).
38. J. H. Koo, W. K. Chow, H. Stretz, A. C.-K. Cheng, A. Bray, and J. Weispfenning, "Flammability Properties of Polymer Nanostructured Materials," *Int'l SAMPE Symposium and Exhibition* **48**:954–963 (2003).
39. R. A. Vaia, G. Price, P. N. Ruth, H. T. Nguyen, and J. Lichtenhan, "Polymer/Layered Silicate Nanocomposites as High Performance Ablative Materials," *Applied Clay Science* **15**:67–92 (1999).
40. J. H. Koo et al., "A Cost-Effective Approach to Evaluate High-Temperature Ablatives for Military Applications," *Naval Engineers J.* **104**:166–177 (1992).
41. M. J. Miller, J. H. Koo, et al., "Evaluation of Different Categories of Composite Ablative for Thermal Protection," AIAA-93-0839, 31st AIAA Aerospace Sciences Meeting, Reno, NV, Jan. 1993.

42. F. Cheung, J. H. Koo, et al., "Prediction of Thermo-Mechanical Erosion of High-Temperature Ablatives in the SSRM Facility," AIAA-95-0254, 33rd Aerospace Sciences Meeting, Reno, NV, Jan. 1995.
43. M. VanMeter, J. H. Koo, et al., "Mechanical Properties and Material Behavior of a Glass Silicone Polymer Composite," *Proc. 40th International SAMPE Symposium*, SAMPE, Covina, CA, 1995, pp.1425–1434.
44. J. H. Koo et al., "Effect of Major Constituents on the Performance of Silicone Polymer Composites," *Proc. 30th International SAMPE Technical Conference*, SAMPE, Covina, CA, 1998.
45. J. H. Koo et al., "Thermal Protection of a Class of Polymer Composites," *Proc. 44th International SAMPE Symposium*, SAMPE, Covina, CA, 1999, pp.1431–1441.
46. MX-4926 Technical Data Sheet, Cytec Engineered Materials, Winona, MN.
47. W. Luehmann, Pratt & Whitney Space Propulsion/Chemical Systems Division, San Jose, CA, personal communication.
48. SC-1008 Technical Data Sheet, Borden Chemical, Louisville, KY.
49. J. H. Koo, C. U. Pittman, Jr., K. Liang, H. Cho, L. A. Pilato, Z. P. Luo, G. Pruetz, and P. Winzek, "Nanomodified Carbon/Carbon Composites for Intermediate Temperature: Processing and Characterization," *Int'l SAMPE Technical Conference* 35:521–534 (2003).
50. J. H. Koo, L. A. Pilato, C. U. Pittman, and P. Winzek, "Nanomodified Carbon/Carbon Composites for Intermediate Temperature," AFOSR Contract No. F49620-02-C-0086 STTR Phase I Final Report, Jan. 2004.
51. J. H. Koo, L. A. Pilato, P. Winzek, K. Shivakumar, C. U. Pittman, Jr., and Z. P. Luo, "Thermo-Oxidative Studies of Nanomodified Carbon/Carbon Composites," *Int'l SAMPE Symposium and Exhibition* 49:1214–1228 (2004).
52. R. Blanski, J. H. Koo, et al., "Polymer Nanostructured Materials for Solid Rocket Motor Insulation-Ablation Performance," *Proc. 52nd JANNAF Propulsion Meeting*, CPIAC, Columbia, MD, May 2004.
53. J. H. Koo, D. Marchant, et al., "Polymer Nanostructured Materials for Solid Rocket Motor Insulation—Processing, Microstructure, and Mechanical Properties," *Proc. 52nd JANNAF Propulsion Meeting*, CPIAC, Columbia, MD, May 2004.
54. P. Ruth, R. Blanski, and J. H. Koo, "Preparation of Polymer Nanostructured Materials for Solid Rocket Motor Insulation," *Proc. 52nd JANNAF Propulsion Meeting*, CPIAC, Columbia, MD, May 2004.
55. J. H. Koo, L. Pilato, et al., "Epoxy Nanocomposites for Carbon Fiber-Reinforced Composites," *Proc. SAMPE 2005 Int'l Symposium*, SAMPE, Covina, CA, May 1–5, 2005.
56. J. H. Koo, L. Pilato, et al., "Nanocomposites for Carbon Fiber-Reinforced Polymer Matrix Composites," AIAA-2005-1928, 46th AIAA/ASME/ASCE/AHS Structures, Structural Dynamics, and Materials Conference, Austin, TX, Apr. 18–21, 2005.
57. J. H. Koo, L. Pilato, et al., "Nanocomposite for Carbon Fiber Reinforced Polymer Matrix Composites," AFOSR STTR Phase I Final Report, submitted to AFOSR, Arlington, VA, Oct. 2004.
58. R. D. Patton, C. U. Pittman, L. Wang, J. R. Hill, and A. Day, "Ablation, Mechanical and Thermal Conductivity Properties of Vapor Growth Carbon Fiber/Phenolic Matrix Composites," *Composites: Part A* 33:243–251 (2002).
59. A. V. Bray, G. Beal, and H. Stretz, "Nanocomposite Rocket Ablative Materials," Final Report, AFOSR Contract No. F49620-02-0013, STTR Phase II Final Report, Jan. 2004.
60. A. F. Grand, "Heat Release Calorimetry Evaluations of Fire Retardant Polymer Systems," *Int'l SAMPE Symposium and Exhibition* 42:1062–1070, 1997.

61. J. H. Koo, S. Venumbaka, P. E. Cassidy, J. W. Fitch, A. F. Grand, and J. Bundick, "Evaluation of Thermally Resistant Polymers Using Cone Calorimeter," *Fire and Materials '98 Int'l Conference*, 1998, pp. 189–193.
62. J. H. Koo, S. Venumbaka, P. E. Cassidy, J. W. Fitch, A. F. Grand, and J. Bundick, "Flammability Studies of Thermally Resistant Polymers Using Cone Calorimetry," *Fire and Mater.* **24**:209–218 (2000).
63. J. H. Koo, S. Venumbaka, P. Cassidy, J. Fitch, P. Clemens, and B. Muskopf, "Evaluation of Fire Safe Polymers/Composites for Marine Application," *Proc. 43rd Int'l SAMPE Symposium and Exhibition* **43**:1077–1089 (1998).
64. J. H. Koo, B. Muskopf, U. Sorathia, P. Van Dine, B. Spencer, and S. Venumbaka, "Fire Performance of Polymeric Matrix Composites for Marine Applications," *Proc. of 2001 Fire and Materials Conference*, Interscience Communication, London, 2001.
65. J. H. Koo, B. Muskopf, G. McCord, P. Van Dine, B. Spencer, U. Sorathia, and S. Venumbaka, "Characterization of Fire Safe Polymer Matrix Composites for Naval Applications," *Int'l SAMPE Symposium and Exhibition* **46**:2170–2182 (2001).
66. MIL-STD-2031 (SH). Fire and Toxicity Test Methods and Qualification Procedure for Composite Material Systems Used in Hull, Machinery, and Structural Applications Inside Naval Submarines. Philadelphia: Department of Defense, 1991.
67. J. W. Gilman, T. Kashiwagi, M. Nyden, J. E. T. Brown, C. L. Jackson, S. Lomakin, E. P. Giannelis, and E. Manias, "Flammability Studies of Polymer Layered Silicate Nanocomposites: Polyolefin, Epoxy, and Vinyl Ester Resins," *Chem. Tech. Polym. Additives*, 249–265 (1999).
68. J. W. Gilman, T. Kashiwagi, E. P. Giannelis, E. Manias, S. Lomakin, J. D. Lichtenhan, and P. Jones, "Nanocomposites: Radiative Gasification and Vinyl Polymer Flammability," *Fire Retardancy of Polymers*, Royal Soc. of Chemistry, Cambridge, 1998, pp. 203–221.
69. PT-30 Technical Data Sheet, Lonza, Basel, Switzerland.
70. K. Shivakumar et al., "Development of Cyanate Ester Based Carbon/Carbon Composites," *Proc. Int'l SAMPE 2000 Symposium*, SAMPE, Covina, CA, May 2000, pp. 1005–1015.
71. F. Abali, K. Shivakumar, N. Hamidi, and R. Sadler, "An RTM Densification Method of Manufacturing Carbon-Carbon Composites Using PT-30 Resin," *Carbon* **41**:893–901 (2003).
72. PT-15 Technical Data Sheet, Lonza, Basel, Switzerland.
73. Hitco 134A Technical Data Sheet, Hitco Carbon Composites, Gardena, CA.
74. Hitco CC139 Technical Data Sheet, Hitco Carbon Composites, Gardena, CA.
75. R. A. Vaia, "Polymer Nanocomposites Open a New Dimension for Plastics and Composites," *Amptiac Quarterly* **6**:17–24 (2002).
76. E. P. Giannelis, "Polymer Layered Silicate Nanocomposites," *Adv. Mater.* **8**:29–35 (1996).
77. J. D. Lichtenhan, N. Q. Vu, J. A. Carter, J. W. Gilman, and F. J. Feher, "Silsequioxane-Siloxane Copolymers from Polyhedral Silsesquioxanes," *Macromolecules* **26**:2141–2142 (1993).
78. M. L. Lake, D. G. Glasgow, C. Kwag, and D. J. Burton, "Carbon Nanofiber Polymer Composites: Electrical and Mechanical Properties," *Int'l SAMPE Symposium and Exhibition* **47**:1794–1800 (2002).
79. M. R. Nyden, J. W. Gilman, R. D. Davis, and J. R. Shields, "High-Throughput Methods for Flammability Screening of Multicomponent Polymer Blends and Nanocomposites," *Int'l SAMPE Symposium and Exhibition* **47**:738–748 (2002).
80. C. T. Vogelson, Y. Koide, L. B. Alemany, and A. R. Barron, "Inorganic-Organic Hybrid and Composite Resin Materials Using Carboxylate-Alumoxanes as

- Functionalized Cross-Linking Agents," *Chem. Mater.* 12:795–804 (2000); U.S. Patent 6,369,183 dated April 9, 2002.
81. C. Zilg et al., U.S. Patent 6,197,849 dated April 6, 2001.
 82. T. Lan et al., U.S. Patent 6,251,980 dated June 26, 2001.
 83. E. N. Gilbert, B. S. Hayes, and J. C. Seferis, "Nanoparticle Modification of Epoxy Based Film Adhesives," *Int'l SAMPE Symposium and Exhibition* 47:41–50 (2002).
 84. S. Spindler-Ranta and C. E. Bakis, "Carbon Nanotube Reinforcement of a Filament Winding Resin," *Int'l SAMPE Symposium and Exhibition* 47:1775–1787 (2002).
 85. C. Chen and D. Curliss, "Resin Matrix Composites: Organoclay-Aerospace Epoxy Nanocomposites, Part II," *SAMPE J.* 37:11–18 (2001).
 86. B. P. Rice, C. Chen, L. Cloos, and D. Curliss, "Carbon Fiber Composites: Organoclay-Aerospace Epoxy Nanocomposites, Part I," *SAMPE J.* 37:7–9 (2001).
 87. C. Chen and D. Curliss, "Processing, Dynamic Studies and Properties of Exfoliated Aerospace Epoxy-Organoclay Nanocomposites," *Mat. Res. Soc. Symp. Proc.*, vol. 703, MRS, Warrendale, PA, 2002, pp. 3–8.
 88. O. Becker, R. J. Varley, and G. P. Simon, "Morphology, Thermal Relaxations and Mechanical Properties of Layered Silicate Nanocomposites Based upon High-Functionality Epoxy Resins," *Polymer* 43:4365–4373 (2002).
 89. O. Becker, Y-B. Cheng, R. J. Varley, and G. P. Simon, "Layered Silicate Nanocomposites Based on Various High-Functionality Epoxy Resins: The Influence of Cure Temperature on Morphology, Mechanical Properties, and Free Volume," *Macromolecules* 36:1616–1625 (2003).
 90. A. Lee, *Proc. POSS Nanotechnology Conference*, Huntington Beach, CA, Sept 25–27, 2002.
 91. C. Pittman, *Proc. POSS Nanotechnology Conference*, Huntington Beach, CA, Sept 25–27, 2002.
 92. J. M. Brown, D. Curliss, and R. A. Vaia, "Thermoset-Layered Silicate Nanocomposites: Quaternary Ammonium Montmorillonite with Primary Diamine Cured Epoxies," *Chem. Mater.* 12:3376–3384 (2000).
 93. C. S. Triantafillidis, P. C. LeBaron, and T. J. Pinnavaia, "Thermoset Epoxy-Clay Nanocomposites: The Dual Role of α,ω -Diamines as Clay Surface Modifiers and Polymer Curing Agents," *J. Solid State Chem.* 167:354–362 (2002).
 94. C. S. Triantafillidis, P. C. LeBaron, and T. J. Pinnavaia, "Homostructured Mixed Inorganic-Organic Ion Clays: A New Approach to Epoxy Polymer-Exfoliated Clay Nanocomposites with a Reduced Organic Modifier Content," *Chem. Mater.* 14:4088–4095 (2002).
 95. C. Pederson, Cytec Engineered Materials, Anaheim, CA, personal communication, 3/03 and CYCOM 977-3 Resin System Technical Data Sheet.
 96. Technical Bulletin No. 27 AEROSIL for Solvent-Free Epoxy Resin, AEROSIL Technical Service Dept., Degussa AG, D-63403 Hanau-Wolfgang, Germany.
 97. J. H. Koo, J. Polidan, et al., "An Investigation of Polymer Nanocomposite Ablatives Characterization," invited lecture at the *30th Annual Conference of the North American Thermal Analysis Society*, Pittsburgh, PA, September 23–25, 2002.
 98. J. H. Koo, R. Blanski, et al., "Nanostructured Ablatives for Rocket Propulsion System: Recent Progress," AIAA-2003-1769, *44th AIAA/ASME/ASCE/AHS Structures, Structural Dynamics, and Materials Conference*, Norfolk, VA, Apr. 7–10, 2003.
 99. J. H. Koo and L. Pilato, "Polymer Nanostructured Materials for Propulsion Systems," Paper AIAA-2005-3606, *41st AIAA/ASME/SAE/ASEE Joint Propulsion Conference*, Tucson, AZ, July 10–12, 2005.
 100. M. H. Young and S. R. Glaittli, *50th JANNAF Propulsion Meeting*, July 2001, CPIA Pub. 705, vol. 2, pp. 1–14.

101. E. C. Mathias and T. N. Johnson, *20th JANNAF Rocket Nozzle Subcommittee Meeting*, Nov. 1999, CPIA Pub. 694, pp. 237–266.
102. D. Marchart, J. H. Koo, et al. “Flammability and Thermophysical Characterization of Thermoplastic Elastomer Nanocomposites,” *ACS National Meeting, Fire and Polymers Symposium*, Philadelphia, PA, Aug. 22–26, 2004.

Current Status, Trends, Future Directions, and Opportunities

8.1 Nanotechnology Research Funding

Nanoscience and Nanotechnology are initiating a new era of integrated, fundamental research at the nanoscale level. It is expected to lead to a more coherent science and engineering education, provide economic nanoscale manufacturing of products, and be an enabling foundation for improving human capabilities and societal outcomes in the long term. The U.S. National Nanotechnology Initiative (NNI) is a visionary program that coordinates 17 departments and independent agencies¹⁻⁸ and had a total budget of U.S. \$961 million in fiscal year 2004. The 2006 NNI budget request for nanotechnology research and development across the Federal Government is \$1.05 billion. Estimated spending for NNI in 2005 is nearly \$1.1 billion, an increase of 9 percent over 2004 expenditures. The increase in spending for nanotechnology over the past five years (from an estimated \$464 million in 2001) reflects the U.S. government's continuing support and commitment to the NNI program, based on its potential to expand knowledge, strengthen the U.S. economy, support national and homeland security, and enhance the quality of life for all citizens.⁴ At least 35 countries have initiated national activities in this field, partially stimulated by the visions and plans of NNI.

8.1.1 Government R&D investments

Following the establishment of the NNI in FY 2001, worldwide interest and investment in nanotechnology research and development (R&D) have grown steadily. The worldwide nanotechnology R&D investments

reported by government organizations have increased eightfold, from U.S. \$432 million to about U.S. \$4.1 billion, between 1997 and 2005 (Table 8.1 and Fig. 8.1). Today, virtually every country that supports scientific and technology R&D has a nanotechnology initiative. The total investment by governments outside the United States surpasses \$3 billion annually, with comparable investment by the private sector.⁶

The annual global impact of products where nanotechnology will play a key role was estimated in 2000 to exceed U.S. \$1 trillion by 2015, which would require about 2 million nanotechnology workers.⁸ This estimate was based on the analysis of existing R&D activities in industries in the U.S., Japan, and western Europe. One notes that U.S. \$1 trillion represents about 10 percent of the U.S. GDP in 2003. If one would extrapolate from previous experience, where for each information technology worker another 2.5 jobs are created in related areas, nanotechnology has the potential to create 7 million jobs overall by 2015 in the global market.

TABLE 8.1 Estimated Government Nanotechnology R&D Investments from 1997 to 2005 (\$ Millions)

Region	1997	1998	1999	2000	2001	2002	2003	2004	2005
EU	126	151	179	200	~225	~400	~650	~950	~1,050
Japan	120	135	157	245	~465	~720	~800	~900	~950
U.S.	116	190	255	270	465	697	862	989	1,081
Others	70	83	96	110	~380	~550	~800	~900	~1,000
Total (%) of 1997	432 (100%)	559 (129%)	687 (159%)	825 (191%)	~1,535 (355%)	~2,350 (547%)	~3,100 (720%)	~3,700 (866%)	~4,100 (945%)

SOURCE: M. Roco, National Science Foundation

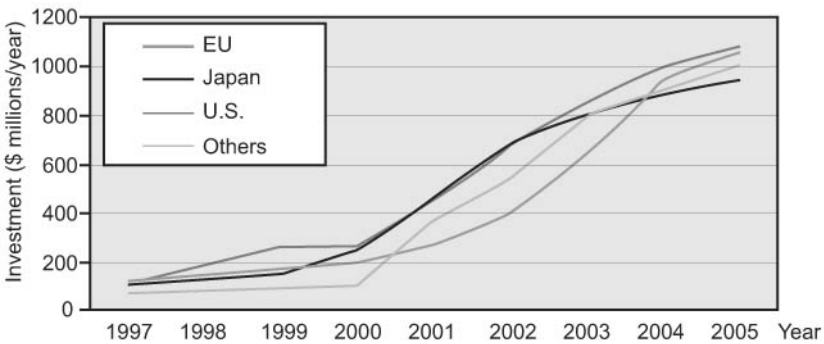


Figure 8.1 Government nanotechnology R&D investments from 1997 to 2005. (Courtesy of M. Roco, National Science Foundation.)

As scientific advances and technical progress continue, most agree that nanotechnology is still in a nascent stage and that its impact on the world economy remains to be seen. There is agreement that significant potential clearly exists. Scientists and engineers have opened a broad net that captures most major research areas in the physical, biological, materials, and engineering sciences. Industry has gained confidence that nanotechnology will provide competitive advantages to both traditional and emerging fields. Significant growth is anticipated in small businesses, large corporations, and the attraction of venture capital investors.

8.2 Nanotechnology Research Output

8.2.1 Publication output

One metric often used to gauge scientific leadership is the number of peer-viewed scientific articles. Figure 8.2 shows the results of a search of one of the principal databases of scientific literature, the Institute for Scientific Information (ISI) Web of Science, a searchable database of about 5400 professional journals, using the keyword *nano**. The chart shows an escalation in the total number of publications since 1989, and especially since 2000. Although the number of publications from the U.S. has grown throughout the period, the percentage of publications originating from the United States has declined from approximately 40 percent in the early 1990s to less than 30 percent in 2004.

Whereas the total number of publications is an indicator of the *quantity* of research output, a better indicator of the *quality* of the output is represented by publication in the most highly regarded scientific journals. A search of three high impact journals, *Science*, *Nature*, and

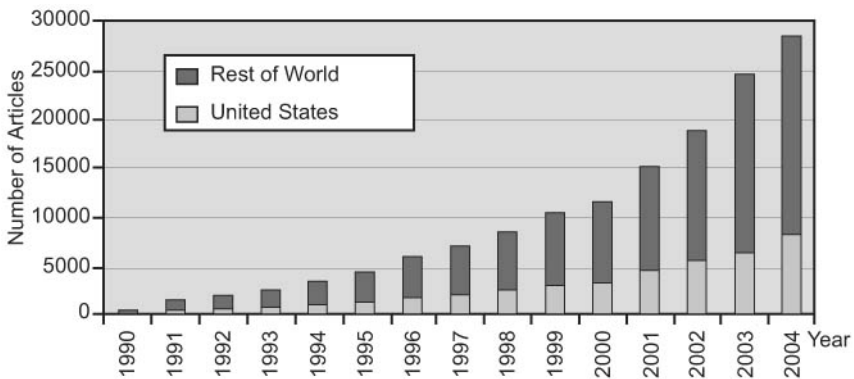


Figure 8.2 Number of articles in ISI Web of Science database found by searching “nano*”. (Courtesy of J. Murday, U.S. Naval Research Laboratory.)

Physical Review Letters, shows a 100 percent increase in the percentage of articles related to nanotechnology in these journals. Among these publications, the U.S. has produced an even larger fraction, over 50 percent, of the nanotechnology-related articles (Fig. 8.3). The data show, however, as did those from the broader selection of publications, that there is a steady increase in the percentage that originates from other countries.

8.2.2 Patent output

Another metric commonly used to gauge leadership in technology innovation is the number of patents and patent applications. Research disclosures (patents) are not proportional to the amount of investment provided to an R&D group because different factors must be considered within each and every organization such as secrecy, company policy not to patent, lengthy delays for technology and patentability to emerge, etc. For example, the timeline of the patents recorded with the U.S. PTO (U.S. Patent and Trade Office) is shown in Fig. 8.4. That office perceives domestic and foreign applications as being the main target for investors, because the U.S. provides the largest single market.

8.2.3 Research areas of focus

In June 2004, NSF sponsored an international meeting related to responsible nanotechnology R&D, at which 25 countries and the European Union were represented. A survey taken at the meeting which indicated that some nations, like the U.S., have broad research programs, whereas others have opted to make targeted research investments.

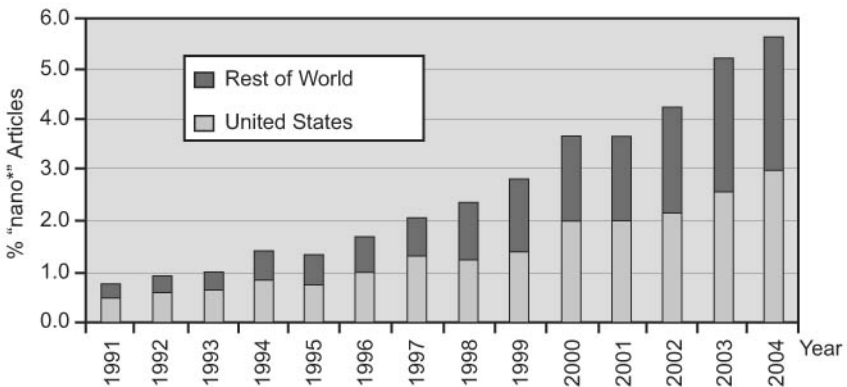


Figure 8.3 Total percentage of articles in *Science*, *Nature*, and *Physical Review Letters* identified by a keyword search on *nano**. (Courtesy of J. Murday, U.S. Naval Research Laboratory.)

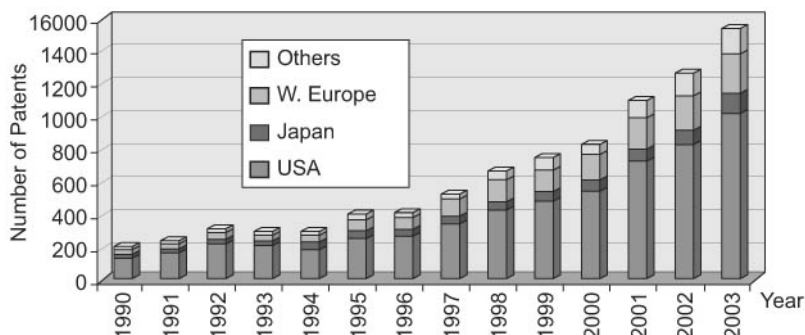


Figure 8.4 Number of nanotechnology-related patents identified by a search of titles and claims of patents in the USPTO database. (Courtesy of Huang, Z., H. Chen, Z.-K. Chen, and M. Roco. 2004. "International Nanotechnology Development in 2003; Country, Institution, and Technology Field Analysis Based on USPTO Patent Database," *Journal of Nanoparticle Research*, 6:325–354.)

Table 8.2 shows the key areas in which various countries are focusing their nanotechnology efforts according to the survey response. These countries appear to be investing especially in materials and manufacturing, biotechnology, and electronics.

8.2.4 Private sector activity

According to an EmTech Research (2005) survey of approximately 600 companies involved in the R&D, manufacture, sale, or use of nanotechnology, the top three companies based on the number of nanotechnology-related patents issued were IBM, Intel, and L’Oreal. Other companies that ranked high were large technology-based businesses. The companies included in Fig. 8.5 range in size, with the number being either very small (< 10 employees) or large (> 1000 employees).

8.3 Nanotechnology Commercialization Prospects

There is a gap between microsystem technology and nanotechnology. Micro- and nanotechnologies are becoming key technologies that have a significant impact on the development of new products and manufacturing technologies for nearly all industrial branches. This newly emerging field includes the use of nanotechnology to achieve better product performance or to create new products (bottom-up). The trend of continuous miniaturization is a challenge to develop suitable processes and materials for use (top-down). At the interface bridging micro- and the nanoworld, this exciting area is attracting interest from those individuals engaged in fundamental research as well as those persons involved in more applied research and related to industrial applications.

TABLE 8.2 Focus Areas of Government Investments in Nanotechnology

Country	Materials/ manufact.	Devices (including electronics & optics)	Energy & environ- ment	Biotech/ medical	Instru- ment develop- ment	Education
Argentina	X					
Australia	X	X	X	X		
Austria						
Belgium	X	X		X		
Brazil	X	X		X		
Canada	X	X		X		
Czech Republic	X	X		X		
European Union	X	X	X	X	X	X
France	X			X		
Germany	X	X		X	X	
India	X	X		X	X	X
Ireland	X	X	X	X		
Israel	X			X		
Italy	X	X		X	X	
Japan	X	X	X	X	X	
Korea	X	X				
Mexico	X					
Netherlands	X	X		X	X	
New Zealand	X					
Romania	X			X		
South Africa	X		X	X		
Switzerland	X	X		X	X	
Taiwan	X	X		X		
United Kingdom	X	X		X		
United States	X	X	X	X	X	X

SOURCE: June 2004 International Dialogue on Responsible Research and Development of Nanotechnology, <http://www.nanoandthepoor.org/international.php>

Although the EU as a whole is pursuing a broad program, individual EU countries (also shown here) have more targeted areas of research.

Depending on the material, most fundamental physical properties change if the geometric size (in at least one dimension) is reduced to a critical value below 100 nm. This size reduction allows tailoring of the physical properties of a macroscopic material if the material consists of nanoscale building blocks with controlled size and composition. Every property has a critical length scale, and if a nanoscale building block is made smaller than the critical length scale, the fundamental physics of that property change. By altering the sizes of those building blocks, controlling their internal and surface

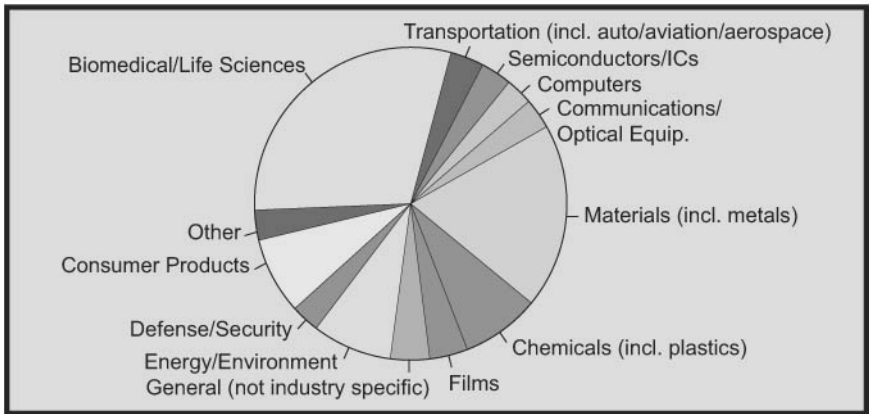


Figure 8.5 Target industries for companies involved in the R&D, manufacture, sale, and use of nanotechnology in 2004 (total number of companies = 599). (Courtesy of *EmTech Research 2005*.)

chemistry, their atomic structure, and their assembly, it is possible to engineer properties and functionalities in completely new ways.

Nanoparticles and nanomaterials possess radically different phenomena and performance, as compared to their larger scale counterparts. Such considerations include quantum effects, statistical time variations of properties, and their scaling within structure size. These nanoparticles and nanomaterials have unique mechanical, electronic, magnetic, optical, and chemical properties, thus providing a panorama to enormous new possibilities of engineered nanostructures and integrated nanodevices with application opportunities in information technology and communications, biotechnology and medicine, photonics and electronics. A selected example includes developments in very high-density data storage and quantum dots. Atomic or molecular units offer the ultimate building blocks for a bottom-up, atom-by-atom synthesis and self-assembly manufacturing. Advanced nanostructured materials such as high-purity, single-wall carbon nanotubes are being considered for microelectronics, sensors, thermal management for microelectronics, and flat panel displays.

Microsystems, including microelectromechanical systems (MEMS), bioMEMS, nanoelectronmechanical systems (NEMS), and optical, electronic, and electrochemical microsystems, offer the promise of a new class of multifunctional devices and systems for numerous applications. These applications include advanced computing, chemical and biological analysis and detection, drug delivery and discovery, tissue engineering, chemical and materials synthesis, and energy conversion and storage. New, advanced microsystems with integrated, nanometer-scale structures and functions present a multidisciplinary challenge.

An overview of the effects and applications of the reduced dimensionality of nanomaterials is listed in Table 8.3.⁹ The addition of nanoparticles to an otherwise homogenous material can lead to a change in macroscopic material behavior. Most material properties may be changed and engineered dramatically through the controlled, size-selective synthesis and assembly of nanoscale building blocks.

Readers should refer to Fecht and Werner's⁹ recent publication that discusses technology marketing trends for early nanotechnologies; research, development, and commercialization in Asia-Pacific nanotechnology; cooperation among small- and medium-sized enterprises boosts commercialization; rapid commercialization of nanotechnology in Japan; and numerous potential applications for nanotechnologies.

8.4 Economics of Nanoparticles

The use and incorporation of nanoparticles within a device or system can be envisioned as a relatively simple or highly complex procedure. Nanoparticles can be used via a simple "drop in" procedure introducing a low-volume fraction of "nano" additive into an existing polymer system without a change in process equipment. Hence no major capital investment is needed for the commercialization of these types of nanomodified materials. Contrary to the facile "drop in" method, there are other proposed uses of nanoparticles that are more complex and may require exceedingly complicated processes, nanoparticle manipulation/functionalization, etc. Either a simple or complex procedure

TABLE 8.3 Effect of Nanomaterials and Potential Applications Due to the Reduced Dimension⁹

Effects	Potential applications
High surface to volume ratio, enhanced reactivity	Catalysis, solar cells, batteries, gas sensors
Lower percolation threshold	Conductivity of materials
Increased hardness with decreasing grain size	Hard coatings, thin protection layers
Narrower bandgap with decreasing grain size	Opto-electronics
Higher resistivity with decreasing grain size	Electronics, passive component, sensors
Increasing wear resistance	Hard coatings, tools
Lower melting and sintering temperature	Processing of materials, low sintering materials
Improved transport kinetics	Batteries, hydrogen storage
Improved reliability	Nanoparticle encapsulated electronic components

contributes favorably or adversely to the timetable and the economics of the resulting nanotech product.

Table 8.4 lists the economics of several common nanoparticles used to manufacture polymer nanostructured materials. The cost of these raw materials represents a wide range of prices. MMT nanoclay is the least expensive—about \$3.50/lb—while SWNT is the most expensive—about \$500/g. Depending on the size of the test article required to demonstrate the feasibility of concept, some of these nanoparticles are cost prohibitive for many current and future applications.

8.5 Current Nanotechnology Commercial Applications

The definition of “commercial product” is one that is both *offered for sale* and *used* in the regular production of a device or component in general commerce. In this section numerous examples of “commercial” and “potential commercial” nanomaterials will be included. Table 8.5 provides an overview of currently available nanotechnology products, the developer/manufacturer, and the benefits of these nanomaterials applied to their prospective applications.¹⁰ Table 8.6 illustrates some of nanotechnology potential applications under development by various composite manufacturers combined with anticipated benefits.¹⁰

An excellent article by Sanchez et al. summarizes the current and potential commercial applications of hybrid organic-inorganic nanocomposites.¹¹ They pointed out that organic-inorganic hybrid materials not only represent a creative way to design new materials and compounds for academic research, but the improved and unusual features of these methods will result in the development of innovative industrial applications. Most of the hybrid materials that are currently commercially available are synthesized and processed by using

TABLE 8.4 Economics of Different Types of Nanoparticles¹⁰

Type of nanoparticles	Cost
MMT nanoclays	\$3.50/lb
Nanosilica	\$8.50/lb
Carbon nanofibers	\$85/lb
POSS	\$500/lb R&D quantity
Multi-wall carbon nanotubes (MWNTs)	\$3,000/lb R&D quantity
Small diameter carbon nanotubes (SDNTs)	\$22,700 (\$50/g) R&D quantity
Single wall carbon nanotubes (SWNTs)	\$227,000/lb (\$500/g) R&D quantity
N-Aluminum oxide	\$11.80/lb
N-Titanium dioxide	\$11.80/lb

TABLE 8.5 An Overview of Current Commercially Available Nanotechnology Products¹⁰

Product	Developer/manufacturer	Benefit/function
Auto sideboards	GM/Basell/Southern Clay Products/Blackhawk	Nano TPO-clay provides stronger, lighter sideboards (Fig. 8.8)
Nylon film	Honeywell/Nancor/Ube/Unitika	Low oxygen barrier film for packaging (Fig. 8.9)
Performance plastics masterbatch	Hyperion	EMI components for office and home appliances
Trousers	Nanotex/Burlington Mills/Eddie Bauer	Stainless trousers
Mattress covers	Nanotex/Seally	Shield for stains
Floor coverings	Nanophase	Vinyl flooring with nanocoating abrasion resistant
Sunscreen	Nanophase	Nanocrystals allow sunscreen to be transparent
Tennis ball	InMat™/Wilson	Coating for butyl rubber core improves pressure seal for longer life (Fig. 8.10)
Red stain and grease removal	Eastman/P&G	Peroxide and nanoparticle to remove stain and grease
Fire retardant power cable	Kabelwerk Eupen	Combining ATH-based compound with organoclay improves fire performance and smoke density (Fig. 8.11)
Basketball shoe pouch	Converse/Triton System	Nanocomposite pouch filled with helium inserts that fits into basketball shoe (Fig. 8.12)
Medical tubing	Foster-Miller	Nylon nanocomposite tubing with improved modulus for medical application (Fig. 8.13)
Chemical Mechanical Planarization	DuPont/Air Products/Others	Nanosilica, nanoCerium oxide, smooth chips
Nano-wax particle	BASF	Self cleaning surfaces
Polymer-clay masterbatch	Nanocor	Molded parts
Nanoclay additives	Sud Chemie	Flame retardant additives
Polycarbonate/ABS	Bayer	Flame retardant polymer blends
Optical coating	Nanofilm	Antistreaking windshield coating
Polycarbonate panels	GE/Cabot	Nanogel translucent aerogel
Rocket fuel	Mach I	Nanoferric oxide additive to rocket fuel

TABLE 8.6 An Overview of Potential Commercial Nanotechnology Products¹⁰

Product	Developer	Benefit/function
Tires	In Mat	Maintain long term tire air pressure, up to 2× as current seals
Power cells	Ballard	Fullerenes for H cells, notebook, auto computer
Drug delivery	Microchip/ChipRx	Medical devices, biosensors for drug delivery
Robots	NYU/USC	Tiny machine to clean ocean, attack germs, space research

conventional soft chemistry based routes developed in the 1980s. The authors grouped all hybrid material processes into three routes:

- Copolymerization of functional organosilanes, macromonomers, and metal alkoxides
- Encapsulation of organic components within sol-gel derived silica or metallic oxides
- Organic functionalization of nanofillers with lamellar structures, etc.

The chemical strategies (self-assembly, nanobuilding block approaches, hybrid MOF [Metal Organic Frameworks], integrative synthesis, coupled processes, bio-inspired strategies, etc.) allow the development of new chemistry to direct the assembly of a large variety of structurally well defined nano-objects into complex hybrid architectures hierarchically organized in terms of structure and functions. This new generation of hybrid materials will result in very promising commercial applications in: optics, electronics, ionics, mechanics, energy, environment, biology, medicine, functional smart coatings, fuel and solar cells, catalysts, sensors, etc. The Sanchez et al. study, reference 11, identifies selective examples of hybrid materials with an implied emerging potential commercialization as well as functional hybrids with real commercial opportunities.

8.5.1 Hybrid compounds for cosmetics

New hybrid compounds are targeted for cosmetics and controlled release of “active ingredients” for applications related to skin care and protection. They are based on the encapsulation of active organic components within porous silica microcapsules. Undesirable skin alterations and melanomas created by sun induced premature skin aging require the use of efficient but biocompatible sunscreens. Conventional commercial sunscreens are directly applied to the skin and usually contain an extremely high amount of active ingredients. These can be detrimental to health especially when they are absorbed by skin and are not photostable, thus generating free radicals that may cause

damage to the DNA. Sol-Gel Technologies Ltd. located in Bet Shemesh, Israel (website: <http://www.sol-gel.com>)¹² provides a safe solution by encapsulating the active organic UV filters in silica micro-capsules. As a result contact of these potent chemicals with skin is reduced and damage from trapped free radicals within the porous host is prevented. These “UV-pearls” are incorporated into a suitable cosmetic vehicle to achieve high Sun Protection Factors (SPF), while providing an improved safety profile as the penetration of the absorbed UV is conveniently reduced. These newly developed products have already been marketed by companies for sunscreens and daily wear cosmetics. Figure 8.6(a) shows the “UV pearls” and Fig. 8.6(b) shows the core-shell capsule for carrying functional contents.

Sol-Gel Technologies Ltd. also developed silica rainbow pearls containing organic dyes for cosmetics applications. These silica active-pearls contain an effective acne medication such as benzoyl peroxide (BP), which is as effective as an antibiotic but do not cause bacterial resistance. Benzoyl peroxide in direct contact with skin causes skin irritation, dryness and hyper-pigmentation in many patients. Encapsulating the benzoyl peroxide active ingredient in a silica shell prevents it from contacting the epidermis while it gradually delivers BP into the follicular region where acne bacteria are found. Sol-gel active-pearls are presently a successful commercial development.

8.5.2 Hybrid materials for protective and decorative coatings

Many interesting and highly effective applications of inorganic-organic hybrid materials have occurred in the area of automotive coatings. Hybrid coatings provide coloration, scratch-resistance, protection from UV, and chemical resistance for the substrate. DuPont with Generation 4[®] has developed a complex mixture of two hybrid polymers cross-linked simultaneously during curing to form a polymer network. This

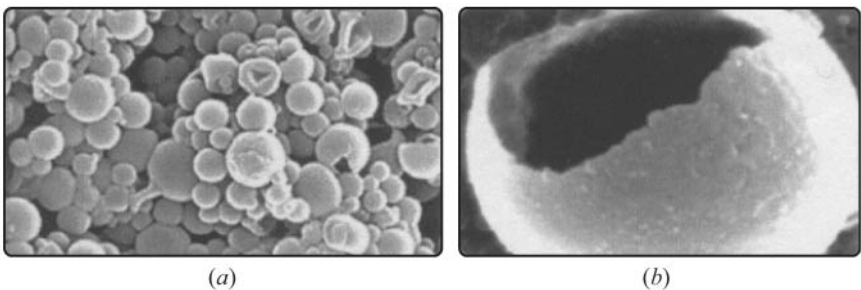


Figure 8.6 (a) Micro-capsules of UV pearls. (b) Micrograph of a core-shell capsule for carrying functional contents.¹²

unique network is partially grafted and partially interpenetrated as a decorative coating for the automotive industry.¹³ This hybrid material consists of a high density acrylate polymer core with organically modified alkoxy silane groups and residual unsaturation. It confers a high modulus and scratch-resistant function, dispersed in a low cross-linked density polymer, which provides film-forming properties. The superior scratch and environmental-etch resistance of these hybrid coatings resulted in their acceptance as topcoats for eight of the ten top-selling automobiles for 1997, including the Ford Taurus, Toyota Camry, and Honda Civic/Del Sol.

Decorative hybrid coatings also encompass an industrial area of interest such as packaging glass, glass sheets for furniture and sanitary appliances, glass in architecture and the building industry. For example a dishwasher-safe ORMOCER[®] color coating is used on glass (DEKOSIL[®]). The main advantages in terms of processing these coatings are the easy reproducibility of the colors and the finishing by conventional wet painting procedures (low curing temperatures < 200°C). From an aesthetic point of view, some requirements such as unlimited color palette and additional decorative effects like color gradients or partial coloration are also considered key features. Another example is the titania siloxane based hybrid organic-inorganic materials developed by several Japanese and European glass packaging industries.¹⁴ These coatings provide a variety of colors, enhance the consumer appeal, and improve the mechanical properties of these glass bottles. These dyed colored bottles are recyclable as uncolored glass because in contrast to conventional colored glass bottles, these glass bottles are color coated. The coloration does not originate from transition metals that are normally dissolved in glass and difficult to remove on re-melting glass for recycling. Conventional colored glass remains colored glass on re-melting.

8.5.3 Hybrid materials for dental applications¹⁵⁻¹⁸

Inorganic-organic hybrid materials can be used as filling composites in dental applications. As shown in Fig. 8.7(a) these composites feature tooth-like properties (appropriate hardness, elasticity, and thermal expansion behavior) and are easy to use by the dentist as they can easily penetrate into the cavity and harden quickly via exposure to blue light. These materials feature minimum shrinkage, are non-toxic, and sufficiently non-transparent to X-rays.

Traditional plastic filling composites have long-term adhesion problems and a high degree of polymerization shrinkage resulting in marginal fissures. The dual character of the ORMOCERs as inorganic-organic

copolymers is the key for improving the properties of dental filling composites. The organic, reactive monomers are contained within the sol-gel process by the formation of an inorganic network. Thus, in the subsequent curing process, polymerization takes place with less shrinkage. Abrasion resistance is significantly enhanced by the existing inorganic Si-O-Si network.

An example of available commercial filling composites based on dental ORMOCERs from Fraunhofer ISC such as “Definite®” and “Admira®” are as shown in Fig. 8.7[b]. In the case of the Admira product, a specifically designed dentine-enamel bonding agent, an adhesive ORMOCER developed in cooperation with VOCO GmbH, is used to make this product especially attractive and brilliant in appearance. In the glass ionomer cement based dental composites novel blue light polymerized carboxyl functionalized ORMOCERs have been developed.

8.5.4 Hybrid materials (polymer-clay nanocomposites - PCNs) with structural properties

The first successful and significant development of polymer-clay nanocomposites (PCNs) was pioneered by Toyota’s researchers¹⁹⁻²³ for high performance reinforced plastics applications in automobiles. The earliest successes in the automotive industry are credited to the sonication process developed by Ford Corporation to better disperse the clay within the polymer. Related to these early disclosures, General Motors Corporation (GMC) developed a step-assist component²⁴ (Fig. 8.8) for 2002 GMC Safari and Chevrolet Astro vans, which is made

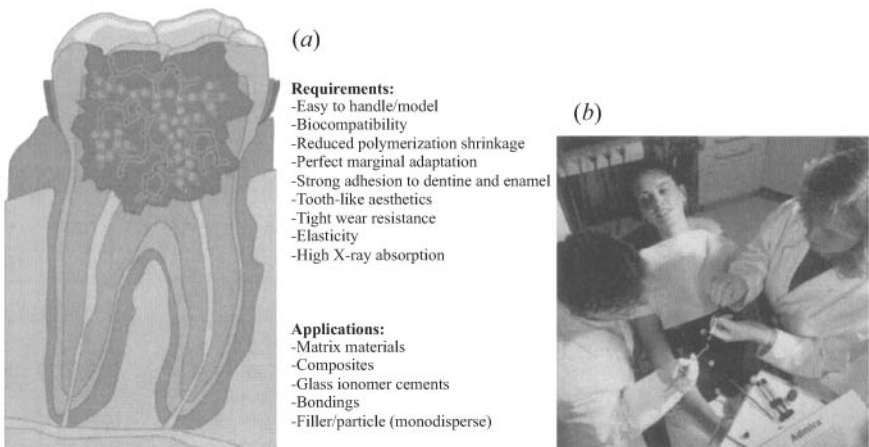


Figure 8.7 (a) Requirements and possibilities of dental applications of ORMOCERs. (b) Application of an ORMOCER as dental filling material.¹¹



Figure 8.8 (a) Partners in development: GM/Basell/Southern Clay Products/Blackhawk for the first commercial nano TPO step assist on Astro and Safari vans. (b) GM R&D manager stepping into a van with a step assist. (Courtesy of SCP.)

of thermoplastic polyolefin-clay nanocomposite. This material is lighter and stiffer, more robust at low temperatures and easily recyclable. GMC also used these PCNs in the lateral protection wire of the 2004 Chevrolet Impala since the PCNs are 7 percent lighter in weight and present a better surface appearance.

New applications of hybrid PCNs are envisaged by the automotive industry for commercialization: PP-clay for bodywork with anti-scratch properties (Dow Plastics/Magma); acetal-clay for ceiling lights (Showa Denko); PP-clay for panes of doors, consoles and interiors decoration (Ford, Volvo) due to aesthetics, recyclability and weight saving properties; nylon-clay for bumpers with enhanced mechanical and weight saving properties (Toyota); nylon-clay for fuel reservoir with air tight properties (Ube America).

Beside the above properties characteristics, the weight advantage provides a significant impact on the environment. It has been reported²⁵ that widespread use of PCNs by U.S. automotive industry could save 1.5 billion liters of gasoline in one year of automotive production and reduce related carbon dioxide emissions by more than 10 billion pounds.

For environmental applications, nanoclays are used as effective reinforcing agents in “green nanocomposites.”²⁶ These renewable-resource-based biodegradable nanocomposites consist of cellulose plastics (plastics made from wood); polyactic acid (corn-derived plastic) or polyhydroxyalkanoate (bacterial polyester). They are attractive materials as substitutes for petroleum feedstock in making the manufacture of biodegradable plastic for the commercial market.²⁷

8.5.5 Hybrid materials (PCNs) with gas barrier properties

Through the incorporation of nanoclays in polymer matrices, it is possible to create a labyrinth within the structure, which physically delays

the passage of gas molecules. The excellent barrier properties of gas and vapor transmission have resulted in applications for food and beverage packaging as well as barrier liners in storage tanks and fuel lines for cryogenic fuels in aerospace systems.²⁸ Bayer Polymers have developed a hybrid material combining silicate nanoparticles with the features of polyamide 6 (PA6) and ethylene vinyl alcohol (EVOH); it is inexpensive with good barrier properties. The silicate modified PA6 is not as attractive a barrier as EVOH but is significantly better than neat PA6.²⁹

Nanocor and Mitsubishi Gas Chemical Company developed the MXD6 high barrier semi-aromatic nylon nanocomposites.^{29,30} Mitsubishi marketed this PCN under the Imperm[®] trade name. The new material features oxygen and carbon dioxide barrier properties that were previously unachievable. Imperm's barrier properties are superior to EVOH and its processing characteristics are ideal for multilayer films, bottles, and thermoformed containers (Fig. 8.9).

Honeywell has developed a polyamide-clay nanocomposite with specific active and passive oxygen barrier properties.²⁹ The passive barriers are the nanoclays, which render it more difficult for oxygen transmission inside the composite, but also conduct the oxygen molecules to specific oxygen-captors. The clay incorporation limits the oxygen transmission up to 15–20 percent of the value for the pure polymer.

Triton Systems and the U.S. Army collaborated on the development of PCNs as non-refrigerated packaging materials, which conserves food freshness for three years.^{29,31}

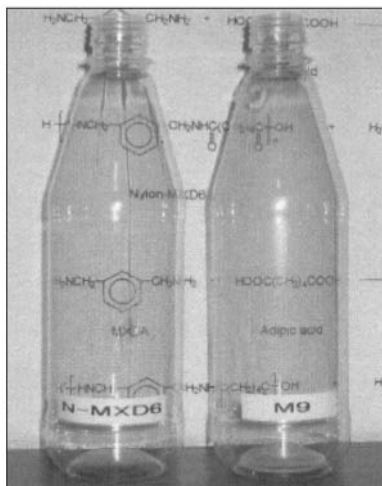


Figure 8.9 Nano-N-MXD6 and N-MXD6 M9 are high gas barrier resins commercially available from Mitsubishi Gas Chemical Co.³⁰

InMat Inc. has developed several applications for their nanocomposite coatings.³² The nanocomposite coating of the Wilson tennis balls maintains the internal pressure for an extended period of time. Figure 8.10 shows the Wilson tennis balls containing a double core. The core is coated by a polymer-clay (vermiculite) nanocomposite that acts as a gas barrier, doubling its shelf life. It is anticipated this technology can be extended to the rubber industry and be incorporated into soccer balls or in automobile or bicycle tires.

The barrier properties of PCNs have also been extended to liquids (solvents) or molecules such as water, since these liquids are responsible in some instances in polymer deterioration. De Bievre and Nakamura of Ube Industries have reported a significant reduction in fuel diffusion through polyamide-6/66 polymers by incorporation of nanoclay, resulting in reduced fuel emissions for fuel tank and fuel line components.^{29,33} InMat Inc. is collaborating with the U.S. Army with regard to the concept of liquid/hydrocarbon barriers.³² Some envisaged applications are protective gloves and coatings for combustibles and fuel tanks.

8.5.6 Hybrid materials (PCNs) with flame retardant properties

Thermal stability and fire retardancy have facilitated the investigation of nanoclay as an FR additive for commodity polymers as reported by

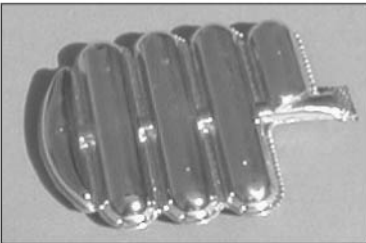


Figure 8.10 The core of this Wilson tennis ball is covered by a polymer-clay nanocomposite coating that acts as a gas barrier, doubling its shelf-life. (Courtesy of SCP.)

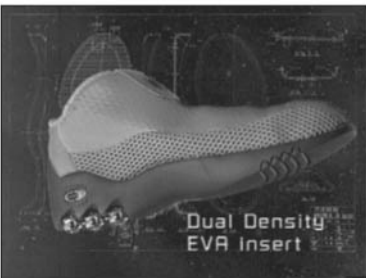
Gilman et al.^{29,34} Gitto (polymer manufacturer) and Nanocor (nanoclay manufacturer) are developing fire retardant polyolefin-clay nanocomposites, since this polymer has a wide range of industrial applications.^{29,35} The heat distortion temperature (HDT) of PCNs can be increased to 100°C and extend their usage to higher temperature applications such as automotive under-the-hood parts. Additional flammability studies are mentioned in Chap. 7.

8.5.7 Hybrid materials (PCNs) with other properties

In some cases, the value of PCNs technology relates to value-added performance of mechanical, barrier or fire retardant properties not present in the neat polymer but occur via the low volume introduction of these organically modified layered silicates (OLS). For example, in contrast to conventional filled polymers that are opaque and exhibit compromised mechanical properties. The introduction of a low volume fraction of OLS that is of nanoscopic dimensions and uniformly dispersed within the polymer results in PCN with optimum transparency and clarity similar to the neat polymer. Further these PCNs exhibit multifunctionality behavior that is unavailable in neat polymer.



Nanocomposite pouch filled with helium



Insert that fits into the shoe

Figure 8.11 Converse basketball shoe pouch by Triton Systems Inc. (Courtesy of SCP.)

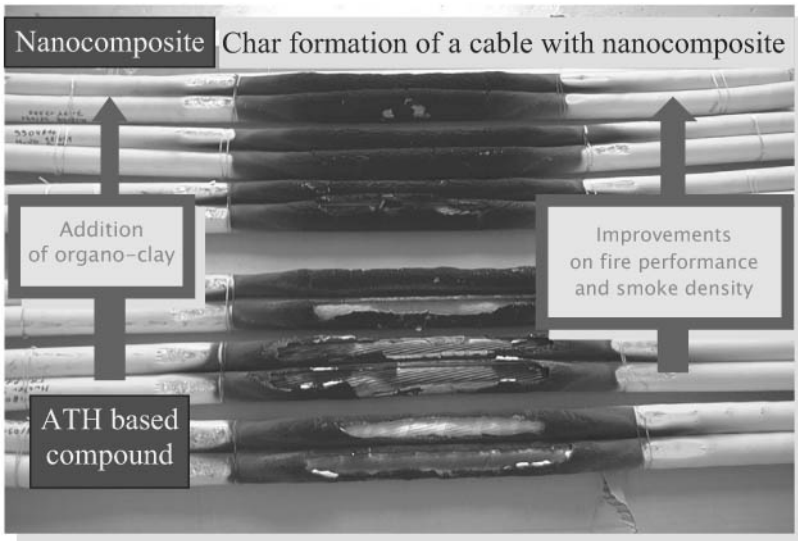
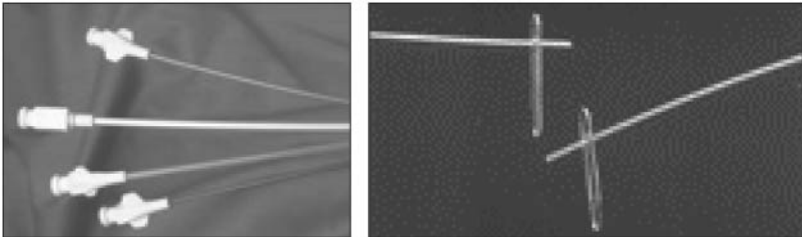


Figure 8.12 Nanocomposite power cable by Kabelwerk Eupen showing charring forming is more efficient, with improvements in fire performance and smoke density. (Courtesy of SCP.)



Tubing with improved modulus

Figure 8.13 Nylon 12 nanocomposite for medical applications with improved modulus. (Courtesy of SCP.)

8.6 Future Directions of the National Nanotechnology Initiative

The future vision of the National Nanotechnology Initiative (NNI) will promote the ability to understand and control matter on the nanoscale level and leads to a revolution in technology and industry. Toward this vision, the NNI will expedite the discovery, development, and deployment of nanotechnology to achieve responsible and sustainable economic benefits, to enhance the quality of life, and to promote national security. The initiative is a multiagency, multidisciplinary program that supports R&D; develops infrastructure; and promotes education, knowledge diffusion, and commercialization in nanotechnology.

Concurrent with the development of new technology options, the NNI is addressing nanotechnology's various societal dimensions.

As the NNI is evolving and maturing, it has recognized the need to assess the initiative and to update its strategic plan by projecting 5 to 10 years into the future. A strategic plan describes the goals of the NNI, as well as the strategy by which those goals are to be achieved. The four goals of the NNI are as follows:⁴

- Maintain a world-class research and development program aimed at realizing the full potential of nanotechnology.
- Facilitate transfer of new technologies into products for economic growth, jobs, and other public benefit.
- Develop educational resources, a skilled workforce, and the support infrastructure and tools to advance nanotechnology.
- Support responsible development of nanotechnology.

Ongoing activities, as well as specific new activities, aimed at achieving each goal are identified. As new materials and devices are created and novel applications developed, the NNI plans to target investments toward opportunities identified by the community via NNI-sponsored workshops, to place greater emphasis on technology transfer and liaison with industry groups, and to complete and operate user facilities.

The plan also includes a description of the investment strategy, including the major subject categories of investment or *program component areas* (PCAs). Whereas the NNI goals embody the vision of the initiative and provide structure of its strategy and plans, PCAs relate to areas of investment that are critical to accomplishing those goals. The program component areas are grouped under seven major subject areas and are defined as follows:⁴

1. Fundamental nanoscale phenomena and processes
2. Nanomaterials
3. Nanoscale devices and systems
4. Instrumentation research, metrology, and standards for nanotechnology
5. Nanomanufacturing
6. Major research facilities and instrumentation acquisition
7. Societal dimensions

Each PCA may include research that ranges from basic to applied, as well as development of applications based on nanotechnology. The original implementation plan for the NNI identified nine *grand*

challenge areas, corresponding to a variety of application areas in which nanotechnology is expected to have a significant impact. Table 8.7 shows the relationships between PCA and the overarching NNI goals. The NNI will provide a balanced and coordinated investment in the program component areas and in a broad spectrum of applications. This process will ensure that the U.S. remains a global leader in the responsible development of nanotechnology and will secure the resulting benefits to the economy, to national security, and to the quality of life of all citizens.

8.6.1 Budget summary⁵

The 2006 NNI budget request for nanotechnology R&D for the federal government is \$1.05 billion. Estimated spending in 2005 is nearly \$1.1 billion, an increase of 9 percent over 2004 expenditures. The increased spending for nanotechnology over the past five years (from an estimated \$464 million in 2001) reflects the U.S.’s continuing support for the NNI program, based on its potential to expand

TABLE 8.7 Relationships Between Program Component Areas and the Overarching NNI Goals

Program Component Areas:	Goal 1: Maintain a world-class research and development program aimed at realizing the full potential of nanotechnology	Goal 2: Facilitate transfer of new technologies into products for economic growth, jobs, and other public benefit	Goal 3: Develop educational resources, a skilled workforce, and the supporting infrastructure and tools to advance nanotechnology	Goal 4: Support responsible development of nanotechnology
Fundamental Nanoscale Phenomena and Processes				
Nanomaterials				
Nanoscale Devices and Systems				
Instrumentation Research, Metrology, and Standards for Nanotechnology				
Nanomanufacturing				
Major Research Facilities and Instrumentation Acquisition				
Societal Dimensions				
	<div style="display: flex; align-items: center;"> <div style="width: 20px; height: 20px; background-color: #cccccc; margin-right: 5px;"></div> critical to goal </div> <div style="display: flex; align-items: center; margin-top: 5px;"> <div style="width: 20px; height: 20px; background-color: #999999; margin-right: 5px;"></div> primary relevance </div> <div style="display: flex; align-items: center; margin-top: 5px;"> <div style="width: 20px; height: 20px; background-color: #666666; margin-right: 5px;"></div> secondary relevance </div>			

SOURCE: Nanoscale Science, Engineering, and Technology Subcommittee (NSET). 2004. *The National Nanotechnology Initiative: Strategic Plan*. Washington, D.C. December 2004.

knowledge, strengthen the U.S. economy, support national and homeland security, and enhance the quality of life for all citizens.

For the first time since the inception of NNI, funding has been classified by program component areas. The five agencies investing the most in nanotechnology R&D are the National Science Foundation, Department of Defense, Department of Energy, National Institutes of Health, and the National Institute for Standards and Technology. Each of the agencies has investments distributed across at least six of the seven PCAs. Funding among the PCAs by all 11 agencies with nanotechnology R&D budgets reflects a balanced strategic investment. Funding of PCAs for 2006 is as follows:

- Fundamental nanoscale phenomena and processes (\$234M)
- Nanomaterials (\$228M)
- Nanoscale devices and systems (\$244M)
- Instrumentation research, metrology, and standards for nanotechnology (\$71M)
- Nanomanufacturing (\$47M)
- Major research facilities and instrumentation acquisition (\$148M)
- Societal dimensions (\$82M)

The societal dimensions PCA includes approximately \$39M for programs directed primarily at environmental, health, and safety (EHS) R&D. Readers are referred to Karn's publication³⁶ on *Nanotechnology and the Environment: Applications and Implications* to explore this subject. An amount of \$43 million was allocated for education-related activities and research on the broad implications of nanotechnology for society, including economic, workforce, and educational, ethical, and legal implications.

In 2006, the NNI will continue to support a broad portfolio of R&D aimed at extending the boundaries of knowledge. As understanding of nanoscale processes and phenomena emerge, greater emphasis is being placed on the development of applications, especially within agencies with focused missions. In addition, funding for research into the potential environmental and health effects of nanotechnology is growing, and interagency planning and coordination in this area is expanding. Programs focused on education at all levels, both in the classroom and in informal settings, are also increasing. The NNI, through the National Nanotechnology Coordination Office and other channels, plans to broaden its activities for public involvement.

8.7 Identified Areas of Opportunity⁶

Priority nanoscale science and technology goals in the next five years are in currently exploratory areas of research (including nanomedicine, energy conversion, food and agriculture, realistic simulations at the nanoscale, and molecular nanosystems), in areas transforming to technological innovation (nanostructured materials, nanoelectronics, catalysts, pharmaceuticals, and development of tools for measurement and simulation), and in areas to advance broad societal goals (such as a better understanding of nature and life, increasing productivity in manufacturing, interdisciplinary education, improvement of human performance, and sustainable development). Societal and educational implications, including environmental research, will increase in importance in NNI as nanotechnology products and services reach the market.

Several generations of nanotechnology products are expected to evolve from relatively simple nanostructures for products such as coatings and hard metals, to active components such as nanoscale transistors, and then to nanosystems with new architectures.

The National Nanotechnology Advisory Panel gained insight into what areas of research were likely to yield high-impact advances. Below is a selection of the near-, mid-, and long-term areas in which nanotechnology is expected to make a significant impact.

8.7.1 Near-term (1 to 5 years)

- Nanocomposites with greatly improved strength-to-weight ratios, toughness, and other characteristics
- Nanomembranes and filters for water purification, desalination, and other applications
- Improved catalysts with one or more orders of magnitude less than precious metal
- Sensitive, selective, reliable solid-state chemical and biological sensors
- Point-of-care medical diagnostic devices
- Long-lasting rechargeable batteries

8.7.2 Mid-term (5 to 10 years)

- Targeted drug therapies
- Enhanced medical imaging
- High-efficiency, cost-effective solar cells

- Improved fuel cells
- Efficient technology for water-to-hydrogen conversion
- Carbon sequestration

8.7.3 Long-term (20+ years)

- Drug delivery through cell walls
- Molecular electronics
- All-optical information processing
- Neural prosthetics for treating paralysis, blindness, and other conditions
- Conversion of energy from thermal and chemical sources in the environment

The above opportunities suggest the potential for technologies that will improve the quality of life for all by providing clean water, affordable energy, and better healthcare.

8.8 Nanotech's Safety Risks

The potential economic impact of nanotechnology is vast. With many products currently on the market and the anticipation of more to come, there are escalating concerns related to the potential environmental, health, and safety (EHS) implications of products utilizing nanotechnology, particularly nanoparticles. These interests were recently expressed during a hearing convened by the U.S. House Science Committee to assess research on the EHS implications of nanotechnology and how the government could facilitate work in this area.

The federal government's nanotechnology research and development (R&D) effort is currently led by National Nanotechnology Initiative (NNI) (see Sections 8.1, 8.5, and 8.6 in this chapter). In 2006, it was pointed out that the requested budget for NNI was \$1.1 billion, and only 3.7 percent was directed toward research on EHS implications (see Section 8.5.1). Readers are referred to Karn's publication,³⁶ "Nanotechnology and the Environment—Applications and Implications," to explore this subject.

Most current uses of polymer material nanotechnology involve composites where the nanoparticles are contained within a polymer matrix. The manufacturers and users of engineered nanomaterials are already taking necessary precautions to minimize exposure to the "nano" particles in the workplace. But the uncertainty of the toxicity of nanoparticles—even in small quantities—requires the determination

of whether selected nanoparticles are benign or toxic. The anxiety originates from the limited number of short-term toxicity studies that have been published to date. The government should provide leadership in this area of research by coordinating the efforts underway in various industrial, academic, and government laboratories. The unification of the toxicology research effort, along with the elimination of regulatory ambiguity that could possibly occur from the resulting data, is critical to facilitate the rapid and responsible development of nanotech product in industry. These two issues—limited EHS data and regulatory ambiguity—are slowing nanotechnology commercialization in the United States today.

The commercialization of products based on nanotechnology may also be threatened by an absence of generally accepted testing methods and standards. Nanoparticles do not necessarily behave like their larger micro- and macro-particle relatives; research is needed to develop a uniform, science-based approach for identification of hazards, assessment of exposure, and management of risks. *In the author's opinion, this research requires immediate attention!*

To further address this situation, more government funds should be allocated for this research. It is recommended that a portion of the NNI budget for Nanotechnology R&D be allocated for EHS. To avoid potential opposition or societal hostility to nanotechnology, the government should consider a public engagement strategy considerably different from education. The strategy should include town meetings, “listening sessions,” and civic forums.

Furthermore, the government should obtain information related to EHS risks from those organizations (small businesses, start-up companies, and other groups) that are currently working in the nanotech field. Many of the exciting and attractive discoveries related to new nanoscale materials are being made in universities and by entrepreneurs in start-up companies. But these entities lack the experience, resources, and funding needed to adequately address the fundamental EHS problems. An integrated procedure that provides and communicates “ongoing” EHS information to these universities and entrepreneurs would greatly contribute to moving products to market.

The government—at all levels: federal, state, and local—needs to knock on the doors of small businesses with useful technical and potential financial assistance with regard to EHS issues. Government website information is not viewed as adequately addressing this problem.

Nanotechnology offers an important opportunity to apply the lessons from prior EHS-related issues by identifying the risks up front, grasping the necessary steps to address them, and engaging in a meaningful dialogue with the stakeholders to shape this technology's

explosive growth. In summary, there is an opportunity to get nanotechnology right the first time!

8.9 Summary

This chapter summarizes the past and current nanotechnology research funding status, and nanotechnology research output in terms of publication, patent, and research area of focus. Nanotechnology commercialization prospects, economics of nanoparticles, and several current nanotechnology commercial applications were included in this chapter. Future directions and areas of opportunities in near-, mid-, and long-term opportunities were identified by NNI. Concerns of potential environment, health, and safety (EHS) implications of products utilizing nanotechnology were discussed.

References

1. M. C. Roco, S. Williams, and P. Alivisatos (eds.), *Nanotechnology Research Directions: IWGN Workshop Report*, Kluwer Academic Publishers, Dordrecht, The Netherlands, 2000. <http://www.wtec.org/loyola/nano/IWGN.Research.Directions/>.
2. R. W. Siegel, E. Hu, and M. C. Roco (eds.), *WTEC Panel Report on Nanostructure Science and Technology*, Kluwer Academic Publishers, Dordrecht, The Netherlands, 1999.
3. U.S. National Nanotechnology Initiative official website: <http://www.nano.gov>.
4. The National Nanotechnology Initiative Strategic Plan, Nanoscale Science, Engineering and Technology Subcommittee, Committee on Technology, National Science and Technology Council, Dec. 2004. <http://www.nano.gov>.
5. The National Nanotechnology Initiative: Research and Development Leading to a Revolution in Technology and Industry, Supplement to the President's FY 2006 Budget, March 2005. <http://www.nano.gov>.
6. The National Nanotechnology Initiative at Five Years: Assessment and Recommendations of National Nanotechnology Advisory Panel, President's Council of Advisors on Science and Technology, May 2005. <http://www.nano.gov>.
7. Defense Nanotechnology Research and Development Programs, Department of Defense, Director, Defense Research and Engineering, May 17, 2005. <http://www.nano.gov>.
8. M. C. Roco, "U.S. National Nanotechnology Initiative: Planning for the Next Five Years," in *The Nano-Micro Interface: Bridging the Micro and Nano Worlds*, H.-J. Fecht and M. Werner (eds.), Wiley-VCH Verlag GmbH, Weinheim, Germany, 2004, pp. 3–9.
9. H.-J. Fecht and M. Werner (eds.), *The Nano-Micro Interface: Bridging the Micro and Nano Worlds*, Wiley-VCH Verlag GmbH, Weinheim, Germany, 2004.
10. J. H. Koo and L. A. Pilato, *Polymer Nanocomposites*, SAMPE Tutorial, SAMPE, Covina, CA, 2005.
11. C. Sanchez, B. Julian, P. Belleville, and M. Popall, "Applications of Hybrid Organic-Inorganic Nanocomposites," *J. Mater. Chem.* **15**:3559–3592 (2005).
12. Sol-Gel Technologies Ltd., Bet Shemesh, Israel. <http://www.sol-gel.com>.
13. I. Hazan and M. Rummel, U.S. Patent No. 5, 162, 426, 1992.
14. T. Minami, *J. Sol-Gel Sci. Technol.* **18**:290, 2000.
15. H. Wolter and W. Storch, *J. Sol-Gel Sci. Technol.* **2**:93, 1994.
16. H. Wolter, W. Storch, and H. Ott, *Mater. Res. Soc. Symp. Proc.* **346**:143, 1994.
17. H. Wolter, W. Glaubitt, and K. Rose, *Mater. Res. Soc. Symp. Proc.* **271**:719, 1992.

18. H. Wolter, W. Storch, and C. Gellerman, *Mater. Res. Soc. Symp. Proc.* **435**:67, 1996.
19. S. Fujiwara and T. Sakamoto, Japanese Kokai Patent Application No. 109998 (1976) (assigned to Unitika K.K., Japan).
20. Y. Fukushima and S. Inagaki, "Synthesis of an Intercalated Compound of Montmorillonite and 6-Polyamide," *J. Inclusion Phenomena* **5**:473–482 (1987).
21. A. Okada, Y. Fukushima, M. Kawasumi, S. Inagaki, A. Usuki, S. Sugiyama, T. Kurauchi, O. Kamigaito, United States Patent No. 4739007 (1988) (assigned to Toyota Motor Co., Japan).
22. M. Kawasumi, M. Kohzaki, Y. Kojima, A. Okada, O. Kamigaito, United States Patent No. 4810734 (1989) (assigned to Toyota Motor Co., Japan).
23. A. Usuki, Y. Kojima, M. Kawasumi, A. Okada, Y. Fukusima, T. Kurauchi, O. Kamigaito, "Synthesis of Nylon 6-Clay Hybrid," *J. Mater. Res.* **8**:1179–1184 (1993).
24. Southern Clay Products, Gonzales, TX. <http://www.scpod.com/gm.html>.
25. Nanocomposites New Low-Cost, High-Strength Materials for Automotive Parts, ATP Project 97-02-0047, National Institute of Standards and Technology, Gaithersburg, MD, 1997.
26. A. K. Mohanty, L. T. Drzal, and M. Misra, *Polym. Mater. Sci. Eng.* **88**:60, 2003.
27. S.L. Wilkinson, *Chem. Eng. News*, 2001, January 22, 61.
28. G. W. Beall, "New Conceptual Model for Interpreting Nanocomposite Behavior," in *Polymer-Clay Nanocomposites*, T. J. Pinnavaia and G. W. Beall (eds.), Wiley & Sons, New York, 2001, pp. 267–279.
29. J. N. Hay and S. J. Shaw, "A Review of Nanocomposites 2000," abstracted version from <http://www.azom.com/details.asp?ArticleID-921>.
30. Multilayer Containers Featuring Nano-Nylon MXD6 Barrier Layers with Superior Performance and Clarity, Mitsubishi Gas Co., Inc. and Nanocor, presented at NavaPac 2003. <http://www.nanocor.com/techpapers.asp>.
31. Triton Systems, Inc., Chelmsford, MA. <http://www.tritonsys.com>.
32. InMat Inc., Hillsborough, NJ. <http://www.InMat.com>.
33. De Bievre and K. Nakamura, "Laminate Structure Excelling in Fuel Permeation Preventing Performance," *PCT Int. Appl.*, 2004, 26. Patent no. WO20004054802.
34. J. W. Gilman, *Appl. Clay Sci.*, 1999, 15, 31.
35. Nanocor, Inc., Arlington Heights, IL. <http://www.nanocor.com>.
36. B. Karn, T. Mascinangioli, W. Zhang, V. Colvin, and P. Alivisatos (eds.), *Nanotechnology and the Environment: Applications and Implications*, ACS Symposium Series 890, American Chemical Society, Washington DC, 2005.

This page intentionally left blank

Index

- Admira, 248
- AEROSIL:
- and aluminum oxide, 43–45
 - applications, 39–40
 - in flame-retardant polymer nanocomposite material, 143, (table)148
 - in NCPMCs, 202, 203–207
 - origins, 36, 37
 - properties of, 38–39
- AEROSIL 300, 143, (table)148
- AEROSIL R202, 203, 204–211
- AEROSIL R805, 204–207, 210, 211
- Aerospace applications, of CNF, 24
- AFM (atomic force microscopy), 80, 92, 118
- Air Force Office of Scientific Research (AFOSR), 177
- Air Force Research Laboratory (AFRL), 67, 172–174, 176, 215
- Alexandre, M., 63
- Alumina, 11
- Aluminum oxide, 36, 44–46
- American Society for Testing and Materials (ASTM), 132
- Apparel applications, (table)244
- Applied Sciences, Inc. (ASI), 19, 24, 160, 184
- Arkema Chemicals, 139
- Army, 250, 251
- ASTM (American Society for Testing and Materials), 132
- Athletic shoes, (table)244
- Atomic force microscopy (AFM), 80, 92, 118
- Automobile industry:
- coatings, 246–247
 - hybrid PCNs, 248–249
 - nanotechnology products, (table)244
- BADGE (bisphenol-A-diglycidylether), 72
- Bakis, C. E., 200
- Barron, A. R., 200
- BASF, (table)244
- Bayer, (table)244, 250
- Becker, O., 109, 110, 116, 200
- Bentonite, 10
- Benzoyl peroxide, 246
- BET surface area, 44, (figure)45
- BioMEMS, 241
- Bismaleimide (BMD) polymer matrix composites, 26
- Bisphenol-A-diglycidylether (BADGE), 72
- Blackhawk, (table)244
- Bondioli, F., 117
- Borden Chemical, SC-1008 (*See* SC-1008)
- Brown, J. M., 104
- Buckytubes, 31–33
- Burnside, S. D., 67
- Cables, 126–132, (table)244, (figure)253
- Cabot, (table)244
- Calorimetry, cone (*See* Cone calorimetry (CC))
- Calorimetry, differential scanning, 80, 93
- Carbon black, 35, 164
- Carbon dioxide, in fire-resistant nanostructured materials, 181
- Carbon fiber-reinforced polymer matrix composites (CPMCs), 198–200 (*See also* Nanocomposites for carbon fiber-enforced polymer matrix composites (NCPMCs))
- Carbon monoxide, in fire-resistant nanostructured materials, 180–181
- Carbon nanofibers (CNFs), 19–26
- applications, 24–26
 - cost of, 19, (table)243
 - definition of, 19
 - elastomer nanocomposites, 215, 216
 - flame-retardant thermoplastic polyurethane nanocomposites, 220–221
 - manufacturing, 20–21
 - mechanical reinforcement requirements, 24
 - NCCCs, 184–185

- NCPMCs, 200, 201, 207–210, 213
 NRAMs, 164, 170–171, 173, 175
 origin, 19
 properties, 20–26
 (*See also* PR-19-PS CNF; PR-24-PS CNF)
- Carbon Nanotechnologies, Inc. (CNI), 31, 33, (figure)34
- Carbon nanotubes, 30–36
 applications, 30
 classifications of, 30–37
 manufacturing, 30
 multiwall carbon nanotubes, 35–38
 origins of, 29–30
 properties, 30–31
 single-wall carbon nanotubes, 31–34
 small-diameter carbon nanotubes, 33–35
 thermal conductivity of, 30
- Carbon/carbon (C/C) structures:
 characteristics, 182
 fabrication of, 188–189
 mechanical properties, 195–196
 thermo-oxidative studies of, 190–195
- Carbon/carbon composites (CCC), 182–183
 (*See also* Nanomodified carbon/carbon composites (NCCCs))
- Carter, L. W., 95
- Cation exchange (CEC), 65, 66, 70
 CC (*See* Cone calorimetry (CC))
 CC139, 183, 195, 196, 197
 CEC (cation exchange), 65, 66, 70
 CEM (Cytec Engineered Materials), 159, 167, 168, 175, 176, 200, 201
- Characterization methods:
 future techniques, 92–93
 overview of, 79–80
 (*See also specific method*)
- Chemical vapor infiltration (CVI)
 process, 184
- Cho, J. W., 96
- Clariant, Exolit AP 750, 126, 130–131
- Clay, MMT (*See* Montmorillonite organoclays (MMTs))
- Clay soil, 10–11
- Cloisite 10A, 17, (table)18, (table)19, 184, 186, 187, 201, 203–205, 208–210
- Cloisite 15A, 17, (table)18, (table)19, 126, 127–132
- Cloisite 20A, 17, (table)18, (table)19, 126, 127, (table)128, 132
- Cloisite 25A, 17, (table)18, (table)19
- Cloisite 30B:
 chemical structure, (table)18
 dry particle sizes, (table)19
 flame-retardant thermoplastic polyurethane nanocomposites, 220, 221, 225, 227, 228
- NCCCs, 184, 185–186
 NCPMCs, 201, 208
 NRAMs, 163, 164–165, 168
 organic modifier, (table)18
 PA11 polymer, 142, (table)148, 150–155, 158
 properties of, 17
 TEM micrograph, (figure)85
- Cloisite 93A, 17, (table)18, (table)19, (table)148, 158
- Cloisite Na⁺, 13, 17, (table)18, (table)19, 184
- CNFs (*See* Carbon nanofibers (CNFs))
- CNI (Carbon Nanotechnologies, Inc.), 31, 33, (figure)34
- Coefficient of thermal expansion (CTE), 224, 228
- Commercial applications, overview, 243–245
- Cone calorimetry (CC), 88–91
 description of, 88–91
 flame-retardant polymer nanocomposites for RP, 148–153
 flame-retardant thermoplastic polyurethane nanocomposites, 225, 227
 Navy submarine application, 174, 177
 Nylon 11 nanocomposites, 141
 polymer nanostructured materials, 174–175, 177
- Converse, (table)244, (figure)252
- Cosmetics, 245–246
- Costs, of nanoparticles, 242–243
- CPMCs (carbon fiber-reinforced polymer matrix composites), 198–200
 (*See also* Nanocomposites for carbon fiber-enforced polymer matrix composites (NCPMCs))
- Crushing powders, 84
- CTE (coefficient of thermal expansion), 224, 228
- Cure temperature, epoxy nanocomposites, 104–108
- Curliss, D., 104, 200
- CVD (chemical vapor deposition)
 synthesis, 35
- CVI (chemical vapor infiltration)
 process, 184

- Cyanate ester resin, 183
 CYCOM 977-3, 200, 201, 210, 211
 Cytec Engineered Materials (CEM), 159,
 167, 168, 175, 176, 200, 201
- De Bievre, 253
 Defense Department, 256
 Degussa, 36, 43, 140, 201
 Dennis, H. R., 96
 Dental applications, 247–248
 Derakane Momentum 441-400 epoxy vinyl
 ester (EVE) resin, 67–68
 DGEBA (diglycidyl ether of bisphenol A)
 epoxy resin, 68, 70–71, 108–116
 Diethyltoluene diamine (DETDA), 109
 Differential scanning calorimetry (DSC),
 80, 93, (table)113
 Diffraction, x-ray, 65, 70, 80–81
 (See also Wide-angle x-ray diffraction
 (WAXD))
 Dispermat mixer, 132
 Diglycidyl ether of bisphenol A (DGEBA)
 epoxy resin, 68, 70–71, 108–116
 DMTA (dynamic mechanical thermal
 analysis), 74, 80, 202, 204–209, 213
 Dow Chemical, 220
 Dow Corning, 217
 Dubois, P., 63
 DuPont, (table)244, 248
 Dynamic mechanical thermal analysis
 (DMTA), 74, 80, 202, 204–209, 213
- Eastman Chemical Company, (table)244
 EDS (energy-dispersive x-ray
 spectroscopy), 83, 86, 119
 Edwards AFB, 173
 Elastomer-based nanocomposites, 55, 67,
 118–121, 215–217
 Electron energy-loss spectroscopy (EELS),
 83–84
 Electropolishing, 84
 Elongation at break, 100, 143, (table)148,
 (figure)150, 158
 EmTech Research, 239
 Emulsion polymerization, 68–69
 Energy Department, 256
 Energy-dispersive x-ray spectroscopy
 (EDS), 83, 86, 119
 Environmental, health, and safety (EHS)
 risks, 258–259
- Environmental applications, 249
 EPDM (ethylene-propylene-diene rubber),
 215–217
 Epon 828, 71, 104, 105, 106
 Epoxy nanocomposites, 103–118
 applications, 103
 cure temperature, 104–108
 DGEBA epoxy resin system,
 108–116
 dispersion of octadecyl ammonium
 ion-modified layered silicates,
 109–116
 general processing of, 104–108
 model of elastic properties, 117–119
 temperature dependence of shear
 moduli, 106–108
 TGAP system, 109–111, 113–115
 TGDDM system, 109–116
 Epoxy resins, 103, 108–116, 200, 201
 Epoxy vinyl ester (EVE) resin, 67–68
 Epoxy-silica nanocomposites, model of
 elastic properties, 117–119
 Equistar, Petrothene XL 07414, 126
 Ethylene vinyl alcohol (EVOH), 250
 Ethylene-propylene-diene rubber (EPDM),
 215–217
 European Union, nanotechnology R&D
 investments, 236
 Exfoliation, exfoliated state, 5
 Exolit AP 750, 126, 130–131
 Extruders, 126, 140, 221
- Fasulo, P. D., 118
 Fecht, H. J., 242
 Filling composites, 247–248
 Film, nylon, (table)244
 Fire resistance, 28
 Fire resistant nanostructured materials,
 176–182
 Fire Testing Technology Ltd. (FTT), 91
 Flame retardant applications,
 (table)244
 Flame retardant properties, hybrid PCNs
 with, 253–254
 Flame retardant thermoplastic polymers:
 development process, 139
 nonhalogenated flame retardant
 polymers for cabling jackets,
 126–132
 polyurethane nanocomposites,
 220–228

- waterborne fire-retardant
nanocomposite coating, 132–138
(*See also* Rapid prototyping (RP),
flame-retardant polymer
nanocomposites for)
- Flammability properties:
flame-retardant thermoplastic
polyurethane nanocomposites,
225, 226
PA11, 142–143, (table)148,
(table)157, 158
polymer nanostructured materials,
176–182
- Flammability testing, 126
(*See also* Cone calorimetry (CC))
- Flatwise tension strength (FWT), 210,
212, 213
- Flexural strength:
NCPMCs, 210–211, 212, 213
PA11, 143, (table)148, (figure)149, 158
- Floor coverings, (table)244
- Ford Motor Company, 248
- Fornes, T. D., 97
- Foster-Miller, (table)244
- Fourier Transform Infrared Spectroscopy
(FTIR), 69
- Fujiwara, S., 96
- G_{1C} values, 211, 213
 G_{2C} values, 212, 213
- Gas-displacement pycnometry, 113
- General Electric (GE), (table)244
- General Motors (GM), (table)244, 248
- Giannelis, E. P., 66, 67, 71, 199
- Gilman, J. W., 177, 199, 251
- Gitto, 251
- Glasgow, D. G., 24
- Government investments, (table)240,
255–256, 258–259
- Graphite, 35, 46
- “Green” nanocomposites, 249
- Haake, CTW 100 extruder, 126
- Halpin-Tsai rule, 118
- Hanse Chemie, 40–43
- Heat capacity, of TPUNs, 224, 226
- Heat of combustion, TPUNs, 228
- Heat release, defined, 91
- Heat release rate (HRR):
AP 750, (figure)130
Cloisite 15A, (figures)127, 130
Cloisite 20A, (figure)127
definition of, 91
fire-resistant nanostructured materials,
179–180
flame-retardant polymer
nanocomposites for RP, 142–143,
(table)148
of TPUNs, 227, 228
waterborne fire-retardant
nanocomposite coating, (figures)
133, (figures)134
Hectorite Na^+ , (table)65
High-shear mixing, 72–74
Hitco, 184, 188–189
Honeywell, (table)244, 250
HRR (*See* Heat release rate (HRR))
- Hybrid materials:
automotive coatings, 246
cosmetics, 245–246
dental applications, 247–248
overview, 243–245
PCNs, 248–253
Hybrid Plastics, Inc., 26, 160
Hyperion, (table)244
- IBM, 239
- Ignitability, 91, 179
- Iijima, S., 30
- IKA mixer, 72, 137
- Imperm, 250
- In-situ polymerization, 69–72, 118
- InMat, Inc., (table)244, 250–251
- Inorganic-organic hybrid materials (*See*
Hybrid materials)
- Institute for Scientific Information
(ISI), 237
- Intel, 239
- Intercalation, 64–67
- Interlaminar shear strength (ILSS),
195–196, 198
- Ion-milling, 84
- Japan, nanotechnology R&D
investments, 236
- Johnson, T. N., 215
- Kabelwerk Eupen, (table)244, (figure)253
Karn, B., 256, 258

- Kevlar, 215, 216
 Koo, J. H., 73, 176, 199
- Lake, M. L., 199
 Lan, T., 71, 114, 200
 Laponites, 15
 Lee, A., 200
 Length scale, importance of, 2
 Lewis-Nielsen equation, 118
 Lichtenhan, J. D., 200
 Lonza Corporation, Primaset PT-15/30, 183
 L'Oreal, 239
 Luehmann, B., 170
- Mach I, (table)244
 Macrosurfaced nanosilica, 40–42
 Mass loss calorimeter (MLC), 91–92, 123, 134
 Mathias, E. C., 215
 Mattress covers, (table)244
 Medical applications, (table)244, (figure)253
 Melt compounding or processing, 13, 96–97, 101–103, 118
 Melt intercalation, 66–67
 Messersmith, P. B., 71
 Microelectromechanical systems (MEMS), 241
 Microsystem technology, 239, 241–242
 Military applications, (tables)25, 103
 Mitsubishi Gas Chemical Company, 250
 MLC (mass loss calorimeter), 91–92, 123, 134
 MMT (*See* Montmorillonite organoclays (MMTs))
 Molteni Labmax mixer, 72
 Montmorillonite Na⁺, (table)65
 Montmorillonite organoclays (MMTs):
 cost of, (table)243
 dispersing process, 13–15
 in emulsion polymerization, 68
 NCCCs, 184, 196, 198
 NCPMCs, 200, 201, 213
 nonhalogenated flame retardant polymers for cabling jackets, 126–132
 NRAMs, 160, 163–164, 170–171, 175, 176
 organic treatment, 12–13
 origins, 10–11
 in-situ polymerization, 70–71
 structure, 11–12
 suppliers, 15–16
 (*See also Cloisite entries*)
 Mulhaupt, R., 72
 Multiwall carbon nanotubes (MWNTs), 35–36, (figures)37, (table)243
 MX-4926:
 fire-resistant nanostructured materials, 178–182
 NRAMs, 159–160, 163, 167–168, 170–171, 173
- Nahin, P. G., 95
 Nakamura, K., 251
 Nanoaluminum oxide, 44–46, (table)243
 Nanoclays, 10–11
 (*See also* Montmorillonite organoclays (MMTs))
 Nanocomposite rocket ablative materials (NRAMs):
 Airforce Research Laboratory Pi-K rocket motor ablation test, 172–174
 experimental results, 164–166
 future research, 176
 heat transfer, 172, 175
 high-shear mixing, 73
 material selection, 163–164
 MX-4926 as controls, 167–168
 overview of, 159–160
 scale ablation test, 168–172
 SSRM ablation test, 166–167, 175
 SSRM experimental approach, 160–163
- Nanocomposites:
 definition of, 5
 length scales of, 3
- Nanocomposites for carbon fiber-enforced polymer matrix composites (NCPMCs), 198–201
 CNF nanoparticle processing and characterization, 207–210
 epoxy resins, 200
 experimental results, 202–203
 material selection, 201–202
 mechanical properties, 210–211
 nanoclay system processing and characterization, 203
 nanosilica system processing and characterization, 203–207

- overview of, 198–201
- processing, 210
- scaling up, 210
- NANOCONE, 43
- Nanocor, Inc., 16, 110, (table)244, 250, 251
- NANOCRYL, 42
- Nanoelectronmechanical systems (NEMS), 241
- Nanomanufacturing, research issues, 256
- Nanomaterials:
 - behavior vs. larger scale counterparts, 241
 - classification of, 4
 - research funding, 256
 - uniqueness of, 3–4
- Nanomer, 184, 186
- Nanometer (nm), definition of, 2
- Nanomodified carbon/carbon composites (NCCCs), 182–198
 - carbon/carbon composite fabrication, 188–189
 - density comparison, (table)193, (table)194
 - experimental results, 185, 197–198
 - high-shear mixing, 73
 - material selection, 183–185
 - mechanical properties, 195–196, (table)197
 - overview of, 182–183
 - physical properties, (table)191
 - processing and characterization of resin/nanoparticle systems, 185–188
 - thermo-oxidative studies, 190–195
 - weight loss comparison, (table)192
- Nanoparticles:
 - behavior vs. larger scale counterparts, 241
 - characteristics of, 10
 - economics of, 242–243
 - for NCCCs, 184
 - types of, overview, 9–10
- Nanophase materials, 4
- Nanophase Technologies, (table)244
- NANOPOL, 43
- Nanoscale science and technology, 3, 257
- Nanosilicas, 38–44, 158, 200, 213, (table)243
 - (See also AEROSIL)
- Nanostructured materials:
 - definition of, 4
 - uniqueness of, 3–4
- Nanotechnology:
 - commercial applications, overview, 243–245
 - commercialization prospects, 239–242
 - definition of, 1
 - future research, 253–258
 - government investments, (table)240
 - patents, 238, 239
 - potential applications, (table)245
 - publications, 237–238
 - research funding, 235–237, 255–256
 - safety risks, 258–260
 - target industries, (figure)241
- Nanotex, (table)244
- Nanotitanium dioxide, 46–47, (table)243
- National Institute of Standards and Technology (NIST), 177, 256
- National Institutes of Health, 256
- National Nanotechnology Advisory Panel, 257
- National Nanotechnology Initiative (NNI), 1, 235, 253–256, 258
- National Science Foundation (NSF), 238, 256
- Naval applications, 126, 176–177
- NCCCs (See Nanomodified carbon/carbon composites (NCCCs))
- NCPMCs (See Nanocomposites for carbon fiber-enforced polymer matrix composites (NCPMCs))
- NEMS (nanoelectronmechanical systems), 241
- Neutron scattering, 80, 92
- NIST (National Institute of Standards and Technology), 177, 256
- NNI (National Nanotechnology Initiative), 1, 235, 253–256, 258
- Nonhalogenated flame retardant polymers for cabling jackets, 126–132
- NRAMs (See Nanocomposite rocket ablative materials (NRAMs))
- NSF (National Science Foundation), 238, 256
- Nuclear magnetic resonance (NMR), 80, 92
- Nylon 6, 95–103
- Nylon 11 (See PA11 (polyamide 11))
- Nylon 12, 139, (figure)253

- Optical coatings, (table)244
 Optical microscopy, 80, 112
 Organic treatments, of silicates, 12–13
 Organically modified layered silicates (OLS), 104, 252
 Organoclays, 95–96
 (See also Montmorillonite organoclays (MMTs))
 Organophilic layered silicate (OLS), 72, 106
 ORMOCER, 247, 248
- PA11 (polyamide 11):
 flame retardancy, 139
 flammability properties, 142–143, (table)148, (table)157, 158
 flammability specimen analyses, 150–155
 fracture surface analyses, 147–150
 mechanical properties, 143, 147, (table)148, (table)157, 158
 peak heat release rate, 158
 processing and characterization of, 140–142
 RILSAN PA11, 139–140
 SLS processing, 155–157
 PA12 (polyamide 12), 139
 Patents, 238, 239
 Paul, D. R., 96, 97, 101
 PCAs (program component areas), 254, (table)255, 256
 PCNs (polymer-clay nanocomposites), 248–253
 Peak erosion, NRAM, 168, 169, 175
 Peak heat release rate (PHRR):
 fire-resistant nanostructured materials, 179
 flame-retardant polymer nanocomposites for RP, 143
 flame-retardant thermoplastic polyurethane nanocomposites, 225, 228
 nonhalogenated flame retardant polymers for cabling jackets, 127, 128–129
 PA11, (table)148
 waterborne fire-retardant nanocomposite coating, 133–134, 135, 137
 PELLETHANE 2102-90A TPU, 220, 221, 222–223, 227, 228
 Petrothene XL 07414, 126
 Phenolic resin, 163, 184, 187–188
 Phenyl, 28
 Phosphorus loading, 130–131
 PHRR (See Peak heat release rate (PHRR))
 Pi-K SRM, 173–174
 Pinnavaia, T. J., 71, 114
 Pittman, C., 200
 PMCs (polymer matrix composites), 55, 103
 PMMA (polymethyl methacrylate), 68–69
 PNMs (polymer nanostructured materials), 4–5, 51–52
 Polyamide 6, 96
 Polyamide 11 (See PA11 (polyamide 11))
 Polyamide 12 (PA12), 139
 Poly(caprolactam) (nylon 6), 159
 Polycarbonate, 139
 Polyhedral oligomeric silsesquioxane (POSS):
 cost of, (table)243
 energy-dispersive x-ray spectroscopy, 86
 features, 27–29
 flame-retardant thermoplastic polyurethane nanocomposites, 221
 high-shear mixing, 73
 NCCCs, 184, 185–186, 187–188
 NRAMs, 164, 169, 175
 origins, 26
 properties, 26–27
 roll milling, 67–68
 Polymer coils, length scales of, 3
 Polymer fillers, length scales of, 3
 Polymer matrices, 52–55
 Polymer matrix composites (PMCs), 55, 103
 Polymer nanocomposites (PNs):
 classifications of, 52–55
 current technology, 9
 Polymer nanostructured materials (PNMs), 4–5, 51–52
 Polymer-clay nanocomposites (PCNs), 248–253
 Polymerization, 54, 68–72, 118
 Polymers, classification of, 52
 Polymethyl methacrylate (PMMA), 68–69
 Polyimide (PI) nanocomposites, 64–65
 Polyimide-montmorillonite (MMT) nanocomposite, 65
 Polypropylene, 118

- Polystyrene, 29–30, 65, 118, 139
- Polyurethane nanocomposites, 220–228
- Polyvinyl silsesquioxane uncured (PVSQ)-PM1285, 164
- POSS (*See* Polyhedral oligomeric silsesquioxane (POSS))
- Powder mechanics, 156, 158
- Power cables, 126–132, (table)244, (figure)253
- PPO, 72
- PR-19-PS CNF:
 - fire-resistant nanostructured materials, 179
 - flame-retardant thermoplastic polyurethane nanocomposites, 221, 222, 225, 227
- NCCCs, 184
- NCPMCs, 207–208, 210, 211
- NRAMs, 164
- PA11 polymer, 147–155
- PR-24-PS CNF:
 - flame-retardant thermoplastic polyurethane nanocomposites, 221, 222, 224, 225, 227
- NCCCs, 184
- NRAMs, 164, 168
- TEM micrograph, (figure)85
- Primaset PT-15, 183, 186–187 (*See also* Nanomodified carbon/carbon composites (NCCCs))
- Primaset PT-30, 183, 185 (*See also* Nanomodified carbon/carbon composites (NCCCs))
- Procter & Gamble, (table)244
- Program component areas (PCAs), 254, (table)255, 256
- Propulsion systems, 215–220
- Publications, 237–238
- PVA-Clay fire retardant coating systems, 133–138
- Pyrograf carbon nanofibers, 19–20, (figure)21
- Rapid prototyping (RP), flame-retardant polymer nanocomposites for:
 - applications, 138–139
 - flammability properties, 142–143, (table)157
 - flammability specimen analyses, 150–155
 - fracture surface analyses, 147–150
 - materials, 139–140
 - mechanical properties, 143, 147, (table)148, (table)157
 - resin/nanoparticle systems, 140–142
 - SLS candidates, 155–157
- Research, future directives, 253–259
- Research funding, 235–237, 255–256, 259
- Research output, 237–239
- Resins:
 - epoxy resins, 103, 108–116, 200, 201
 - epoxy vinyl ester (EVE) resin, 67–68
 - for high-shear mixing, 72
 - phenolic resins, 163, 184, 187–188
 - thermoplastic olefin (TPO), 118–121
 - thermosetting of, 52, 53–54
- Rheology, 93
- RILSAN PA11, 139–140
- Rocket ablative materials (*See* Nanocomposite rocket ablative materials (NRAMs))
- Rocket fuel additives, (table)244
- Roll milling, 67–68
- Rubber modified epoxy nanocomposites, 71
- Safety risks, 258–260
- Sakamoto, T., 96
- Sanchez, C., 63, 243
- Saponite Na⁺, (table)65
- SAXS (small-angle x-ray scattering), 86–88
- SBS (short-beam interlaminar shear strength), 212, 213
- SC-1008:
 - fire-resistant nanostructured materials, 178, 179
 - NRAMs, 160, 163–164, 169, 173
- Scanning electron microscopy (SEM):
 - EPDM-Kevlar, 216–217
 - and high-shear mixing, 73
 - for microstructural analyses of flammability specimens, 150–155
- NCPMCs, 202
- NRAMs, 176
- PVA-30% clay, (figure)136
- TPO nanocomposites, 119
- Scanning probe microscopy (SPM), 80
- Scanning tunneling microscopy (STM), 80
- Science, Nature, and Physical Review Letters*, 237–238
- SDNTs (small-diameter carbon nanotubes), 33–35, (table)243

- Seferis, J. C., 200
- Selective laser sintering (SLS), 138–139, 155–157
- SEM (*See* Scanning electron microscopy (SEM))
- Shivakumar, K., 153
- Short-beam interlaminar shear strength (SBS), 212, 213
- Silica, 11
- Silicon carbide, 46
- Silicon dioxide, 36
- Silicon-rubber-based nanocomposites, 67
- Simon, G., 109
- Simulated solid rocket motor (SSRM), 160–163, 166–167
- Single-wall carbon nanotubes (SWNTs), 31–33, (table)243
- SLS (selective laser sintering), 138–139, 155–157
- Small-angle x-ray scattering (SAXS), 86–88
- Small-diameter carbon nanotubes (SDNTs), 33–35, (table)243
- Smalley, Richard E., 31
- Smoke ratio, fire-resistant nanostructured materials, 180–181
- SO1458 POSS (*See* Trisilanolphenyl-POSS-SO1458)
- Sol-Gel Technologies Ltd., 246
- Solution intercalation, 64–65
- Southern Clay Products (SCP), 10, 13, 15–16, 118, 126, 160, (table)244
- SPM (scanning probe microscopy), 80
- SSRM (simulated solid rocket motor), 160–163, 166–167
- Stain removers, (table)244
- Standards, 259
- STM (scanning tunneling microscopy), 80
- Submarines, fire-safe polymeric materials, 176–177
- Sud Chemie, (table)244
- Sunscreens, (table)244, 246
- SWNT (single-wall carbon nanotubes), 31–33, (table)243
- Synthesis methods, 61–65
- Synthetic Mica Na⁺, (table)65
- TEM (*See* Transmission electron microscopy (TEM))
- Tennis balls, (table)244, 250–251
- Tensile strength, 143, (table)148, 158, 196, 198
- Tetrafunctional tetraglycidyl diamino diphenylmethane (TGDDM), 109–116
- Tetraglycidyl 4, 4'-diaminodiphenyl methane (TGDDM), 72
- TGA (thermal gravimetric analysis), 80, 93, 215–216
- TGAP (trifunctional triglycidyl *p*-amino phenol), 109, 110, 111, 113–115
- Thermal conductivity, of TPUNs, 225, 226, 228
- Thermal gravimetric analysis (TGA), 80, 93, 215–216
- Thermo-oxidative studies of CCC, 190–195
- Thermoplastic elastomers (TPEs), 214–228
- flame-retardant thermoplastic polyurethane nanocomposites, 220–228
- propulsion systems, 215–220
- TPSiV X1180, 217–220
- Thermoplastic polyolefin (TPO) nanocomposites, 118–121
- Thermoplastic polyurethane elastomer nanocomposites (TPUNs), 221–228
- Thermoplastic polyurethane elastomers (TPUs), 220–228
- Thermoplastic-based nanocomposites: characteristics of, 52–53
- examples of, (table)53
- high-temperature applications, overview, 125
- melt intercalation, 66–67
- nylon 6 nanocomposites, 95–103
- in-situ polymerization, 70–71 (*See also* Flame retardant applications)
- Thermoset-based nanocomposites: characteristics of, 52, 53–54
- examples of, (table)54
- flammability properties, 176–182
- in-situ polymerization, 71 (*See also* Epoxy nanocomposites; Nanocomposite rocket ablative materials (NRAMs); Nanocomposites for carbon fiber-enforced polymer matrix composites (NCPMCs); Nanomodified carbon/carbon composites (NCCCs))
- THF, 185, 186
- 3D Systems Vanguard HS machine, 156
- Titanium dioxide, 36, 46–47

- Toyota Research group, 65, 70, 96, 248
- TPEs (*See* Thermoplastic elastomers (TPEs))
- TPO (thermoplastic polyolefin)
nanocomposites, 118–121
- TPSIV X1180, 217–220
- TPUNs (thermoplastic polyurethane elastomer nanocomposites),
221–228
- TPUs (thermoplastic polyurethane elastomers), 220–228
- Transmission electron microscopy (TEM),
81–86
advantages of, 81–82
aluminum oxide, 44
clay dispersion, 86
Cloisite clay nanocomposites,
(figures)129
description of, 81–86
disadvantages of, 86
epoxy nanocomposites, 104–106
example of, 84–85
flame-retardant polymer development
for RP, 141
flame-retardant thermoplastic
polyurethane nanocomposites,
221–223, 226
and high-shear mixing, 73
limitations of, 85–86
macrosurfaced nanosilica,
(figure)42
NCCCs, 184, 186, 187, 188, 197
NCPMCs, 202–207, 213
NRAM, 164–166
PVA-Clay fire retardant coating
systems, (figure)136, (figure)138
sample preparation, 84
thermoplastic elastomers, 218–219
thermoplastic nanocomposites, 70
titanium dioxide, 46
- Trifunctional triglycidyl *p*-amino phenol
(TGAP), 109, 110, 111, 113–115
- Trisilanolphenyl-POSS-SO1458:
in flame-retardant thermoplastic
polyurethane nanocomposites,
221, 227
in NCCCs, 186, 187
SSRM approach, 164
TEM micrograph, (figure)85
- Triton Systems, (table)244, 250,
(figure)252
- Ube Industries, (table)244, 251
- Unitika, 96, (table)244
- Ultimate tensile strength (UTS)
(measurement), 196, 198
- Vacuum assisted resin transfer molding
(VARTM), 42
- Vaia, R. A., 66, 67, 96, 104, 159, 199
- Vapor-grown carbon fibers (VGCFs), 19
- Varley, R., 109
- VGCFs (vapor-grown carbon fibers), 19
- Vinyl, 28
- Volcanic ash, 10–11, (figure)12
- Wang, K., 116
- Waterborne fire-retardant nanocomposite
coating, 132–138
- Werner, M., 242
- Werner Pfeleider extruder, 140, 221
- Wide-angle x-ray diffraction (WAXD):
clay dispersion, 86
description of, 80–81
DGEBAs nanocomposites, 71, 111
flame-retardant thermoplastic
polyurethane nanocomposites, 224
and high-shear mixing, 73
NCCCs, 185
NCPMCs, 202
NRAM, 164
TGDDM nanocomposites, (table)
112
- Wilson, (table)244, 250–251
- X-ray diffraction (XRD), 65, 70, 80–81
(*See also* Wide-angle x-ray diffraction
(WAXD))
- Young's modulus, 143, (figure)149
- Zilg, C., 200

ABOUT THE AUTHOR

Joseph H. Koo is currently a senior research fellow and director of Solid Freeform Fabrication Consortium in the Department of Mechanical Engineering at the University of Texas at Austin, Austin, TX. He is chairman of the newly established SAMPE Nanotechnology Committee and immediate past chairman of the AIAA Materials Technical Committee. Dr. Koo has 30 years of industrial and academic experience in program and engineering management and has published over 200 papers on thermal, material, and optical sciences in a variety of science journals and conference proceedings.



McGraw-Hill's DIGITAL ENGINEERING LIBRARY

www.digitalengineeringlibrary.com



A Dynamic Online Source of WORLD-RENOWNED ENGINEERING TITLES Combined with Innovative Technology

Digital Engineering Library Features:

- A powerful online resource of engineering content from the field's premier publisher
- 12 major areas of engineering with more than 500 major subtopics

The 12 major areas of engineering include:

- Aerospace Engineering
- Bio Engineering
- Chemical Engineering
- Civil Engineering
- Communications Engineering
- Construction & Architectural Engineering
- Electrical Engineering
- Engineering Math & Science
- Environmental Engineering
- Industrial Engineering
- Materials Science & Engineering
- Mechanical Engineering

- 5,000+ Chapters derived from 170+ outstanding McGraw-Hill Titles including:

- *Marks' Standard Handbook for Mechanical Engineers*
- *Perry's Chemical Engineers' Handbook*
- *Roark's Formulas for Stress and Strain*

- Pay-Per-View Access
- Chapters available in PDFs
- Ultra-efficient search or topical browse
- Late-breaking industry news from *Engineering News Record*
- Search the *McGraw-Hill Dictionary of Engineering* with more than 18,000+ entries
- Bookmark, highlight, e-mail articles, and annotate to add your own personal notes and comments to the text



Browse list of topics, search, preview and purchase individual articles!

Contact Us: call 888-307-5984 (outside the U.S.: 1-614-759-3663)

www.digitalengineeringlibrary.com